CZECH TECHNICAL UNIVERSITY IN PRAGUE

FACULTY OF MECHANICAL ENGINEERING

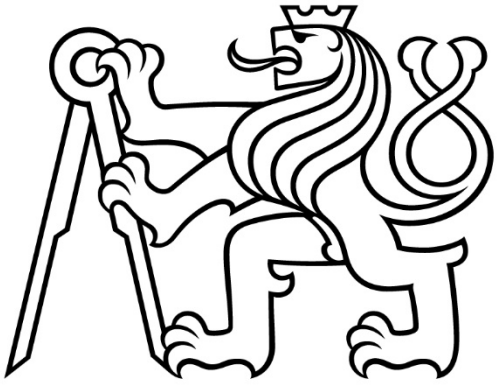

DOCTORAL THESIS STATEMENT

CZECH TECHNICAL UNIVERSITY IN PRAGUE
Faculty of Mechanical Engineering
Department of Environmental Engineering

Dissertation
on

Stratification in storage tanks for heat pumps

Ing. Yogender Pal Chandra

Doctoral Study Programme: Mechanical Engineering

Study Field: Environmental Engineering

Supervisor: doc. Ing. Tomáš Matuška, Ph.D.

Dissertation thesis statement for obtaining the academic title of “Doctor” abbreviated to “Ph.D.”

Prague March 2024

SHRNUTÍ

Pro zajištění vysoké kvality akumulace tepla a vysoké účinnosti při jeho získávání se v zásobnících tepla často využívá tepelného vrstvení (stratifikace). Motivace pro využití stratifikace spočívá v tom, že mísení vrstev v zásobníku může být během provozního cyklu minimalizováno tak, že na konci ohřevu objemu zásobníku může být z horní části odebírána voda o vysoké teplotě, čímž se dosahuje vysoké tepelné účinnosti na straně odběru, zatímco v dolní části může být odebírána voda o nízké teplotě a tak udržena vysoká účinnost na straně jímání obnovitelného tepla. Výzkum stratifikace zahrnuje posouzení široké škály konceptů, které se vyskytují okolo ústředního tématu zásobníků tepla, především jejich návrhu a modelování.

Tato práce je zpracována jako „Disertace publikacemi“. K průvodnímu textu této práce je připojeno celkem 5 publikací (článků), které představují 3 hlavní výzkumné studie. Celkem 4 články jsou publikovány v recenzovaném impaktovaném časopise ležícím v prvním kvartilu (Q1), zatímco 1 článek je publikován v recenzovaném impaktovaném časopise ležícím v prvním decilu (D1).

V první studii je představena jak experimentální tak numerická práce. Samotná studie je založena na systematické a komplexní rešeršní práci, např. bylo diskutováno použití více-uzlového a „plug-flow“ přístupu k modelování různých rozložení teploty. Modely byly kategorizovány jako lineární, stupňovité, spojitě-lineární a obecné třízónové modely pro rozložení teploty. Následně byla demonstrována dynamika degradace teplotního gradientu a ovlivňující parametry v pohotovostním i dynamickém režimu. Kromě toho byl ukázán přehled současných metod a postupů k vyhodnocování stratifikačního chování a jeho kvantifikaci. To zahrnuje geometrické parametry, uvažování konstrukčního návrhu, jako návrh vtoku, poměr rozměrů nádrže či specifikace materiálu stěny a také provozní parametry pro omezení mísení. Praktické techniky a metody byly představeny novým způsobem a rozšiřují základ praktických aplikací a výzkumných postupů.

Na základě rešerše bylo dále kvantifikováno turbulentní mísení na základě teplotního profilu, MIX čísla a Richardsonova čísla. Pro nalezení optimálních provozních podmínek v režimu vybíjení zásobníku byly vytvořeny různé CFD modely a experimentálně ověřeny na vlastním laboratorním zkušebním zařízení pro různá nátoková zařízení. Hodnocené parametry pak zahrnují průtok, rozdíl teplot ΔT a dále konstrukci nátoku do zásobníku, takže mezi nimi byla stanovena

vzájemná závislost. Výsledky numericky prokázaly, že provozní podmínky zásobníku lze optimalizovat vhodnou volbou konstrukce nátoku. Tato výzkumná zjištění mohou sloužit jako vodítko pro optimalizaci návrhu zásobníku tepla, konkrétněji návrhu založeného na vhodném nátokovém zařízení integrovaném s konkrétním zdrojem tepla, neboť teplotní stratifikace a *COP* zdroje tepla, tj. například tepelného čerpadla, jsou neodmyslitelně korelovány. Tepelná čerpadla jsou zařízení s vysokým průtokem a nízkým ΔT, na rozdíl od solárních systémů jako zařízení s nízkým průtokem a vysokým ΔT. Vhodná volba nátokového zařízení pro konkrétní provozní podmínky zdroje tepla je proto kritická.

Druhá studie je zaměřena především na vývoj vhodného exergetického modelu kvantifikujícího degradaci stratifikace v zásobníku tepla na základě druhého termodynamického zákona, který byl sledován pro přizpůsobení rovnic vyjadřujících entropii a exergii. Nové modely prošly přísným validačním procesem. Nejprve byla provedena experimentální validace, poté byl využit přístup založený na datech za použití LSTM neuronové sítě. LSTM model reprodukoval výsledky vypočtené nově vyvinutým exergetickým modelem, a výsledky vypočtené kvantitativním přístupem odpovídají výsledkům datového přístupu. Součástí procesu validace modelu bylo porovnání výsledků s pracemi jiných autorů. Stejně důležitým bylo i podrobení dat časové řady analýze statistické nejistoty z pohledu Gaussova rozdělení. Bylo zjištěno normální rozdělení nejistoty s 95 % datovými body v rozmezí 5% nejistoty. Nakonec, byly tyto rovnice přizpůsobeny datové vrstvě, aby bylo možné v reálném čase zaznamenávat výsledné stratifikační chování při akumulaci tepla a topného faktoru *COP* tepelného čerpadla během cyklu nabíjení/vybíjení zásobníku tepla. Takové vyhodnocení v reálném čase poskytuje lepší pohled na energetickou účinnost systému OZE jako zdroje tepla a může tak být pomocí expertům a výzkumníkům.

Ve třetí studii je demonstrováno použití inteligentní datové vrstvy pro vyhodnocování a predikci výsledného chování stratifikovaného zásobníku tepla integrovaného s tepelným čerpadlem. Modelování dat, jejich získávání, zpracování a transformace se provádí dynamicky. Byla vyvinuta metoda k využití rámce datové vrstvy k vizualizaci energetické účinnosti akumulace tepla v reálném čase tak, aby vyhovovala exergetickému modelu podle druhého termodynamického zákona. To umožňuje expertům intuitivně porozumět energetické účinnosti jejich zařízení pomocí nového datového řetězení. Datová vrstva vyhodnocuje degradaci vrstvení (ve smyslu generování entropie) pomocí nového modelu podle druhého termodynamického

zákona odvozeného v této třetí studii. Kromě entropie také vypočítává *COP* tepelného čerpadla při různých provozních parametrech.

SUMMARY

To assure high quality thermal storage and high efficiency of its acquisition, thermal stratification is often employed in thermal storage tanks. The motivation of stratification lies in the fact that mixing of layers can be minimized during operational cycle of the tank so that high temperature water could be taken at the load end, thus maintaining high thermal efficiency at demand side, while low temperature water can be drawn at lower bottom, thus maintaining the high efficiency at renewable heat collection side. The investigation of stratification entails the assessment of a wide variety of concepts to be embodied around the central theme of the thermal storage, especially its design and modelling.

This thesis is put forward as "Thesis by publication." In total 5 papers, which represent three main research studies, are attached together to accompanying text in this thesis. Meaning, 4 papers are published in first quartile (Q1) peer-reviewed impacted journal, while 1 paper is published in first decile (D1) peer-reviewed impacted journal.

In the first study both experimental and numerical work is presented. The study is based on systematic comprehensive review work. For instance, multi-node and plug-flow approach to model various temperature distribution models are resurfaced. These models are categorized as linear, stepped, continuous-linear and general three-zone temperature distribution models. Subsequently, the dynamics of thermo-cline decay and influencing parameters both during standby and dynamic mode were demonstrated. In addition, a survey of state-of-the-art methods and practices to ascertain the performance improvement and its quantification were illustrated. This includes geometrical parameters – such as, structural design incorporation, essentially – inlet design, tank aspect ratio and wall material specification, and also, operational parameters to curb down the inlet mixing. Practice techniques and methods which were presented here in a novel way, extend towards the ground of practical application and research procedures.

Furthermore, based on review, quantification of turbulent mixing was achieved on the basis of temperature profile, MIX number, and Richardson number. Various CFD models were developed and experimentally validated on the own laboratory test rig in order to find the optimal working conditions in discharge mode for different inlet devices. The evaluated parameters include flow rate, ΔT, and design of inlet device (diffuser), henceforth a direct interdependence between

each was thus established. The results proved numerically that the tank working conditions can be optimized by proper selection of inlet device. These research findings can serve as guidelines to optimize the storage tank design, more specifically, inlet device-based design integrated with heating system, as thermal stratification and *COP* of heating system i.e. heat pumps, for example, are inherently correlated. Heat pumps are high flow rate and low ΔT devices, while, solar systems are low flow rate and high ΔT devices. Thus, the suitable choice of inlet device for a particular operating condition is critical.

Second study is mainly focused on development of suitable exergetic models quantifying stratification decay of thermal storage based on second law of thermodynamics which was observed in tailoring the entropy and exergy equations. The new models underwent strict validation process. Firstly, experimental validation was achieved. Secondly, data driven approach using LSTM neural network was utilized. The LSTM model reproduced the results calculated by newly developed exergetic model thus the results calculated by quantitative approach is validated by data driven approach. Finally, the results were also compared with the work of other authors as a part of validation process. Equally important, time series data thus collected underwent statistical uncertainty analysis. Probability distribution of error in terms of Gauss distribution was analyzed. It was observed that the uncertainty was normally distributed with 95% data points falling under 5 % uncertainty range. In conclusion, it was made possible to fit these equations to the customized data layer in order to stream in real time the end to end stratification performance of thermal energy storage, and *COP* of heat pump during charge/discharge cycle. This real time evaluation gives a better perspective about the energy efficiency of RES system and thus could help experts and researchers.

In the third study, application of intelligent data layer for evaluating and predicting end to end performance of heat pump integrated stratified thermal energy storage system is demonstrated. The data modelling – acquisition, curation, and transformation is done in situ (dynamically). A method was developed to utilize of data-layer framework to visualize in real-time energy efficiency of thermal storage, in other words, to fit the developed second law of thermodynamics-based exergy model. This will help experts to intuitively understand the energy efficiency of their devices using novel data pipeline. The data layer evaluates stratification decay (in terms of entropy generation) using the novel second law model derived in the third study. In addition to entropy it also calculates *COP* of the heat pump at different operational parameters.

Acknowledgement

I express my gratitude to:
Tomas Matuska as my supervisor, for his guidance and useful critique and providing me grounds for this creative and scientific work,
My parents, family members and friends,
Josephus for his constant support and guidance,
and the Almighty Lord.

Declaration

I declare that work done in this thesis entitled, “Stratification in storage tanks for heat pumps” submitted towards fulfilment of Ph.D. degree at *Department of Environmental Engineering, Faculty of Mechanical Engineering, Czech Technical University in Prague*, is an authentic record of work carried out by me under the supervision and guidance of doc. Ing. Tomáš Matuška, Ph. D.

Ing. Yogender Pal Chandra

Contents

Nomenclature

$\boldsymbol{c}$	thermodynamic specific heat capacity (J/kg·K)
$\boldsymbol{E}$	energy content of j^{th} fluid layer
$\boldsymbol{g}$	acceleration due to gravity (m/s^2)
$\boldsymbol{h}$	height (m)
$\boldsymbol{L}$	characteristic length pertaining to tank (m)
$\boldsymbol{M_E}$	moment of energy (J·m)
$\boldsymbol{M_{exp}}$	moment of energy of experimental tank (J·m)
$\boldsymbol{M_{ful\text{-}mix}}$	moment of energy of fully mixed tank (J·m)
$\boldsymbol{M_{str}}$	moment of energy of perfectly stratified tank (J·m)
MIX	MIX number (dimensionless)
Ri	Richardson number
$\boldsymbol{v}$	velocity component in *y* direction (m/s)
$\boldsymbol{V}$	volume (m^3)
$\boldsymbol{y_j}$	vertical distance between nodes (mm)
$\boldsymbol{T}$	temperature (°C)
$\boldsymbol{T_{hp,out}}$	heat pump output temperature (°C)
$\boldsymbol{T_{hp,in}}$	heat pump inlet temperature (°C)
$\boldsymbol{T_i}$	temperature of i^{th} layer (°C)
$\boldsymbol{\xi}$	exergy (kJ)

Greek

$\boldsymbol{\beta}$	coefficient of thermal expansion (1/K)
$\boldsymbol{\rho}$	fluid density (kg/m^3)
$\boldsymbol{\Delta s}$	thermodynamic entropy production (J/K)
$\boldsymbol{v_{hp}}$	heat pump flow rate/circulation pump flow rate m^3 /s
η	Stratification efficiency

Introduction

Background and motivation

Thermal energy storage (TES) is the essential part of renewable energy systems. This is because it is the only solution against noncoincidence of supply and demand, especially with solar systems. Improving the performance of this central component can significantly decrease the auxiliary energy demand for both the space and domestic hot water heating. For designing or performing building energy simulations of heating systems including the storage tanks it is essential to adopt the integrated and dynamic simulation approach. According to Campos Celador et al. [1], storage tank models can help to determine the annual saving and subsequent decision-making to increase it right at the design phase of the system. Stratified storage tank is a cost-effective building heat storage technology which facilitates the reduction in auxiliary heating demands, reduction in primary energy savings, discounting the consumer costs, while promoting the lower carbon footprints [2, 3]. The simple concept of thermal stratification lies in the fact that colder water being denser than hot water is withdrawn from the bottom and is circulated to the energy collection side (source side). This increases the efficiency of energy collection especially with renewables – solar thermal and/or heat pump, as it increases with decrease in inlet water temperature. Consequently, hot water is made to enter at the top of the tank which promotes the stratification.

High performance of such TES employing water as storage medium is undeniably indispensable. For this purpose, an effective TES device should satisfy these technical prerequisites (Fig. 1):

- Thermal stratification: the water tank should be able to sustain hot and cold water separately without any physical barrier, in other words, continuous or stepped temperature distribution of water across the height of the tank should be practiced.
- Mixing of hot and cold volume of water induced due to different operational cycle's viz. charging and discharging should be minimized.
- The tank design should minimize the dead water weight.

- The tank design should minimize the heat losses.

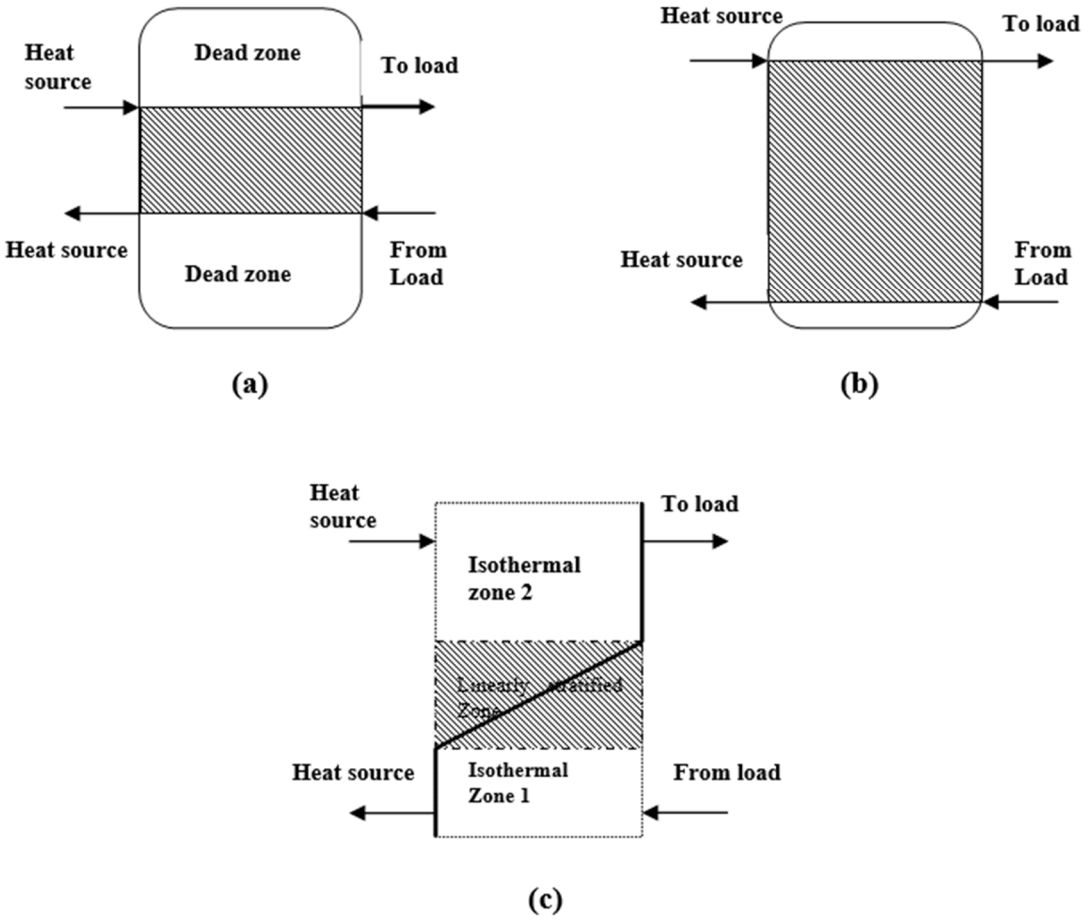

Fig. 1. (a) and (b) Different positions of inlets and outlets in storage tank, and (c) indication of thermal stratification in the same.

Two counteracting forces i.e. buoyant forces and gravity are responsible for movement of the newly introduced fluid inside tank. High density or low temperature fluid layers have the tendency to settle down as early as possible, while low density or high temperature layers have the propensity to move towards the upper hot layers. In addition, the momentum with which water is introduced into the bulk impacts the core fluid and hence decides how it will react with rest of the fluid layers. After the fluid layers are settled at their respective positions, thermal stratification is built up forming a thermocline region which can be described by different temperature distribution models such as linear, stepped or three zone model. This thermocline serves as the thermal barrier

to separate the hot and cold-water regions. Hot water is extracted from the upper part to feed the load, while cold water is extracted from the lower region to circulate to the energy addition loop. Thus, thermal stratification is maintained within the tank during the different operation cycles. Nevertheless, this stratification starts to fade away due to different hydrodynamic and/or thermal contingencies which need to be controlled.

Stratified water tanks can either be directly heated or indirectly heated by addition of a heat exchanger between energy source and the tank. Directly heated water tanks are highly effective at thermal exchange, however they are weak at maintaining the stratification due to high mixing and turbulence. Henceforth, they are usually equipped with different structural design changes viz. inlet stratifiers, baffle plates, diffuser systems etc. In addition, the performance of the immersed type thermal system can be significantly improved by correctly crafting the inner arrangement of the coils. The simulation results validated by experimental findings by Celador et al. [4] concluded that sophisticated inner arrangement can improve the performance and effectiveness of hot water preparation up to 15%.

The primary purpose of the thermal energy storage is to maximize the availability (or exergy) in the form of useful energy gain [5]. Energy and Exergy analysis both are used to quantify the performance of the TES. Exergy analysis, on the other hand, is a second law based thermodynamic investigation which provides gain over energy analysis in a way – firstly, it puts into account the temperature differences for the same energy content storages – this is particularly required for stratified storages as they sustain spatial temperature variations or thermocline, which could be stepped or linear [6]. Secondly, it considers the causes and location of quantitative losses due to mixing of fluids at different temperatures, and losses towards the environment. The working of TES moreover is governed by operating cycles, typically, energy addition, storage, and energy removal cycles. Careful thermal management and control of these cycles could result in increased performance of the thermal recovery.

Yaici et al. [7] performed a CFD analysis to evaluate the influence of geometrical and operational parameters on performance of the tank in charging mode. The results confirmed that a controlled optimization between both geometrical and operational variables is rudimentary for an appropriately designed storage tank. Geometrical factors include aspect ratio representing the effect of varying tank height with fixed diameter and vice versa, and also inlet and outlet position with respect to the top and bottom wall of tank. The operational parameters include mass flow rate,

inlet temperature variation and the effect of initial water temperature variation. The results concluded that the low mass flow rate instills increased level of thermal diffusion, axial wall conduction, and thermal conduction within the hot and cold-water layers, due to increase in thermal exchange time – thus, increasing the thermocline thickness and decreasing the stratification.

Objectives

This Ph.D. thesis investigates the behavior of thermal energy storage (TES) experimentally and with the help of simulation. The point of focus throughout this thesis is the thermal stratification assessment carried using pre-established indices found in the literature, using own custom built second law model and also using CFD code. The three specific objectives of this thesis are:

1. Design and simulate the methodology to separate the good from the bad operational parameters during TES operation from the view of stratification quality and thus efficiency of renewable heat sources connected to TES.
2. Design and validate own custom built second law model to quantify the availability of the energy that is being added and subsequently removed during charge and discharge cycle of TES.
3. Design and build an intelligent IoT stream processing unit to fit the second law model previously developed and predict the second law stratification efficiency in real time.

Solution Methods

Investigation of stratification efficiency of TES can be done by either energy or exergy analysis. Energy analysis uses first law of thermodynamics. This entails various stratification indices such as MIX number, Richardson number etc. These stratification numbers consider the temperature gradient rather than the exergy/entropy as in the case of second law modelling. Study 1 revolves around this strategy to evaluate TES stratification behavior. In this study quantification of turbulent mixing was achieved on the basis of temperature profile, MIX number, and Richardson number. Temperature dat was collected using experimental setup as described in Fig. 2.

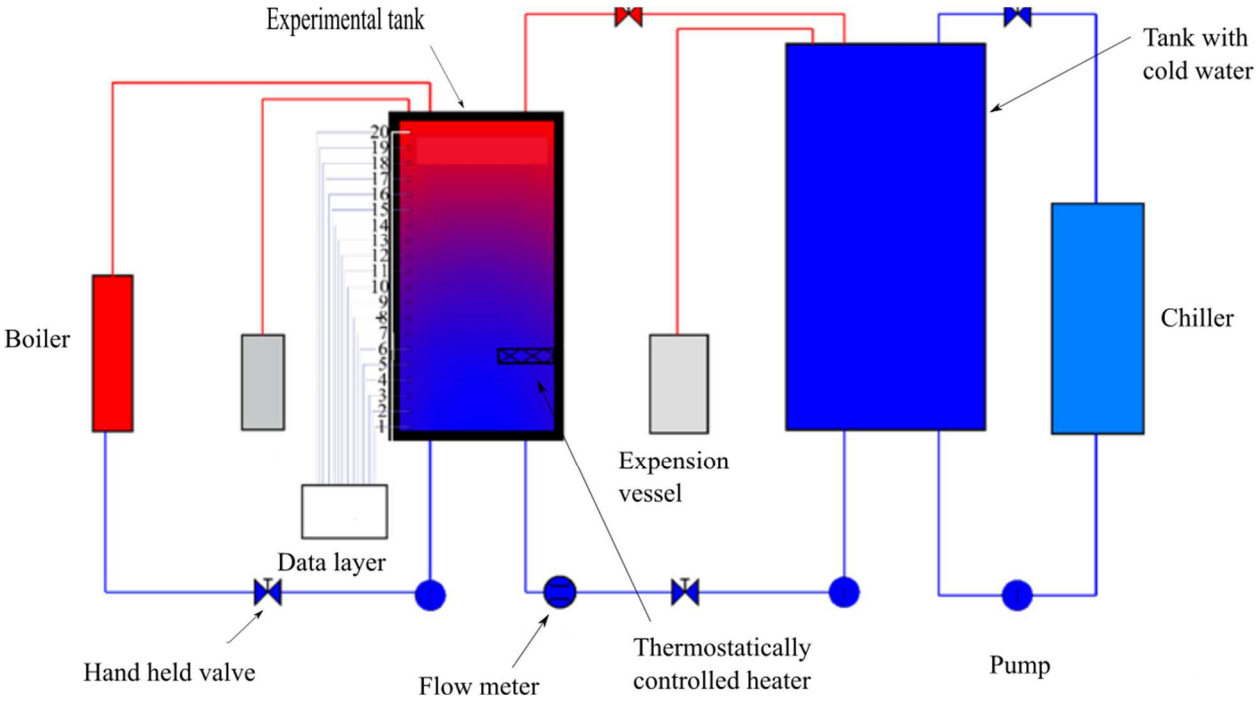

Fig. 2 Schematic of experimental setup

The experimental setup as shown in Fig. 2 consists of primary cylindrical hot water storage tank with following parameters: 397 L in volume, 550 mm diameter and 1905 mm overall height. The tank is connected to the secondary tank with chilled water in order to perform discharging cycles. To measure the vertical distribution of temperature, 20 Pt100 temperature sensors were attached around to the outer surface of tank wall in the vertical direction, dividing the tank into 20 equal fluid layers. Charging of the tank was performed using two methods. Firstly, by

thermostatically controlled electric heater which is present in the lower half of the tank, secondly, by an external electric boiler. Experimental tank can be set for various mixed conditions, 60 °C and 50 °C for example. Discharging process is carried out by regulating manually operated valve as shown in Fig. 2. A pump is also used for discharging. In addition, tank with chilled water is connected to the thermostatic chiller to cool it down after each discharging cycle. The evaluated parameters included fluid flow rate, ΔT (between heat pump outlet and TES temperature). These parameters were also investigated for different diffuser design (in CFD analysis), henceforth a direct interdependence between each was thus established. Refer Renewable Energy paper in Study 1 for more information.

CFD models for given designs were developed and experimentally validated on the test rig in order to find the optimal working conditions in discharge mode. This accounted for the operational parameters influencing stratification efficiency in TES. The influence of operational parameters was also recognized in the Study 1 and was further explored in Study 2. The results proved numerically that the tanks working conditions can be optimized by proper selection of inlet device. For instance, slotted type inlet device sustained maximum stratification even in as adverse a condition as of turbulent inflow & low ΔT. Perforated and simple inlet devices were capable of delivering best discharge efficiency only at low flow rate of 200 l/h and were showing insignificant dependency on ΔT. To establish these facts, MIX number and Richardson numbers were recognized earlier in the Study 1. MIX number evaluates the tank on the basis of both vertical temperature distribution and the total energy stored in the tank. Accordingly, it postulates the mixing process in the tank by evaluating the moment of energy of individual water layers. Moment of energy of thermal storage tank is calculated to account for energy location by summation of the sensible energy content up to j^{th} vertical segment, weighted with the height of its location (Eq. 1 & 2). MIX number varies between 0 and 1.

$$M_E = \sum_{j=1}^{j} y_j . E_j \tag{1}$$

$$MIX = \frac{M_{str} - M_{\exp}}{M_{str} - M_{full-mix}} \tag{2}$$

MIX number for 60 – 10 °C (60 °C being TES temperature, and 10 °C being discharge temperature) at flow rates of 200, 400, 600 and 800 l/h discharging flow rate was calculated for each inlet device. MIX for 200 l/h has the lowest ascent, followed by 400 l/h, then 600 l/h; finally,

800 l/h has the highest ascent of MIX number suggesting more intense mixing with 800 l/h discharging rate (refer Fig. 3 in Renewable Energy paper within study 1). Richardson number Ri is a dimensionless number which characterizes the ratio between potential energy required for vertical mixing and the turbulent kinetic energy available for such process (Eq. 3).

$$Ri = \frac{g\beta\Delta TL}{v^2} \tag{3}$$

A small Ri signifies mixed storage, while high Ri number indicates stratified one. Ri is increased as flow rate is decreased from 800 to 200 l/h. For example, Ri at τ^* (dimensionless time) = 0.6 for 800 l/h is nearly 75, while for 200 l/h it is approximately 120, τ^* = 0.6 being the dimensionless time at which 60% of tank volume is already discharged. Numerical solution for one such operational parameter is shown in Fig. 3.

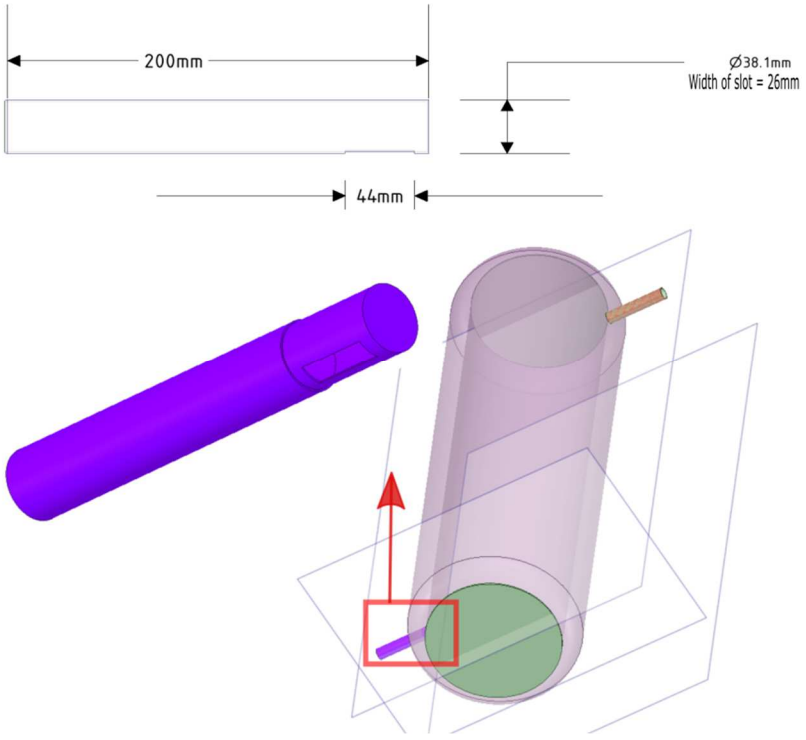

(a)

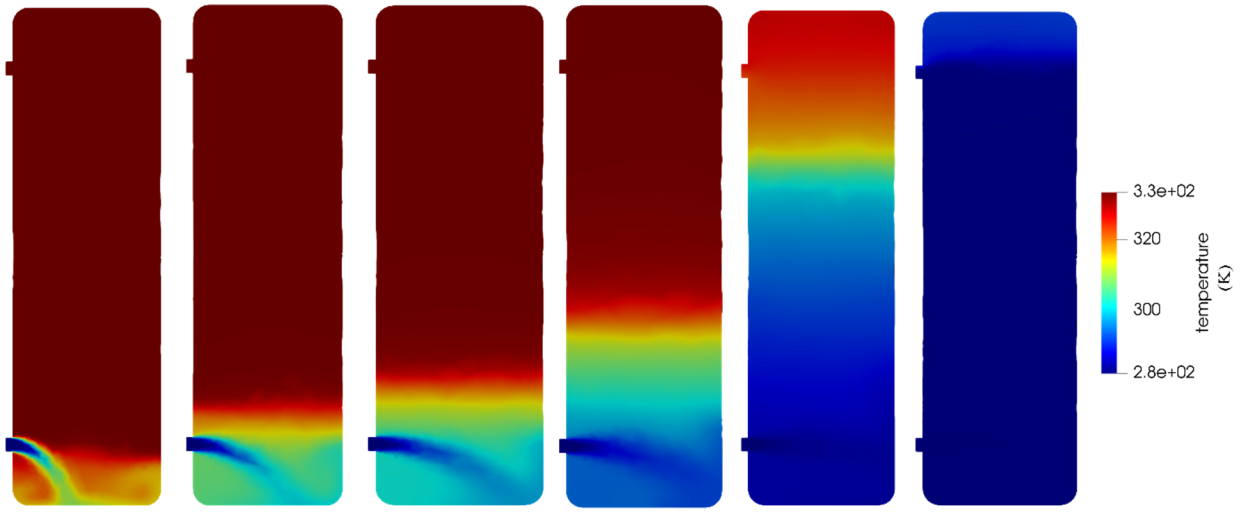

(b)

Fig. 3 Numerical analysis of TES (a) TES physical model, (b) temperature contours

As narrated the behavior of TES is governed by operating cycles, namely energy addition, storage and retrieval. Evaluating TES for non-transient conditions might not lead to full end to end energy quantification. This is termed as research and performance gap in the current methods. As an advancement to the limitation of current indices, second law models were developed and the data was fitted using the data layer. The model allowed to calculate end to end entropy, exergy and availability of the system. Eq. 4 and 5 represent the derived second law models fitted by data layer. Eq. 4 is entropy change (where n is the number of layers), Eq. 5 is exergy, while Eq. 6 is the stratification efficiency of TES. The derivation is depicted in study 2.

$$\Delta s_{total} = \int_0^H \rho(h)\cdot c(h)\cdot (V/n)\cdot \ln\left(\frac{T_{hp}}{T_i}\right)dh. \tag{4}$$

$$\xi = \int_0^t \rho(T)\cdot \dot{v}_{hp}\cdot c(T)\cdot [T_{hp,out}(t)-T_{hp,in}(t)]dt - T_0\int_0^H \rho(h)\cdot (V/n)\cdot c(h)\ln\left(\frac{T_{hp}}{T_i(h)}\right)dh \tag{5}$$

$$\eta_{st}(ch) = \frac{\int_0^t \rho(T)\cdot \dot{v}_{hp}\cdot c(T)\cdot [T_{hp,out}(t)-T_{hp,in}(t)]dt - T_0\int_0^H \rho(h)\cdot (V/n)\cdot c(h)\ln\left(\frac{T_{hp}}{T_i(h)}\right)dh}{\int_0^t \rho(T)\cdot \dot{v}_{hp}\cdot c(T)\cdot [T_{hp,out}(t)-T_{hp,in}(t)]dt} \tag{6}$$

To validate the second law models an experimental setup with water-water heat pump and water storage tank 397 L as investigated TES has been arranged. Speed controlled heat pump has nominal heat output 6.1 kW and coefficient of performance 4.78 at B0/W35 conditions and 50 Hz. In addition, an intelligent data layer was developed which collected and fitted the previously developed second law models. The data modelling – acquisition, cleaning, and transformation is done in situ (dynamically). Data-layer framework visualized real-time energy efficiency of TES using second law models developed in Study 3. Data layer served as the entry point for all the sensors connected to the TES integrated with heat pump system. For this task novel data layer was devised and programmed using Raspberry Pi-4 systems (Fig.4). Wide range of computing packages was observed which is not limited to PostgreSQL (to store/retrieve dynamic data that is being collected from sensors (RTD, current loop, Modbus)), Pandas/Numpy (to do all the scientific data computing, parsing, transformation, and curation), MatPlot-Lib/Seaborn for an in-situ animated visualization of the stratification decay. This considerably improved the intuitive understanding of stratification decay in real time, thus improving the advanced laboratory testing of HP integrated TES systems serving as information addition to the practice. The data layer consists of two Raspberry Pi (Raspi1 & Raspi2) mini computers, both running on Raspbian – Debian Linux operating system. Raspi1 stores temperature data from 19 Pt100 sensors located at various locations of the test bench, while Raspi2 stores the flow rate data, all in real time. Each 5th second the data is logged into each of the Raspi's PostgreSQL-DBs tables. In addition, a short code snippet running in Raspi1 also fetches wattmeter readings. Wattmeter data is used to measure the performance factor of the heat pump. All the data is used to fit together second law model to calculate the exergy/entropy and thus stratification efficiency. Raspi1 also retains 'Flask server' which is constantly logging the data on web-based application server (Fig. 5). The process diagram of data layer is described in more detail in Fig. 6.

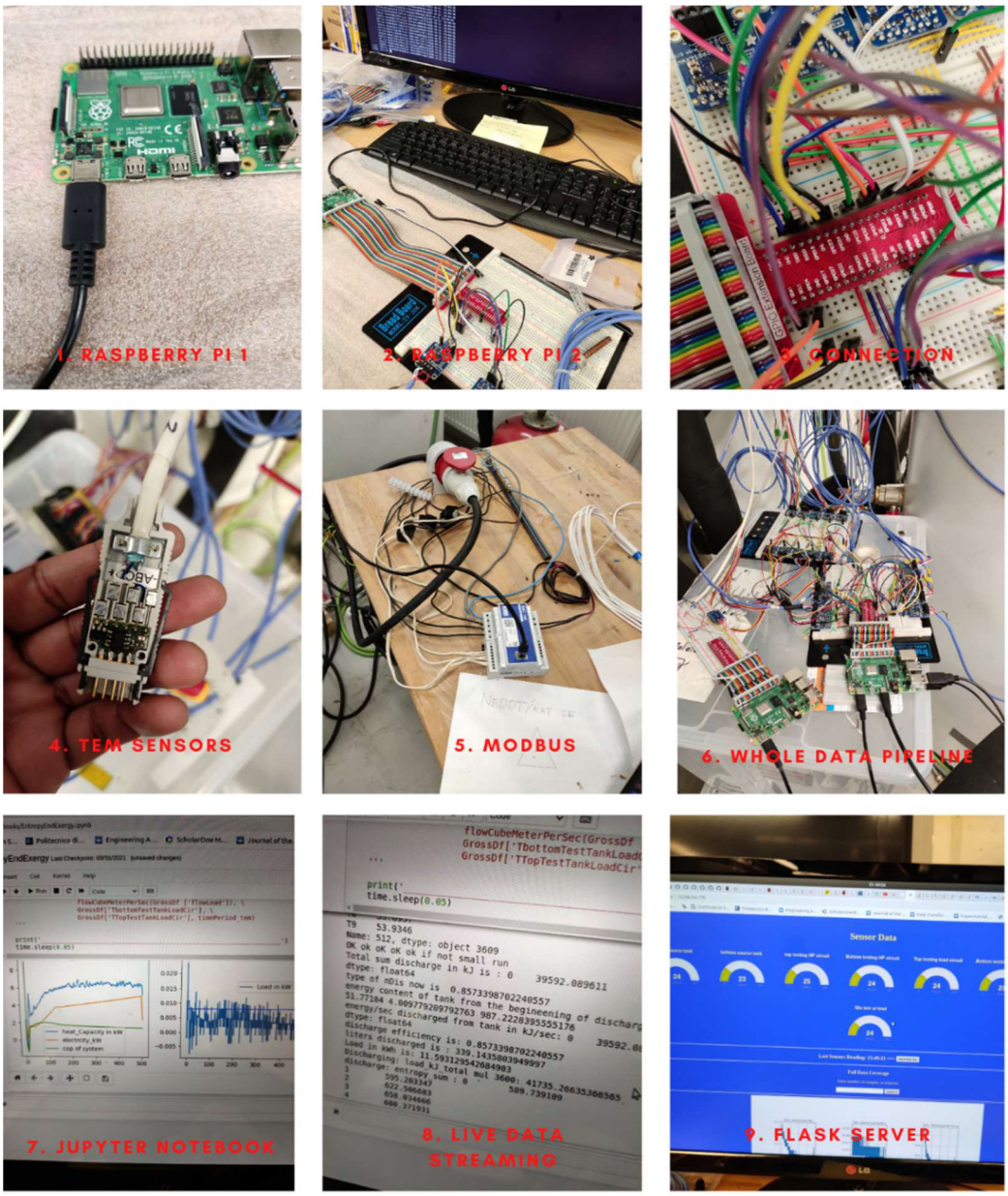

Fig. 4 Intelligent data layer

Fig. 5 Flask server

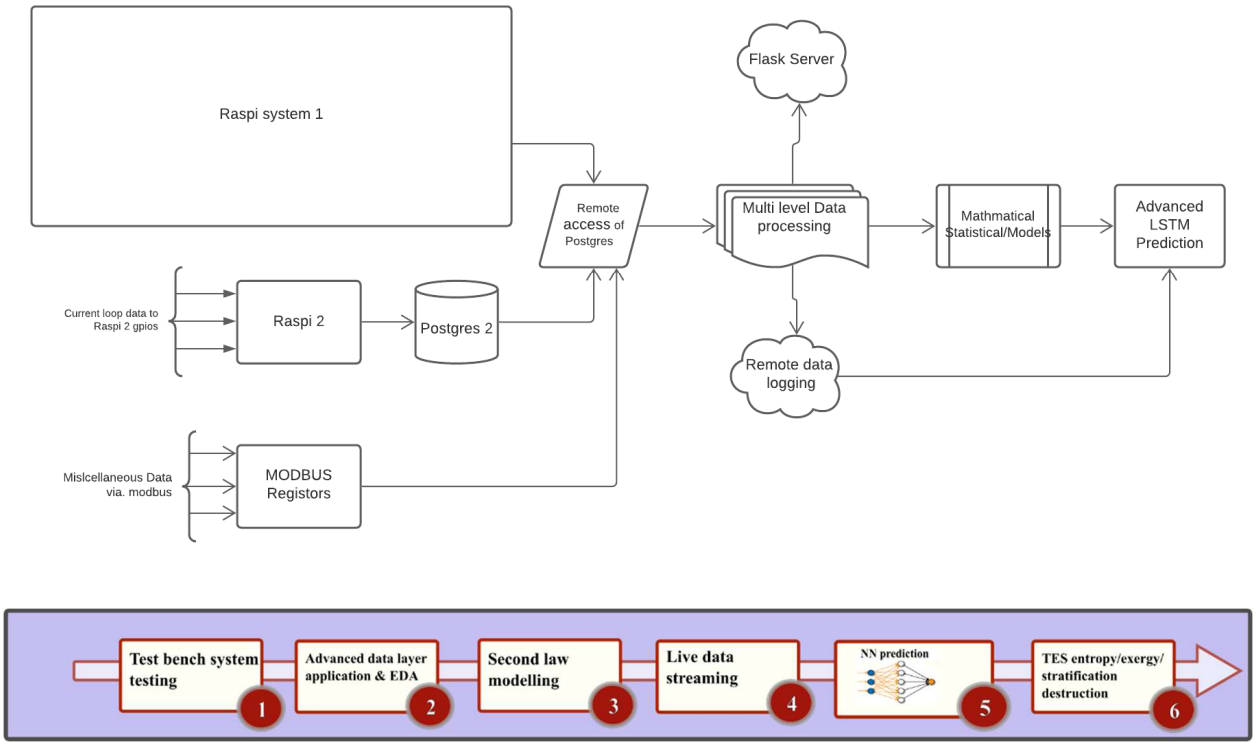

Fig. 6 Detailed process diagrams for data layer

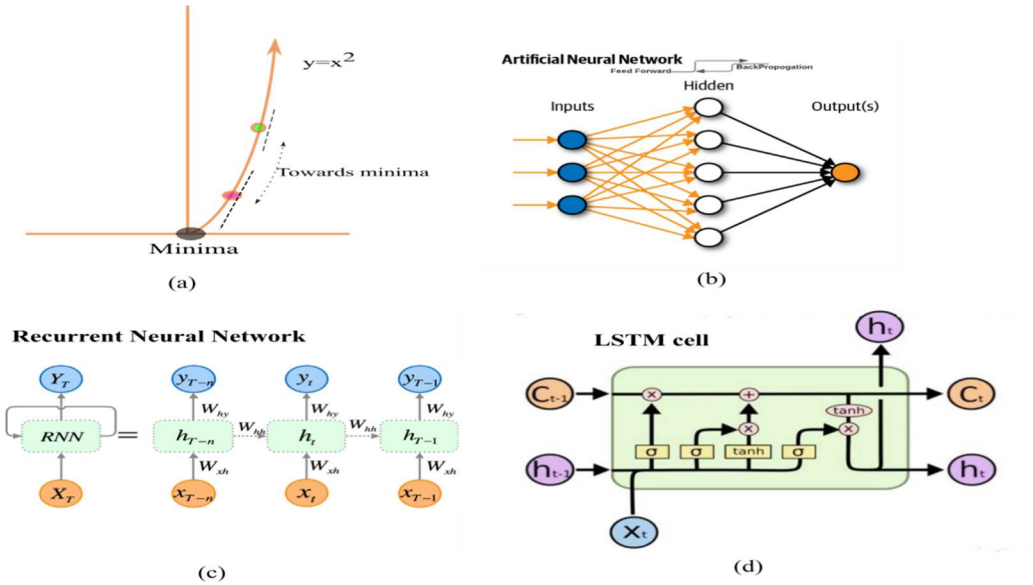

Fig. 7 NN architecture [8, 9]

Data layer was also equipped with hyper tuned neural network models to predict the stratification efficiency during each operating cycle. This incorporate applied deep learning (DL) framework utilizing long short-term memory (LSTM), and multilayer perceptron (MLP) to model the layered temperature and to predict the entropy generation during charging and discharging loop (Fig. 7b-d). Fig. 7 shows the architecture of the neural network used for prediction.

This is another non-traditional way of evaluating TES other than first or second law modelling. Neural networks in this fashion served as the entry point of the data produced by second law model that was developed and used during study 3. The results predicted by neural networks corroborated the results obtained by second law model. In this way, the neural network modelling validated the results of second law models. Model training and weight adjustment use a technique called stochastic gradient descent. In this technique, the network repeatedly determines the coefficient of the loss function where it has its local minima (Fig. 7a). Fig. 8 shows information flow with regards to LSTM modelling and quantitative model fitting by data layer.

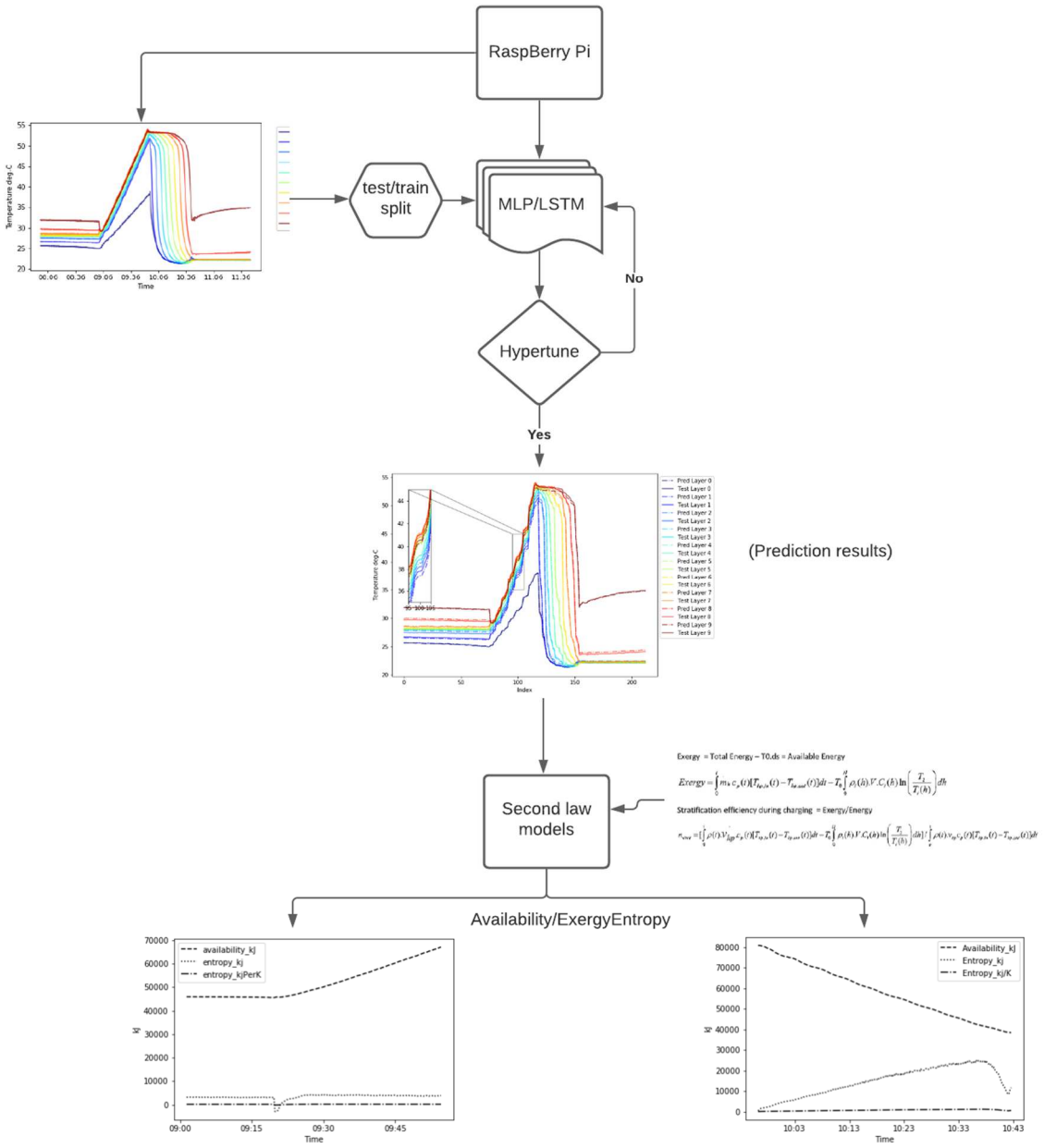

Fig. 8 Complete workflow of data layer from data injection to model fitting and prediction

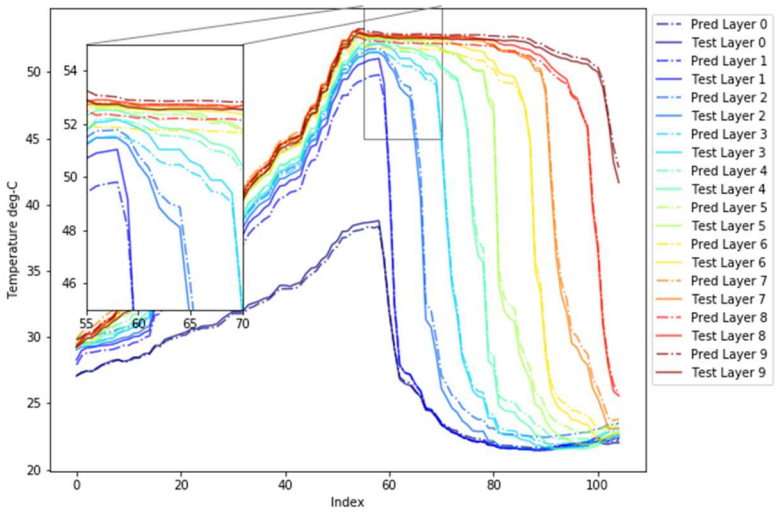

(a)

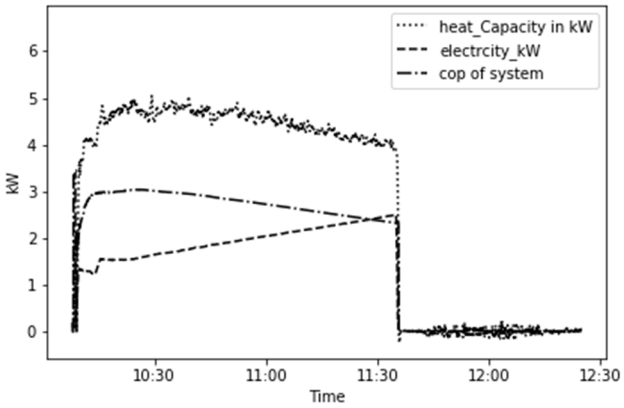

(b)

Fig. 9 Data collected by data layer, (a) temperature distribution, (b) heat pump parameters

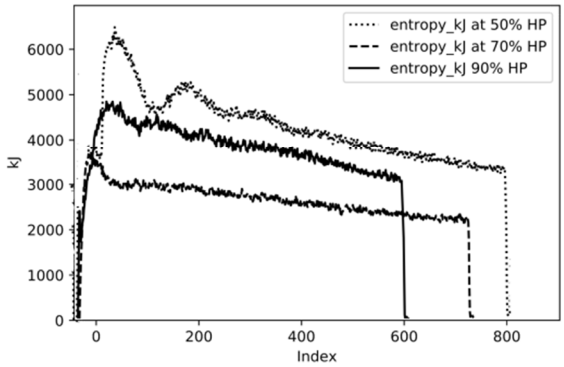

(a)

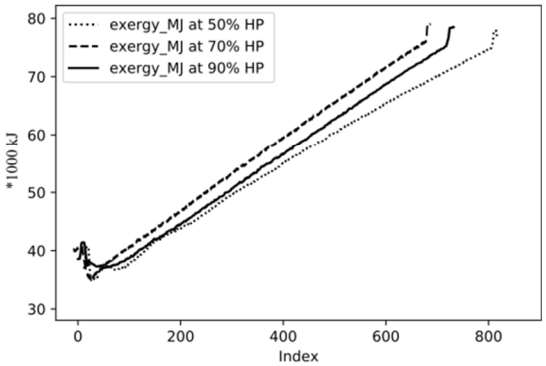

(b)

Fig. 10 During charging at different heat pump compressor speeds (a) entropy generation, (b) exergy in TES

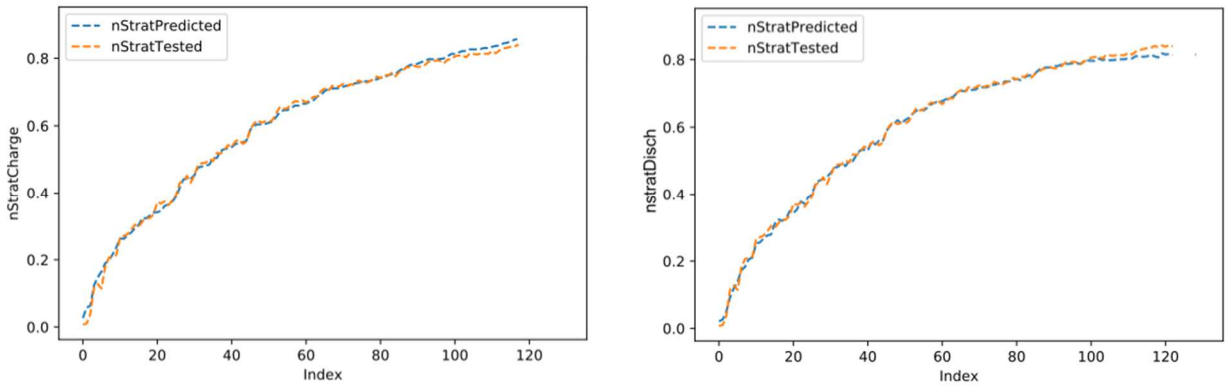

(a) (b)

Fig. 11 Stratification efficiency (validation) during (a) charge, and (b) discharge

Fig. 9 shows the work of data layer. The sooner the data layer collects the data from experimental setup, it dynamically plots the temperature profile of TES and heat pump parameters. Heat pump parameters include heat capacity, electricity consumption, and *COP* of the heat pump. These data points are collected for charge and discharge cycles. Fig. 9 also shows the predicted values of temperature. Fig. 10 shows the work of second law models developed in this thesis. Entropy and exergy generation in the TES at different compressor speeds were calculated during charge and discharge cycles. Fig. 10 however shows the results of second law models during charging. Entropy generation was found to be highest at slowest compressor speed.

The credibility of results obtained was ascertained at each stage. Ingested data in the data layer underwent linear regression to ascertain credibility of collected sensor data. Afterwards, statistical error distribution was performed (ref. Fig. 6 in the Renewable Energy paper within study 1 and Fig. 7 in Journal of Energy Storage paper within study 2). Second law models were validated using data driven as well as quantitative approach. Refer Fig. 11, Fig. 15 and Fig. 17 in the Journal of Energy Storage within Study 2 for validation using data driven approach. Finally, neural network modelling was validated itself. Fig. 12 in the same paper shows the parameters such as mean squared error and validation mean squared error. Validation is also shown in the Fig. 11.

Thesis Organization

This thesis is presented as "Thesis by publication". Five papers are bundled together to prepare this thesis. One paper among these is published in D1 (Decile 1), while four are published in Q1 (Quartile 1).

Objective coverage by Study 1: *Design and simulate the methodology to separate the good from the bad operational parameters during TES operation.*

(Design of operational parameters, stratification quantification, experimentation and CFD analysis are addressed by paper 1 & 2)

- **Paper 1:**

  Yogender Pal Chandra, and Tomas Matuska. Stratification analysis of domestic hot water storage tanks: A comprehensive review, Energy and Buildings 187 (2019) 110-131

  (Q1 – top 25%, Impact Factor: 7.201)

  DOI: https://doi.org/10.1016/j.enbuild.2019.01.052

  Citations (WoS): 63

  Yogender Pal Chandra: 80% contribution. Investigation, Data curation, Formal analysis, Software, Validation, Writing - original draft, Visualization.

  Tomas Matuska: 20% contribution. Conceptualization, Methodology, Writing - review & editing, Supervision, Project administration, Funding acquisition

- **Paper 2:**

  Yogender Pal Chandra, and Tomas Matuska. Numerical prediction of the stratification performance in domestic hot water storage tanks, Renewable Energy 154 (2020) 1165-1179

  (Q1 – top 25%, Impact Factor: 8.634)

  DOI: https://doi.org/10.1016/j.renene.2020.03.090

  Citations (WoS): 35

  Yogender Pal Chandra: 80% contribution. Investigation, Data curation, Formal analysis, Software, Validation, Writing - original draft, Visualization.

  Tomas Matuska: 20% contribution. Conceptualization, Methodology, Writing - review & editing, Supervision, Project administration, Funding acquisition

Objective coverage by Study 2: *Design and validate the custom built second law model to quantify the availability of the energy that is sbeing added and subsequently removed during charge and discharge cycle of TES*

- **Paper 3**: Yogender Pal Chandra, Gwang Jim Kim, Tomas Matuska. Second law performance prediction of heat pump integrated stratified thermal energy storage system using long short-term memory neural networks, Journal of Energy Storage 61 (2023) 106-699

  (Q1- top 25%, Impact factor: 8.907)

  DOI: https://doi.org/10.1016/j.est.2023.106699

  Citations (WoS): 1

  Yogender Pal Chandra: 80% contribution. Investigation, Data curation, Formal analysis, Software, Validation, Writing - original draft, Visualization.

  Gwang Jim Kim: 1% contribution. Conceptualization, Methodology

  Tomas Matuska: 19% contribution. Writing - review & editing, Supervision, Project administration, Funding acquisition

Objective coverage by Study 3: *Design of intelligent IoT stream processing unit to fit the second law model previously developed*

- **Paper 4:** Yogender Pal Chandra, and Tomas Matuska, Intelligent data systems for building energy workflow: Data pipelines, LSTM efficiency prediction and more, Energy and Buildings 267 (2022) 112135

  (D1 – top 10%, impact Factor: 7.201)

  DOI: https://doi.org/10.1016/j.enbuild.2022.112135

  Citations (WoS): 0

  Yogender Pal Chandra: 80% contribution. Investigation, Data curation, Formal analysis, Software, Validation, Writing - original draft, Visualization.

  Tomas Matuska: 20% contribution. Conceptualization, Methodology, Writing - review & editing, Supervision, Project administration, Funding acquisition

- **Paper 5:** Yogender Pal Chandra, and Tomas Matuska. Energy modeling of thermal energy storage (TES) using intelligent stream processing system, Energy Reports 8 (2022) 1321 – 1335

  (Q1 – top 25%, Impact Factor: 4.937)

  DOI: https://doi.org/10.1016/j.egyr.2022.08.012

  Citations (WoS): 0

Yogender Pal Chandra: 60% contribution. Investigation, Data curation, Formal analysis, Software, Validation, Writing - original draft, Visualization.

Tomas Matuska: 40% contribution. Conceptualization, Methodology, Writing - review & editing, Supervision, Project administration, Funding acquisition

Results & Achievements of objectives

Research gaps and performance gaps were identified during Study 1. The ***first objective*** of this Ph.D. thesis was design, operational parameters, stratification quantification, using experimentation and CFD analysis. This is presented in ***Study 1***. In this study, quantification of turbulent mixing was achieved on the basis of temperature profile, MIX number, and Richardson number (indices observed in ***Study 1***).

Research gap:

- The research gap was observed during ***Study 1***. More specifically, MIX number was picked and utilized to quantify the stratification in TES experimentally. *Study 1* extended the work of Haller et. al [1,3] in terms of experimental investigation of the same. In addition, CFD methods and models were developed to collect, model, and curate the data and were validated using experimental results. Their work was further extended by investigating MIX number for various TES operational and inlet design characteristics.
- G. Rosengarten et. al [2] proposed second law approach in characterizing TES with application to solar energy water heater. Their work was further extended by simplifying their model, customizing it for temperature dependent thermophysical properties and applying it in real time mode in both charge and discharge cycle. These models were later customized for our TES use-case. This is presented in the ***Study 2.***

Performance gap:

- Energy disbursement in renewable energy system is a transient state process. A streaming data layer edge device was developed which analyses the energy efficiency of renewable energy system in real time. This is very novel approach in such analysis.
- G. Rosengarten et. al [2] analyzed renewable energy system in single discharge cycle. This dissertation focuses on automated analysis of full charge and discharge cycle giving more insight into energy disbursement from electric grid to load.

Results: The evaluated parameters include flow rate and ΔT, henceforth a direct interdependence between each was thus established. Various CFD models were developed and experimentally validated on the test rig in order to find the optimal working conditions in discharge mode. The results for different diffuser designs proved numerically that the tank working conditions can be optimized by proper selection of inlet device. For instance, slotted type inlet

device sustained maximum stratification even in as adverse a condition as of turbulent inflow & low ΔT. Perforated and simple inlet devices were capable of delivering best discharge efficiency only at low flow rate of 200 l/h and were showing insignificant dependency on ΔT. However, as flow rate is increased, ΔT dependency increased. Seeing the compounded benefits of slotted inlet devices and decreased ΔT, it was concluded that slotted inlet device delivered comparatively better thermal performance at both adverse conditions i.e. high flow & low ΔT and high flow & high ΔT, however, failed to outshine the rest of the inlet devices at low flow rate & low ΔT, and low flow rate & high ΔT. These research findings can serve as guidelines to optimize the storage tank design, more specifically, inlet device-based design integrated with heating system, as thermal stratification and *COP* of heating system (heat pumps), for example, are inherently correlated. Heat pumps are high flow rate and low ΔT devices, while, solar systems are low flow rate and high ΔT devices, Thus, opting for accurate choice of inlet device for a particular operating condition is critical.

The ***second objective*** of this Ph.D. thesis was to design and validate the custom built second law model to quantify energy/exergy dispersal during TES charging and discharging. This is presented in ***Study 2.*** To quantify the system performance, second law efficiencies (exergy, and entropy) of TES along with *COP* of heat pump system were introduced. It also proposes optimized modelling framework of one complete charge/discharge cycle which can further be appended over a longer time horizon. A tailored second law-based exergy equations to be fitted to the data layer for real time streaming of entropy/exergy in TES and *COP* was derived. Stratification decay was also predicted using Neural Networks.

Results: Three distinct compressor speeds and tapping rates were studied using this data-streaming edge device and their exergy disbursement was studied in live mode. It was observed that entropy generation was maximum at highest discharge rate of 800 l per hour i.e. 25,000 kJ (while only 3000 kJ for 900 l/h of charging rate). Furthermore, entropy generation has not only impact on stratification efficiency, however also on performance factor of the heat pump. Making it extremely essential to adjust for inlet flow rate and compressor speed ratio. *COP* of 3.2 was obtained at 70 % compressor speed, while at the same time maximum discharge efficiency was registered at lowest discharge flowrate of around 450 l/h.

The ***third objective*** of this Ph.D. thesis was to design intelligent IoT stream processing unit to fit the second law model previously developed. This is presented in ***Study 3***. This study

demonstrates the application of intelligent data layer with neural networks for evaluating and predicting end to end performance of heat pump integrated stratified thermal energy storage (TES) system. The data modelling – acquisition, curation, and transformation is done in situ (dynamically). This study is a 'method-based' study to demonstrate the data-layer framework and its application in assessing energy efficiency of renewable energy system by fitting the custom second law exergy models previously developed, all in real time. This real time analysis can help researchers to intuitively understand the energy efficiency of renewable energy systems in high expertise labs.

Results: The data-streaming edge device was comprised of two *Raspberry-Pi* mini computers, running on Raspbian operating system. Both stored and processed the TES and heat pump data in live mode in master slave architecture. The data was stored in Postgres-SQL database, from where it was processed and ingested to custom real time interactive dashboarding system. The data layer streams, end-to-end (from electric gird to user tapped water) exergy balance of heat pump integrated TES system in live mode. This makes sure that the engineer has clear understanding of the percentage of grid output being consumed as entropy during charging/discharging, and what percentage of it is available to user as the tapped water. For that matter, real time dash-boarding was built. Prediction modelling was also performed using deep learning frameworks.

Validation of results:

A neural network model using LSTM was developed and was used to predict the temperature of TES layers and its stratification efficiency. The error range for temperature and efficiency prediction was observed to be 5 % and 2 % respectively (ref. Fig. 17 in the Journal of Energy Storage paper) as shown within Study 2. The LSTM model reproduced the results calculated by exergetic model thus the results calculated by quantitative approach is validated by data driven approach. The data-driven approach is agnostic and makes no assumptions - but does not give any clue how and which inputs influence the output. The quantitative approach works with assumptions but shows clearly the quantitative relationship between input features and the calculated output, thus helps to deepen the understanding of the processes. Data driven approach in theory is bias-free.

In addition, time series data thus collected underwent statistical uncertainty analysis. Probability distribution of error in terms of gauss distribution was analyzed. Error was roughly

normally distributed with 95 % of data points falling under 5 % error (ref. Fig. 7 in the Journal of Energy Storage paper).

Conclusion

This thesis emphasizes the importance of thermal stratification in heat storage systems, and how it can improve the efficiency and exergy of the system. A well-stratified tank is able to deliver higher exergy with less heat input compared to a mixed isothermal tank. To achieve this, it is important to maintain a stable vertical temperature gradient during all operation cycles of the tank. This can be achieved through careful monitoring of hydrodynamics and thermodynamics, and the management of inlet-outlet configuration, such as the position, shape, and type of diffuser, hot water inlet, bulk water temperature difference, and draw-off rate. Other parameters such as thermal conductivity and aspect ratio of tank is also important in this regard. The degree of mixing in the tank can be measured through various parameters, which require accurate temperature measurements of each water layer using temperature sensors. The research is furthered to develop calculation methodology for the same.

CFD part of the thesis focuses on the influence of various inlet devices on stratification degradation. Three types of inlet devices (slotted, perforated, and simple) were simulated in a transient manner to understand their performance under different operational conditions, such as flow rate and ΔT. The results showed that the slotted inlet device performed best at high flow rates and low ΔT, which is suitable for heat pump-based storage tanks. However, for solar system-based storage tanks, which require low flow rates and high ΔT, the application of slotted inlet devices did not make much difference in stratification efficiency. CFD model validation was also performed. CFD data was plotted against the experimental data. In addition, mesh independent study was also performed. The study also highlighted the importance of stratification indices, such as temperature evolution, MIX number, and discharging efficiency, in assessing the performance of storage tanks. These indices use first law approach to assess the stratification. Later on, second law approach was used as second objective.

Furthermore, the second law of thermodynamics was considered in developing equations for entropy and exergy. The models and the edge devices allow for real-time monitoring of TES performance and heat pump efficiency during charge/discharge cycles. Advanced deep learning algorithms specifically LSTM neural networks were used to model the data collected by edge device and to predict the TES layered temperature and efficiency. The neural network prediction is considered as data driven approach to evaluate the stratification. And it is also used to validate

the quantitative models developed. The error between quantitative and predicted results lied within 5% range. The exergy balance presented in the thesis measures the effective utility of the heat pump integrated with the TES system.

Lastly, a methodology was developed to study the stratification of TES in real-time mode using custom-built data-stream processing edge devices and exergetic (quantitative) models. The study tested a TES integrated heat pump used for a single-family house for stratification efficiency and energy balance, and applied custom exergy models using a custom data streaming edge device to study end-to-end energy expenses. Overall, the study provides a promising approach to real-time experimental based optimization of TES systems.

Overall, these methodologies can be used for high expertise lab testing of TES systems.

Value addition to the theory:

The theoretical aspect of this thesis was to identify a research gap related to TES and stratification indices to quantify thermal stratification in TES. CFD models and algorithms were developed to understand the applicability of temperature distribution and stratification indices to quantify the stratification in TES. This knowledge was later used in experiments. It was found that first law models were static and focused on TES only. In order to evaluate the TES along with heat pump, and that also dynamically and in a transient state manner, second law models were developed. Mathematical equations were derived in the theoretical part of this thesis and were used to measure how well a TES system was stratified. More specifically, thermodynamic models were developed to quantify exergetic expenses in TES integrated heat pump. This methodology of evaluating the TES along with heat pump is proposed as an improvement plan over first law models.

Value addition to the practice:

A real-time performance evaluation and streaming edge device was developed for the heat pump integrated with a thermal energy storage (TES). The edge device observed the exergetic models (previously developed in theoretical part) to demonstrate and quantify the entropy generation in TES and its effects on the *COP* of the heat pump during charging and charging cycles. Optimization of the circulation flow rate and compressor speed was also achieved using the above. Overall, this methodology provides a better perspective on the energy efficiency of renewable energy systems and could help researchers in this field. In short, value addition to practice is the data layer setup in the testing lab, predictive modelling using the data layer and

subsequent second law model fitting and validation. Using both the models (theoretical addition) and data layer (practical addition), researchers can gain more inference in renewable energy systems in tightly controlled specialized and high expertise labs.

Study 1

Design and simulate the methodology to separate the good from the bad operational parameters during TES operation

Paper 1: Stratification analysis of domestic hot water storage tanks: A comprehensive review, Energy and Buildings, Elsevier

In this paper, different parameters to measure the stratification and thus the level of mixing are suggested, some of such measures are capable of spotting the accurate time on which mixing has appeared. Thus, these parameters are plainly rudimentary to be calculated as far as testing of commercial storage tanks is considered. Adding to this, these parameters require the accurate temperature of each water layer to be calculated – thus rendering the need for actual temperature distribution inside the tank to be measured by a series of temperature sensors. To understand this, a temperature-distribution schema is also been produced in this paper. Further research could be centered on the invention of calculation methods to calibrate this inconsistency of ever-changing shape and size of thermal layers of water segments and fixed location of temperature sensors. To sum up, this information could be clubbed together with new modelling techniques and water consumption patterns to accommodate a better stratification enhancement right during design phase of TES system.

Paper 2: Numerical prediction of the stratification performance in domestic hot water storage tanks, Renewable Energy, Elsevier

In this paper quantification of turbulent missing was achieved on the basis of temperature profile, MIX number, and Richardson number. The evaluated parameters include flow rate, ΔT, and diffuser design, henceforth a direct interdependence between each was thus established. Various CFD models were developed and experimentally validated on the test rig in order to find the optimal working conditions in discharge mode. The results proved numerically that the tank working conditions can be optimized by proper selection of inlet device. In this paper quantification of turbulent missing was achieved on the basis of temperature profile, MIX number, and Richardson number. The evaluated parameters include flow rate, ΔT, and diffuser design, henceforth a direct interdependence between each was thus established. Various CFD models were

developed and experimentally validated on the test rig in order to find the optimal working conditions in discharge mode. The results proved numerically that the tank working conditions can be optimized by proper selection of inlet device. These research findings can serve as guidelines to optimize the storage tank design e more specifically, inlet device-based design integrated with heating system, as thermal stratification and *COP* of heating system e heat pumps, for example, are inherently correlated. Heat pumps are high flow rate and low ΔT devices, while, solar systems are low flow rate and high ΔT devices, Thus, opting for accurate choice of inlet device for a particular operating condition is critical.

Energy & Buildings 187 (2019) 110–131

Contents lists available at ScienceDirect

Energy & Buildings

journal homepage: www.elsevier.com/locate/enbuild

Stratification analysis of domestic hot water storage tanks: A comprehensive review

Yogender Pal Chandra[a,*], Tomas Matuska[b]

[a] Department of Environmental Engineering, Faculty of Mechanical Engineering, Czech Technical University in Prague, Technicka 4, 166 07 Prague 6, Czech Republic

[b] University Center for Energy efficient Buildings, Czech Technical University in Prague, Trinecka 1024, 273 43 Bustehrad, Czech Republic

ARTICLE INFO

Article history:
Received 1 June 2018
Revised 23 December 2018
Accepted 25 January 2019
Available online 3 February 2019

Keywords:
Thermal stratification
Thermal energy storage
Domestic hot water tank (DHWT)

ABSTRACT

To assure high quality thermal storage and high efficiency of its acquisition, thermal stratification is often employed in domestic hot water tanks. The whole motivation of stratification lies in the fact that mixing effect can be minimized during operational cycle of the tank so that high temperature water could be taken at the load end, thus maintaining high thermal efficiency at demand side, while low-temperature water can be drawn at lower bottom, thus maintaining the high efficiency at energy collection side. The study of stratification entails the assessment of a wide variety of concepts to be embodied around the central theme of the tank – its design and modelling. This paper presents a systematic review pertaining to various such concepts. For instance, multi-node and plug-flow approach to model various temperature distribution models are considered. These models are categorized in paper as linear, stepped, continuous-linear and general three-zone temperature distribution models. Subsequently, the dynamics of thermocline decay and influencing parameters both during standby and dynamic mode will be demonstrated. In addition, a survey of state of the art methods and practices to ascertain the performance improvement and its quantification will be illustrated. This includes geometrical parameters – such as, structural design incorporation, essentially – inlet design, tank aspect ratio and wall material specification, and also, operational parameters to curb down the inlet mixing. Practice techniques and methods which are presented here in a novel way, extend towards the ground of practical application and research procedures.

1. Introduction

Energy demand whether it is heating or cooling is occasionally matched with availability in case of renewable energy sources applications – especially, solar systems or heat pump systems. Henceforth, energy efficient storage not only ensures high actual heat output but also maintains the usable temperature level to cover the demand in all operation cycles. Sensible thermal energy storage (TES) works on the basic principle of increasing the temperature of storage medium such as water, oil, sand or rock beds. Thus amount of energy stored is directly proportional to the temperature difference, the mass of the medium and the heat capacity of the same. Water has comparatively high heat capacity (4.2 kJ/kg.K), hence this makes it broadly a logical choice for building heating and cooling purpose. In addition to high specific heat capacity, water is easily available, non-toxic and widely suitable for nearly all purposes, hence promoting it for a whole range of sensible thermal energy storage applications in buildings. High performance of such TES employing water as storage medium is undeniably indispensable. For this purpose, an effective TES device should satisfy these technical prerequisites [1–3]:

- Thermal stratification: the water tank should be able to sustain hot and cold water separately without any physical barrier, in other words, continuous or stepped temperature distribution of water should be practiced.
- Mixing of hot and cold volume of water induced due to different operational cycle's viz. charging and discharging should be minimized.
- The tank design should minimize the dead water weight.
- The tank design should minimize the heat losses.

The simple concept of thermal stratification lies in the fact that colder water being denser than hot water is withdrawn from the bottom and is circulated to the energy collection side (source side). This increases the efficiency of energy collection especially with renewables – solar thermal and/or heat pump, as it increases with decrease in inlet water temperature. Consequently, hot water is made to enter at the top of the tank which promotes the strati-

* Corresponding author.
E-mail address: yogenderpal.chandra@fs.cvut.cz (Y.P. Chandra).

https://doi.org/10.1016/j.enbuild.2019.01.052
0378-7788/

Nomenclature

A	area (m^2)
c_p	specific heat (J/kg K)
E	energy content of fluid element/ node (J)
Ex	exergy (J)
F	fraction of recoverable heat
F^c	collector control function
F^L	collector load function
g	gravitational acceleration (m/s^2)
Gr	Grashof number
h	height from the tank bottom (m)
h^e	enthalpy (J/kg)
H	tank height (m)
j	water layers
J	number of water layers
k	thermal conductivity (W/m K)
L	length (m)
m	mass of fluid segment (kg)
$\dot{m}$	mass flow rate (kg/s)
$\dot{m}_s$	mass flow rate of stream (kg/s)
$\dot{m}$	mass flow rate of tank (kg/s)
N	entropy generation number
P	recoverable heat (J)
Pe	Peclet number
Q	thermal energy/heat (J)
q	heat flux (W/m^2)
Re	Reynolds number
Ri	Richardson number
S	entropy (J/K)
T	temperature (°C/K)
t	time (s)
t^*	dimensionless time
u	internal energy (J/kg)
υ	velocity (m/s)
U_T	heat loss coefficient of tank per unit area (J/m^2 K)
V	volume (m^3)
$\dot{V}$	volumetric flow rate (m^3/s)
y	vertical distance from bottom of tank to centre of node

Greek symbols

α	thermal diffusivity (m^2/s)
β	coefficient of thermal expansion (1/K)
δ	thermocline thickness (m)
ρ	density (kg/m^3)
ζ	coefficient of stratification evaluation as defined by McCarthy and Woods [130]
ξ	symbol used by Shah and Furbo [74] to define exergy efficiency
ψ	symbol used by Fernandez-Seara [72] to define exergy efficiency
ϕ	temperature distribution in Jth zone

Subscripts

a	ambient condition
b	tank bottom
c	collector
cold	pertaining to cold inlet
del	delivery
dis	pertaining to fully discharged conditions
exp	pertaining to experimental conditions
full-mix	pertaining to fully mixed conditions
L	pertaining to load requirement of storage tank
out	pertaining to outflow exergy availability
outlet	pertaining to outlet conditions
s	pertaining to stream of entrained fluid
str	condition for stratified situation
st	pertaining to stored condition in tank
t	tank top
T	pertaining to bulk tank temperature

fication due to low density of hot water [4–6]. However, if the hot water and cold water are allowed to mix, the available temperature and thus quality of energy supplied at load will be decreased. Accordingly, to make domestic water storage most economical, feasible and practicable – stratification technology has evolved a lot in recent decades. As for simplest case, a design pre-requisite, as mentioned above – minimization of dead water weight is ensured by regulating proper inlet-outlet positions (as shown in Fig. 1)

The central component of the whole system is the storage tank as it is not only responsible for storage capacity but also for thermal efficiency of the whole system. Since, thermal performance of storage tank can be affected by many parameters, in this paper, a detailed portray of such parameters is attempted. Firstly, various hydraulic schemes employing the stratification technology along with each ones' benefits and shortcomings are investigated, this is followed by a descriptive insight into mathematical mechanics of stratification definition. In addition, the factors concerning hydrodynamics and thermodynamics of fluid flow are considered, which include – operating temperatures, flow conditions, inlet velocity and momentum, natural convective flows within the hot and cold water, re-circulative flows due to vertical wall conduction, mixing induced forced convection during charging and discharging, heat exchange between storage tank and environment. Secondly, parameters concerning the geometry of storage tank – thermo-physical properties of tank material and insulation, method of fluid and energy addition and extraction during charging and discharging, diffuser and stratifier shape and type are also explored. Lastly, different methodologies and performance indicators which can be utilized to test and evaluate a storage tank are reported. The underlying meta-analysis is performed by reviewing the literature and case studies ranging within the diverse topic of theoretical exergy and energy analysis of thermal systems along with numerical plus experimental studies on hot water storages available to this date. This is not exclusive of even the aspects of optimization strategies in distributed district heating as detailed by Sameti and Haghighat [136–138] and state of the art technology of solar water storage wall [139]. This is done to make a contrasting effect as the theoretical understanding of thermal systems in general, and application of the same in explanation of stratification in storage tanks was juxtaposed.

Many researchers have presented their studies regarding thermal stratification in water storage tanks. Rodrigues et al. [7] had carried out a non-dimensional analysis to represent the transient natural convection model for domestic storage tank. They identified that heat losses through the walls are controlled by Rayleigh number, overall heat loss coefficient, and aspect ratio of the tank, while Prandtl number has negligible influence. A study performed over 10 different shapes of storage tanks by Yang et al. [8] revealed that sharp corner shaped tanks had the maximum level of thermal stratification, as no velocity field was found in the stratification region for such tanks. Also, all the circulation patterns occur in the isothermal region and in the boundary layer. In addition, the capacity of thermal energy storage is detrimental by surface to volume ratio of the tank. Li et al. [9] experimentally determined the effective discharging efficiency of storage tank working with slotted inlet, direct inlet and shower type inlet. The study demon-

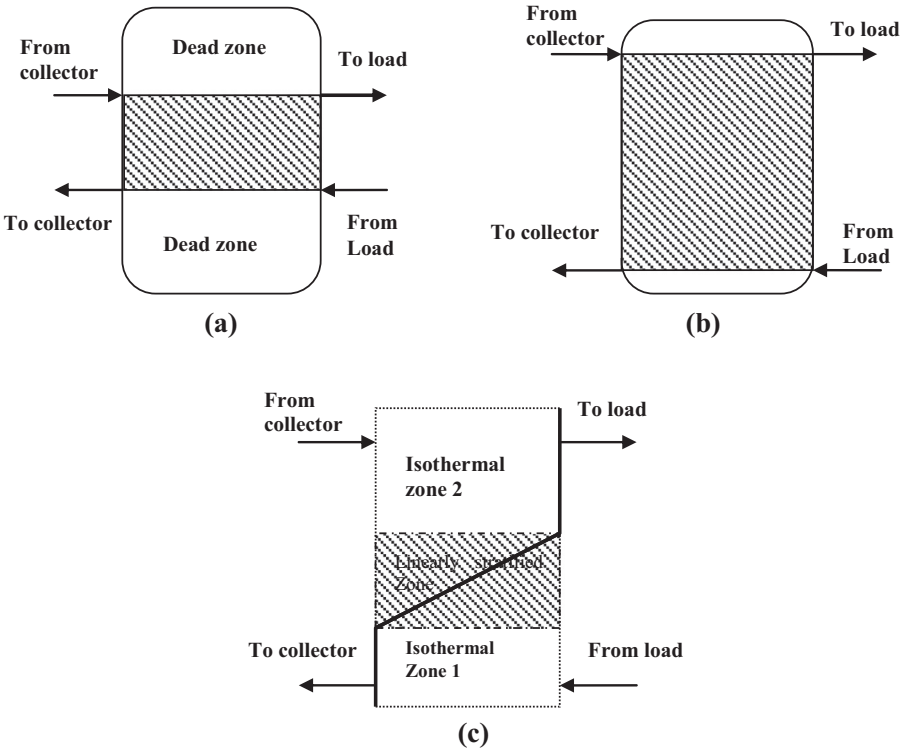

Fig. 1. (**a**) and (**b**) Position of inlet and outlet for efficient and economic concerns in SDHW, and (**c**) thermal stratification in the same.

strated that mixing was considerably prevented with slotted inlet, hence ensuring better stratification throughout discharging. It was also concluded that low flow rates with slotted inlet maintained higher temperature of tapped water for longer period of time. Ievers and Lin [10] quantified the level of thermal stratification in seven three dimensional models as analyzed in Fluent. They established that higher aspect ratio essentially leads to higher thermal stratification – with an increase of aspect ratio from 2.5 to 5, in total 30% betterment in stratification was observed. They also concluded that high mass flow rate at inlet and outlet results in strong jets which strike the walls before diffusing, thus creating strong degradation in thermal layers. It was noticed that an increase of 0.05 kg/s in mass flow rate resulted in 32% of the volume of the tank to be de-stratified, even though it is a well-recognized fact that the position of inlet/outlet plays a major role. This can be corroborated by the fact that reassembling the inlet and outlet positions and moving them 150 mm away from top and bottom of tank resulted in 28% reduction in thermal stratification. Lavan and Thompson [11] studied the variation in extraction efficiency and thermal stratification during discharge cycle with different parameters such as inlet position and geometry, mass flow rate, aspect ratio and inlet/outlet temperature difference. They reduced the effect of these parameters to inlet Reynolds number (characterizing inlet conditions) and Grashofs number (characterizing tank conditions). They concluded that discharging efficiency has much higher influence on position of cold water inlet port rather than outlet port. Henceforth, it was highly suggested that the inlet port should be as close to the storage tank bottom as possible. Abdelhak et al. [12] conducted computational studies and compared vertical and horizontal tanks during discharge mode. They concluded that horizontal position of tank instills larger recirculation patterns due to increased area of thermal conduction between layers, leading to larger amount of stratification decay and lower discharge efficiency. Also, larger amount of vortex patterns near the outlet makes the hottest layers of water to slide away, thus decreasing the draw off temperature. In addition, Richardson number was also assessed to characterize the adverse mixing in horizontal tank which comes out to be unfavourably lower in contrast to vertical tank. Castell et al. [13] investigated various dimensionless numbers to evaluate the stratification in hot water tanks. Castell et al. [13] investigated various dimensionless numbers to evaluate the stratification in hot water tanks. The authors calculated Mix number, Peclet number, Richardson number, Reynolds number and discharge efficiency for their discharging experiment. The study illustrated that only Richardson number and Mix number were able to portray the correct stratification picture in the tank for the entire working range of experiments, while rest of the parameters viz. Reynolds number, Peclet number, and discharge efficiency did not show any clear representation as these numbers were fairly constant. Anderson et al. [14] performed experimental study to compare the fabric stratification pipes with conventional non flexible stratifier for heating/cooling and stratified cooling tests. The results indicated that Mix number in case of fabric stratifier was dramatically reduced during the heating tests because horizontal heat transfer from hot fabric pipe to cold water of the tank was lower, as concluded by the authors. In addition, 2 layer fabric stratification pipe outperformed the rigid stratifier in cooling tests. Hahne et al. [15] studied the flow and heat transfer characteristics in hot water storage tank during charging process. They described the flow and heat transfer characteristics and thus thermal stratification through Richardson number, Peclet number, charging efficiency and Fourier number. Charging efficiency strongly depends on charging temperature difference – increased charging temperature difference instills higher buoyancy forces against turbulent kinetic energy of inflow (increasing the Richardson number) hence inhibiting the direct discharge on inflow jet. Increase in charging velocity also reduces the Richardson number thus increasing the mixing and reducing the charging efficiency. However, this effect is reduced at increased charging temperatures. The effect of Peclet number is also conjoined along with the Richardson number by

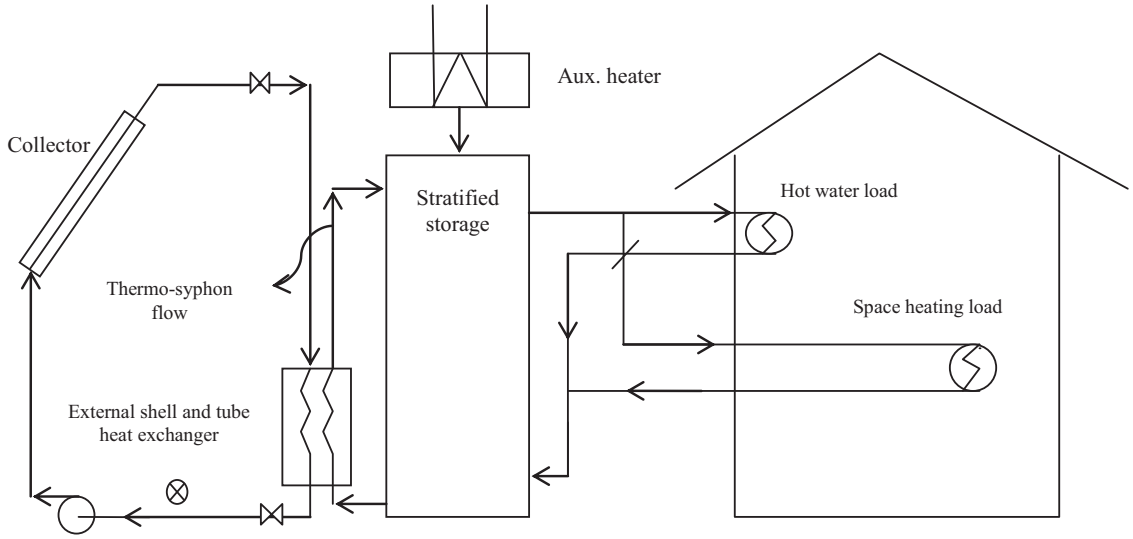

Fig. 2. Solar domestic hot water (SDHW) combisystem with external heat exchanger.

the authors – at low Richardson number, the increase in Peclet number leads to weak heat transfer between hot and cold fluid thus improving the charging efficiency. Yaici et al. [16] performed a CFD analysis to evaluate the influence of geometrical and operational parameters on performance of the tank in charging mode. The results confirmed that a controlled optimization between both geometrical and operational variables is rudimentary for an appropriately designed storage tank. Geometrical factors include aspect ratio representing– the effect of varying tank height with fixed diameter and vice versa, and also inlet and outlet position with respect to the top and bottom wall of tank. The operational parameters include – mass flow rate, inlet temperature variation and the effect of initial water temperature variation. The results concluded that the low mass flow rate instills increased level of thermal diffusion, axial wall conduction, and thermal conduction within the hot and cold water layers, due to increase in thermal exchange time – thus, increasing the thermocline thickness and decreasing the stratification. Contrary to that, high mass flow rate increases the mixing, henceforth, a direct trade-off between effects of thermal diffusion and mixing should be taken into account while choosing the proper mass flow rate. Miller [17] conducted numerical analysis to study the effect of tank walls on the thermocline degradation. The study illustrated that if the thermal conductivity of the fluid is low (as in the case of water), the thermocline degradation due to thermal diffusion or conduction between hot and cold water layers is comparatively slow – provided tank material also has low thermal conductivity. However, if the tank wall material has the thermal conductivity much higher as compared to fluid, the convection currents increases the effective conductivity of the fluid, resulting in an increased thermocline degradation rate. As a comparison, steel tank showed 6 times higher degradation then the glass tank. Also, the convection currents fill up the whole flow field i.e. entire tank is influenced by these currents and are not confined only to water wall interface. A yet another study has been performed by Hess and Miller [18] to investigate the effect of storage tank wall on thermocline dynamics. The numerical results with the help of Laser Doppler Velocimeter (LDV) made some significant observations: vortex formation was observed near the top of the tank wall – this was due to the fact that the velocity field was found to be a function of height and radius, also velocity switched direction from downward to upward direction and vice versa (depending upon the radial position). This bidirectional velocity field was due to counter acting convection induced buoyant force and pressure gradient. Even though, the velocities measured in the studies were very small (maximum axial velocity was 0.3 cm/s at $Ra = 3.7 \times 10^8$), they are responsible for thermocline degradation in some measures. Evans et al. [19] performed experimental and analytical study to understand the transient natural convection in a vertical cylinder exposed to uniform heat flux at the walls. The author divided the system into 3 regions namely: boundary layer, mixing layer and the core region. Boundary layer is the thin region that extends along the boundary of the wall and is responsible for convection currents and the energy discharge into the mixing region. Mixing region is the region where convection currents after taking energy from the walls mixes with the core. Core is the rest of fluid region which is under plug flow. The dye trace method indicated some results: (1) the maximum boundary layer thickness was less than 0.05 inch for aspect ratio = 3, (2) the boundary layer fluid, after taking energy from the tank wall, ascends up *via.* boundary layer and is consequently discharged into the mixing region – which was said to be constituted as upper 10% of the tank, (3) below the mixing region the radial temperature gradients are small and the warmer fluid descends downwards as colder fluid is fed through the boundary layers – eventually to be discharged into mixing region again – thus, constituting internal flow leading to expansion of thermocline. This internal flow also constitutes the progression of linear temperature gradient in the core.

2. Stratification in domestic thermal storage tanks

For thermo-syphon systems, in general, flow rate in the energy collection loop is maintained very low (approx. 0.7 l/min), while in the energy delivery loop it is maintained comparatively higher [7]. Thermo-syphon systems are simplest in the market, employing solar flat plate collectors as energy collecting side, besides this, thermal reservoir or storage tank, auxiliary heating device, heat exchanger, connecting tubes and valves are some important components in a typical solar domestic hot water system (SDHW). Even though the inlet rate is directly proportional to water consumption which is preset depending upon the operational cycle and load pattern, Helwa et al. [20] concluded that the stratification sternly depends upon load pattern and ultimately to inlet parameters.

Fig. 2 represents the concept of solar domestic hot water system (SDHW) with space heating and hot water load. Heat is extracted from the collector loop *via.* external heat exchanger through thermo-syphon. Thermal stratification is maintained in this kind of schematic design when hot water drops to the level where its density matches with the bulk water inside the tank.

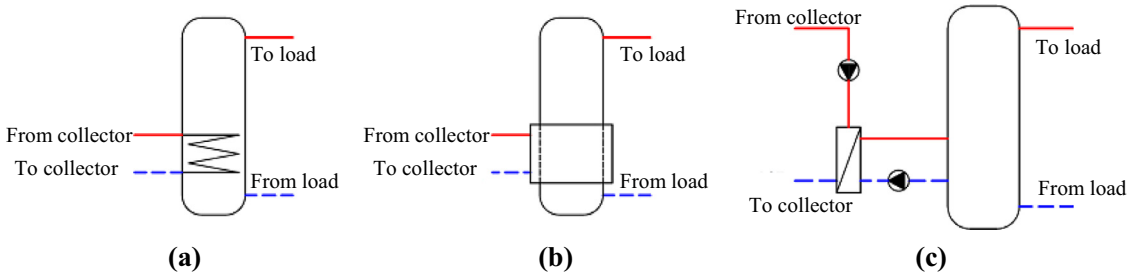

Fig. 3. Common schemes in DHW tank (a) immersed heat exchanger (b) mantle heat exchanger (c) external shell and tube heat exchanger (adapted from Han et al. [26]).

Two counteracting forces i.e. buoyant forces and gravity are responsible for movement of the newly introduced fluid inside tank. High density or low temperature fluid layers have the tendency to settle down as early as possible, while low density or high temperature layers have the propensity to move towards the upper hot layers. In addition, the momentum with which water is introduced into the bulk impacts the core fluid and hence decides how it will react with rest of the fluid layers. After the fluid layers are settled at their respective positions, thermal stratifications is built up forming a thermocline region which is governed by different temperature distribution models such as linear, stepped or three zone model. This thermocline serves as the thermal barrier to separate the hot and cold water regions. Hot water is extracted from the upper part to feed the load, while cold water is extracted from the lower region to circulate to the energy addition loop. Thus thermal stratification is maintained within the tank during the different operation cycles. Nevertheless, this stratification starts to fade away due to different hydrodynamic and/or thermal contingencies which need to be controlled.

2.1. Domestic hot water (DHW) tank's configuration

Stratified water tanks can either be directly heated or indirectly heated by addition of a heat exchanger between energy source and the tank. Directly heated water tanks are highly effective at thermal exchange, however they are weak at maintaining the stratification due to high mixing and turbulence. Henceforth, they are usually equipped with different structural design changes viz. inlet stratifiers, baffle plates, diffuser systems et cetera. Indirect heating, on the other hand, reduces the efficacy of thermal transport from energy addition loop to the stratified tank due to addition of extra heat exchanger which is not always 100% effective, even though it may or may not promise better stratification by reducing mixing and turbulence or by promoting the natural buoyancy within the fluid layers of the tank. For example, consider the case of immersed heat exchanger in which a heating coil is completely immersed in the tank, this design promotes intense undesirable mixing (refer Fig. 3a). Although immersed coil tanks are highly undesirable for their lack in stratification perspective, yet load side immersed heat exchangers are utilized quite prominently in Europe for solar domestic hot water (SDHW) and space heating (SH) combisystems. The reason for this is – it provides facility to separate the water loop which is dedicated to human consumption thus minimizing the chances for oil or algae contamination. In addition, the performance of the immersed type thermal system can be significantly improved by correctly crafting the inner arrangement of the coils. The simulation results validated by experimental findings by Spur et al. [21] concluded that sophisticated inner arrangement can improve the performance and effectiveness of hot water preparation up to 15%. On contrary, external heat exchangers provides rapid flexibility to customize the storage tank according to the stratification requirements. Henceforth, storage tanks used in United States of America are frequently using external shell and tube heat exchangers with two circulating pumps in which one circulation pump is utilized to circulate antifreeze solution in energy collection loop through solar collector while other one is used for energy addition into storage tank through external heat exchanger [22]. Wide range of studies have been performed by Parent et al. [23] and Lin et al. [24] on natural convection or thermo-syphon thermal systems in which need for external pump is eliminated. All the authors concluded that even though the external heat exchanger has effectiveness of thermal exchange ranging from 40 to 99%, thermal systems employing it have enhanced thermal performance due to improved thermal stratification, better cost effectiveness and better consistency and reliability with little restoration (refer Fig. 3c).

Mantle heat exchangers in contrast to external shell and tube heat exchanger facilitates a greater heat transfer area with better effectiveness of thermal exchange (refer Fig. 3b). Mantle type thermal systems prominently find their usage in Denmark and Austria owing to their simplicity in design and construction, cost effectiveness and enhanced thermal efficiency for the same reason discussed above. Webster et al. [25] as quoted by Han et al. [26] concluded experimentally, that overall performance of thermal system working on eight immersed tube heat exchanger was drastically reduced owing to the stratification degradation viewpoint of immersed heat exchanger in contrast to mantle heat exchanger based thermal system. This prompted the use of mantle type thermal system which facilitated the enhanced thermal performance by not only increasing the heat exchange area by two and a half times but also by improving the thermal stratification in storage tank. Further research regarding modelling and testing, and effect of water consumption pattern on thermal performance and stratification in mantle heat exchangers based thermal systems is performed by Knudson et al. [27]. Author established the fact that draw-off induced mixing, which actually amounts to 40% of the total mixing in typical Danish thermal systems, caused approximately 10% of underutilization of net solar gain. Rosengarten et al. [28] studied the effect of temperature distribution, tank cross section, and delivery temperature on exergy and stratification. They concluded that stratification efficiency as well as energy and exergy analysis should be used to ascertain the performance of mantle heat exchanger based thermal systems. Additional computational and flow characteristics based studies have been done by various researchers in [29–32]. Schemes as indicated by Han et al. [26] namely immersed coil, external heat exchanger and mantle heat exchanger type are shown in Fig. 3. Authors concluded that for immersed heat exchanger type storage tank, the inner arrangement of heat exchanger considerably effects the stratification of the tank.

2.2. Hydraulic schemes for indirectly heated combisystems

Even though the stratification efficiency and cost efficacy are best sorted qualities to conceptualize and characterize any DHW and space heating (SH) combisystem, this promptly instills the

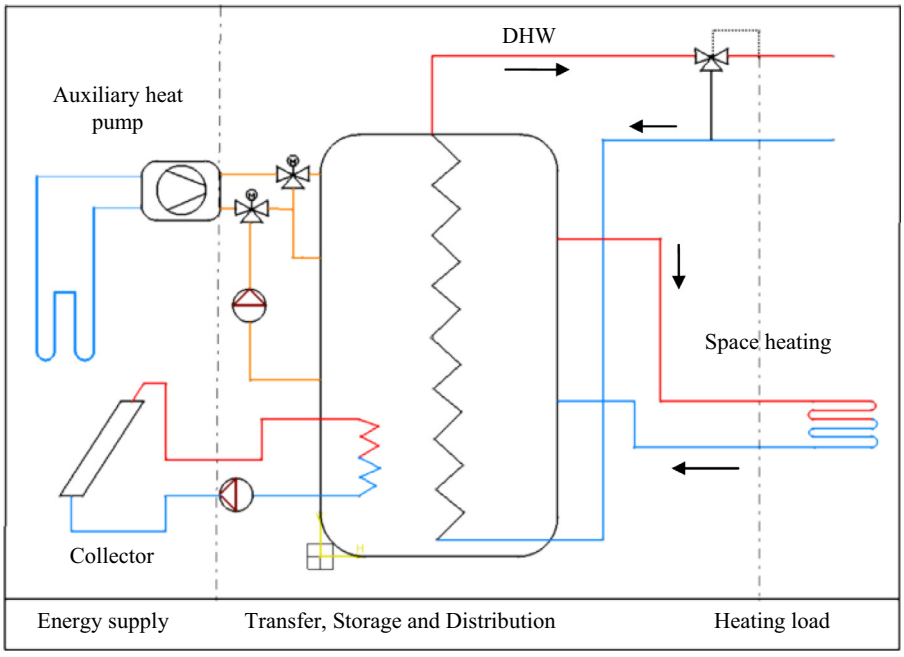

Fig. 4. Hydraulic scheme for indirectly heated (immersed tube) DHW and SH combisystem.

fact – application of mantle heat exchangers and avoiding any immersed tube heat exchangers should be practiced. However, as design parameters of the thermal systems are based on steady state models, despite the fact – solar availability, thermal accumulation and thermal consumption are a lot more transient, this leads to drop back rather a gain right at design stage. Henceforth, a compromise is made between the efficiency and the flexibility of usage which also facilitates the usage of various stratifier devices to curb any augmented de-stratification. This explains – why storage tank is incorporated with dual type heat exchangers? *Viz.* either immersed tube and mantle heat exchanger or immersed and shell and tube heat exchanger. This is explained in next sub section.

2.2.1. DHW and SH combisystem with immersed tube heat exchanger

Fig. 4 gives a detailed schematic of the domestic hot water (DHW) and space heating (SH) combisystem. This system incorporates a heat pump (possibly a ground source heat pump (GSHP) or ground coupled heat pump (GCHP)) as an auxiliary heat supply in addition to solar collector. As illustrated, storage tank is fitted with two immersed tube heat exchangers, one is load side coil for domestic hot water supply, and other one is at the bottom part for collector loop. The auxiliary heat pump is controlled by storage set point temperature which depends upon the DHW and SH requirements. A controller detects the solar gain and thus is able to switch to the solar collector loop instead of heat pump (or both can be operated simultaneously) depending upon the set point temperature. The heating water from GSHP is directed to the respective location of the tank through the external switching *via.* 3-way valves, this enables the release of near to same density of hot water as of the surrounding fluid thus maintaining stratified heat transfer.

2.2.2. DHW and SH combisystem with immersed tube and mantle heat exchanger

Fig. 5 illustrates the usage of immersed and mantle heat exchanger in a compact combisystem. This system consists of 250 l or 650 l storage tank surmounted by mantle heat exchanger which is coupled to solar collector. A dual load side immersed coils one at the upper part and other at the lower part of the tank serves for the DHW preparation. A differential controller regulates the collector loop by switching it on if the collector's absorber temperature is considerably higher than the temperature in the mantle. The SH and DHW is controlled by two sensors, the room thermostat figures out whether there is SH demand which is pre-calibrated by user and outdoor sensor controls both heat pump and solar collector heat input.

3. Stratification analysis

3.1. Energy and exergy analysis

The primary purpose of the thermal energy storage is not – as the name suggests it is – however is to maximize the availability (or exergy) in the form of useful energy gain from the storage. In other words, the purpose of thermal energy storage contrastingly should not be to maximize the heat storage rather contrary is to minimize the destruction of available stored exergy. Bejan [33–36] initiated the second law involvement in analyzing the thermal energy storage and correspondingly he tried to optimize its design and working parameters as opposed to first law inclusion in energy analysis. Bejan [33] referring to the direct trade-off between optimum work stored in TES and work recovery from it, suggested that designing TES for maximum energy storage doesn't necessarily leads to optimized TES thermodynamically – irreversibility must not be compromised to design the TES. Bejan [34] clearly illustrated that "*the mission of the storage device is to temporarily store exergy, not energy*." This irreversibility effect on practically all the TESs, as a characteristic, is demonstrated in Fig. 6 in which a hot gas is irreversibly exchanging its heat with the cold fluid, and hence exhibit the following exergy losses – firstly, irreversible heat exchange with cold fluid during a finite temperature difference ΔT, secondly, heat transfer to ambient during environmental cooling of gas which is again against the finite temperature difference ΔT, and finally, gas flow across the ΔP to overcome friction. This implies that only a segment of incoming exergy is ever stored in the fluid. To see the effect of diminishing returns of the incoming exergy, an entropy generation mapping is produced by Eq. (1).

$$\dot{S}_{gen} = \dot{m}c_p \ln\frac{T_o}{T_\infty} + \frac{Q_o}{T_o} + \frac{d}{dt}(mc\ln T) \tag{1}$$

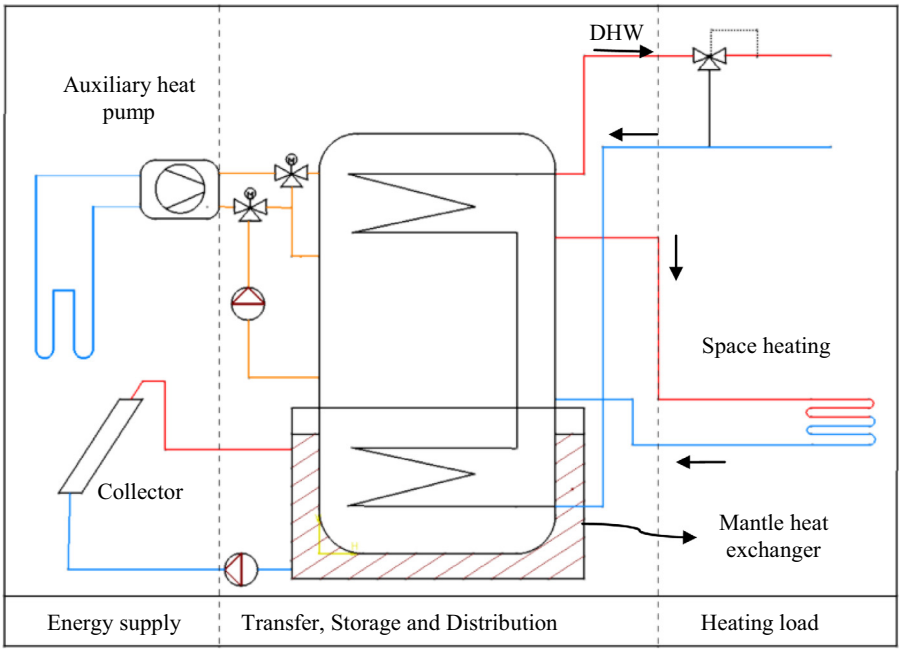

Fig. 5. Hydraulic scheme involving mantle and immersed tube heat exchanger for DHW and SH combisystem.

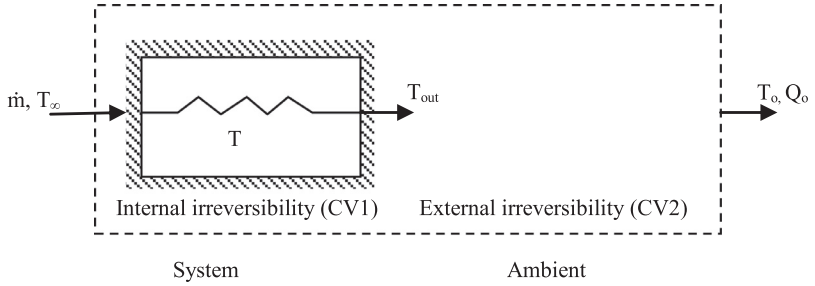

Fig. 6. Irreversibility in TESs.

where, $Q_o = \dot{m}c_p(T_{out} - T_o)$, and $\dot{S}_{gen}$ is the entropy generated during the exchange process or during the charging cycle of TES. Taking this equation to the dimensionless form:

$$\frac{1}{mc}\int_o^t \dot{S}_{gen}dt = \theta\left(\ln\frac{T_o}{T_\infty} + \tau\right) + \ln(1+\tau\eta_1) - \tau\eta_1 \tag{2}$$

where η_1 is the first law efficiency and is given by Eq. (3)

$$\eta_1 = \frac{mc(T - T_o)}{mc(T_\infty - T_o)} \tag{3}$$

and,

$$\tau = \frac{T_\infty - T_o}{T_o}, \theta = \frac{\dot{m}c_p}{mc}t \tag{4}$$

Entropy generation number N_s is defined as ratio of exergy spent to the total energy injected. Eq. (2) multiplied by T_o would signify the exergy loss out of supplied exergy due to systems irreversibility, in this context, N_s is defined as:

$$N_s = \frac{T_o}{E_x}\int_0^t \dot{S}_{gen}dt = 1 - \frac{\tau\eta_I - \ln(1+\tau\eta_I)}{\theta[\tau - \ln(1+\tau]} \tag{5}$$

Or in other words, $N_s = 1 - \eta_{II}$, where, η_{II} is the second law efficiency of charging of storage. Noteworthy point is that: as the dimensionless time θ increases, N_s – the entropy generation number increases – thus leading to more exergy destruction, $N_s = 0$ is the excluding case for reversible process, thus the value of N_s oscillates between 0 and 1.

Adding to the Bejan's studies Krane [37–39] showed that thermodynamic irreversibility during heat addition and storage cycles can destroy up-to 60% to 80% of the availability that has entered the system. Energy efficiency of a TES can be termed as the ratio of energy recovered during the discharging cycles to the energy supplied to the storage during charging cycle. This consideration of utilizing first law analysis is however insufficient in practice to evaluate the performance of any TES as it doesn't provides any information regarding: (a) how closely the system is approaching the ideal one, (b) the comparative temperatures of recovered and supplied energy, and (c) the duration of storage within which the heat can be recovered at desired temperature. In addition, the energy analysis alone leads to poor and invalid comparison of two different TESs operating at different conditions – this has resulted in broader perspective and acceptance for both energy and exergy analysis to evaluate any TES. Exergy analysis, on the other hand, is a second law based thermodynamic investigation which provides gain over energy analysis in a way – firstly, it puts into account the temperature differences for the same energy content storages – this is particularly advantageous for stratified storages as they sustain spatial temperature variations or thermocline, which may be continuous, stepped or linear. Secondly, it takes into account the causes and location of quantitative losses due to mixing of fluids at different temperatures, and losses towards the environment. Thus leveraging for betterment in design and optimization of TES.

More researchers – Bjurstrom and Carlsson [41], Mathiprakasam and Beeson [42], and Taylor et al. [43] preferred second law optimization of stratified storage devices.

The working of TES moreover is governed by operating cycles, typically, energy addition, storage, and energy removal cycles. Careful thermal management and control of these cycles could result in increased performance of the thermal recovery. This section of review explains the exergy and energy analysis of stratified storages, however in an analytical manner to provide a practical insight in a physical temperature distribution model of a typical TES. Moreover, temperature distribution and thus the energy and exergy analysis is usually evaluated through numerical methods – this however in non-general terms doesn't necessarily provide practical insights and physical outlook up to core excellence plus these analytical expressions are far more useful in thermo-economic optimization in thermal storage systems as reported by Zubair and Al-Naglah [40]. Since for an ideal liquid, the specific energy e and specific exergy w can be represented by Eq. (6) and (7), where temperature T is height dependent.

$$e(h) = c(T(h) - T_o) \tag{6}$$

$$w(h) = c[(T(h) - T_o) - T_o \ln(T/T_o)] = e(h) - cT_o \ln(T(h)/T_o) \tag{7}$$

Therefore,

$$Ex = E - mc_pT_o \ln(T_e/T_o) \tag{8}$$

where, T_e is the equivalent temperature of stratified fluid having same exergy as that of mixed fluid and is represented by Eq. (9).

$$T_e \approx \exp[\frac{1}{H}\int_0^H lnT(h) \cdot dh] \tag{9}$$

Now since energy content of mixed storage is considered to be equal to that of energy content of stratified storage, this implies, $E_m = E$, continuing for exergy of mixed storage:

$$Ex_m = E_m - mc_pT_o \ln(T_m/T_o) \tag{10}$$

where, T_m is the equivalent temperature of the mixed storage and $T_m \neq T_e$, as T_e has high degree of stratification dependence, while T_m is independent of stratification. Eqs. (8) and (10) gives the exergy difference between stratified and mixed storage, this is a negative quantity – that is to say, exergy is always lost – for example, during the process of mixing and other irreversibilities.

$$Ex - Ex_m = mc_pT_o \ln(T_m/T_e) \tag{11}$$

3.2. Modelling and analysis of thermal stratification

The main task of modelling of the thermal stratification is to develop computational procedure adequate enough of accuracy and generality to predict the various flow fields and scaler transport terms pertaining to thermocline. As a matter of fact, in addition to charging and discharging cycles, transient behaviour of tank stratification is generally more sought phenomenon to predict the tank performance. One dimensional numerical modelling, in addition to its simplicity and computational savings, is more favourable when long-term (standby) storage tank conditions are required to be simulated. Temperature distribution and its mathematical expressions are one of the most important considerations and point of investigations vis-à-vis to stratification study of the storage tank. Theory describing the thermal stratification is analytically modelled through the first principle, where energy balance is performed over each control volume thus leading to a series of coupled partial differential equations in vertical height and time. Fig. 7 shows a physical description of thermally stratified tank where it is divided into J equal elements and the adjoining

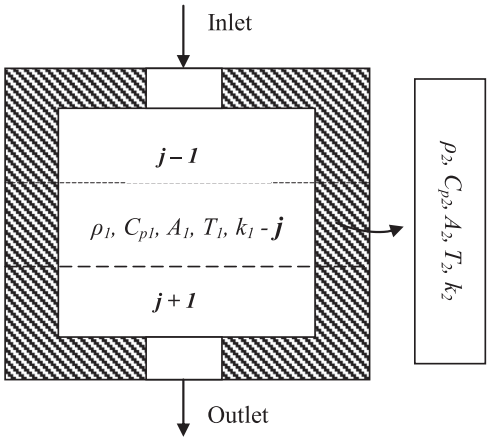

Fig. 7. Control volume description of the tank.

Eqs. (12) and (13) represents the energy balance for the water and the tank walls. A complete analytical model and solution can be referred in Yoo and Pak [50] and Cole and Bellinger [51]. Oppel et al. [52] and Zurigat et al. [53] introduced and studied the effective diffusivity factor (EDF) to incorporate turbulent mixing, represented by $\varepsilon^{in}{}_{eff}$, at the inlet region. Oppel et al. [52] developed and studied one-dimensional model to investigate the variable flow rate effects including turbulent mixing at inlet during charging and discharging.

$$k_1A_1\frac{\partial^2T_1}{\partial x^2} - \rho_1c_{p1}A_1\upsilon\frac{\partial T_1}{\partial x} - \rho_1c_{p1}A_1\frac{\partial T_1}{\partial t} = -hl(T_2 - T_1) \tag{12}$$

$$k_2A_2\frac{\partial^2T_2}{\partial x^2} - \rho_2c_{p2}A_2\frac{\partial T_2}{\partial t} = hl(T_2 - T_1) \tag{13}$$

Many more thermocline predictions, in other words, temperature distribution models have been developed and their comparison study is presented by Zurigat et al. [54], however, they are categorized largely into – multi-node methodology, plug flow methodology and plume entrainment methodology. Multi-node approach entails the tank division into N sections, rendering the energy balance equation and thus resulting N number of differential equations for each section that may be solved for the temperature of each as a function of time and elevation. Plug flow incorporates the up and down movement of bulk fluid section as cold water is added or hot water is removed during different working cycles. To illustrate, as load return cold water is added from the bottom it pushes forward the hot water in piston push fashion – there is only bulk fluid flow – while all other fluid movement is assumed to be restricted. Unlikely, if inlet temperature varies – its tendency to find the matching density layer is adopted by imposing the mixing in the model as explained by plume entrainment model.

3.2.1. Multi-node model

Fig. 8 shows a 3 node tank. Collector return finds its matching position depending on how close to any node its temperature is. For instance, with a three node model having temperatures 60, 55, and 50 °C each the collector return at temperature of 52 °C shifts towards node 3 (node 3 being the lower segment of water at 50 °C). A collector and load control function as defined by Duffie and Beckman [1], given by Eq. (14), is re-introduced to regulate which node is receiving the water from collector and from the return load.

$$F_j^c = \begin{cases} 1 & if\ j = 1\ and\ T_{c,\,o} > T_{s,\,1} \\ 1 & if\ T_{s,\,j-1} \geq T_{c,\,o} > T_{s,\,j} \\ 0 & if\ j = 0\ or\ if\ j = N+1 \\ 0 & otherwise \end{cases} \tag{14}$$

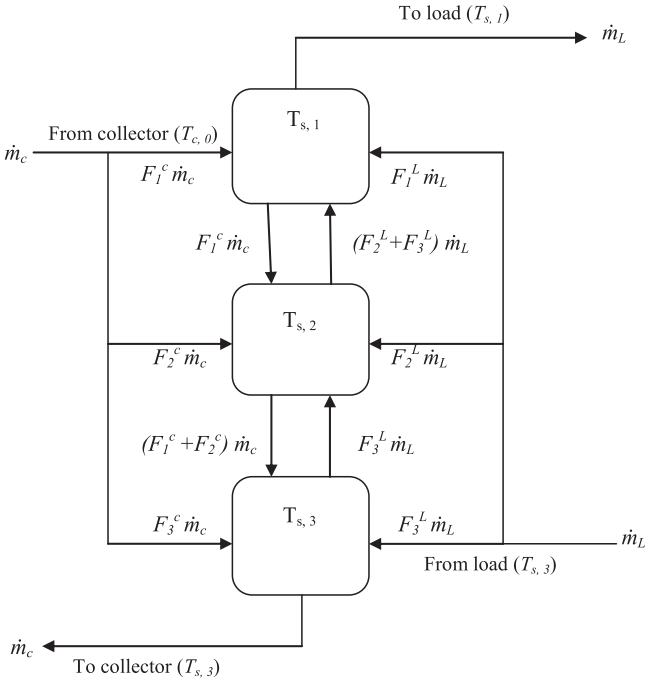

Fig. 8. The 3 Node methodology in tank stratification, adapted from Ref. [1].

Similar control function is defined for load return as well. The flow of fluid element in these 3 nodes are controlled by two control functions as illustrated in Fig. 8.

Considering these functions, an energy balance equation can thus be established pertaining to any node '*j*' (as shown by Eq. (15)) and can be solved using Crank Nicolson, Ranga–Kutta or some other numerical method. However, due to additional factors such as stratification destruction through wall conduction, diffusion and mixing may leads to a complicated nature of this equation thus rendering the usage of computational techniques. More insight can be taken from Close et al. [55] who established a 3 node mathematical model with control function to guide the water.

$$m_j \frac{dT_{s,j}}{dt} = \left(\frac{UA}{c_p}\right)_j (T_a - T_{s,j}) + F_j^c \dot{m}_c (T_{c,o} - T_{s,j}) + F_j^L \dot{m}_L (T_{L,r} - T_{s,j}) \tag{15}$$

3.2.2. Plug flow model

The plug flow model somehow categorises the fluid into fragments of variable sizes and temperature. The number of fragments and their volume vary primarily on tank volume, the net flow from heat source and load, and time step used for simulation. Fig. 9 demonstrates the concept of plug flow [1, 44,56]. Four fragments of fluid with V_i *and* temperature T_i are shown on an horizontal scale for clear understanding. Volume of fluid V_c delivered at a temperature T_c by heat source (e.g. collector) in one time step of simulation is $\dot{m}\ \Delta t/\rho$ (see step 1). Simultaneously, although they are shown sequentially, V_L fluid element i.e. load return equal to $\dot{m}_L\ \Delta t/p$ adds up at the bottom as $T_L > T_4$ (see step 2). Thus making a shift in the whole profile a bit upward which is equal to $V_c - V_L$, on contrary, the shift is downward if this value is positive. In addition, the fraction of fluid which is pushed outside the boundary of the stratified tank is refunded to load and/or the heat source. In fact the average conveyed temperature at the load side would be as given by Eq. (16):

$$T_{del} = \frac{V_c T_c + (V_L - V_c)}{V_L} \tag{16}$$

Temperature profile in the case of plug flow is calculated by solving the differential equation given by Eq. (17):

$$\rho V_j c_p \frac{dT_j}{dt} = -UA(T_j - T_a) + kA_{j-1}\frac{T_{j-1} - T_j}{\Delta h_{j-1}} - kA_j \frac{T_j - T_{j+1}}{\Delta h_j} \tag{17}$$

Alizadeh [57] developed two one dimensional models namely turbulent and displacement mixing models in order to study the vertical temperature distribution in horizontal plug flow stratified tank. During the experimental validation, it was found that stratification remains intact for a non-dimensional time $t = 0.4$, however, stratification deviates from idealised plug flow in the top half of the tank due to turbulent Kelvin – Helmholtz mixing.

3.2.3. Plume entrainment model

During the non-peak hours of solar availability, the cooler collector return water is driven downwards owing to higher density. This descending cold water starts to entrain-along the surrounding hot water layers as it makes its way towards the bottom of the tank. This whole process is termed as plume entrainment and is well represented in Fig. 10. That is to say, plume entrainment is the process of heating the descending water where it rearranges its position in the tank according to the matched available density of surrounding fluid. Phillips and Pate [45] illustrated by experimentation that low temperature incoming water at 10 °C, if introduced in the tank with practically linear temperature profile, that is to say – temperature varied from 15 °C to 54 °C in a continuously linear manner, settles down to around fluid segment at 35 °C. This highly infers the fact that the descending plume must have had entrained-along sufficient quantity of tank water during its short cruising which has raised its temperature by 30 °C.

With the assumption of zero horizontal temperature gradients and smaller cross sectional area of plume compared to tank, energy equations separately for the plume entrained (Eq. (18)), and tank (Eq. (19)) can be written as:

$$c_p \frac{\partial(\dot{m}_s T_s)}{\partial x} = c_p T_T \frac{\partial \dot{m}_s}{\partial x} \tag{18}$$

$$\rho A c_p \frac{\partial T_T}{\partial t} = -c_p \frac{\partial(\dot{m}_T T_T)}{\partial x} + c_p T_T \frac{\partial \dot{m}_T}{\partial x} + kA \frac{\partial^2 T_T}{\partial x^2} - U_T P_T (T_T - T_a) \tag{19}$$

where the term – $c_p\ \delta(\dot{m}_T T_T)/\delta_x$ characterises the control volume advection from tank, while, $+ c_p T_T\ \delta\dot{m}/\delta_x$ characterises the energy entrained from the tank to the plume. A more sophisticated theory on entrainment can be found and adapted through Schlichting and Gersten [46]. Han and Wu [49] developed a model based on partial differential equations governing the heat and mass flow in the viscous entrainment driven inlet of the storage tank and utilised the implicit finite difference method to solve it. It was found out through TRNSYS solar energy simulation that viscous entrainment process resulted in unacceptably fast increase in bottom temperature of the tank when the inlet temperature is colder than the top tank temperature. Henceforth, aspect ratio and tank capacity do not contribute adequately towards the overall performance when other models were used – thus overestimating tank performance. Further detailing in effects of plume entrainment in the performance of domestic hot water tanks is done by Csordas [58]. Authors tried to minimize its effects through specific collector outlet temperature (SCOT) and fixed collector temperature rise (FCTR) flow control strategies. More intricate models involving the two dimensional flow and temperature field visualization has been studied by Chan et al. [59], Cabellie [60] and Guo and Wu [61]. Cabellie [60] numerically studied the flow and temperature field under forced and free convection for different values of Reynolds and Grashoffs numbers falling under the practical situations of computational mesh domains.

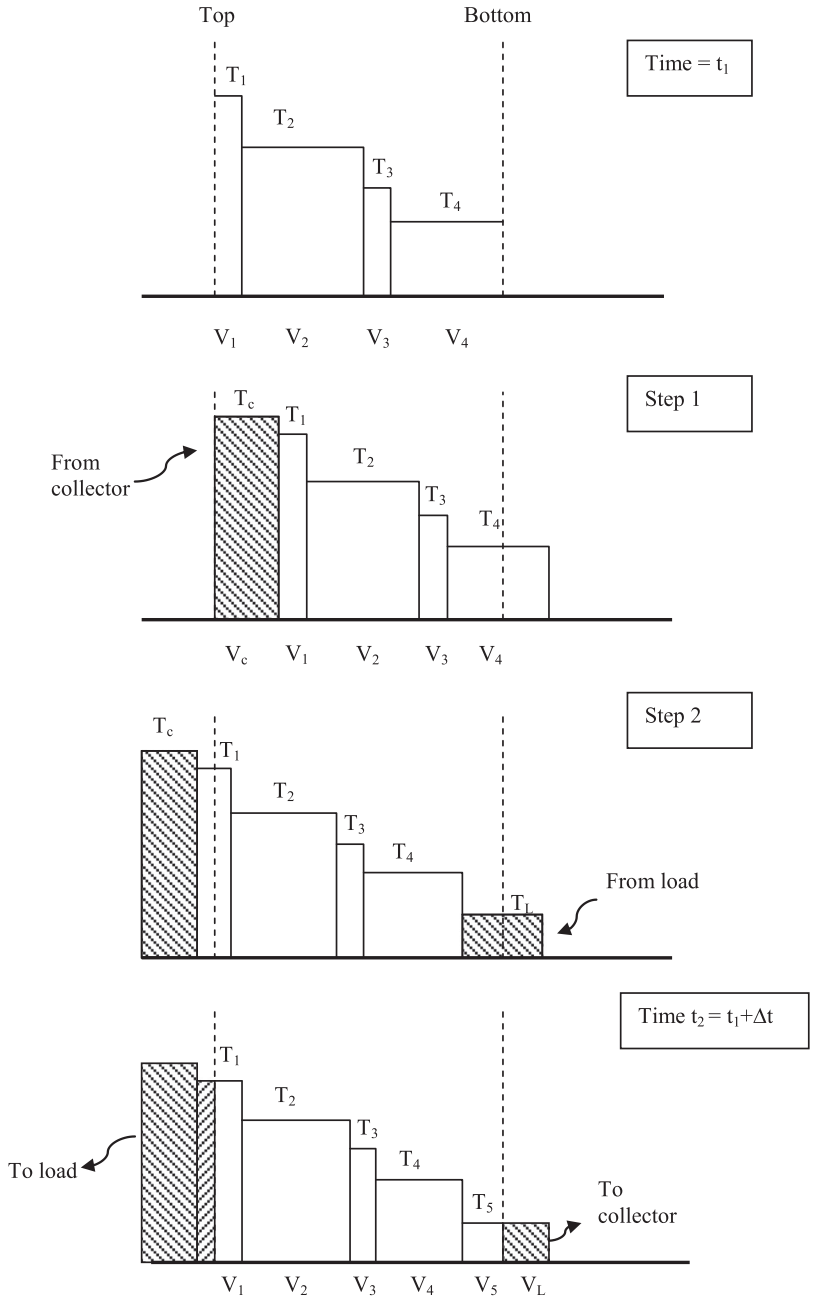

Fig. 9. Plug flow model of stratification in a tank, adapted from Ref. [56].

3.2.4. More considerations in temperature distribution

Various temperature distribution models on stratification as followed by Rosen [47] are summarised here. These include linear, stepped, continuous-linear, general, basic three zones, and general three zones temperature distribution model. In addition, their corresponding expression of mixed (T_m) and equivalent (T_e) temperatures as a function of height are also estimated. Linear temperature distribution model is considered to be the simplest of all in which temperature varies in a linear fashion with the tank height, that is to say, the variation is from T_b to T_t from $h=0$ to $h=H$. Stepped temperature distribution model incorporates J zones as shown in the Fig. 11. Each of these zone is at a certain constant temperature as expressed by the equation in the figure. Continuous linear temperature distribution model, on the other hand, constitutes the same J zones, however, temperature variation – instead of being stepped, establishes a linear profile from bottom to top. This is shown in Fig. 11, where $\phi_j\ (h)$ basically represents the temperature distribution in jth zone – essentially, continuous between each. Also, mean temperature in each zone j is represented by $(T_m)_j$. General linear, on contrary, combines the same J horizontal zones and again the temperature variation is linear, however, not essentially continuous between zone. Refer Fig. 11, where $_j\ (h)$ characterizes temperature distribution in zone j, whereas $(T_t)_j$ and $(T_b)_j$ signifies top and bottom temperature of the same zone.

On the other hand, general three zone and basic three zone model can be generalised as a subdivision of continuous linear model – in a sense, they only have three zones. Temperature variation is essentially linear in each zone, while it is continuous across each zone (refer Fig. 11.). Likewise, basic three zone model can be assumed as a subclass of general three zone model – in a sense, temperature of top and bottom zones stays constant, while temperature in the middle zone varies linearly between temperature of

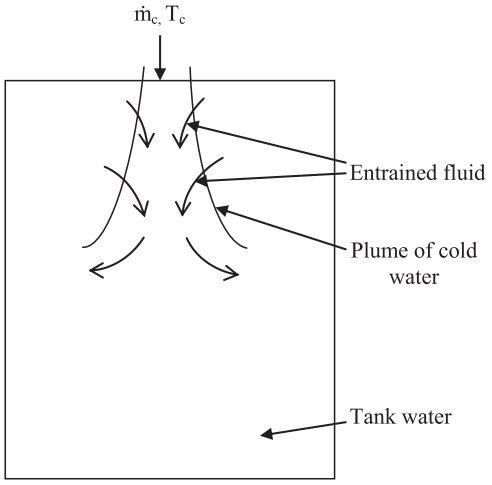

Fig. 10. Plume entrainment model of tank stratification.

top and bottom as shown in Fig. 11. Each of the above mentioned models can be used depending upon to their ease of employability and flexibility to correctly portray the actual temperature distribution. For instance, linear model although basic and easy to be utilised, does not fit to wide-ranging stratification situations. This facilitates the usage of the stepped and continuous model which can be fitted to any temperature distribution, provided – zones are made small. Three zone models on the other hand, are more flexible and can be implemented to any temperature distribution model which has two zones of marginally varying or constant temperature, i.e. upper and lower zone along with a thermocline zone which eventually grows as thermal diffusion follows. Even though three zone models find their usage in nearly all practical temperature distribution models, Mavros et al. [48] suggested that a larger number of zones or layers can actually more closely idealises the plug flow and thus can better predict the stratification.

4. Thermocline dynamics

4.1. Thermocline decay (de-stratification) in dynamic mode

Thermocline is a part of bulk fluid stored in the vessel which separates the hot and cold water owing to density difference. A good sharp stratification not only inhibits the mixing and entropy production during various operation cycles, but also reduces the ineffective volume or dead zone of the tank – which may sums up to 25% of the volume [62]. More than a temperature distribution – as predicted in Fig. 11, thermocline is bit of a dynamically changing layer, which is changing its shape and size with every cycle reversal. In other words, contrary to the common research schema – where hot and cold water are separated with a steep (near to zero thickness) thermocline, however in actual practice, thermocline is considerably thick and is changing its shape and depth both in static and dynamic mode of working. Thus mandating the strict avoidance of largely varying discharge temperature difference due to reaching of thermocline near the outlet port. This is assisted by the cycle reversal the sooner the thermocline reaches outlet port during energy removal. Even though this is a better control strategy then the fully charge and fully discharge one, it has some ground level drawbacks. Firstly, it instils the inefficient utilization of tank volume due to some finite height of thermocline which is prohibited anywhere near the outlet port. Secondly, the entrainment of the thermocline by the incoming water whenever the water is added in both the charge and discharge cycle.

This entrainment process as discussed in the previous section increases the thickness of thermocline by various mechanisms such as Kelvin–Helmholtz instability or engulfment mechanism – incoming water is engulfed by the surrounding water due to difference in their velocities and temperatures [63,64]. This is also aggravated by viscous shear on thermocline by the previously formed K-H eddies and vortices thus resulting to eddy advection into thermocline region due to viscous shear of formed K–H vortices, henceforth, increasing the horizontal span and side by side vertical travel rate of the thermocline through tank during dynamic cycles. Fig. 12 illustrates the dynamics of the mixing process due to entrainment caused by incoming water. Other investigators have researched the physical mechanism of mixing through plume entrainment interaction at a sharp density interface [65–67]. Fig. 13 demonstrates this process in chronological order. For instance, firstly the high momentum turbulent fluid with finite difference in velocity and temperature as compared to the surrounding fluid encounters the stratified fluid or thermocline (Fig. 13a), after gathering enough turbulent kinetic energy it breaks the stratified layers (in contrast to buoyancy driven flow) called the wave breaking as illustrated in Fig. 13b [68–70]. Finally, this cold incoming water entrains the hot stratified water and K – H instability or engulfment starts to take place (Fig. 13c and d).

This eddy advection of mass and energy can be considered to be equivalent to diffusion rate at the interface of the thermocline as represented by Eq. (20)

$$A\upsilon_e \rho c_p \Delta T = kA\frac{dT}{d\delta} \tag{20}$$

where, υ_e is the entrainment velocity, c is the heat capacity, ΔT is the temperature difference between two layers, k is the heat conductivity, and δ is the thermocline thickness.

Furthermore, Knudson et al. [71] demonstrated that the net energy utilization of a small solar thermal system is diminished by 10–16% each time the tank is getting mixed in the lower 40% of the portion of tank during each discharging cycle. For further information regarding dynamic mode operations and concerned de-stratification due to mixing phenomena, Fernandez-Seara et al. [72], Al-Najem and El-Reface [73], Shah and Furbo [74], Davidson et al. [75] can be referred.

4.1.1. Dynamic mode parameters (influence of Richardson number)

Whenever two fluids with different density interact, buoyancy force comes into existence and influences both mixing and motion of two fluids. Turbulence associated to shear flow of the incoming fluid can induce vertical mixing in the stratified fluid if the available turbulent kinetic energy is sufficiently high enough to overcome the potential energy required for vertical mixing. This turbulent mixing due to incoming fluid may cause reduction of temperature gradient or decay in thermocline. In other words, denser water is mixed up with the low density water – disrupting the vertical temperature gradient – moving the centre of mass of the water tank system upwards – subsequently, increasing its potential energy. Energy consideration permits the explanation of gradient Richardson Number which estimates the proportion of kinetic energy available for turbulent mixing. Accordingly, this dimensionless number characterizes the ratio between potential energy required for vertical mixing and the turbulent kinetic energy available for such process. In other words, potential energy available for moving up the centre of mass of the system versus turbulent kinetic energy available for it. The expression can be summarised by Eq. (21) and by Eq. (22) in terms of bulk properties

$$Ri = \frac{W}{K.E.} = -\frac{\frac{g}{\rho}\frac{d\rho}{dz}}{\left(\frac{\partial \upsilon}{\partial z}\right)^2} \tag{21}$$

Model description	Temperature distribution	Mixed temperature (T_m)	Equivalent temperature (T_e)
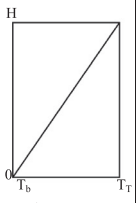 Linear tem. Distribution	$T(h)=\frac{T_t-T_b}{H}h+T_b$	$T_m=\frac{T_t+T_b}{2}$	$T_e=\exp\left[\frac{T_t(\ln T_t-1)-T_b(\ln T_b-1)}{T_t-T_b}\right]$
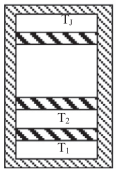 Stepped tem. distribution	$T(h)=\begin{Bmatrix}T_1, & h_0\le h\le h_1\\ T_2, & h_1<h\le h_2\\ \cdots\\ T_k, & h_{k-1}<h\le h_k\end{Bmatrix}$	$T_m=\sum_{j=1}^{J}\left(\frac{h_j-h_{j-1}}{H}\right)T_j$	$T_e=\exp\left[\sum_{j=1}^{J}\left(\frac{h_j-h_{j-1}}{H}\right)\ln T_j\right]$
Continuous linear temperature distribution model	$T(h)=\begin{Bmatrix}\phi_1(h), & h_0\le h\le h_1\\ \phi_2(h), & h_1<h\le h_2\\ \cdots\\ \phi_k(h), & h_{k-1}<h\le h_k\end{Bmatrix}$ Where, $\phi_j(h)=\frac{T_j-T_{j-1}}{h_j-h_{j-1}}h+\frac{h_jT_{j-1}-h_{j-1}T_j}{h_j-h_{j-1}}$	$T_m=\sum_{j=1}^{J}\left(\frac{h_j-h_{j-1}}{H}\right)(T_m)_j$ Where, $(T_m)_j=\frac{T_j+T_{j-1}}{2}$	$T_e=\exp\left[\sum_{j=1}^{J}\left(\frac{h_j-h_{j-1}}{H}\right)\ln(T_e)_j\right]$ Where, $(T_e)_j=\begin{cases}\exp\left[\frac{T_j(\ln T_j-1)-T_{j-1}(\ln T_{j-1}-1)}{T_j-T_{j-1}}\right] & \text{if } T_j\ne T_{j-1}\\ T_j & \text{if } T=T_{j-1}\end{cases}$
General linear temperature distribution model	$T(h)=\begin{Bmatrix}\phi_1(h), & h_0\le h\le h_1\\ \phi_2(h), & h_1<h\le h_2\\ \phi_3(h), & h_2<h\le h_3\end{Bmatrix}$ Where, $\phi_j(h)=\frac{(T_t)_j-(T_b)_{j-1}}{h_j-h_{j-1}}h+\frac{h_j(T_b)_j-h_{j-1}(T_t)_j}{h_j-h_{j-1}}$	$T_m=\sum_{j=1}^{J}\left(\frac{h_{t,j}-h_{b,j}}{H}\right)(T_m)_j$ Where, $(T_m)_j=\frac{(T_t)_j+(T_b)_j}{2}$	$T_e=\exp\left[\sum_{j=1}^{J}\left(\frac{h_{t,j}-h_{b,j}}{H}\right)\ln(T_e)_j\right]$ Where, $T_{e,j}=\begin{cases}\exp\left[\frac{T_{t,j}(\ln T_{t,j}-1)-T_{b,j}(\ln T_{b,j}-1)}{T_{t,j}-T_{b,j}}\right] & \text{if } T_{t,j}\ne T_{b,j}\\ T_{t,j} & \text{if } T_{t,j}=T_{b,j}\end{cases}$
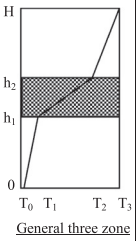 General three zone	$T(h)=\begin{Bmatrix}\phi_1(h), & h_0\le h\le h_1\\ \phi_2(h), & h_1<h\le h_2\\ \phi_3(h), & h_2<h\le h_3\end{Bmatrix}$ Where, $\phi_j(h)=\frac{T_j-T_{j-1}}{h_j-h_{j-1}}h+\frac{h_jT_{j-1}-h_{j-1}T_j}{h_j-h_{j-1}}$ With, $j=1, 2, 3$	$T_m=\sum_{j=1}^{3}\left(\frac{h_j-h_{j-1}}{H}\right)(T_m)_j$ Where, $(T_m)_j=\frac{T_j+T_{j-1}}{2}$	Same as continuous linear model with $J=3$
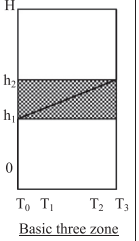 Basic three zone	$T(h)=\begin{cases}T_1, & 0\le h\le h_1\\ \frac{T_2-T_1}{h_2-h_1}h+\frac{h_2T_1-h_1T_2}{h_2-h_1}, & h_1\le h\le h_2\\ T_2, & h_2\le h\le H\end{cases}$	$T_m=x_1T_1+x_2\frac{T_1+T_2}{2}+x_3T_2$ Where, $x_j=\frac{h_j-h_{j-1}}{H}$	$T_e=\exp\begin{bmatrix}x_1\ln T_1\\ +x_2\frac{T_2(\ln T_2-1)-T_1(\ln T_1-1)}{T_2-T_1}\\ +x_3\ln T_2\end{bmatrix}$

Fig. 11. Various temperature distribution models in tank stratification.

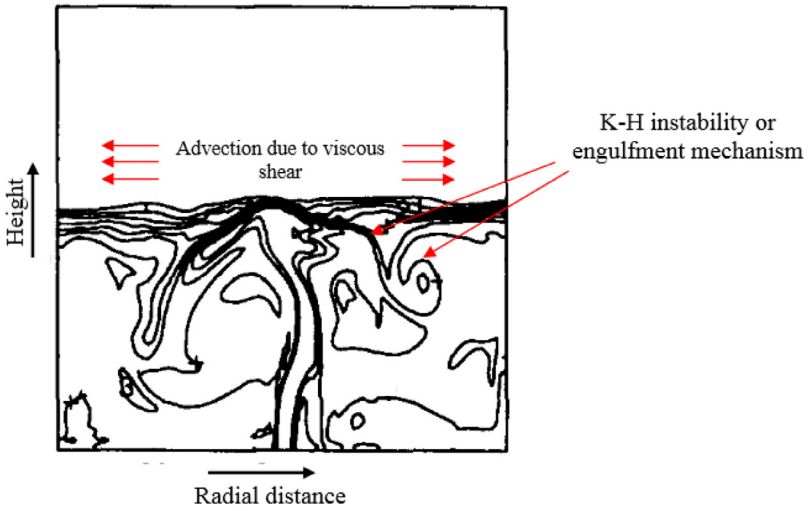

Fig. 12. Mechanism of mixing due to entrainment process during dynamic cycle, adapted from Ref. [63].

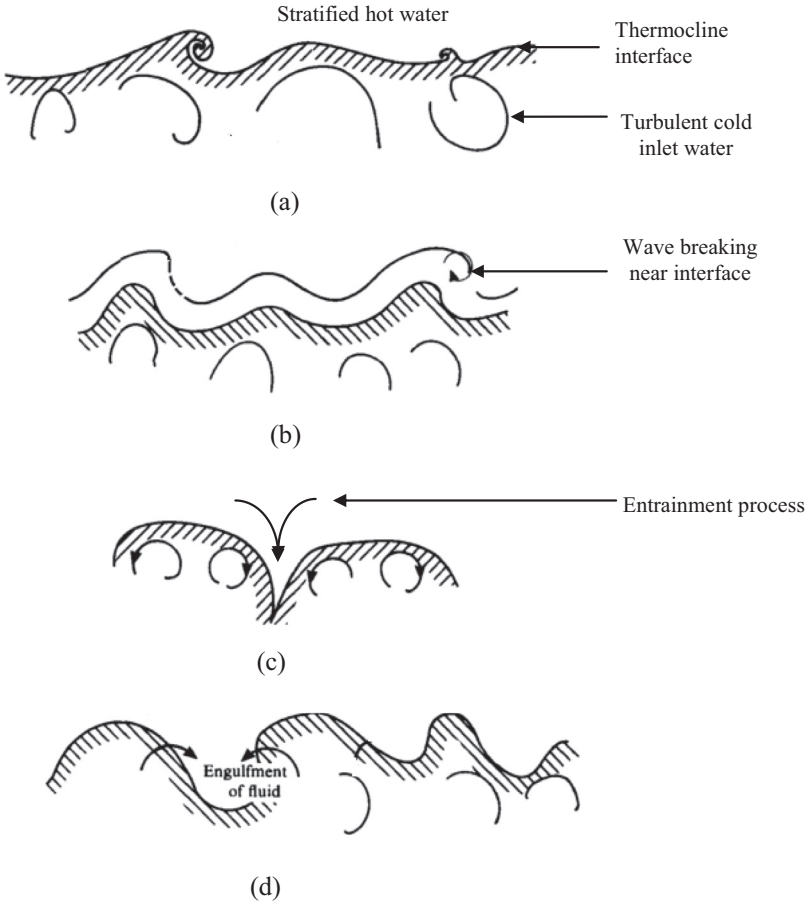

Fig. 13. Physical process of mixing, (a) interaction of cold water with thermocline, (b) wave breaking and subsequent breaching in thermocline, (c) entrainment starts along with, (d) engulfment process.

$$Ri = \frac{g\beta\Delta TL}{\upsilon^2} \tag{22}$$

where g is the acceleration due to gravity, β is the coefficient of thermal expansion, ΔT is temperature difference between inlet and bulk tank temperature, L is characteristic length and υ is the characteristic inlet velocity. It is evident that the high value of Ri characterises low potential for mixing and vice-versa. More specifically, for flows with comparatively larger Ri values – high density gradient leaves a little space for turbulent mixing through plume entrainment. Usually a critical value of Ri is taken, below which turbulent shear stresses break down the density gradient through plume entrainment and mixes with the tank water through wave breaking and engulfment mechanism. Typical value of critical Richardson number is 0.25 [76,77].

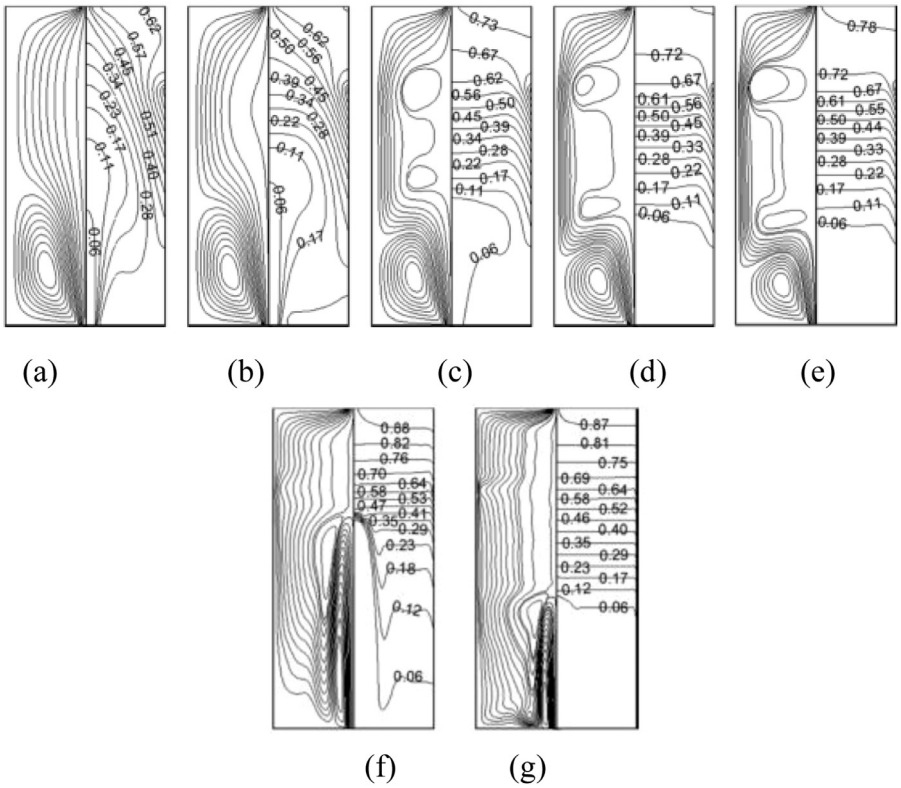

Fig. 14. Streamlines and isotherms at (a) $Re = 500$, $Ri = 0.01$, (b) $Re = 500$, $Ri = 0.1$, (c) $Re = 500$, $Ri = 1$, (d) $Re = 500$, $Ri = 4$, (e) $Re = 500$, $Ri = 10$, (f) $Re = 5 \times 10^3$, $Ri = 20$ and, (g) $Re = 5 \times 10^3$, $Ri = 40$, adapted from Ref. [78].

Low *Ri* inflow has fairly high momentum as compared to buoyant force. This leads to easy penetration of inflow into the thermocline region. More specifically, during discharge cycle, high *Ri* inflow has inadequately low momentum thus making it incapable of penetrating upper hot layers. In a similar manner, during charging cycle, the hot inlet water with high *Ri* number could not gather sufficient amount of momentum in order to penetrate deep into the colder bottom region. To visualise the effect of Richardson number on stratification, Dehgan and Barzegar [78] varied the dimensionless Richardson number in their computational experiment ranging within 0.01–10 for a typical value of Reynolds number $Re = 500$. This range of *Ri* includes both laminar and turbulent regime. Streamlines and isotherms for these values of *Ri* and *Re* are given in Fig. 13. As low *Ri* cold water (Fig. 14a–c) enters the tank bottom, it breaches longitudinally deeper into the tank stratified layers or thermocline, reaching out straight to the outlet. This enhances high mixing in already established sharp temperature gradient *via.* entrainment – and, subsequent fluid engulfment and above all, eddy advection as explained already – thus, destabilising thermocline by decreasing the temperature gradient in vertical direction. As *Ri* is increased (Fig. 14d and e), instead of penetrating into the thermocline (due to unavailability of enough turbulent kinetic energy) the cold incoming water diffuses around the cold bottom region of the tank, and only after thermally communicating with the walls, losing its momentum and finding proper suitable temperature layers finds its way in vertical direction. This makes sure that the cold incoming water doesn't interfere with the hot water in the top portion of the tank thus preserving the stable stratification.

Fig. 14f and g show higher values of Reynolds number (forced convection dominated) and Richardson number (buoyancy dominated) illustrating the better establishment of stratification during discharging. This behaviour is very much important to avoid the fluctuating delivery temperature during discharging. In addition to the fluctuating delivery temperatures, mixing during discharge cycle can cause up-to 23% decrease in energy addition from the tanks perspective [79].

4.1.2. *Influence of Reynolds number*

The influence of inlet fluid velocity on the temperature field of tank as characterised by inlet Reynolds number is shown by Fig. 15. Each of Fig. 15a–c represents the buoyancy driven incoming flow (i.e. *Ri* greater than 1) with $Re = 100$. Accordingly, cold incoming water find its way radially towards the walls of the tank where it communicates thermally, exchanges heat from upper hotter regions, just to find the proper area suiting the temperature demands of surrounding. As the *Re* is increased, or in other words, *Ri* is decreased, the cold inlet water not only straight away finds its way penetrating axially deep into the thermocline region, but also causes eddy diffusion or shear driven vortex in the bottom cold part of tank (refer Fig. 15e and f). This eddy diffusion intensifies the mixing and entrainment process by providing further momentum to subsequent incoming cold fluid.

4.1.3. *Influence of Peclet number* Pe

Peclet number in terms of vertical mixing in tanks is defined as ratio of rate of advection of flow quantities to the rate of diffusion of the same quantity driven by vertical gradient such as temperature gradient in tank. It is represented by Eq. (23).

$$Pe = \frac{\upsilon . H}{\alpha} \tag{23}$$

where α is the thermal diffusivity, and

$$\upsilon = \frac{\dot{V}}{\pi . r^2_{\tan k}} \tag{24}$$

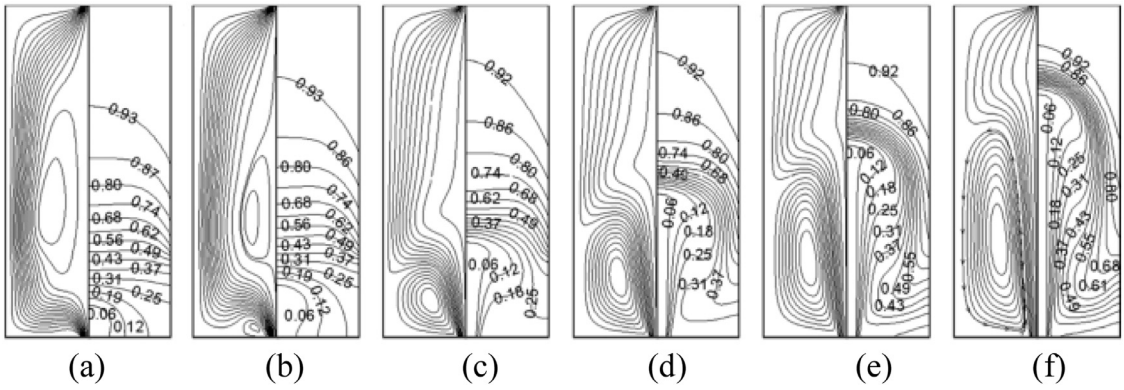

Fig. 15. Streamlines and isotherms at (a) $Re = 100$, (b) $Re = 200$, (c) $Re = 400$, (d) $Re = 600$, (e) $Re = 800$ and, (f) $Re = 1000$ presented in Ref. [78].

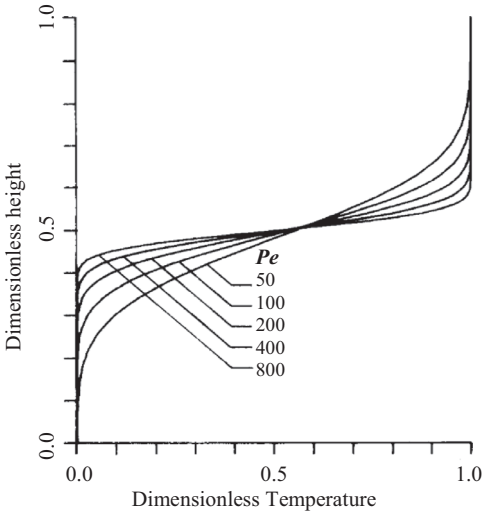

Fig. 16. Effect of Peclet number on thermocline.

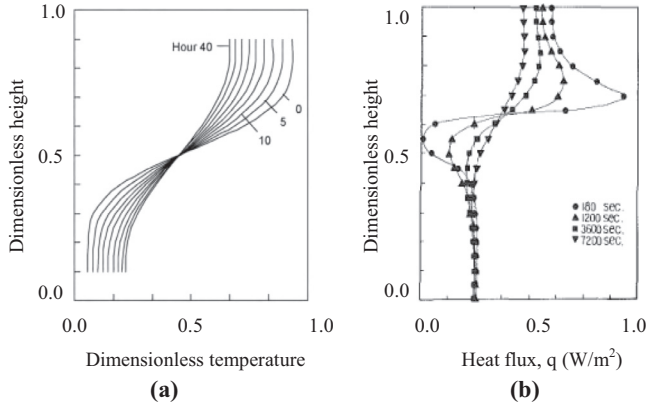

Fig. 17. (a) Temperature distribution, and (b) wall flux in a bare wall tank, originally presented in Ref. [68].

The influence of *Pe* on the thermocline is demonstrated in Fig. 16, where temperature profile of a tank is given for 5 different values of *Pe*. For instance, higher value of *Pe* implies higher value of inlet velocity which eventually gets disbursed for horizontal advection, however more importantly – it implies a lower value of thermal diffusivity due to vertical temperature gradient. In other words, higher value of *Pe* leads to shortened vertical diffusion height, thus leading to lower thermocline decay.

4.2. Thermocline decay in standby mode

Buoyancy driven flow or natural convective flow arising in the tank due to heat loss to the ambient and axial wall conduction is a prevailing de-stratification phenomenon along with thermal diffusion during the standby mode. Upper hot layers are constantly losing heat through tank walls, making the adjacent fluid slightly colder then bulk fluid. This temperature difference serves as impetus to natural convective flow – the colder fluid flow downwards along the vicinity of tank wall, whereas, the relatively hotter fluid at the centre escalates upwards. This constitutes a natural recirculation loop inside tank thus resulting in an enhanced fluid conductivity [68]. Transient natural convective flows in a tank as known as buoyancy driven flows have been widely studied numerically and experimentally by Papanicolao and Belessiotis [79], Oliveski et al. [80], Patterson and Armfield [81], Hyun [82], Patterson and Imberger [83]. The de-stratifying effect of natural convective flows during standby conditions are caused by axial wall conduction, thermal diffusion, and ambient losses from the top hot layers. This can be visualized by Fig. 17a where the temperature in the lower layers is unfavourably incremented, while temperature at top layers is reduced considerably.

Fig. 17b shows the wall-water heat flux calculated by Fourier's law [68]. The large positive values near the top portion of the tank indicates the downward heat flow if the internal tank wall is uninsulated. Similarly, negative value near the bottom portion is the heat flux transferred from water to walls in a normalised value. As the time increase the span of heat flux decreases. This is due to the increase in ambient losses from top hot layers thus decreasing axial wall conduction with time. Natural convective flows and resulting de-stratification due to axial wall conduction is reduced to minimum when the thermal conductivity of wall and the fluid is same as stated by Jaluria and Gupta [5] or when fluid side surface of tank is insulated and outside surface is conductive as demonstrated by Shyu and Hsieh [84].

Fan and Furbo [85] conducted a CFD analysis of a stratified tank for natural convective flows due to heat losses during standby mode. Fig. 18a and b shows the axial wall conduction along with temperature profile and local velocity magnitude pertaining to the buoyancy driven convective flows. It is apparent from the Fig. 18a that there is full rotating loop of thermal energy flowing from high energy upper layers to lower energy bottom layers *via.* conducting tank walls. At height of 1.58 m from the tank there is a downward flow of approximately 5 mm/s near the vicinity of the tank walls. Near the centre of the tank the fluid is moving both downwards and upwards due to heat loss from the top of the tank. At a height of 1.12 m from the tank bottom, the downward flow is very feeble, even though the temperature difference between height 1.58 m

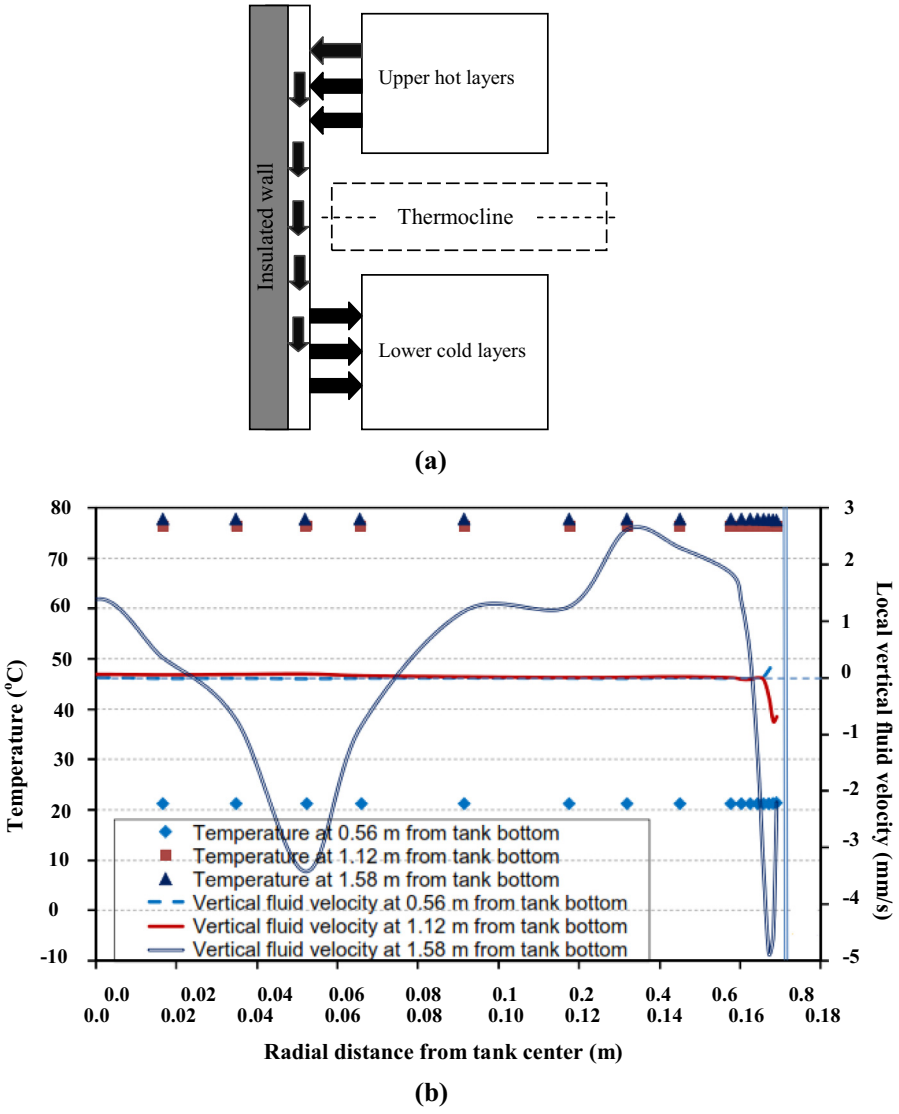

Fig. 18. (a) Axial wall conduction and, (b) Temperature and velocity profile of natural convective flows, originally presented in Ref. [85].

and 1.12 m is merely 3 K. This is due to the presence of stratification layers at the mid region of the tank. Furthermore, as there is a heighten axial wall conduction in thicker tank walls, and increased ambient losses in thinner tank walls with the fact that ambient losses are the major causes of thermocline degradation in an uninsulated tank – an optimal tank geometry design is opted [86]. In addition to ambient losses and axial wall conduction, thermal diffusion due to temperature gradient inside tank is also responsible for de-stratification, however, Nelson et al. [87] concluded that in most cases of storage tank operations it can be considered as insignificant. An extensive research in axial wall conduction and thermal diffusion due to temperature gradient is done experimentally as well as numerically by Miller [88], Sherman et al. [89], Murthy et al. [90] and Parrini et al. [91].

5. Stratification improvement parameters

5.1. Geometrical parameters

Geometrical parameters include tank size, wall thickness and aspect ratio, inlet port – position, shape, length to diameter ratio and type of diffuser, stratifiers – type and shape to control the inlet momentum, insulation – inner wall insulation and type, outside wall insulation.

To begin with, inlet structure can have a very dramatic influence on the thermal stratification of tank, this mandates the demanding need to optimise it in every aspect [92–94]. Since primary mixing takes place during the dynamic cycle of charging and discharging Al-Najem and El-Reface [95] concluded and stated in their study that turbulent mixing arising due to mixing at inlet and outlet ports cannot be neglected as they take the sole responsibilities for thermocline decay. Lavan and Thompson [11] concluded in their experimental study that the inlet position has a much more influence on the stratification decay during the charging mode as compared to the outlet position. During charging process, mixing is initiated by momentum and temperature of incoming jet. A lot of literature is available on the direct inlet and its effects on stratification [74,96,97]. If the inflow jet temperature is comparatively colder than the surrounding it will entrain downwards thus destabilising the stratification. Similarly, if the inlet jet has high momentum, turbulence thus generated will initiate intense mixing in the top layers. Adding to this, concerning the inlet temperature – Eames and Norton [93] concluded in their experimental studies that single inlet port having a variable inlet temperature can even upsurge mixing during charging process due to entrainment.

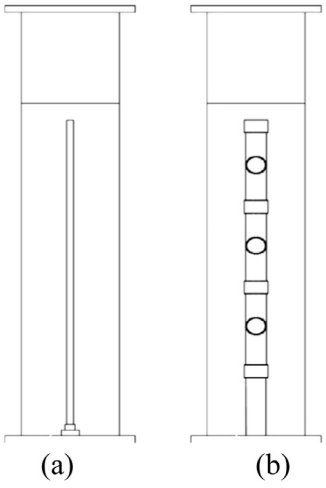

Fig. 19. (a) Flexible polymer pipe and, (b) plastic pipe having holes with flaps to prevent counter flow, adapted from Ref. [103].

It was also stated that a number of ports at different heights can improve the stratification and thus the extraction efficiency of a tank. Concerning the inlet momentum, Li et al. [9] studied different inlet structures i.e. slotting-type, direct, and shower inlet type. The authors concluded that slotting type inlet performed best to reduce the momentum of the incoming cold water and was effective to reduce the mixing during discharge mode. Direct type inlet was comparatively better than the shower type inlet. A similar study on the influence of inlet devices was undertaken by Moncho-Esteve et al. [98] and Carlsson [99] and it was evident that a sintered bronze conical diffuser has more impact in preserving the stratification during charging as compared to conventional bronze elbow inlet. Matrawy and Farkas [100] studied the flow rate and its effect on the stratification. Alizadeh [57] noted in their experimental and numerical studies that higher flow rate irrespective of the surrounding temperature induces strong mixing in the surrounding area thus producing a uniform temperature in a pre-established stratification. Additionally, stratification is even best established smoothly when heat is added at certain level depending upon the surrounding bulk water temperature by usage of special inlet stratification device during charge mode. Inlet stratifier is a type of pipe with arrangement of valves designed to allow water to enter the tank at right thermal level [101]. It can be of various kinds for example a vertical polymer pipe having openings at different locations with or without non-return valves. Non-return valves make sure that water travels only from pipe to tank and not vice versa. Another example can be a porous manifold situated in the tank [102]. Fig. 19 illustrates the basic idea of stratification devices used in charging. Dragsted et al. [103] studied experimentally two types of stratifiers namely a rigid plastic pipe with holes and flaps at every 30 cm of length to prevent counter flow, and a flexible polymer based stratifier with holes along its entire length. Authors made conclusion that both type were able to maintain stratification by deliberately directing water at proper location. Flexible polymer due to its flexibility maintained the counter flow at bay. It was also concluded that the flexible polymer stratifier outperformed the plastic stratifier with holes and flaps at low flow rates of 1–2 l/min, while latter performed better at high flow rates of around 41 l/min. More studies regarding the thermal performance of tanks with different stratifiers have been done by Shah et al. [104], Anderson and Furbo [105], Anderson et al. [14], Anderson et al. [106], Gracia-Maria et al. [107].

Size or aspect ratio of storage tank holds an important role in the standby heat losses. Natural convection due to axial wall conduction and ambient heat losses primarily depends on surface area and hence tank's aspect ratio. Bouhdjar and Harhad [108], Abdoly and Rapp [109] studied the influence of aspect ratio on stratification and performance of storage tanks and concluded that the longer tank with thin walls have better stratification. Fan and Furbo [85] performed experimental and numerical studies on convection flow patterns arising due to axial wall conduction and thus evaluated the standby heat losses and subsequent flow regimes for varying tank volume and aspect ratio. The authors concluded that with an increase in height to diameter ratio from 1 to 5 the convective currents in terms of volume flow rate decreased considerably from 6 l/min to 0.12 l/min. Lastly, it was also concluded that as the tank volume is increased the increase in tanks aspect ratio doesn't actually reduces the axial wall conduction. Ievers and Lin [10] also evaluated and concluded numerically that an increase in aspect ratio from 2.5 to 5 not only increased the degree of stratification up to 30.69% but also decreased the initial mixing at inlet. Chauvet et al. [110] concluded in their study that increase in aspect ratio reduces de-stratification during dynamic mode on the expense of increased ambient heat losses. This leads to an optimal aspect ratio usage between 3 and 4 [111,112]. On contrary, large aspect ratio has impractical dimensions making the tank unsuitable to be used in modern homes. Adding to this, higher aspect ratio also increases the surface area of the tank which can prompt even more convection currents due to increased ambient losses, hence demanding a need for better insulation. Furthermore, as there is an elevated axial wall conduction in thicker tank walls, and increased ambient losses in thinner tank walls with the fact that ambient losses are the major causes of thermocline degradation – an optimal tank wall thickness of about 3 mm is opted [86]. Armstrong et al. [113] performed investigation on wall material specification and concluded that reduction in wall thickness from 1 mm to 0.7 mm decreased the usable volume loss through convection by 13%. The authors also illustrated through numerical techniques that copper walls having higher thermal conductivity then steel and polyethylene have higher rates of counter rotating convection currents due to higher wall flux. Gasque et al. [114] conducted numerical study on inner lining materials and suggested that steel as inner lining material encouraged mixing through thermal diffusion and axial wall conduction, while placing expanded polystyrene (EPS) or poly methyl methacrylate (PMMA) improved discharging efficiency with decreased thermal diffusion and heat leakage due to surrounding walls.

5.2. Operational parameters

As Gasque et al. [114] and various others stated that the tank material specification including inner lining material is prerequisite information to be gathered beforehand to design a tank for better performance during standby mode. However, for dynamic mode of operation the inlet mixing overtakes any other thermocline decay causes – thus requiring the operational parameters – such as, draw-off rate with different inlet-outlet port arrangements and their designs to be taken care of. Fernandez-Seara et al. [72] performed an experimental analysis with three different inlets and 2 different outlets i.e. 6 different inlet and outlet configurations were studied with 3 different draw-off rates of 5, 10 and 15 l/min. The main purpose of the analysis was to configure the best inlet – outlet configuration in terms of stratification performance. The results suggested that a particular type of inlet-outlet port configuration with a specific draw-offs and inflow rates contributes towards better discharge efficiency, better thermocline establishment and the sensitivity of system. This effect is also reflected in the energy and exergy efficiencies for each configuration. Jordan and Furbo [115] illustrated through TRNSYS simulation that fixed inlet during the discharge cycle can lead to a decrease in ef-

Table 1
Dimensionless numbers and their influence on stratification as stated by earlier researchers.

Author	Dimensionless number	Value limit	Impact on stratification
Berkel et al. [116]	Richardson number	$Ri \approx 15$	Clear mixing occur at $Ri = 9.8$, while $Ri \approx 15$ could be considered as apt design condition
Zurigat et al. [92]	Richardson number	$Ri > 3.6$	Influence of inlet geometry such as side inlet perforated inlet etc. on stratification can be neglected
Guo and Wu [61], Sliwinski [118]	Richardson number	$Ri >> 1$	Thermal stratification would be assisted due to decreased forced convection and improved temperature gradient
Cabelli [60], Lavan and Thompson [11]	Flow parameters (Reynolds number, Grashof number)	$Re < 400$ and, $Gr < 80{,}000$	The ratio Gr/Re^2 has greater influence on fluid movement at inlet
Brown and Lai [119]	Reynolds number, Richardson and inverse Peclet number	$Re < 1000$	Degree of stratification is a function of the Richardson number and inversed Peclet number at low Richardson number, however this dependency reduces at high Richardson number
Al-Nimr [120]	Peclet number	At high Peclet number	The stratification destruction due to axial wall conduction is reduced considerably
Yoo and Pak [50], Yoo et al. [121]	Peclet number	$Pe = 50$–800	Sharp thermocline at Peclet number
Dehghan and Barzegar [78]	Reynolds number and Grashof number	$Re < 2000$ and, $Gr < 10^{10}$	Even at high values of Grashof/Richardson number, influence of inlet/outlet geometry cannot be compromised
Shin et al. [122]	Tank size and Froude number	At all limits	Large sized tanks are insensitive to the Froude number and thus to the inflow turbulence does not affect the temperature gradient

fective solar fraction from 60% to 56% due to inlet mixing, while increasing the annual mean temperature of lower 15% of the tank to 2.5 K. Shah and Furbo [74] studied the entrance effect of 3 type of inlet designs (normal pipe, hemispherical baffle, and plate inlet) for 9 draw-off tests. The results showed that for the pipe inlet – 68% of the tank was completely mixed after first draw-off of only 21% of the tank volume. With baffle inlet at least 39% of the tank was mixed, while, only 21% of the tank was affected with the usage of plate type inlet for the same draw-off. Lavan and Thompson [11] experimentally studied the influence of inlet and bulk temperature difference, mass flow rate and port location on stratification during the discharge test of a fully mixed tank at temperature 40.6 °C. Authors deduced the effect of above mentioned parameters to dimensionless numbers such as inlet Reynolds number and Grashof number. In other words, volume flow rate and inlet diameter, which are very detrimental to mixing intensity and inlet mixing layers were recognised and thus were represented by inlet Reynolds number, while the inlet and bulk water temperature difference was characterised by Grashof number. It was suggested that the inlet location should be as close as possible to the bottom for better stratification. The extraction efficiency increased directly as ΔT was increased. At higher values of ΔT, ascending cold fluid in the discharge process dropped back due to higher Grashof number as evident by Fig. 14. Many researchers compared their analytical calculations and tried to associate and include these findings with the dimensionless groups pertaining to the stratification study in storage tanks. This resulted with a concrete prefabricated information regarding the tank geometry, flow velocity, temperatures of inlet and outlet to characterise the performance and level of mixing. Dimensionless numbers such as inlet Reynolds number, Peclet number, Richardson number and Froude number were measured to directly correlate the effect of parameters of thermal, hydrodynamic and tank design on stratification and mixing. These dimensionless numbers as used by some of the authors are tabulated in Table 1. Richardson number plays an important role in defining the level of mixing, however researchers have different rather inconsistent range. Berkel at al. [116] for instance, stated that thermal efficiency nearly remained same when Ri was greater than 15. Zurigat et al. [92] on the other hand stated that one dimensional modelling will not be applicable below Richardson number 3.6 if inlet mixing correlations for each inlet design is not employed – thus inlet mixing plays a greater part for $Ri < 3.6$. Shah and Furbo [74] on the other hand evaluated the inlet impact during draw-offs and thus on the deliverable energy content. Authors concluded that the exergy and entropy change and thus the energy content during draw-off is considerably influenced by the Richardson number. Ramsayer [117] on contrary evaluated that for the flows with $Ri > 0.2$, inlet flow and geometry does not influence the mean temperature gradient.

6. Indices of stratification

To compare the performance of different storage tanks in terms of stratification, performance or evaluation indices are measured and assessed. These indices are specified in terms of firstly, temperature gradient as defined by Huhn [123], together with its decay as represented by Shuy et al. [124], and secondly, efficiencies of stratification, ranging from 0 to 100%, 0% for fully mixed while 100% for fully stratified tank. In other words, stratification efficiency directly characterises the level of mixing as its larger value signifies perfect plug flow. Most of the efficiency parameters as characterised by Panthalookaran et al. [125], Dincer and Rosen [126], Haller et al. [127], Han et al. [26] are evaluated on the basis of either first law of thermodynamics – the energy method, or the second law approach – the exergy or entropy method. In addition, stratification is also evaluated in terms of thermocline thickness as represented by Bahnfleth and Song [128] and percentage ratio of undisturbed or unmixed water volume as defined by Kandari [129]. Even though these methods are experimented and applied successfully, yet these are applicable for constant inlet temperature.

6.1. Stratification numbers

Stratification number is the ratio of mean of the temperature gradients at any time during charging or discharging to the maximum mean temperature gradient as, illustrated by Eq. (25) [72]. Eq. (26) defines the mean of the temperature gradients, while Eq. (27) defines the maximum mean temperature gradient of whole process of charging or discharging. Accordingly, the highest temperature in the equation represents the maximum water temperature during the start of the process, while minimum temperature is the inlet temperature, thus giving the mean maximum

temperature gradient of the form of Eq. (27).

$$Str(t) = \frac{\overline{(\partial T/\partial z)_t}}{\overline{(\partial T/\partial z)}_{\max}} \tag{25}$$

$$\overline{\left(\frac{\partial T}{\partial z}\right)_t} = \frac{1}{J-1} \cdot \left[\sum_{j=1}^{J-1}\left(\frac{T_{j+1}-T_j}{\Delta z}\right)\right] \tag{26}$$

$$\overline{\left(\frac{\partial T}{\partial z}\right)}_{\max} = \frac{T_{\max}-T_{in}}{(J-1)\cdot\Delta z} \tag{27}$$

Davidson et al. [75] quoted McCarthy and Wood [130] who proposed a coefficient to evaluate the level of stratification which is the product of the ratio of actual temperature difference between water at top and bottom of tank to the ideal temperature difference (temperature difference between boiling water and the cold inlet water) and ratio of the actual average temperature of the tank to the average temperature calculated when linear vertical temperature profile is calculated, according to Eq. (28).

$$\zeta = \frac{\Delta T_{actual}}{\Delta T_{ideal}} \cdot \frac{(T_{avg})_{actual}}{(T_{avg})_{ideal}} \tag{28}$$

Wu and Bannerot [131] defined the stratification factor *ST* as the mass weighted mean square deviation of water temperature in the tank from the mean temperature of storage tank divided by total mass of tank, as followed in Eq. (29). It basically focuses on temperature gradient and not the degree of mixing, this makes it the perfect gauge for the deviation of temperature profile from that of perfect isothermal tank at T_{avg}, however, this does not portray the energy stored or the degree of mixing. This implies if the tank gets mixed up or becomes isothermal the ST takes value of zero, irrespective of energy content.

$$ST = \frac{1}{m_{store}} \cdot \sum_{j=1}^{J} m_j \cdot \left[T_j - T_{avg}\right]^2 \tag{29}$$

Liu et al. [158] characterised the degree of thermal stratification in a tube bundle by modifying the stratification factor developed by Wu and Bannerot [131] by incorporating the relative height of each tube bundle in the mean square temperature variation formulae as given by Eq. (30).

$$ST = \frac{1}{m_{store}} \cdot \sum_{j=1}^{J} m_j \cdot \left[T_j - T_{avg}\right]^2 \left(\frac{h}{H}\right) \tag{30}$$

6.2. First law efficiencies

First law stratification efficiency calculates the fraction of recoverable energy during the process of charging or discharging for a constant inlet temperature and mass flow rate. Abdoly and Rapp [109], Nelson et al. [132] approached in a similar a fashion – the first law efficiency in terms of recoverable heat as a measure of thermocline degradation in thermally stratified tank. They specified the quantity *P* as the recoverable heat or reusable heat in any region of the thermocline, which by arbitrary definition could be most significantly explained as the quantity of heat which has not been degraded or dropped in temperature more than 20% of its original temperature towards the incoming cold water (refer Eqs. (31) and (32)). Thus, following the definition for any small region *j*:

$$P_j = m_j(T_j - T_{inlet}), \quad if \ \frac{T_j - T_{inlet}}{T_{outlet} - T_{inlet}} \geq 0.8 \tag{31}$$

$$P_j = 0, \quad if \ \frac{T_j - T_{inlet}}{T_{outlet} - T_{inlet}} < 0.8 \tag{32}$$

where m_j is the mass of the region of water with assumption of unity as the specific heat capacity. Henceforth, the total recoverable heat is the sum total all regions as given by Eq. (33) below.

$$Q = \sum_{j=1}^{J} P_j \tag{33}$$

The fraction of recoverable heat any time *t* is given by Eq. (34):

$$F(t) = Q(t)/Q_0 \tag{34}$$

where, Q_0 is the total heat stored in the stratified storage. This concept of first law stratification efficiency is also revisited by Haller et al. [127] and originally used by Dincer and Rosen [126] and Fernandez-Seara et al. [72], as summed by Eq. (35):

$$\eta = \frac{\int_0^{t_d} \dot{m} \cdot c_p \cdot |T_{outlet} - T_{inlet}|\, dt}{m_{store} \cdot c_p \cdot |T_{initial} - T_{inlet}|} \tag{35}$$

where t_d is the time at which the temperature difference has been dropped for more than 20% of its original temperature towards the incoming cold water ($|T_{outlet} - T_{inlet}| < 0.8 \cdot |T_{initial} - T_{inlet}|$).

Chan et al. [59], Shah et al. [104], Bouhdjar and Harhad [108] defined and used the storage efficiency in terms of effective energy stored versus total inflow energy as given by Eq. (36).

$$\eta = \frac{\rho c_p V[T_{avg}(t) - T_{outlet}]}{\rho c_p \dot{V} \cdot t[T_{inlet} - T_{initial}]} \tag{36}$$

6.3. Second law efficiencies

Exergy quantifies the work that can be extracted from the tank, henceforth, exergy analysis can be used as a parameter to assess the benchmark of theoretical thermal performance of the tank. Rosen et al. [133] and Rosen [47] indicated (also illustrated in Section 3) that a storage tank with better temperature gradient will apparently contain more amount of exergy in contrast to similar storage tank with equal amount of energy content but comparatively lower stratification level. Second law efficiency or exergy efficiency in case of discharging process, as defined by Fernandez-Seara [72], is the ratio of cumulative exergy delivered by the water draw-off to the initial exergy stored by the water in the tank (refer Eqs. (37), (38) and (39)).

$$\eta_{\psi,d}(t) = \frac{Ex_{out}(t)}{Ex_{st}(t=0)} \tag{37}$$

$$Ex_{out}(t) = \int_0^t \left(\rho \cdot \dot{V}\right)_{out} \cdot [(h^e{}_{out} - h^e{}_0) - T_0 \cdot (S_{out} - S_0)] \cdot dt \tag{38}$$

$$Ex_{st}(t=0) = \sum_{j=1}^{J} \{(V \cdot \rho)_j \cdot [(u_j - u_0) - T_0 \cdot (S_j - S_0)]\} \tag{39}$$

Shah and Furbo [74] defined the calculation formulae for exergy efficiency as the ratio of exergy of the experimental tank to the exergy of a fully stratified tank as given by Eqs. (40)–(42).

$$\eta_\xi = \frac{Ex_\xi(\exp)}{Ex_\xi(str)} \tag{40}$$

where,

$$Ex_\xi = E_{\exp} - \sum_{j=1}^{J} m_j \cdot c_p \cdot T_{cold} \cdot \ln\left(\frac{T_j}{T_{cold}}\right) \tag{41}$$

$$E_{\exp} = \sum_{j=1}^{J} m_j \cdot c_p \cdot (T_j - T_{cold}) \tag{42}$$

Exergy efficiency η_{ξ} varies from 0 to 1, for 0 being fully mixed while 1 being perfectly stratified tank. Shah and Furbo [74], in addition, specified the entropy efficiency as the ratio of entropy difference between fully stratified storage tank and the fully discharged tank to the entropy difference between experimental tank and the fully discharged tank, according to Eq. (43). Many more researchers Homan [134], Huhn [123], Van Berkal [135], Rosengarten et al. [28], Panthalookran et al. [125] evaluated thermal storage devices based on second law principle.

$$\eta = \frac{Ex_{str} - Ex_{dis}}{Ex_{\exp} - Ex_{dis}} \tag{43}$$

6.4. Other indices of stratification efficiency

6.4.1. Extraction efficiency

Lavan and Thompson [11] used and defined the extraction efficiency as the percentage of volume that can be discharged for not less than 90% of the temperature difference between initial storage temperature and inlet temperature, as given by Eq. (44).

$$\eta = \dot{V}t^*/V \tag{44}$$

where t^* is the time at which the difference between draw-off and inlet temperature of water drops to not more than 10% of the initial value *i.e.*$(T - T_{inlet})/(T_{outlet} - T_{inlet}) = 0.9$.

6.4.2. Mix number

In contrast to the stratification numbers, which focuses on the temperature profiles – temperature gradients or the temperature deviations in the tank, Mix number evaluates the tank on the basis of both vertical temperature profile as well as the total energy stored in the tank. In other words, Mix number is based on both the energy and temperature distribution inside tank, accordingly, it postulates the mixing process in the tank by evaluating the moment of energy M_E. Moment of energy of thermal storage tank is calculated to account for energy location by doing summation of the sensible energy content up to jth vertical storage segment, weighted with the height of its location, as given by Eq. (45).

$$M_E = \sum_{j=1}^{J} y_j \cdot E_j \tag{45}$$

where y_j is the distance measured from bottom of the tank to the centre of the node j, while the energy content of node j is $E_j = \rho_j \cdot C_p \cdot V_j \cdot T_j$. A larger value of moment of energy implies lower amount of mixing. Mix number is the ratio of the difference between moment of energy of fully stratified and experimental storage to the difference between moment of energy of fully stratified and fully mixed storage, according to Eq. (46).

$$MIX = \frac{M_{str} - M_{\exp}}{M_{str} - M_{full-mix}} \tag{46}$$

Mix number varies from 0 to 1 and is used as a parameter to evaluate the performance of storage tank. Value 0 represents full stratification in tank, while 1 represents complete mixing. The energy content being the same for both experimental as well as fully stratified tank.

7. Conclusion

Thermal performance of heat storage system depends on the degree of stratification. A well stratified tank is always capable of delivering higher exergy plus improved degree of utilization with lesser amount of heat input as compared to the mixed isothermal tank having the same energy content. The idea behind generating and maintaining a good thermal stratification is to keep a stable vertical temperature gradient during all the operation cycle of tank. A stable thermocline can be maintained for example during charging/discharging cycle by carefully monitoring hydrodynamics and thermodynamics of operational parameters. Careful management of inlet-outlet configuration – position, shape, type of diffuser, hot water inlet and bulk water temperature difference, and draw-off rate are all measures to minimize mixing and maximise stratification. Mixing process is influenced by the rate of entrainment which is further controlled by K-H instability where incoming water is engulfed by surrounding water due the velocity and temperature difference. In this paper, different parameters to measure the stratification and thus the level of mixing are suggested, some of such measures are capable of spotting the accurate time on which mixing has appeared. Thus these parameters are plainly rudimentary to be calculated as far as testing of commercial storage tanks is considered. Adding to this, these parameters require the accurate temperature of each water layer to be calculated – thus rendering the need for actual temperature distribution inside the tank to be measured by a series of temperature sensors. This is particularly difficult sometimes firstly because of non-availability of inside temperature distribution of a commercially available storage tank in general, and secondly it is a tedious or even near to impossible to correctly place the sensors according to the ever changing thermal pattern of tank inside. In other words, location of sensors depend on the temperature distribution of water layers (which is changing with time) and not the vice versa. To understand this, a temperature distribution schemas is also been produced in this paper. This includes linear temperature distribution model, stepped distribution model, continuous linear distribution model, basic 3 zone model and general 3 zone model. Further research could be centred on the invention of calculation methods to calibrate this inconsistency of ever changing shape and size of thermal layers of water segments and fixed location of temperature sensors. To sum up, this information could be clubbed together with new modelling techniques and water consumption patterns to accommodate a better stratification enhancement right during design phase of TES system.

References

[1] J.A. Duffie, W.A. Beckman, Solar Engineering of Thermal Processes, Wiley, New York, 1974.
[2] C.W.J. Van Koppen, L.S. Fischer, A. Dijmans, Stratification effects in the short and long term storage of solar heat, Presented Int. Solar Energy Cong., 1978.
[3] A. Cabelli, Storage tanks - a numerical experiment, Sol. Energy 19 (1977) 45–54.
[4] S.K. Gupta, Y. Jaluria, Transient thermal effects in an enclosed water body due to heated water discharge for heat rejection and solar energy storage, Energy Convers. 21 (1981) 3–8.
[5] Y. Jaluria, S.K. Gupta, Decay of thermal stratification in water body for solar energy storage, Sol. Energy 28 (1982) 137–143.
[6] A.A. Dehghan, A. Barzegar, Thermal performance behaviour of a domestic hot water solar storage tank during consumption operation, Energy Convers. Manage. 52 (2011) 468–476.
[7] I. Rodríguez, J. Castro, C.D. Pérez-Segarra, A. Oliva, Unsteady numerical simulation of the cooling process of vertical storage tanks under laminar natural convection, Int. J. Therm. Sci. 48 (4) (2009) 708–721.
[8] Z. Yang, H. Chen, L. Wang, Y. Sheng, Y. Wang, Comparative study of the influences of different water tank shapes on thermal energy storage capacity and thermal stratification, Renew. Energy 85 (2016) 31–44.
[9] Shu-hong Li, Yong-xin Zhang, Yang Li, Xiao-song Zhang, Experimental study of inlet structure on the discharging performance of a solar water storage tank, Energy Build. 70 (2014) 490–496.
[10] S. Ievers, W. Lin, Numerical simulation of three-dimensional flow dynamics in a hot water storage tank, Appl. Energy 86 (12) (2009) 2604–2614.
[11] Z. Lavan, J. Thompson, Experimental study of thermally stratified hot water storage tanks, Sol. Energy 19 (5) (1977) 519–524.
[12] O. Abdelhak, H. Mhiri, P. Bournot, CFD analysis of thermal stratification in domestic hot water storage tank during dynamic mode, Build. Simul. 8 (4) (2015) 421–429.
[13] A. Castell, M. Medrano, C. Solé, L.F. Cabeza, Dimensionless numbers used to characterize stratification in water tanks for discharging at low flow rates, Renewable Energy 35 (2010) 2192–2199.

[14] E. Andersen, S. Furbo, J. Fan, Multilayer fabric stratification pipes for solar tanks, Sol. Energy 81 (2007) 1219–1226.
[15] E. Hahne, Y. Chen, Numerical study of flow and heat transfer characteristics in hot water stores, Sol. Energy 64 (1–3) (1998) 9–18.
[16] Wahiba Yaïci, Mohamed Ghorab, Evgueniy Entchev, Skip Hayden, Three-dimensional unsteady CFD simulations of a thermal storage tank performance for optimum design, Appl. Therm. Eng. 60 (2013) 152–163.
[17] C.W. Miller, The effect of a conducting wall on a stratified fluid in a cylinder, in: AIAA 12th Thermo-physics Conference, 1977, pp. 27–29.
[18] C.F. Hess, C.W. Miller, An experimental and numerical study on the effect of wall in a thermocline type cylinder enclosure - I, Sol. Energy 28 (1982) 145–152.
[19] L.B. Evans, R.C. Reid, E.M. Drake, Transient natural convection in a vertical cylinder, AIChE J. 14 (1968) 251–259.
[20] N.H. Helwa, A.M. Mobarak, M.S. El-Sallak, H.H. E1-Ghetany, Effect of hot-water consumption on temperature distribution in a horizontal solar water storage tank, Appl. Energy 52 (1995) 185–197.
[21] Roman Spur, Dusan Fiala, Dusan Nevrala, Doug Probert, Performances of modern domestic hot-water stores, Appl. Energy 83 (2006) 893–910.
[22] Patrice Pinel, Cynthia A, Ian Beausoleil-Morrison Cruickshank, Adam Wills, A review of available methods for seasonal storage of solar thermal energy in a residential applications, Renew. Sustain. Energy Rev. 15 (2011) 3341–3359.
[23] M.G. Parent, Th.H. Van der Meer, K.G.T. Hollands, Natural convection heat exchangers in solar water heating systems: theory and experiment, Sol. Energy 45 (1990) 43–52.
[24] J.Y. Lin, R.J. Shyu, L.J. Fang, Study of thermal stratification in storage tank with charging, J. Chin. Soc. Mech. Eng. 8 (2) (1987) 87–94 Chung-Kuo Chi Hsueh Kung Ch'eng Hsuebo Pao.
[25] T.L. Webster, J.P. Coutier, J. Wayne Place, M. Tavana, Experimental evaluation of solar thermosiphon with heat exchanger, Sol. Energy 38 (4) (1987) 219–231.
[26] Y.M. Han, R.Z. Wang, Y.J. Dai, Thermal stratification within the water tank, Renew. Sustain. Energy Rev. 13 (2009) 1014–1026.
[27] S. Knudsen, Consumer's influence on the thermal performance of small SDHW systems - theoretical investigations, Sol. Energy 73 (1) (2002) 33–42.
[28] G. Rosengarten, G. Morrisonç, M. Behnia, A second law approach to characterising thermally stratified hot water storage with application to solar water heaters, ASME *J. Solar Energy Eng.* 121 (1999) 194–200.
[29] J.A. Khan, R. Kumar, Natural convection in vertical annuli: a numerical study for constant heat flux inner wall, ASME J. Heat Transf. 111 (1989) 909–915.
[30] A. Nasr, G.L. Morrison, M. Behnia, Computational study of flow and heat transfer characteristics of annular and vertical cavities, in: Proceedings of 2nd CASCM'97, 1997.
[31] B.B. Rogers, L.S. Yao, The effect of mixed convection instability of heat transfer in a vertical annulus, Int. J. Heat Mass Transfer 33 (1) (1990) 79–90.
[32] S. Knudsen, G.L. Morrison, M. Behnia, S. Furbo, Analysis of the flow structure and heat transfer in a vertical mantle heat exchanger, Sol. Energy 78 (2005) 281–289.
[33] A. Bejan, Two thermodynamic optima in the design of sensible heat units for energy storage, ASME J. Heat Transf. 100 (1978) 708–712.
[34] A. Bejan, The thermodynamic design of heat and mass transfer processes and devices, Heat and Fluid Flow 8 (4) (1987) 258–276.
[35] A. Bejan, Entropy Generation Through Heat and Fluid Flow, John Wiley & Sons Inc., New York, NY, 1982.
[36] A. Bejan, The thermodynamic design of heat and mass transfer processes and devices, Int. J. Heat Fluid Flow 8 (1987) 258–276.
[37] R.J. Krane, A Second-Law analysis of the optimum design and operation of thermal energy storage systems, Int. J. Heat Mass Transfer 30 (1987) 43–57.
[38] R.J. Krane, Second-Law analysis of thermal energy storage systems: fundamentals and sensible heat systems, in: Energy Storage Systems, Kluwer Academic Publishers, Dordrecht, 1989, pp. 37–67.
[39] R.J Krane, Second-law analysis of thermal energy storage systems: latent heat systems, in: Energy Storage Systems, Kluwer Academic Publishers, Dordrecht, 1989, pp. 69–88.
[40] S.M. Zubair, M.A. Al-Naglah, Thermoeconomic optimization of a sensible-heat thermal energy-storage system: a complete storage cycle, J. Energy Res. Technol. 121 (1999) 286–294.
[41] H. Bjurstrom, B. Carlsson, An exergy analysis of sensible and latent heat storage systems, Heat Recov. Syst. 5 (1985) 233–250.
[42] B. Mathiprakasam, J. Beeson, second law analysis of thermal energy storage devices. *Proc. AIChE Symp. Series, National Heat Transfer Conference*, Seattle, Washington.
[43] M.J. Taylor, R.J. Krane, J.R. Parsons, Second-Law optimization of a sensible heat thermal energy storage system with a distributed storage element—part I: development of the analytical model, ASME J. Energy Resour. Technol. 113 (1991) 20–26.
[44] J.K. Kuhn, G.F. VanFuchs, A.P. Zob, Developing and upgrading of solar system thermal energy storage simulation models, draft report for DOE, Boeing Comput. Serv. Company (1980).
[45] W.F. Phillips, R.A. Pate, Mass and energy transfer in a hot liquid energy storage system, in: Proceedings of the American Section of the International Solar Energy Society, Orlando, Florida, 1977.
[46] H. Schlichting, K. Gersten, Boundary Layer Theory, eighth ed., Springer, 2003.
[47] M.A. Rosen, The exergy of stratified energy storages, Sol. Energy 71 (3) (2001) 173–185.
[48] P. Mavros, V. Belessiotis, D. Haralambopoulo, Stratified energy storage vessels: characterization of performance and modelling of mixing behaviour, Sol. Energy 52 (4) (1994) 327–336.
[49] S.M. Han, S.T. Wu, Computer simulation of a solar energy system with a viscous-entrainment liquid storage tank model, in: Proceedings of the Third Southeastern Conference on Application of Solar Energy, 1978, pp. 165–182.
[50] H. Yoo, EE-Tong Pak, Theoretical model of the charging process for stratified thermal storage process, Sol. Energy 51 (6) (1993) 513–519.
[51] R.L. Cole, F.O. Bellinger, Natural thermal stratification in tanks, 1982, pp. 82–85. *Argonne National Laboratory Report* ANL-.
[52] F.J. Oppel, A.J. Ghajar, P.M. Moretti, Computer simulation of stratified heat storage, Appl. Energy 23 (1986) 205–224.
[53] Y.H. Zurigat, A.J. Ghajar, P.M. Moretti, Stratified thermal storage tank inlet mixing characterization, Appl. Energy 30 (1988) 99–111.
[54] Y.H. Zurigat, K.J. Maloney, A.J. Ghajar, A Comparison study of one-dimensional models for stratified thermal storage tanks, J. Sol. Energy Eng. 111 (1989) 204–210.
[55] D.J. Close, A design approach for solar processes, Sol. Energy 11 (2) (1967) 112–122.
[56] E.M. Kleinbach, W.A. Beckman, S.A. Klein, Performance study of one dimensional models for stratified thermal storage tanks, Sol. Energy 50 (2) (1993) 155–166.
[57] S. Alizadeh, An experimental and numerical study of thermal stratification in a horizontal cylindrical solar storage, Sol. Energy 66 (6) (1999) 409–421.
[58] G.F. Csordas, A.P. Brunger, K.G.T. Hollands, M.F. Lighstone, Plume entrainment effects in solar domestic hot water systems employing variable-flow-rate control strategies, Sol. Energy 49 (6) (1992) 497–505.
[59] A.M.C. Chan, P.S. Smereka, D. Giusti, A Numerical study of transient mixed convection flows in a thermal storage tank, ASME J. Solar Energy Eng. (105) (1983) 246–253.
[60] A. Cabelli, Storage tanks – a numerical experiment, Sol. Energy 19 (1977) 45–54.
[61] K.L. Guo, S.T. Wu, Numerical study of flow and temperature stratifications in a liquid thermal storage tank, ASME J. Solar Energy Eng. 107 (1985) 15–20.
[62] C.J. Hoogendoorn, R.G. Bakker, E.J.J Herweijer, W. Plokker, Thermal stratification in water vessels for energy storage, in: INTERSOL 85: Proc. 9th Biennial Congress Int. Solar Energy Sot., Montreal, Canada, 1985, pp. 829–833.
[63] J. van Berkel, Mixing in thermally stratified energy storage stores, Sol. Energy 58 (4 – 6) (1996) 203–211.
[64] J. van Berkel, C.C.M. Rindt, A.A. van Steenhoven, Thermocline dynamics in thermally stratified store, Int. J. Heat Mass Transfer (2002) 343–356.
[65] S.S. Shy, Mixing dynamics of jet interaction with a sharp density interface, Exp. Thermal Fluid Sci. 10 (1995) 355–369.
[66] M.A. Hussain, M.W. Wildin, Studies on mixing on the inlet side of the thermocline in diurnal stratified storage, in: Proceedings in Thermastock 1991, Scheveningen, The Netherlands, 1991, pp. 5–7. *pp 8.5-1 through 8*.
[67] G.C. Christodoulou, Interfacial mixing in stratified flows, I. Hydraulic Res. 24 (2) (1986) 17–92.
[68] Ruey-Jong Shyu, Jian-Yuan Lin, Liang-Jyi Fang, Thermal analysis of stratified storage tanks, ASME J. Solar Energy Eng. 111 (1989) 54–61.
[69] S.J. Caughey, S.G. Palmer, Some aspects of turbulence through the depth of the convective boundary layer, J. R. Met. Soc. 105 (1979) 811–827.
[70] R.A. Brost, J.C. Wyngaard, A.H. Lenschow, Marine stratocumulus layers. Part 11. Turbulence Budgets, J. Atmos. Sci. 39 (1982) 81S837.
[71] S. Knudsen, G.L. Morrison, M. Behnia, S. Furbo, Analysis of flow structure and heat transfer in vertical mental heat exchanger, Sol. Energy 78 (2005) 281–289.
[72] Jose Fernandez-Seara, Francisco J, Jaime Sieres Uiah, Experimental analysis of a domestic electric hot water storage tank. Part II: dynamic mode of operation, Appl. Therm. Eng. 27 (2007) 137–144.
[73] N.M. Al-Najem, M.M. El-Reface, A numerical study for the prediction of turbulent mixing factor in thermal storage tanks, Appl. Therm. Eng. 17 (1997) 1173–1181.
[74] Louise Jivan Shah, Simon Furbo, Entrance effects in solar storage tanks, Sol. Energy 75 (2003) 337–348.
[75] J.H. Davidson, D.A. Adams, J.A. Miller, A coefficient to characterize mixing in solar water storage tanks, ASME J. Solar Energy Eng. 116 (1994) 94–99.
[76] Y. Chia-Shun, Dynamics of Nonhomogeneous Fluids, first ed., Macmillan Series in Advanced Mathematics and Theoretical Physics, 1965.
[77] J.S. Turner, Buoyancy Effects in Fluids, Cambridge University Press, 1973.
[78] A.A. Dehghan, A. Barzegar, Thermal performance behaviour of a domestic hot water solar storage tank during consumption operation, Energy Convers. Manage. 52 (2011) 468–476.
[79] E. Papanicolaou, V. Belessiotis, Phenomena and conjugate heat transfer during cooling of water in an underground thermal storage tank, J. Heat Transfer 126 (2004) 84–96.
[80] Rejane De Cesaro Oliveski, Arno Krenzinger, A Horacio, Vielmo, Cooling of cylindrical vertical tanks submitted to natural internal convection, Int. J. Heat Mass Transfer 46 (2003) 2015–2026.
[81] J.C. Patterson, S.W. Armfield, Transient features of natural convection in a cavity, J. Fluid Mech. 219 (1990) 469–497.
[82] Jae Min Hyun, Transient process of thermal stratifying an initially homogeneous fluid in an enclosure, Int. J. Heat Mass Transfer 27 (1984) 1936–1938.
[83] John Patterson, Jorg Imberger, Unsteady natural convection in a rectangular cavity, J. Fluid Mech. 100 (1980) 65–86.

[84] R.J. Shyu, C.K. Hsieh, Unsteady natural convection in enclosure with stratified medium, ASME J. Solar Energy Eng. 109 (1987) 127–133.
[85] Jianhua Fan, Simon Furbo, Buoyancy driven flow in a hot water tank due to standby heat loss, Sol. Energy 86 (2012) 3438–3449.
[86] C.K. Yee, F.C. Lai, Effects of a porous manifold on thermal stratification in a liquid storage tank, Sol. Energy 71 (4) (2001) 241–254.
[87] J.E.B. Nelson, A.R. Balakrishnan, M.S. Srinivasa, Parametric studies on thermally stratified chilled water storage systems, Appl. Therm. Eng. 19 (1999) 89–115.
[88] C.W. Miller, The effect of a conducting wall on a stratified fluid in a cylinder, in: Proceedings of the AIAA 12th Thermophysics Conference, Albuquerque, U.S.A., 1977, pp. 1–9.
[89] C. Sherman, B.D. Wood, J. Masson, Effect of vertical wall conduction on temperature relaxation in thermally stratified liquid thermal storage tanks, in: Proceedings of ISES Conference, Atlanta, U.S.A., 1979, pp. 591–595.
[90] S. Satyanaryana Murthy, J.E.B. Nelson, T.L. Sitharama Rao, Effect of wall conductivity on thermal stratification, Sol. Energy 49 (1992) 273–277.
[91] F. Parrini, S. Vitale, L. Castellano, Rational analysis of mass, momentum and heat transfer phenomena in liquid storage tanks under realistic operating conditions: 2. Application to a feasibility study, Sol. Energy 49 (1992) 95–106.
[92] Y.H. Zurigat, P.R. Liche, A.J. Ghajar, Influence of the inlet geometry on mixing in thermocline thermal energy storage, Int. J. Heat Mass Transfer 34 (1) (1991) 115–125.
[93] P.C. Eames, B. Norton, The effect of tank geometry on thermally stratified sensible heat storage subject to low Reynolds number flows, Int. J. Heat Mass Transfer 1 (4) (1998) 2131–2142.
[94] N. Altuntop, M. Arslan, V. Ozceyhan, et al., Effect of obstacles on thermal stratification in hot water storage tanks, Appl. Therm. Eng. 5 (14) (2005) 2285–2298.
[95] N.M. Al-Najem, M.M. El-Reface, A numerical study for the prediction of turbulent mixing factor in thermal storage tanks, Appl. Therm. Eng. 17 (1997) 1173–1181.
[96] A. Aviv, S. Morad, Y. Ratzon, G. Ziskind, R. Letan, Experimental and numerical study of mixing in a hot-water storage tank, ASME J. Solar Energy Eng. 131 (1) (2009) 1–6.
[97] J.D. Chung, S.H. Cho, C.S. Tae, H. Yoo, The effect of diffuser configuration on thermal stratification in a rectangular storage tank, Renew. Energy 33 (10) (2008) 2236–2245.
[98] Ignacio José Moncho-Esteve, María Gasque, Pablo González-Altozano, Guillermo Palau-Salvador, Simple inlet devices and their influence on thermal stratification in a hot water storage tank, Energy Build. 150 (2017) 625–638.
[99] P.F. Carlsson, Heat storage for large low flow solar heating system, in: Proceedings of ISES Solar World Congress, 5, 1993.
[100] K.K. Matrawy, I. Farkas, Optimum mass flow rate through the solar domestic hot water system, in: Provisional proceedings of Eurotherm, 49, 1996, pp. 39–46. seminar number.
[101] J Nico, L. van Ruth, New type of valve for solar thermal storage tank stratification, Energy Procedia 91 (2016) 246–249.
[102] S. Wang, J.H. Davidson, Selection of permeability for optimum performance of a pours tube thermal stratification manifold, Sol. Energy 112 (2015) 472–485.
[103] Janne Dragsted, Simon Furbo, Mark Dannemand, Federico Bava, Thermal stratification built up in hot water tank with different inlet stratifiers, Sol. Energy 147 (2017) 414–425.
[104] Louise Jivan Shah, Elsa Andersen, Simon Furbo, Theoretical and experimental investigations of inlet stratifiers for solar storage tanks, Appl. Therm. Eng. 25 (2005) 2086–2099.
[105] E. Andersen, S. Furbo, Fabric inlet stratifiers for solar tanks with different volume flow rates, in: Proceedings EuroSun 2006 Congress, Glasgow, Scotland, 2006.
[106] E. Andersen, S. Furbo, M. Hampel, W. Heidemann, H. Müller-Steinhagen, Investigations on stratification devices for hot water heat stores, Int. J. Energy Res. 32 (2008) 255–263.
[107] Eugenio García-Marí, María Gasque, Rosa Penélope Gutiérrez-Colomer, Federico Ibáñez, Pablo González-Altozano, A new inlet device that enhances thermal stratification during charging in a hot water storage tank, Appl. Therm. Eng. 61 (2) (2013) 663–669.
[108] A. Bouhdjar, A. Harhad, Numerical analysis of transient mixed convection flow in storage tank: influence of fluid properties and aspect ratios on stratification, Renewable Energy 25 (2002) 555–567.
[109] M.A. Abdoly, D. Rapp, Theoretical and experimental studies of stratified thermocline storage of hot water, Energy Convers. Manage. 22 (1982) 275.
[110] L.P. Chauvet, S.D. Probert, D.J. Nevrala, Thermal-energy stores for supplying domestic hot-water and space-heating, Appl. Energy 48 (2) (1994) 163–190.
[111] K. Hariharan, K. Badrinarayana, S. Srinivasa Murthy, M.V. Krishna Murthy, Temperature stratification in hot-water storage tanks, Energy 16 (7) (1991) 977–982.
[112] N.J.E. Bhasker, M.V. Krishnamurthy, Research Report on Experimental Studies of Thermal Stratification, IIT, Madras, India, 1978.
[113] P. Armstrong, D. Ager, I. Thompson, M. McCulloch, Improving the energy storage capability of hot water tanks through wall material specification, Energy 78 (2014) 128–140.
[114] María Gasque, Pablo González-Altozano, Daniel Maurer, Ignacio José Moncho-Esteve, Rosa Penélope Gutiérrez-Colomer, Guillermo Palau-Salvador, Eugenio García-Marí, Study of the influence of inner lining material on thermal stratification in a hot water storage tank, Appl. Therm. Eng. 75 (2015) 344–356.
[115] Ulrike Jordan, Simon Furbo, Thermal stratification in small solar domestic storage tanks caused by draw-offs, Sol. Energy 78 (2005) 291–300.
[116] J. Van Berkel, C.C.M. Rindt, A.A. Van Steenhoven, Modelling of two layers stratified stores, Sol. Energy 67 (1–3) (1999) 65–78.
[117] R.M. Ramsayer, Numerische Untersuchung der Strömungs und Wärme transportvorgänge bei der thermischen Beladung eines Warmwasserspeichers, Institut Für Thermodynamik und Wärmetechnik, Universität Stuttgart, Germany, 2001 Student report.
[118] B.J. Sliwinski, A.R. Mech, T.S. Shih, Stratification in thermal storage during charging, International Conference on Heal Transfer, 1978.
[119] N.M. Brown, F.C. Lai, Experimental study of stratification in a liquid storage tank with a pours manifold, in: *Proceedings of HT - FED04, ASME Heat transfer/Fluids Engineering* Summer Conference, North Carolina, 2004.
[120] M.A. Al-Nimr, Temperature distribution inside a solar collector storage tank of finite wall thickness, ASME J. Solar Energy Eng. 115 (1993) 112–116.
[121] Hoseon Yoo, Charn-Jung Kim, Chang Wook Kim, Approximate analytical solutions for stratified thermal storage under variable inlet temperature, Sol. Energy 66 (1) (1999) 47–56.
[122] Mi-Soo Shin, Hey-Suk Kim, Dong-Soon Jang, Sang-Nam Lee, Young-Soo Lee Hyung-Gi Yoon, Numerical and experimental study on the design of a stratified thermal storage system, Appl. Therm. Eng. 24 (2004) 17–27.
[123] R. Huhn, Beitrag zur thermodynamischen Analyse und Bewertung von Wasserwarmespeichern in Energieumwandlungsketten. Ph.D. Thesis, Technische Universitat Dresden, Germany,
[124] R.J Shyu, J.Y. Lin, L.J. Fang, Thermal analysis of stratified storage tanks, ASME J. Solar Energy Eng. 111 (1989) 54–61.
[125] V. Panthalookaran, W. Heidemann, H. Muller-Steinhagen, A new method of characterization for stratified thermal energy stores, Sol. Energy 81 (2007) 1043–1054.
[126] Ibrahim Dincer, Marc A. Rosen, Thermal Energy and Storage Systems and Applications, second ed., Wiley.
[127] M.Y. Haller, C.A. Cruickshank, W. Streicher, S.J. Harrison, E. Andersen, S. Furbo, Methods to determine stratification efficiency of thermal energy storage processes – review and theoretical comparison, Sol. Energy 83 (2009) 1847–1860.
[128] W.P. Bahnfleth, J. Song, Constant flow rate charging characteristics of a full-scale stratified chilled water storage tank with double-ring slotted pipe diffusers, Appl. Therm. Eng. 25 (2005) 3067–3082.
[129] A.M. Kandari, Thermal stratification in hot storage-tanks, Appl. Energy 35 (1990) 299–315.
[130] D.E. McCarthy, B.D. Wood, Experimental investigation of solar storage tank stratification coefficients, in: Proceedings of the Journal of Solar Energy Engineering, Conference American Solar Energy Society, American Solar Energy Society, Boulder, 1990, pp. 95–100.
[131] L. Wu, R.B. Bannerot, Experimental study of the effect of water extraction on thermal stratification in storage, in: Proceedings of the 1987 ASME-JSME-JSES Solar Energy Conference, Honolulu, 1987, pp. 445–451.
[132] J.E.B. Nelson, A.R. Balakrishnan, S.S. Murthy, Experiments on stratified chilled water tanks, Int. J. Refrig. 22 (1999) 216–234.
[133] M.A. Rosen, R. Tang, I. Dincer, Effect of stratification on energy and exergy capacities in thermal storage systems, Int. J. Energy Res. 28 (2004) 177–193.
[134] K.O. Homan, Internal entropy generation limits for direct sensible thermal storage, ASME J. Energy Resour. Technol. 125 (2003) 85–93.
[135] J. van Berkel, Thermocline entrainment in stratified energy stores Ph.D. Thesis, Technische Universiteit Eindhoven, The Netherlands, 1997.
[136] Sameti, Haghighat, Optimization approaches in district heating and cooling thermal network., Energy Build. 140 (2017) 121–130.
[137] Sameti, Haghighat, Integration of distributed energy storage into net-zero energy district systems: optimum design and operation, Energy 153 (2018) 575–591.
[138] Sameti, Haghighat, Optimization of 4th generation distributed district heating system: design and planning of combined heat and power, Renew. Energy 130 (2019) 371–387.
[139] Samite, A new design of solar water storage wall: a system-level model and simulation, Energy Syst. 9 (2018) 361–383.

Renewable Energy 154 (2020) 1165–1179

Contents lists available at ScienceDirect

Renewable Energy

journal homepage: www.elsevier.com/locate/renene

Numerical prediction of the stratification performance in domestic hot water storage tanks

Yogender Pal Chandra [a, *], Tomas Matuska [b]

[a] Department of Environmental Engineering, Faculty of Mechanical Engineering, Czech Technical University in Prague, Technicka 4, 166 07, Prague 6, Czech Republic

[b] University Centre for Energy Efficient Buildings, Czech Technical University in Prague, Trinecka 1024, 273 43, Bustehrad, Czech Republic

ARTICLE INFO

Article history:
Received 13 November 2019
Received in revised form
25 February 2020
Accepted 17 March 2020
Available online 20 March 2020

Keywords:
Thermal stratification
Thermal energy storage
Domestic hot water tank

ABSTRACT

An efficient storage retains thermal stratification and improves the discharging performance. Turbulent mixing between hot and cold water is the prime source of stratification destruction. In this paper quantification of turbulent missing was achieved on the basis of temperature profile, MIX number, and Richardson number. The evaluated parameters include flow rate, ΔT, and diffuser design, henceforth a direct interdependence between each was thus established. Various CFD models were developed and experimentally validated on the test rig in order to find the optimal working conditions in discharge mode. The results proved numerically that the tank working conditions can be optimized by proper selection of inlet device. For instance, slotted type inlet device sustained maximum stratification even in as adverse a condition as of turbulent inflow & low ΔT. Perforated and simple inlet devices were capable of delivering best discharge efficiency only at low flow rate of 200 l/h and were showing insignificant dependency on ΔT. However, as flow rate is increased, ΔT dependency increased. Seeing the compounded benefits of slotted inlet devices and decreased ΔT, it was concluded that slotted inlet device delivered comparatively better thermal performance at both adverse conditions i.e. high flow & low ΔT and high flow & high ΔT, however, failed to outshine the rest of the inlet devices at low flow rate & low ΔT, and low flow rate & high ΔT. These research findings can serve as guidelines to optimize the storage tank design – more specifically, inlet device based design integrated with heating system, as thermal stratification and COP of heating system – heat pumps, for example, are inherently correlated. Heat pumps are high flow rate and low ΔT devices, while, solar systems are low flow rate and high ΔT devices, Thus, opting for accurate choice of inlet device for a particular operating condition is critical.

1. Introduction

Thermal energy storage (TES) is the essential part of renewable energy systems. This is because it is the best solution against non-coincidence of supply and demand, especially with solar systems. Improving the performance of this central component can significantly decrease the auxiliary energy demand for both the space and domestic hot water heating [1]. For designing or performing building energy simulations of heating systems including the storage tanks it is essential to adopted the integrated and dynamic simulation approach. Campos Celador et al. [16] demonstrated that storage tank model can have significant effect on annual savings and subsequent decision making right at the design phase of the system. Stratified storage tanks are cost effective building heating technology leading to reduction in auxiliary heating demands, reduction in primary energy savings, discounting the consumer costs, while promoting the lower carbon footprints [17,18].

Thermal stratification is the phenomenon usually employed and encouraged to improve the performance of storage tanks i.e. enhanced charging and discharging efficiency [1,2]. Thermal stratification ensures the hot and cold water to be stored simultaneously without any physical barrier inside the tank. In other words, continuous or stepped water temperature distribution is practiced in stratified tank. More precisely, hot water driven by buoyancy has the tendency to rise towards the upper fluid layers in the tank, while cold water has the tendency to settle at the bottom of the tank. This phenomenon naturally creates the stratification in

* Corresponding author.
E-mail addresses: yogenderpal.chandra@fs.cvut.cz, yogender027mae@gmail.com (Y.P. Chandra), tomas.matuska@fs.cvut.cz (T. Matuska).

https://doi.org/10.1016/j.renene.2020.03.090
0960-1481/

Nomenclature

C_p	specific heat capacity [J/kg-K]
E_j	energy content of jth fluid layer
g	acceleration due to gravity (m/s^2)
L	characteristic length pertaining to tank (m)
$\dot{m}$	mass flow rate (kg/m^3)
m_{store}	mass of stored water (kg)
M_E	moment of energy (J m)
MIX	MIX number
M_{exp}	moment of energy of experimental tank (J m)
$M_{ful\text{-}mix}$	moment of energy of fully mixed tank (J m)
M_{str}	moment of energy of perfectly stratified tank (J m)
q	internal heat generation [J/s-m]
r	unit replacement time (s)
Ri	Richardson number
t*	dimensionless time
T	temperature (^{o}C)
T_{in}	inlet temperature
T_{buk}	bulk storage temperature (^{o}C)
T_{inlet}	inlet temperature (^{o}C)
T_{outlet}	outlet temperature (^{o}C)
$T_{initial}$	initial tank temperature (^{o}C)
t	time (s)
u	velocity component in x direction (m/s)
u_{avg}	average velocity in x direction
v	velocity component in y direction (m/s)
$\dot{V}$	volumetric flow rate (l/h)
V_{in}	inlet velocity (m/s)
V_T	tank volume
w	velocity component in z direction
W	potential energy (J)
y_j	jth location of fluid layer

Greek

ρ	fluid density (kg/m^3)
β	coefficient of thermal expansion (1/K)
ΔT	bulk storage and inlet temperature difference (K)
∇	differential operator
λ	Thermal conductivity [W/K-m]
τ_{ij}	viscous stress [N/m2]
f_i	body force [N/kg]
μ	dynamic viscosity [kg.m/s]
η_d	discharging efficiency

Abbreviations

div	divergence operator
grad	gradient operator
K.E.	kinetic energy (J)

the tank. Abdelhak et al. [3] performed CFD simulations and studied the effect of inlet mixing for vertical and horizontal tanks. They concluded that vertical tanks are far better at inhibiting the vertical mixing. Fernandez et al. [6] studied three inlet-outlet devices and identified the most effective stratification sustaining device. Other important parameters include flow rate, the bulk storage & inlet temperature difference. Considerable research based on bulk storage and inlet temperature has been done by Baeten et al. [10]. The authors provided a novel method to model the buoyancy effects and the mixing between inlet and bulk fluid layers which can be implemented in the building energy simulations. Water jets and their effect on stratification as studied experimentally and numerically by Shah and Furbo [8] confirmed the interdependence of inlet design at different flow rate and the quality of stratification. A divergent conical type diffuser is supposed to suppress the mixing effects at inlet due to better diffusion of water thus enhancing stratification [11,12] while, bronze conical diffusers, PEX pipe, Solvis with/without T-pipe, and EyeCular Technologies stratifier are very frequently available [34]. In other situation, de-stratification can occur due to many factors such as ambient heat loss, heat conduction within fluid layers and tank wall, turbulent inlet mixing in dynamic mode [4,5]. Shin et al. [4] performed various bench scale and large-scale experiments and identified among various factors determining the stratification. The loading time critically influences the stratification performance. As loading time increases, stratification decreases. Fan and Furbo [5] studied the dynamics of stratification during heat loss to ambient. Heat loss factor was introduced and used to investigate the buoyancy driven currents between layers caused by natural convection.

A lot of research has been carried out to optimize the storage tanks with the help of computational fluid dynamics CFD [3,19]. Abdelhak et al. [3] numerically studied the heat transfer characteristics of vertical and horizontal tank. Authors concluded that mixing is restricted at the inlet of the vertical tank thus enhancing the stratification in contrast to the horizontal tank. Also, smaller Richardson number was obtained for horizontal tanks. Eames and Norton [19] studied the influence of tank geometry on stratification. Authors found that low inlet jet velocities subject to less cross-sectional dependency on thermocline development. It was also evident in the research that single jet accommodating variable temperature inlet degrades the thermal stratification. Many authors performed finite volume analysis to study thermocline dynamics and inflow geometry dependency. CFD performance parameters such as temperature and streamline contours, were studied along with stratification numbers, discharging/charging efficiency, Richardson number [7]. Kaloudis et al. [9], El-Amin et al. [21], Simon and Wenxian [20] explored the temperature evolution at different heights of the tank during the dynamic cycles of charging or discharging and compared the results for different inlet device positions and types using a three-dimensional finite volume approach. Kaloudis et al. [9] performed Large Eddy Simulation (LES) on the thermocline development and mixing process during discharging. Thermocline thickness, entropy and exergy generation were subsequently calculated to quantify mixing. Two distinct phases of discharging process were identified – intrusion region at the early stage of discharge, and the resultant mixing during overall process. El-Amin et al. [21] performed finite volume method (FVM) and PIV analysis of the turbulent horizontal jet inlet in the storage tanks. Authors visualized the stratification phenomena through CFD contours and PIV methods. Altuntop et al. [22] numerically studied the influence of obstacles on stratification in hot water tanks. Tank with obstacles having a hole at the center appeared to have better stratification then tank without any obstacle. Han et al. [23], in their review work stated that the numerical simulations are undoubtedly becoming the most attractive tools to visualize the complex thermocline behavior in hot water storage tanks based on renewable energy perspective. Numerical simulations based on finite volume methods critically depend upon the assumptions and the quality of model. Likewise, Haller et al. [24] stated that two-dimensional analysis overestimates the thermocline thickness, henceforth, three dimensional simulations are more practical in simulating the more complex fluid behavior in thermal storage

tanks. Khurana et al. [25], Savicki et al. [26], Zachár [27], Toyoshima and Okawa [28], Njoku et al. [29], Gasque et al. [30] performed three dimensional simulations to capture the physics behind the stratified flows in the hot water storage tanks. Khurana et al. [25] studied the influence of ribs in the storage tank. The authors concluded that process of stratification takes place more slowly in the ribbed tank then in the smooth walled tank. These ribs are demonstrated to be simple means to reduce stratification in the liquid hydrogen. Savicki et al. [26] developed and studied 3D model of cylindrical storage tank and established some correlation to predict the temperature profile and thermal stratification with time. These correlations are said to facilitate the modelling of solar collectors and thermal storage tanks as it can provide the reference data without having to do experiments on experimental facility. Toyoshima and Okawa [28] performed experimental and 3D CFD of the impinging buoyant jet and its effect on the transient temperature distribution in the tank.

Empirical correlation was proposed to predict the height of the impinging vortex relative to momentum and buoyancy of the inlet jet, which was finally supplemented by 3D CFD analysis. Njoku et al. [29] in their overview study detailed all the practices in the CFD modelling in the recent past. Accordingly, authors favored 3D modelling rather then 2D for Energy and Exergy analysis of storage tanks. Authors also mentioned about the usage of Artificial Neural Networks (ANN) in 1D modelling of stratified tanks. Geczy-Vıg and Farkas [31], for example developed an ANN model to predict the stratified layer temperatures in the storage tank with an accuracy of as low as 0.77 °C and 0.22 °C with load and no-load conditions respectively. ANN modelling requires a large amount of experimental data, as training and validation are its intrinsic part. Neurons are first trained on the experimental data and then validated subsequently on different set of data which is not seen by the neurons to keep the overfitting checked. Kalogirou and Panteliou [32] trained ANN to predict the long-term performance of solar domestic hot water storage systems in terms of monthly hot water output from a draw-off of 35 °C and 40 °C. Wang et al. [33] developed and performed numerical and experimental study on the novel equalizer. They analyzed their device by calculating temperature profile, MIX number, and fill efficiency. Authors recognized the flow suppressing influence of their device which resulted in less mixing as demonstrated by reduced MIX number and other indices.

The motivation of this work is to assess the operational characteristics of hot water storage tanks during dynamic cycle. The results of which later can be executed in storage devices based on discrete heat addition type – heat pump or otherwise. To begin with, experimental study of discharging process with simple inlet was carried out. Stratification assessment was done with the assistance of different performance indices – MIX number, Richardson number and temperature profiles and discharging efficiency. The discharging process with simple inlet was numerically simulated and was further compared with the CFD model of slotted and perforated inlet.

2. Experimental characterization – application to simulated methods

The experimental setup as shown in Fig. 1 consists of primary cylindrical hot water storage tank with following parameters: 397 L in volume, 550 mm diameter and 1905 mm overall height. Tank diameter along with insulation is nearly 750 mm, top insulation thickness is 120 mm while bottom insulation thickness is 50 mm. The tank is connected to the secondary cold tank which is almost double the size, and acts as the source for cold water inlet. In addition, cold tank is connected to the thermostatic chiller to cool it down after each discharging cycle. Each tank is incorporated with an expansion vessel to accommodate any volumetric change during heating/cooling. To measure the vertical distribution of temperature, 20 PT-100 temperature sensors were attached around the outside of tank wall in the vertical direction, dividing the tank into 20 equal fluid segments. The distance between adjacent sensors was 8 cm. 2 PT-100 sensors were also placed at inlet and at outlet of the tested tank to track incidental temperature deviations. Charging of the tank was performed using two methods. Firstly, by thermostatically controlled electric heater which is present in the lower half of the tank, secondly, by an external electric boiler. Experimental tank can be set for various mixed conditions, 60 °C and 50 °C for example. Discharging process is carried out by regulating manually operated one-way valve as shown in Fig. 1 (b). There are basically two water circuits, in addition to external heater or boiler circuit. The circuit involving cold water tank and hot water tank and, the circuit involving the cold-water tank and the thermostatic chiller. The Discharging process includes shutting off the chiller circuit by regulating various manual valves and carefully following the flowmeter readout for the flow of 200, 400, 600 and 800 l/h. The sensor outputs were recorded by *ALMEMO* data acquisition system at 5 s intervals. Flow rate was measured by *Sitrans F M Mag 5000* flow meter which is a transmitter-based flow meter by *Siemens* with an accuracy of 0.4% ± 1 mm/s. When discharging process was completed the tank to tank circuit was shut down and the chiller circuit is opened to cool down the cold tank for further experiments. Experiments were replicated to assess the experimental accuracy and error analysis was performed.

2.1. Parametric analysis and energy methods

A series of experiments with different flow rates was performed. The experiment results obtained with simple inlet device were used to validate CFD simulations. Initially, the water in the tank was uniformly heated to 60 ± 0.5 °C by the electric heater to ensure that the water in the tank had the same initial temperature and had no thermal stratification. The inlet water temperature was maintained at 10 ± 0.5 °C during discharging. The discharging test of each inlet was carried out at four flow rates i.e. 200 l/h, 400 l/h, 600 l/h, and 800 l/h. The temperature distribution and outflow water temperature were recorded in order to analyze the influence of the flow rates on the vertical temperature distribution in the tank during discharging. The evolution of temperature with dimensionless time (t*) at different nodal location (20 nodes) is shown in Fig. 2. The dimensionless time (t*) was calculated by dividing the current discharging time (in the time series) with the unit replacement time as established by Eq. (1). To illustrate, the replacement time is defined as the time taken by the volume of water in the tank to be fully replaced by incoming cold water, thus unit replacement time differs for different inlet flow rates. Each experiment actually lasted a unit replacement time.

$$t^* = \frac{t}{r} \tag{1}$$

$$r = \frac{V_T}{\dot{V}} \tag{2}$$

The experimental results were analyzed in one-unit replacement time at different flow rates. When the flow rate was 200 l/h, the unit replacement time was 1.98 h. Similarly, the unit

(a)

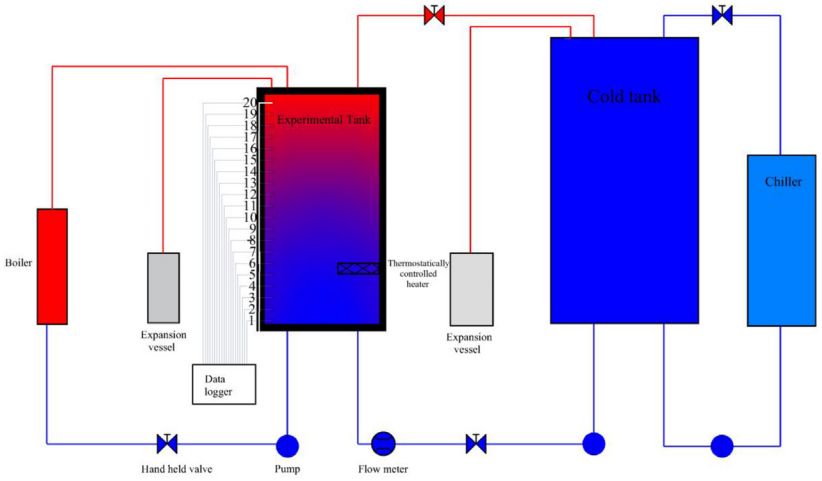

(b)

Fig. 1. Schematic of experimental setup.

replacement time for 400, 600, and 800 l/h's is 0.99, 0.66 and 0.50 h respectively. It is quite apparent that 200 l/h exhibits better stratification as compared to rest of the flow rates. Temperature values of the upper layers are higher and more stable than their counter parts for higher flow rates. Mixing is highest for 800 l/h. Top 20th layer is showing unusual behavior for all the flow rates, as it is not playing any role in the discharging process, due to its geometrical presence above the tank outlet, which actually doesn't participate in plug flow. The temperature of the 18th layer is on its lowest value of 52 °C for 800 l/h while its 59.2 for 200 l/h during 60% of discharge.

2.1.1. MIX number

MIX number evaluates the tank on the basis of both vertical temperature distribution and the total energy stored in the tank [13,14] (Eq. (4)). This is in contrast to assessment of temperature profiles where vertical temperature gradients or the temperature deviations in the tank are evaluated with time. Accordingly, it postulates the mixing process in the tank by evaluating the moment of energy M_E of individual water layers [15]. Moment of energy of thermal storage tank is calculated to account for energy location by summation of the sensible energy content up to *j*th vertical segment, weighted with the height of its location, as given by Eq. (3).

$$M_E = \sum_{j=1}^{j} y_j.E_j \tag{3}$$

$$MIX = \frac{M_{str} - M_{\exp}}{M_{str} - M_{full-mix}} \tag{4}$$

Fig. 3 shows the calculated values of MIX number for 60–10 °C discharging process at flow rates of 200, 400, 600 and 800 l/h respectively. MIX number varies between 0 and 1 as suggested by Eq. (4). 200 l/h has the lowest ascent, followed by 400 l/h, then 600 l/h; finally, 800 l/h has the highest ascent of MIX number. It is evident from figure that at t* = 0.4 MIX number for 200 l/h is approximately 0.4 while for 800 L/h it is 0.6.

2.1.2. Richardson number

Richardson number is quite prominently used to assess stratification by many authors [8]. This dimensionless number characterizes the ratio between potential energy required for vertical mixing and the turbulent kinetic energy available for such process. A small *Ri* number signifies mixed storage, while high *Ri* number

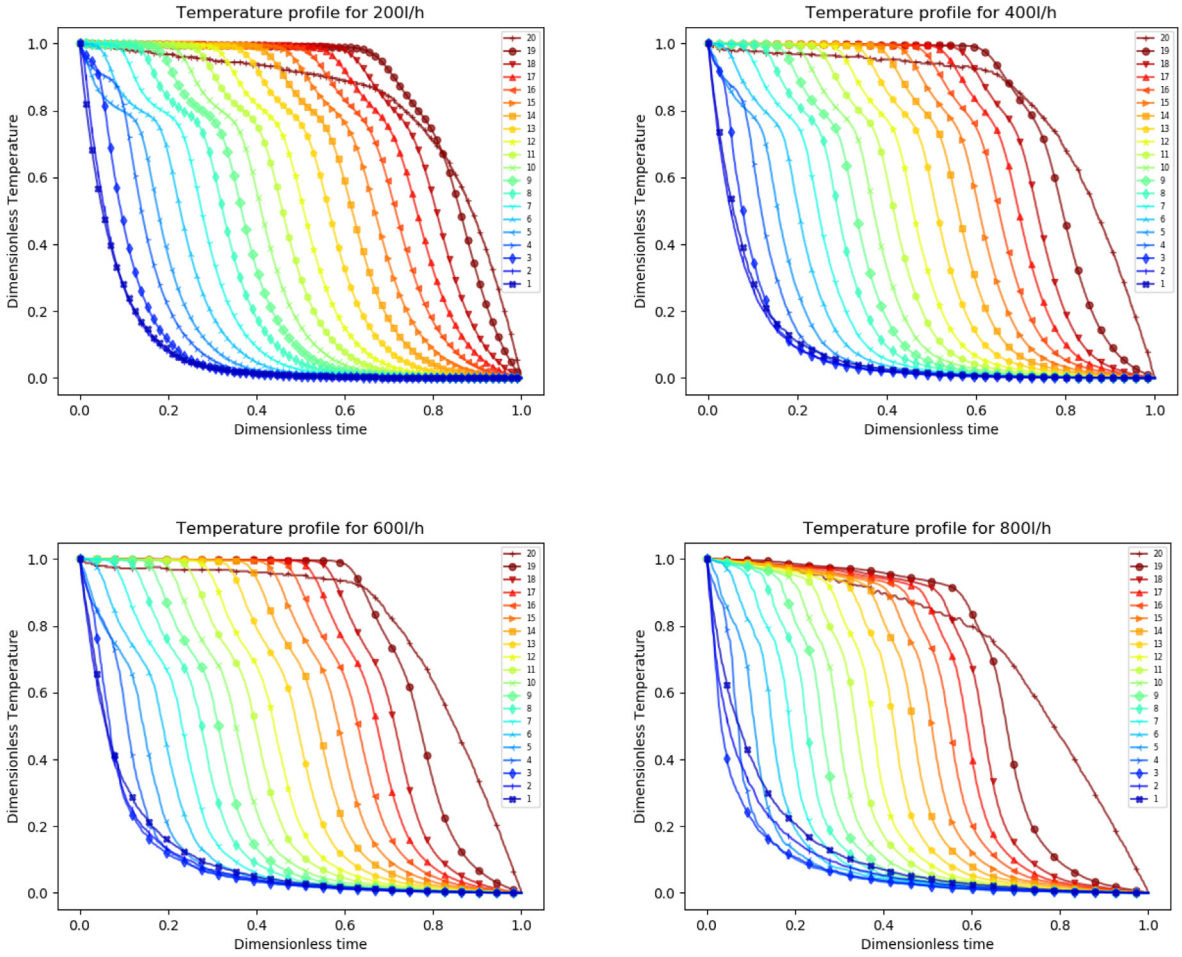

Fig. 2. Temperature evolution at different flow rates.

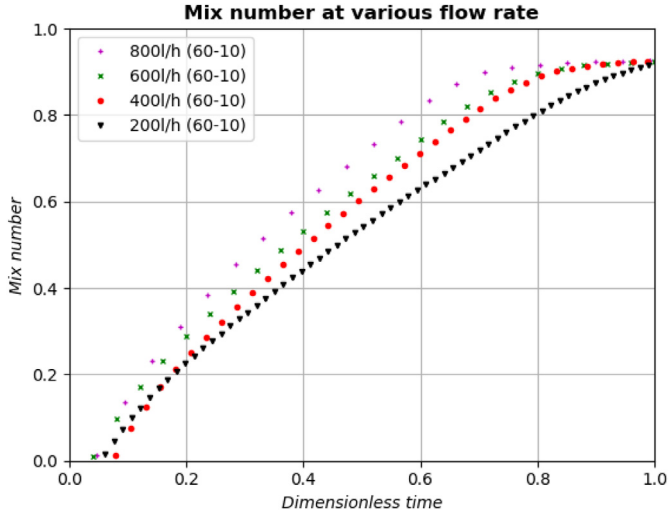

Fig. 3. MIX number evaluation.

indicates stratified one. This is explained in Eqs. (5) and (6)

$$Ri = \frac{W}{K.E.} = \frac{\frac{g}{\rho}\frac{d\rho}{dz}}{\left(\frac{\delta v}{\delta z}\right)^2} \tag{5}$$

$$Ri = \frac{g\beta\Delta TL}{\nu^2} \tag{6}$$

Whenever two fluids with different density interact, buoyancy force comes into picture and influences mixing and motion of two fluids, thus determining stratification. In reality, the Richardson number ($Ri = Gr/Re^2$) is always considered an influential factor. Fig. 4 represents the evolution of the Richardson number as a function of the dimensionless time for different discharging processes. As per definition, tank sustains better stratification at lower flow rates. In other words, Ri is increased as flow rate is decreased from 800 to 200 l/h. For example, Ri at $t^* = 0.6$ for 800 l/h is nearly 75, while for 200 l/h it is approximately 120, t^*=0.6 being the dimensionless time at which 60% of tank volume is already discharged.

2.2. Error analysis

Quantification of data uncertainty is an important part in predicting the precision of the measured random variables. In the series of measurements demonstrated above, time series data was dealt with. With this type of data series, statistical parameters such as mean, standard deviations, probabilistic distribution of error (gauss distribution) etc. can be easily employed to understand the data variability, uncertainty propagation and the error analysis. A series of experiments were performed on the single variable set to confirm reproducibility of the results. Consequently, percentage

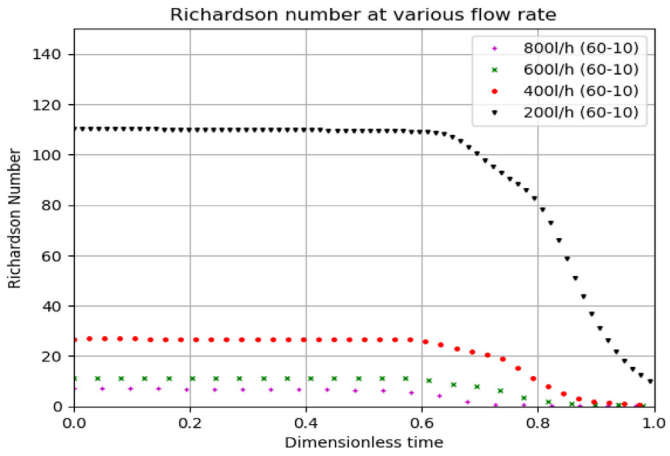

Fig. 4. Richardson number evaluation.

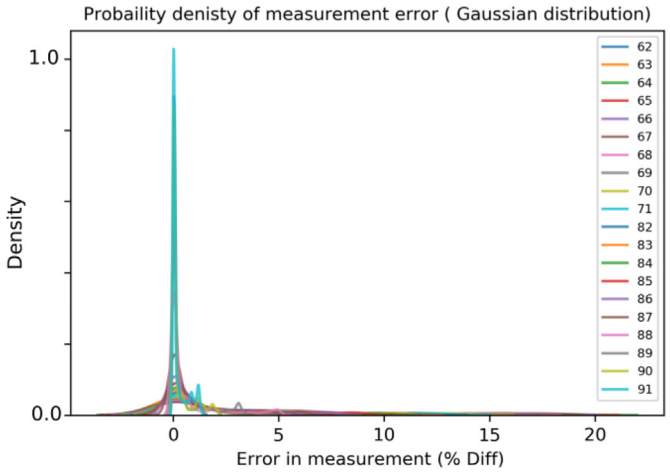

Fig. 5. Probability distribution of Error.

error was determined on each progressive and consecutive set of data points. This was resumed until the 90% of the data values fall within 1 or 2 standard deviation. Fig. 5 shows the probability density distribution of the error measurement of one the consecutive set of data points. It is nearly normally distributed. More than 95% of the values fall within 5% of the error. Fig. 6 shows the count of the measured values of each of the temperature sensor and the error associated with it. It demonstrates statistically, that rather 600 data values have next to 0–0.5% error. There are some values with 5% and even 15% error but these values are not dense. In addition, uncertainties of the measuring devices used in the experiments are given in Table 1.

3. Numerical modelling

3.1. Physical domain and conditions

Computational domain serves as the model of the physical tank under test which was described in section 2. It is created with three distinct cell zone conditions, first for the fluid volume, second for the tank wall thickness and the third for the tank insulation. Incoming fluid has the uniform temperature and velocity. Three distinct geometries of tank inlet namely simple inlet, perforated inlet and slotted inlet are considered. All the geometric models are created in space claim modeler of the *ANSYS* academic research, version 19.2. Geometry creation was followed by mesh generation, and finally 3D transient simulation was performed. The approach of polyhedral mesh was appropriately chosen for the current geometry due to its promising accuracy and faster convergence in fewer iteration. Grid refinement and optimization procedures were adopted and minimum orthogonal quality of 0.45 was ensured. The mesh is more refined at the inlet and outlet with addition of inflations layers to capture the velocity fluctuations. This greatly enhances the numerical accuracy. Mesh independency study was performed on the mesh sizes – 830 685 cells and 980 783 cells and 1 118 564. As the mesh with 1 118 564 cells did not provide improved results, mesh with 980 783 cells was adopted for further analysis, thus maintaining the best trade off between accuracy and computational time. The working assumptions are as follows: working fluid i.e. water is incompressible, any influence of viscous dissipation is neglected, and pressure gradients are assumed to be small enough that temperature dependence on pressure is negligible. Thermo-physical properties are temperature dependent, therefore, density, specific heat, dynamic viscosity, thermal conductivity is fitted with polynomial relation with temperature. Accordingly, after establishing the credibility of the results, with simple inlet device – through experimental validation and mesh independency study, all its working setup was finally regressed to the slotted and perforated inlet. Finally, predictability study was performed on slotted and perforated inlet devices and the results were compared with the simulated inlet. Fig. 7(a) and (b) illustrates perforated slotted inlet devices respectively. While Fig. 7(c) and (d) shows the meshed tank with simple inlet device as used in experimental environment.

3.2. Governing equations

Partial differential equations (PDEs) governing the fluid flow in tank includes continuity, momentum and energy equations. In accordance with fluid dynamics, Reynolds number at the inlet for 800 l/h discharge rate was found to be 6440 which makes the phenomenon in the turbulent regime. A variety of turbulence models are available to simulate turbulent flows for specific conditions. In this study, standard k-ϵ model was adopted to simulate the buoyancy induced mixing and stratification phenomenon. Equations (7)–(11) are represented in Cartesian coordinates below.

Continuity equation:

$$\nabla \cdot u_i = \frac{\partial u}{\partial x} + \frac{\partial v}{\partial y} + \frac{\partial w}{\partial z} = 0 \tag{7}$$

Energy equation:

$$\rho C_p \frac{\partial T}{\partial t} = div(\lambda \overrightarrow{grad} T) + T\beta \frac{\partial P}{\partial t} + q + \varphi \tag{8}$$

where,

$$\varphi = -\frac{2}{3}\mu(div\ \vec{u})^2 + 2\mu S_{ij}\frac{\partial u_i}{\partial x_j} \tag{9}$$

$$S_{ij} = \frac{1}{2}\left(\frac{\partial u_i}{\partial x_j} + \frac{\partial u_j}{\partial x_i}\right) \tag{10}$$

Momentum equation:

$$\frac{\partial(\rho u_i)}{\partial t} + \sum_{j=1}^{3}\frac{\partial}{\partial x_j}(\rho u_j u_i) = -\frac{\partial P}{\partial x_i} + \sum_{j=1}^{3}\frac{\partial \tau_{ij}}{\partial x_j} + \rho f_i \tag{11}$$

Boundary conditions taken into considerations to solve these

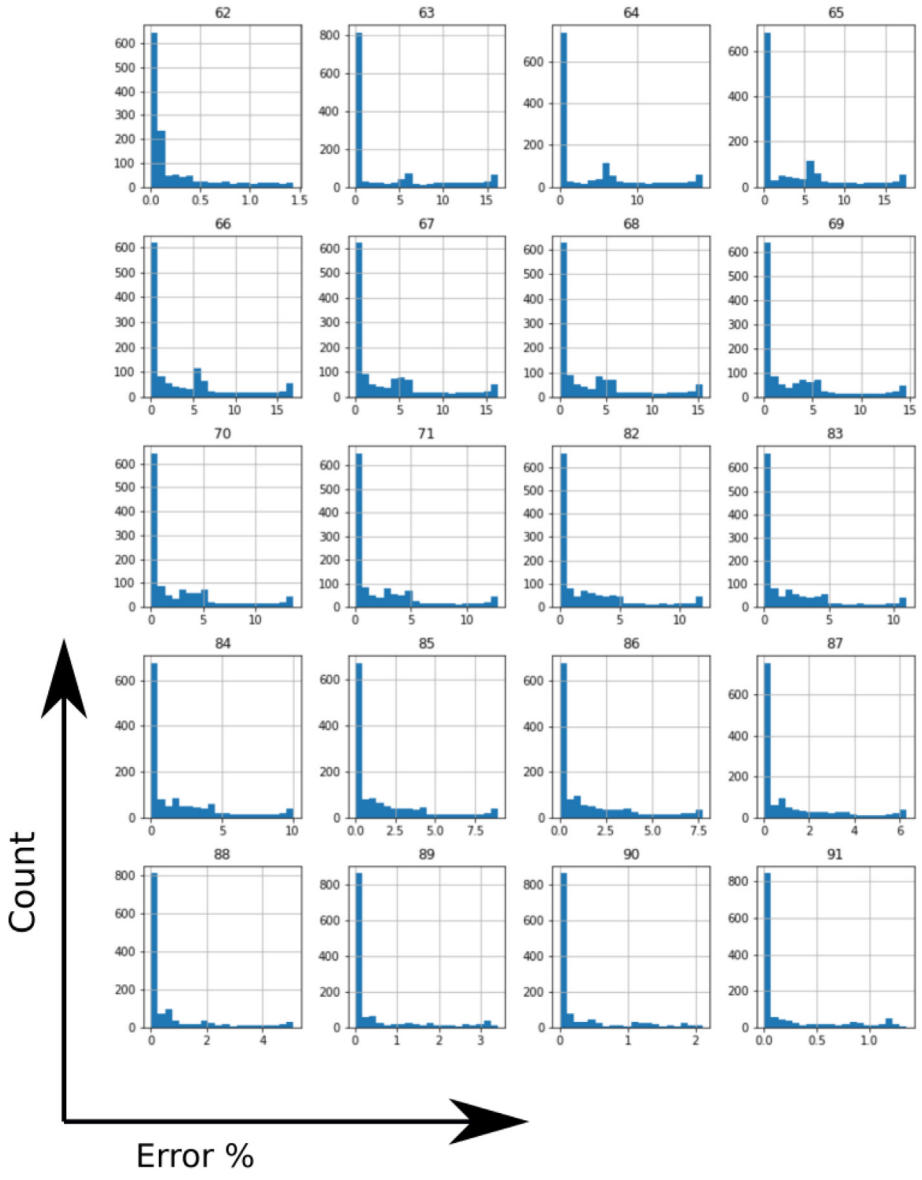

Fig. 6. Statistical analysis to understand error distribution.

Table 1
Uncertainty of measuring units used in experiments.

Device	Uncertainty
Flow meter (Sitrans F M Mag 5000)	0.4% ± 1 mm/s
Temperature sensor (Pt100)	±0.05 °C from −80 °C to 200 °C
Thermostatic heater	±0.5 °C

equations are as follows: velocity inlet and pressure outlet boundary conditions. All three inlet devices were evaluated for flow rate (velocity), and bulk storage & inlet temperature difference (ΔT). Likewise, simulations were performed for tank bulk temperature of 60 °C, and inlet temperature of 10 °C & 30 °C. Accordingly, two conditions of high and low ΔT were formulated. Bulk storage temperature of 60 °C with 30 °C inlet temperature results in low ΔT (30 K). High ΔT constitutes 60 °C bulk storage temperature while 10 °C inlet temperature thus amounting $\Delta T = 50$ °C. Flow rates for both the conditions were 800 l/h and 200 l/h respectively.

The above-mentioned equations are solved with the boundary conditions assigned as follows:

- Flow inlet and flow outlet boundary conditions

$$V_{in} = u_{avg} = (V / A_{cross\ \ sec\ tional}); \quad T = T_{in} \tag{12}$$

- Pressure outlet boundary conditions
- Wall boundary conditions: No slip wall conditions
- Adiabatic wall condition
- Turbulent or laminar flow conditions according to the flow rate:

3.3. Thermo-physical properties

Properties of water are temperature dependent, henceforth density, specific heat capacity, thermal conductivity and dynamic viscosity are the expressed in polynomial fitted expressions as given in Eq (13–16).

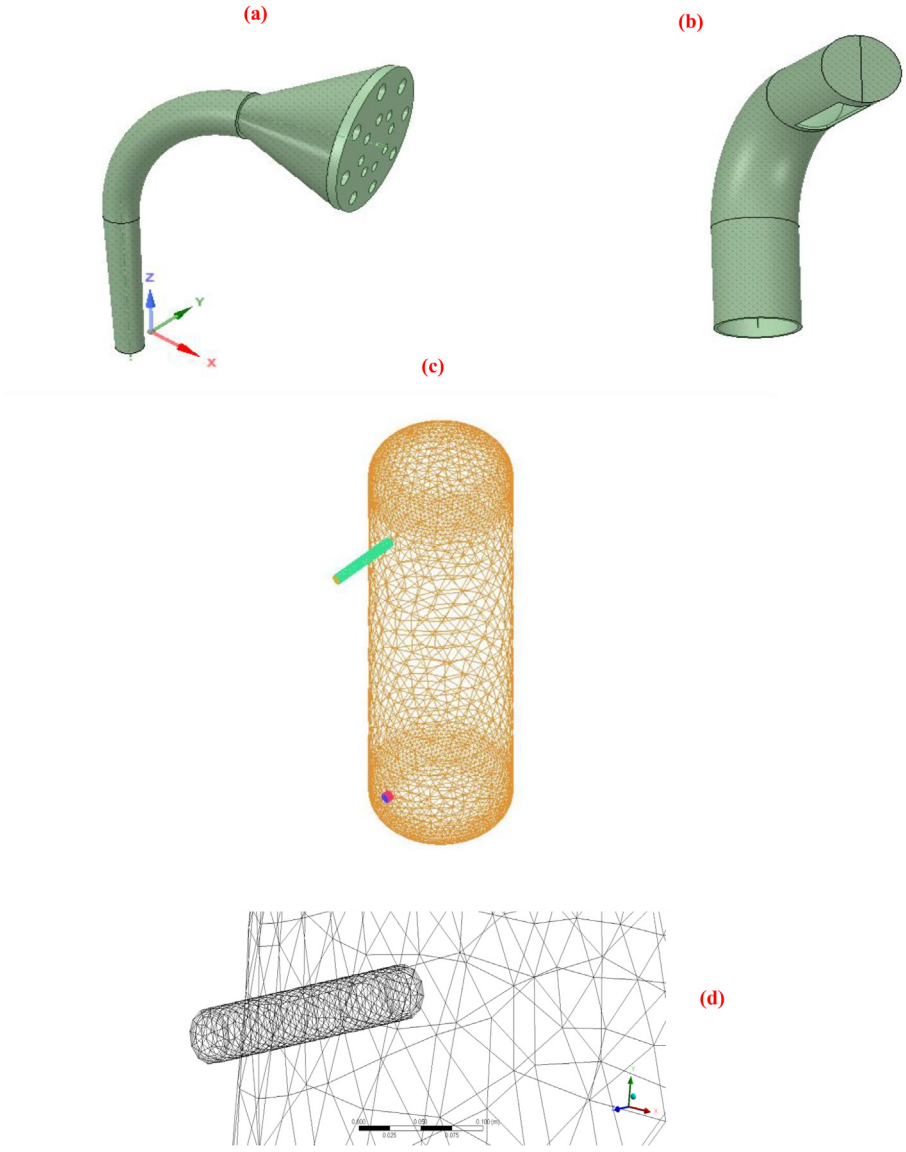

Fig. 7. (a) Perforated inlet, (b) Slotted inlet, (c) and (d) Mesh for simple inlet storage tank.

$$\rho = 999.8 + 0.06755T - 0.008788T^2 + 7.824T \times 10^{-5}T^3 - 5.734 \times 10^{-7}T^4 + 1.901 \times 10^{-9}T^5 \quad (13)$$

$$C_p = 4.217 - 0.00338T + 0.0001142T^2 - 1.924 \times 10^{-6}T^3 + 1.724 \times 10^{-8}T^4 - 6.156 \times 10^{-11}T^5 \quad (14)$$

$$\mu = 0.001789 - 5.994 \times 10^{-5}T + 1.383 \times 10^{-6}T^2 - 2.105 \times 10^{-8}T^3 + 1.811 \times 10^{-10}T^4 - 6.51 \times 10^{-13}T^5 \quad (15)$$

$$\lambda = 0.5558 + 0.002425T - 1.839 \times 10^{-5}T^2 + 1.46 \times 10^{-7}T^3 - 1.934 \times 10^{-9}T^4 + 1.106 \times 10^{-11}T^5 \quad (16)$$

3.4. Numerical method

As soon as the models with three different inlet devices are modelled in *Space Claim* available in *ANSYS* 19.2, cell zone conditions in each were allotted and fixed as solid or fluid, in accordance to the common practice. The models were subsequently exported for meshing where they were discretized to the finitude of smaller sub-elements. One such meshed model with simple inlet is shown in Fig. 7(c) and (d). PDEs (7)–(11) are coupled and nonlinear, therefore in order to solve them further step of numerical discretization follows with pressure-based solver in *Fluent*. In addition, natural and buoyancy induced convection are also incorporated in the momentum equation by introducing density as a function of temperature and activating gravity in *Fluent*. Furthermore, energy and momentum equations have conjugated convective terms which are approximated and spatially discretized by employing second order upwind scheme. Precise SIMPLE algorithm is engaged to ascertain the coupling of pressure and velocity. Before starting the simulation, energy checkbox is selected for *ANSYS* to solve heat transfer equations, followed by, k- ϵ framework,

Table 2
Flow rate and Reynolds number boundary conditions at inlet.

Flow rate (l/h)	Re
200	1400
400	2840
600	4270
800	6440

to ensure turbulent flow, depending upon the case as listed in Table 2. Finally applying the above-mentioned boundary conditions at appropriate named selection. Thermo-physical properties of water as enlisted in Eq (13) – (16) are allotted in the user defined polynomial fitted properties. Inlet water flow velocity ($V/A_{cross\ sectional}$) as enlisted in Table 2 with temperature of 10 °C and 30 °C was applied at inlet boundary condition. A report file containing the information of 20 fluid layers with their coordinates and temperature was defined in *Solution Monitors* tab of *Fluent*. This report file will ensure that the temperature value of each nodal layer will be correctly stored for every 250th iteration, thus later can be easily analyzed with different data processing package such as *Pandas* in *Python* language. For the purpose of plotting the results, statistical data visualization packages such as *Matplotlib* and *Seaborn in Python* were employed. The unsteady or transient simulations were initialized with tanks temperature of 60 °C. The unsteady or transient case was initialized and was run on *Czech Technical University's* cloud computers running on 4 *Intel Xeon* processors. With the exception of continuity, convergence criteria for all other equations were set to 10^{-6}. Continuity equation is most difficult to converge; therefore, it was relaxed as a regular practice to 10^{-4}. An initial time step of 2×10^{-4} was chosen to assist in convergence until flow was fully developed. Later it was increased to 0.02 to make the simulation time feasible.

3.5. Model validation

In order to establish the credibility of results, numerical simulations necessitate the need for validation. In this section results obtained by simulations are compared with experiments especially with the case of simple inlet device. Fig. 8 shows the evolution of temperature contours of discharging process having flow rate of 200 l/h. The thermocline development of the process is visible, cold water enters the tank and entrains the hot water along while settling down towards the bottom of tank. The induced mixing causes thermocline thickness to increase while it propagates

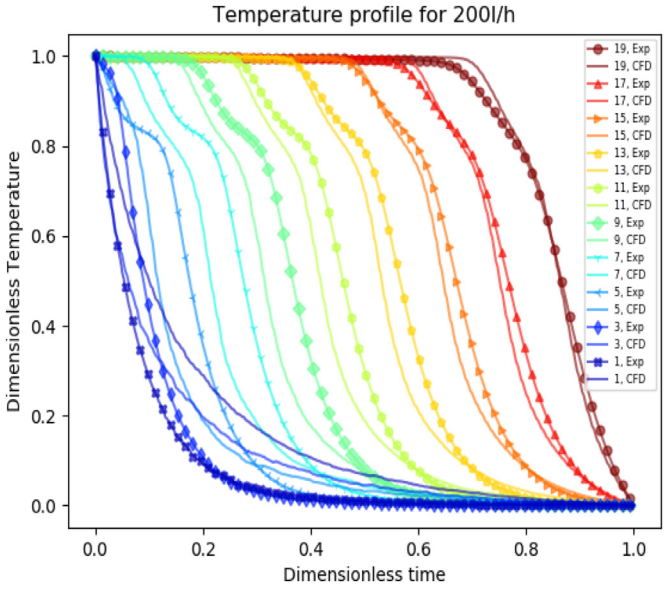

Fig. 9. Temperature profiles for comparison between Experiments and CFD.

towards the outlet during the whole process. The unit replacement time for 200 l/h is 1.98 h. Fig. 9 demonstrates the comparison of temperature profiles between experimental and simulated results with simple inlet device for the flow rate of 200 l/h. As the discharging proceeds, temperature in each layer decreases due to cold water mixing with the hot water. Experimental data acquired from odd numbered PT-100 sensors on the stratified tank were plotted for comparison with corresponding node layers in simulated system. The significant difference at the bottom of the tank is seemed to be due to non-established fully developed flow near the bottom, this then leads to unstable thermocline capture, resulting in high error near the bottom at the early stages of the simulation. As discharging progresses, thermocline establishes and flow was fully developed, resulting the decrease in error. The error was significantly low in the top position of the tank. In addition, generally there is always a tradeoff between the error management and time expenditure by any numerical simulations.

Once the simulated model was validated with experimental results, further simulation with perforated and slotted inlet device will become valid and can lead to higher accuracy. Mesh independence study is also an important aspect of CFD simulations.

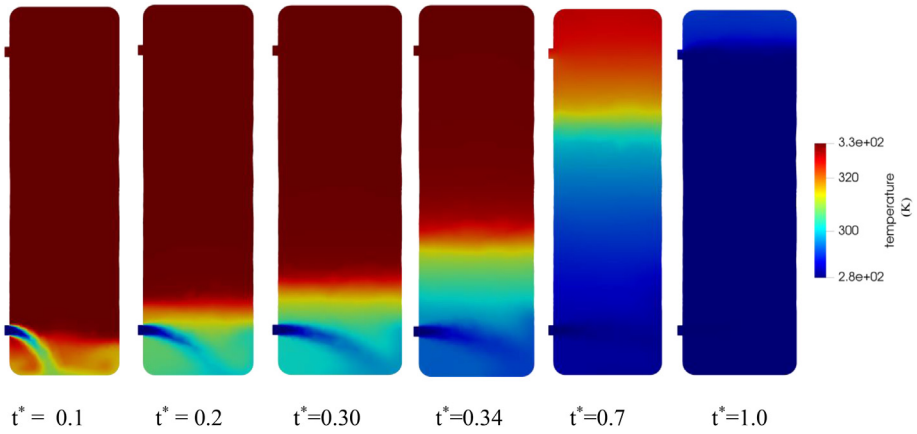

Fig. 8. Temperature contours of discharging through simple inlet device at flow rate 200 l/h & $\Delta T = 50$ K.

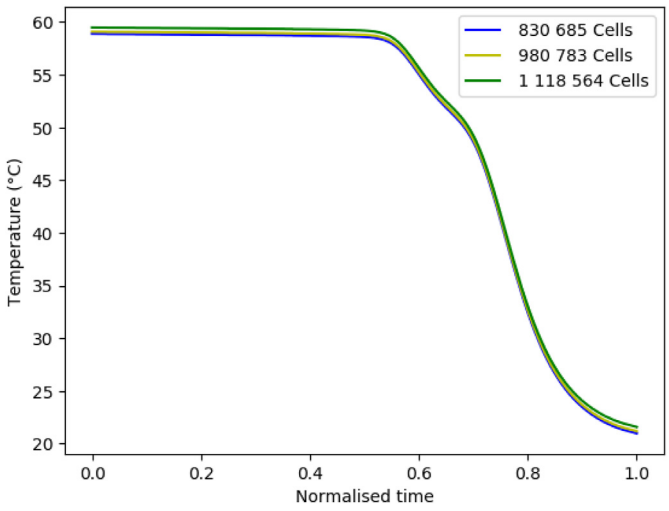

Fig. 10. Mesh independence test.

Mesh independency test is performed on mesh sizes with, 830 685 cells, 980 783 cells and 1 118 564 cells. Case with 1 118 564 performed no better than the case 980 783, henceforth, there was no reason to increase the cells beyond 980 783 and this case was used for all further simulations. This ensured best compromise between computational time and accuracy of results. Fig. 10 plots the outlet temperature for three different meshes.

4. Results and discussions

Once the initial CFD model is validated with experiments and is verified for mesh independence test, the subsequent analysis of different models become more reliable and more accurate. Figs. 11 and 12 respectively give the dynamic temperature contours of perforated and slotted inlet devices at 200 l/h & $\Delta T = 50$ K (i.e $T_{bulk} = 60$ °C & $T_{inlet} = 10$ °C) for different location in time during the discharge. To obtain these clear visual representations, dataset visualization package *ParaView* was employed. Correspondingly, the simulation data files were imported from the Fluent to the *ParaView* and plotted at selected time intervals to obtain the desired contours. Accordingly, the evolution of transient thermocline thickness can be easily visualized through these time dependent temperature contours both for perforated and slotted inlet devices. Likewise, as the discharging process proceeded, incoming low temperature and high-density fluid entrains and mixes with the bulk fluid at inlet thus creating a continuous thermocline. In addition, while the plug flow continues, thermocline thickness increases due to further exchange of heat and mass through convection, diffusion and conduction between layers, even though convection constitutes major part of the thermal exchange. In real sense, density induced buoyant force as governed by flow parameters such as flow rate and ΔT determines the mixing which eventually propagates throughout the tank, i.e. with increase in the dimensionless time, thermocline thickness increases and drifts from bottom to the top of the tank. Figs. 11 and 12 shows the numerical model in detail. It is not intended to measure the thermocline thickness directly for each case of simulated perforated and slotted inlets, however it can be examined through indices of stratification – temperature profiles, MIX number and discharging efficiency as discussed in the following subsection. Richardson number is excluded from this analysis, as it is kept constant for each case – by making ΔT and flow rate fairly constant.

The following sub-sections are tailored to understand the behavior of inlet devices on stratification performance of tank. Simulated simple, perforated and slotted inlet devices are tested for various dynamic mode parameters. These parameters – inlet flow rate and ΔT, are varied for all the three inlet devices, and essentially, indices of stratification – temperature profile, MIX number, and discharging efficiency are calculated and compared. It was consequently found that the indices of stratification demonstrated in the following sections are highly sensitive to inlet flow rate and ΔT. Therefore, for further analysis, flow rate and ΔT are preset and thus classified as high or low depending upon their fluid dynamics properties. For example, flow rate of 800 l/h is regarded as high flow rate owing to its turbulent nature with Re = 6440, while flow rate of 200 l/h is laminar, hence low flow, with Re = 1400. Likewise, $\Delta T = 30$ K accounting for the tank conditions – 60 °C as bulk storage temperature, and 30 °C as inlet temperature is termed as high ΔT, while $\Delta T = 50$ K corresponding to 60 °C as bulk storage temperature, and 10 °C as inlet temperature is termed as low ΔT. These two variables are primarily adjusted for selected inlet devices, and finally, indices of stratifications were appointed to evaluate the results.

4.1. Dynamics of stratification performance at high flow rate (800 l/h) and low $\Delta T = 30$ K

Fig. 13 shows the evolution of temperature with dimensionless time for the case of slotted, simple and perforated inlet devices at 800 l/h, $\Delta T = 30$ K. In other words, flow rate, bulk storage temperature and inlet temperature respectively are 800 l/h, 60 °C and 30 °C. This is the condition of turbulent flow with Re = 6440. The dimensionless discharging time was introduced to compare and analyze the discharging performance at different flow rates. Conspicuously, when the flow rate is 800 l/h, the unit replacement time for each inlet device is 0.50 h, as it was ensured that the volumetric discharge rate is kept constant for each device. This also ensured that the Richardson number is also fairly constant for the same ΔT, thus making comparison grounds even smoother. To illustrate, dimensionless temperature values corresponding to odd numbered fluid layers are plotted and mapped with dimensionless time for each case. It is evident that slotted inlet exhibits better stratification performance as seen by its lower temperature decay of nearly every layer due to impeded mixing. This is especially the case with high flow rate of 800 l/h (Re = 6440) when turbulent mixing is the major culprit in de-stratification, and there is no time for heat sinking through diffusion and conduction between layers, slotted inlet performs best by subduing the mixing and smoothly guiding the cold water. In other words, the higher density fluid is smoothly guided towards the lower portion of the tank, thus acting as buffer in establishing the counter active forces of buoyancy and gravity. When the tank is nearly 80% discharged, temperature of 18th layer with slotted type device is 39.9 °C, while with simple and perforated inlet its 27.6 °C and 22 °C respectively. So there was straight 30.7% and 44.8% percent decrease in the temperature of the 18th layer by changing the inlet device from slotted to simple and from slotted to perforated inlet device. This behavior can be seen in the rest of the layers as well, however, apparently, distinction in the temperature differences in the respective layers of each inlet devices is not very significant in the lower part of the tank (lower then 13th layer), and thus the reason layers 15 to 19 are hued in red. Moreover, Fig. 14 illustrates the variation of MIX number with dimensionless time as the discharging process proceeds. As expected MIX number varies from 0 to 1. Since the temperature decay rate of the lower portion of tank doesn't make much difference for each case, MIX number of the slotted inlet starts to depart approximately after half of discharging process. This is suggested to be improving the tank stratification in the upper part of tank by

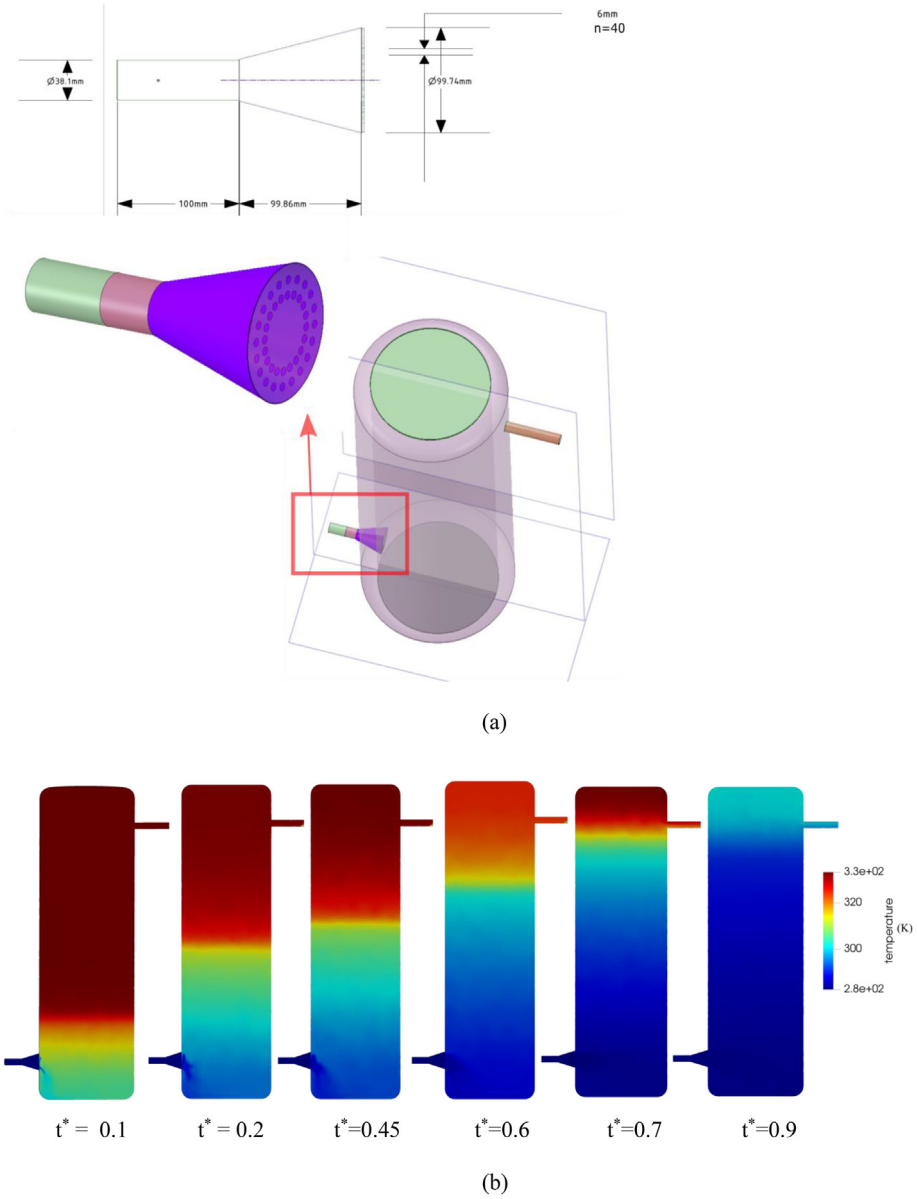

Fig. 11. (a) Perforated inlet characterization, (b) Temperature contours of discharging through perforated inlet at flow rate 200 l/h & $\Delta T = 50$ K.

inducing mixing inhibiting effects of slotted inlet device. As a comparison, MIX number of slotted inlet device at 60% of discharged tank is nearly 0.6, while its 0.8 and 0.85 for simple and perforated respectively. In conclusion, tank with slotted inlet exhibits better stratification performance compared to the other two.

This is corroborated by Fig. 15 demonstrating the discharge efficiency variation with flow rate and ΔT. Discharge efficiency as given in Eq. (17) is defined as the fraction of recoverable heat for the fraction of the discharging time t_d at which the bulk storage and inlet temperature difference has not decreased to 20% of the initial value, i.e. $(|T_{outlet} - T_{inlet}| < 0.8 \cdot |T_{initial} - T_{inlet}|)$.

$$\eta_d = \frac{\int_0^{t_d} \dot{m} \cdot c_p \cdot (T_{outlet} - T_{inlet}) dt}{m_{store} \cdot c_p \cdot (T_{initial} - T_{inlet})} \tag{17}$$

Discharge efficiency of slotted inlet at 800 l/h and ΔT as 30 K is 84%, which is comparatively higher than that of simple inlet (77.8%) and perforated inlet (76.5%).

4.2. Dynamics of stratification performance at low flow rate (200 l/h) and low $\Delta T = 30$ K

Fig. 16 shows the evolution of temperature with dimensionless time for the case of slotted, simple and perforated inlet devices at 200 l/h, $\Delta T = 30$ K. In other words, flow rate, bulk storage temperature and inlet temperature respectively are 200 l/h, 60 °C and 30 °C. Evidently, temperature profiles are showing the same behavior in all the three cases. This can be interpreted by the fact that at low flow rate and low ΔT, when flow is laminar (Re = 1440) de-stratification is not entirely caused by intense mixing, but rather by heat sinking through natural convection diffusion and conduction among fluid layers near thermocline. Consequently, it makes sense that all the three inlet devices are nearly performing equally regardless of the flow rate and ΔT. Also, it can be seen that the tank's bottom layers – 1st, 3rd, 5th, and 7th were deviating a little from each other – slotted inlet device lagging behind in terms of temperature then the rest of its peers, however, they are already

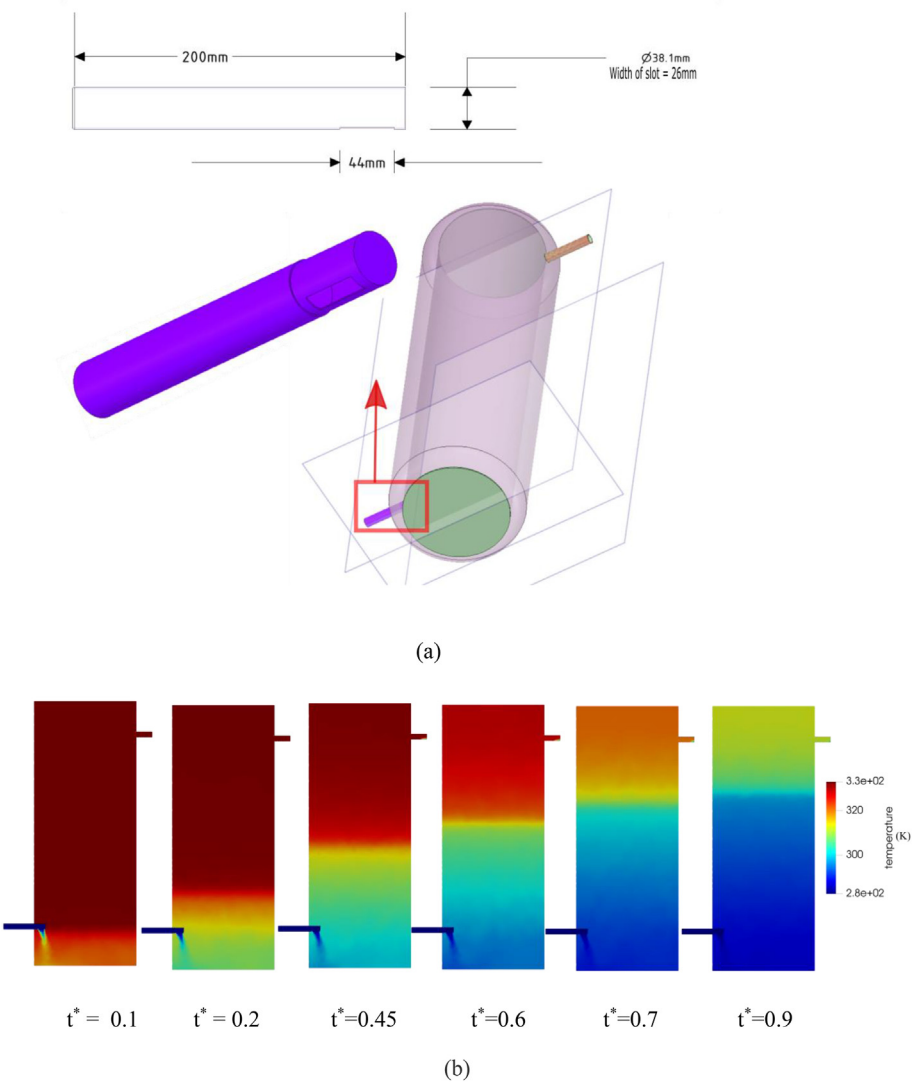

Fig. 12. (a) Slotted inlet characterization, (b) Temperature contours of discharging through slotted inlet at flow rate 200 l/h & $\Delta T = 50$ K.

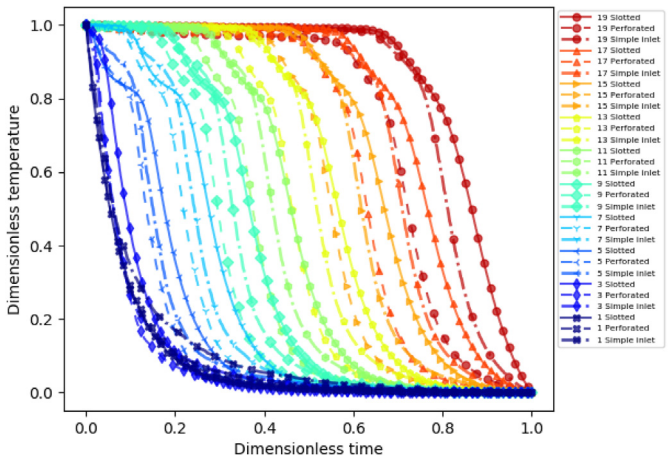

Fig. 13. Temperature profile at 800 l/h and $\Delta T = 30$ K.

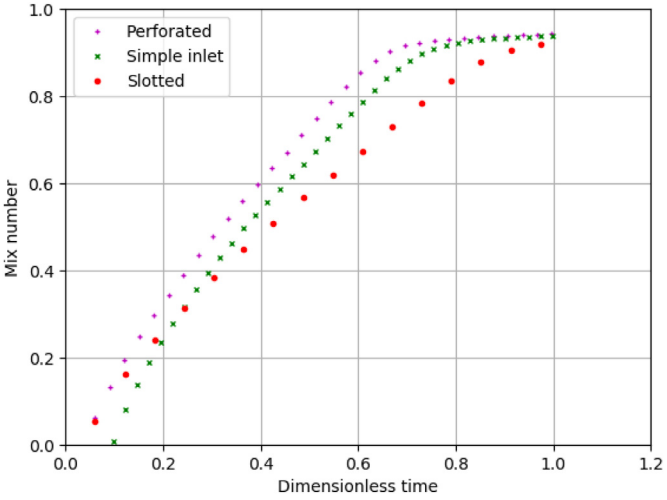

Fig. 14. MIX number at 800 l/h and $\Delta T = 30$ K.

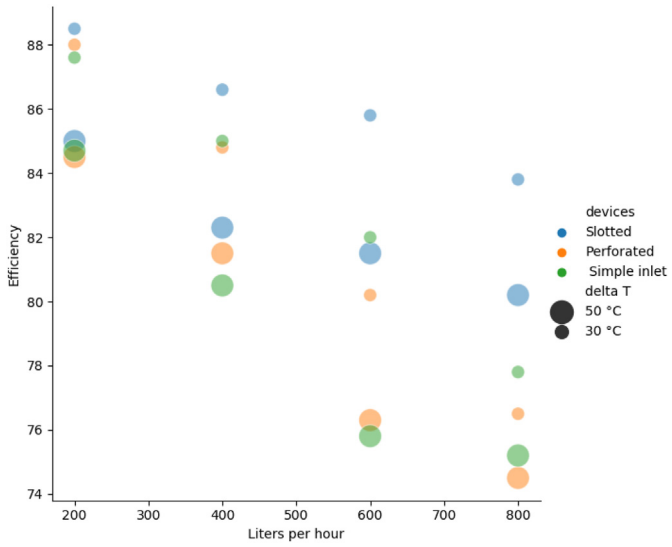

Fig. 15. Variation of discharging efficiency with flow rate and ΔT.

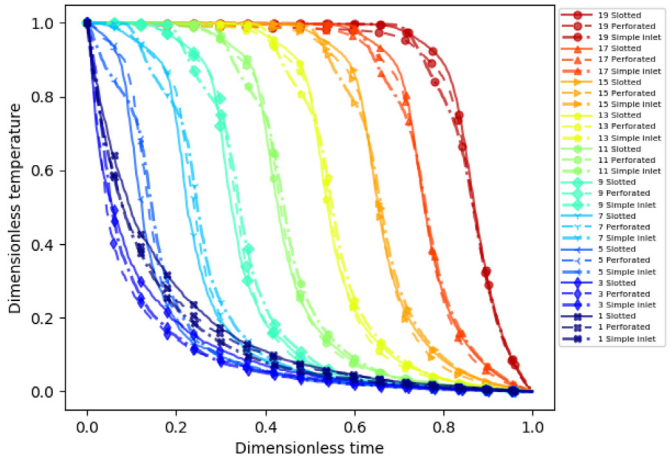

Fig. 16. Temperature profile at 200 l/h and $\Delta T = 30$ °C.

established at the top most layers (layers 13th, 15th, 19th). Likewise, MIX number is behaving correspondingly – MIX for slotted inlet device is diverged during nearly half of the discharging time ($t^* = 0.4$), while catching up again with the rest (Fig. 17). In addition, MIX for slotted inlet device suggests that the tank is comparatively poorly stratified during the half of time of discharging ($t^* = 0.5$), as the area under the curve for slotted inlet is higher than that of the rest of the inlets. However, this is quickly subdued by the upper stratified layers and the overall stratification of the tank is improved. Thus, equalizing all the three inlet devices in the second half of the discharging time. Besides, it can also be seen that the perforated inlet is diverging, but nevertheless, alike stratification performance, as corroborated by the temperature and MIX number analysis subjects to similar thermal performance as illustrated by discharging efficiency in Fig. 15. Accordingly, discharge efficiency for slotted, perforated, and simple inlet is 88.5%, 88% and 87.6% respectively. Henceforth, from this analysis it can be deduced that slotted inlet, perforated inlet and simple inlet performed approximately same in terms of thermal performance and stratification performance for the condition of low flow rate and low ΔT.

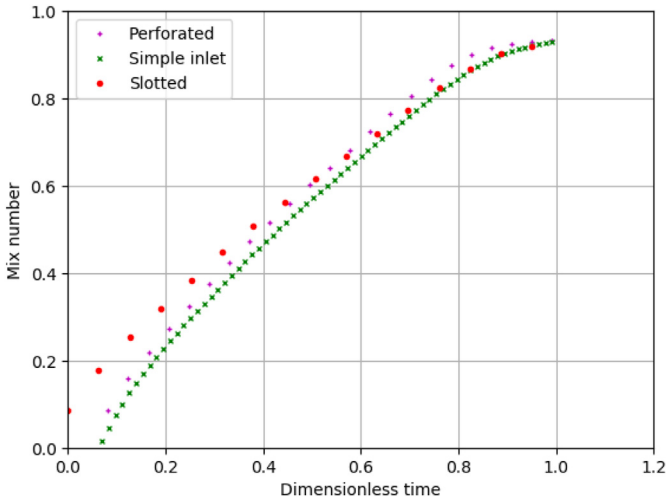

Fig. 17. MIX number at 200 l/h and $\Delta T = 30$ K.

4.3. Dynamics of stratification performance at high flow rate (800 l/h) and high $\Delta T = 50$ K

Fig. 18 show the evolution of temperature with dimensionless time for the case of slotted, simple and perforated inlet devices at 800 l/h, $\Delta T = 50$ K. That is, flow rate, bulk storage temperature and inlet temperature respectively are 800 l/h, 60 °C and 10 °C. To illustrate, slotted inlet device is preforming better as shown by its lower temperature decay at high Reynolds number (Re = 6440) which is of turbulent nature. Again, with flow rate of 800 l/h, the unit replacement time is 1.98 h for each case of inlet devices, however, the temperature decay rate of each layer is contrastingly different. This might be explained in terms of combined action of restrained turbulent mixing of slotted inlet and high temperature difference ΔT between bulk storage and inlet temperature. At the dimensionless time of $t^* = 0.6$, temperature of 13th layer is 18.5 °C, 9.0 °C, and 9.6 °C, respectively for slotted, perforated and simple inlet devices. In other words, there is nearly 51% decrease in temperature of 13th layer when simple inlet is used instead of slotted inlet device. This trend can be observed in the rest of the layers as well. Fig. 19 demonstrates the MIX number analysis of slotted inlet at t* = 0.6 in the same process, while the MIX number of simple and perforated is nearly 0.8. As a result, area under the MIX curve for

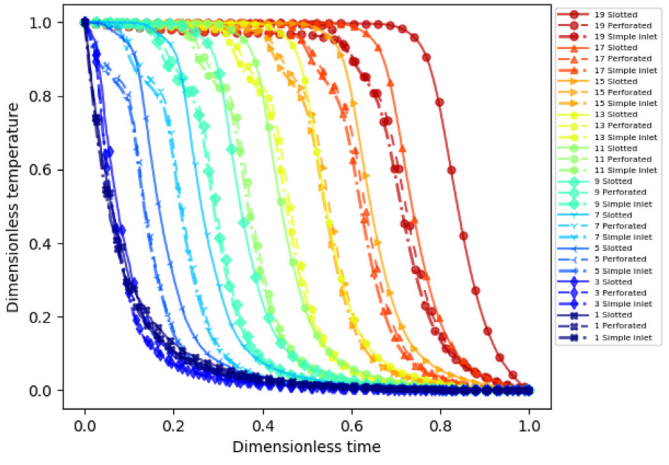

Fig. 18. Temperature profile at 800 l/h and $\Delta T = 50$ K.

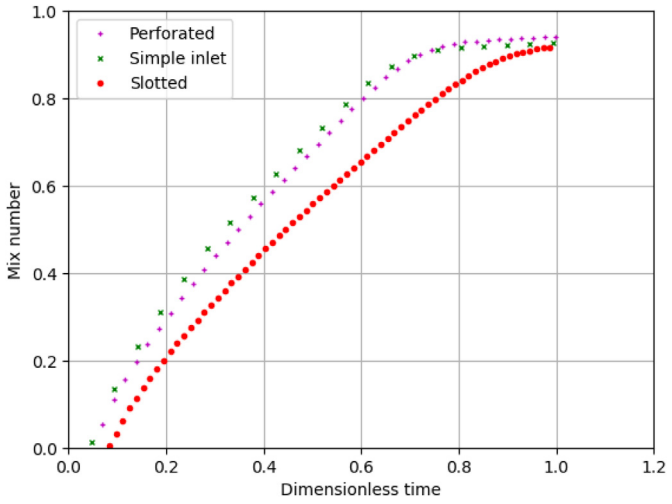

Fig. 19. MIX at 800 l/h and $\Delta T = 50$ K.

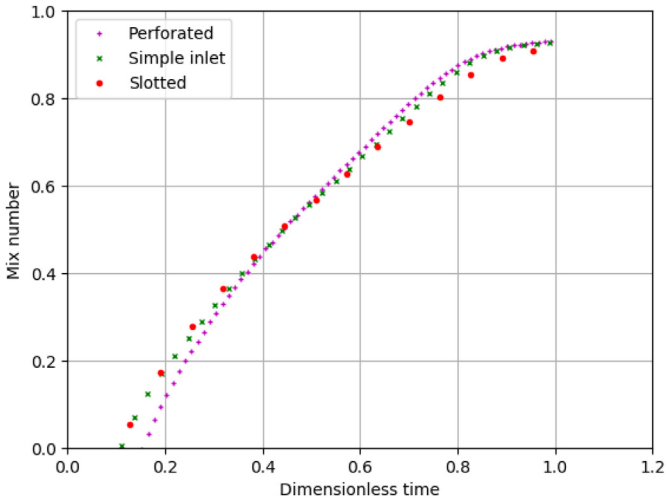

Fig. 21. MIX number at 200 l/h and $\Delta T = 50$ K.

slotted inlet is significantly lower compared to the rest of the two – indicating better stratification performance during the discharge. Fig. 15 contrastingly inspects the discharging efficiency of the processes with $\Delta T = 30$ K and $\Delta T = 50$ K having same flow rate of 800 l/h. Likewise, slotted inlet device has the discharging efficiency of nearly 81%, while perforated and simple inlets at 800 l/h & $\Delta T = 50$ °C have discharging efficiency of 74.5% and 75.2% respectively. In case of flow rate = 800 l/h & $\Delta T = 30$ K, slotted inlet has efficiency of 84% (see Fig. 15). Furthermore, the lowest efficiency at 800 l/h is 74.5% in case of perforated inlet at $\Delta T = 50\%$, while the highest efficiency which is 84%, belongs to the slotted inlet at $\Delta T = 30$ K. Correspondingly, there is a 10% efficiency span among all the discharging processes.

4.4. Dynamics of stratification performance at low flow rate (200 l/h) and high $\Delta T = 50$ K

Fig. 20 show the evolution of temperature with dimensionless time for the case of slotted, simple and perforated inlet devices at 200 l/h, $\Delta T = 50$ K. That is, flow rate, bulk storage temperature and inlet temperature respectively are 200 l/h, 60 °C and 10 °C. Here the temperature profiles are showing the same time dependencies for all the three cases. This again like in the previous section 4.2, follows the same instance of low Reynolds number (Re = 1440). In other words, laminar flow condition permits the convection, conduction, and diffusion between the layers in thermocline as the main source of de-stratification – stronger than the turbulent mixing –therefore, slotted inlet device did not assist too much. Conclusion that can be deduced from here is that stratification, or mixing, at low flow rate shows bare minimum ΔT or inlet device dependency. However, as the flow rate is increased, dependency on ΔT also increases. Fig. 21 demonstrates the MIX number for this discharging process. Area under the curve is the same for each device, suggesting that the tank is equally stratified for each case where flow rate is low and ΔT is high. The other noticeable observation is that the MIX number for the slotted inlet for processes: 200 l/h & $\Delta T = 50$ K and 800 l/h and $\Delta T = 30$ K is nearly the same i.e. 0.6 at t* = 0.6 (see Figs. 21 and 14). In the same conditions MIX number for perforated and simple inlet device quantitatively differ. This can be interpreted as the mixing damping effects of slotted inlet device at higher flow rates which even gets compounded when ΔT is decreased. The same can be seen in Fig. 15. As the flow rate is increased, the slope of efficiency curve decreases (generally for all the cases), due to decrease in efficiency at higher flowrates. However, in the case of slotted inlet device, slope associated with $\Delta T = 30$ K is much higher than the slope associated with $\Delta T = 50$ K, signifying the combined damping effect the slotted inlet device offers.

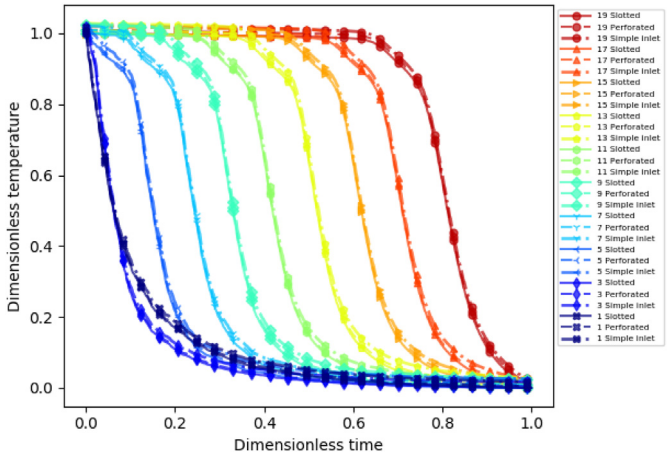

Fig. 20. Temperature profile at 200 l/h and $\Delta T = 50$ K.

5. Conclusion

In this study, a system of CFD models was developed to research the discharging performance of three types of inlet devices relating to domestic hot water storage tanks. An attempt was made to understand how each inlet device performs in discrete operational conditions – flow rate and ΔT. The basic idea behind this study was to find possibilities to optimize storage tanks, with integrated heating device with potential use in – solar systems or heat pumps. For instance, heat pump based storage tank pertains to high flow rate and low ΔT, while, solar system based storage tank pertains to low flow rate and high ΔT. Accordingly, slotted, perforated, and simple inlet devices were simulated in transient manner and were examined for two fundamental operational variables - flow rate and ΔT. Numerical data of simple inlet device was compared with experiments to confirm the veracity of further simulations. Numerical solution was in agreement with the experimental data, thus implying that the predicted behavior of slotted and perforated

inlet was reliable. Stratification indices such as temperature evolution, MIX number and discharging efficiency were calculated for each case and following conclusion derived.

1. Slotted inlet device performed no better than the rest of the inlet devices at low flow rate of 200 l/h, at a particular ΔT. For example, percentage increase in discharge efficiency, when slotted inlet was used instead of perforated or simple inlet device, in both instances differed a mere 1–2%
2. Slotted inlet device started outshining the rest as the flow rate was increased. Mixing damping effects of slotted inlet device were even compounded at higher flow rates when ΔT was decreased from 50 K to 30 K, giving not less than minimum 8.7% increase in discharge efficiency at 800 l/h, within the maximum efficiency difference span, which is 10%.
3. It is predicted, that for the application of heat pumps which demand high flow rate and low ΔT, slotted inlet device can exhibit the best thermal performance. While, for the application of solar systems, demanding low flow rate but high ΔT, application of slotted inlet might not make much difference in thermal efficiency.

These research findings can be used in predicting and thus optimizing the real time dynamic behavior of storage tanks, classified according to their heat addition - solar systems or heat pumps.

Declaration of competing interest

No conflict of interest exists.

CRediT authorship contribution statement

Yogender Pal Chandra: Investigation, Data curation, Formal analysis, Software, Validation, Writing - original draft, Visualization. **Tomas Matuska:** Conceptualization, Methodology, Writing - review & editing, Supervision, Project administration, Funding acquisition.

Acknowledgment

This work has been supported by the Ministry of Education, Youth and Sports within National Sustainability Programme I (NPU I), project No. LO1605 - University Centre for Energy Efficient Buildings – Sustainability Phase.

References

[1] Y.P. Chandra, T. Matuska, Stratification analysis of domestic hot water storage tanks: a comprehensive review, Energy Build. 187 (2019) 110–1331.
[2] Y.H. Zurigat, P.R. Liche, A.J. Ghajar, Influence of the inlet geometry on mixing in thermocline thermal energy storage, Int. J. Heat Mass Tran. 34 (1) (1991) 115–125.
[3] O. Abdelhak, H. Mhire, P. Bournot, CFD analysis of thermal stratification in domestic hot water storage tank during dynamic mode, Build. Simulat. 8 (4) (2015) 421–429.
[4] M.S. Shin, H.S. Kim, D.S. Jang, S.N. Lee, Y.S. Lee, H.G. Yoon, Numerical and experimental study on the design of a stratified thermal storage system, Appl. Therm. Eng. 24 (2004) 17–27.
[5] J. Fan, S. Furbo, Thermal stratification in a hot water tank established by heat loss from the tank, Sol. Energy 86 (2012) 3460–3469.
[6] J. Fernańdez-Seara, F.J. Uhia, J. Sieres, Experimental analysis of a domestic electric hot water storage tank. Part II: dynamic mode of operation, Appl. Therm. Eng. 27 (2007) 137–144.
[7] W. Yaici, M. Ghorab, E. Entchev, S. Hayden, Three-dimensional unsteady CFD simulations of a thermal storage tank performance for optimum design, Appl. Therm. Energy 60 (2013) 152–163.
[8] L.J. Shah, S. Furbo, Entrance effects in solar storage tanks, Sol. Energy 75 (2003) 337–348.
[9] E. Kaloudis, D.G.E. Grigoriadis, E. Papanicolaou, T. Panidis, Large eddy simulation of thermocline flow phenomena and mixing during discharging of an initially homogeneous or stratified storage tank, Eur. J. Mech. B Fluid 4 (2014) (0).
[10] B. Baeten, T. Confrey, S. Pecceu, F. Rogiers, L. Helsen, A validated model for mixing and buoyancy in stratified hot water storage tanks for use in building energy simulations, Appl. Energy 172 (2016) 217–229.
[11] E. García-Marí, M. Gasque, R.P. Gutiérrez-Colomer, F. Ibáñez, P. GonzálezAltozano, A new inlet device that enhances thermal stratification during charging in a hot water storage tank, Appl. Therm. Energy 61 (2013) 663–669.
[12] I.J. Moncho-Esteve, M. Gasque, P. González-Altozano, G. Palau-Salvador, Simple inlet devices and their influence on thermal stratification in a hot water storage tank, Energy Build. 150 (2017) 625–638.
[13] J.H. Davidson, D.A. Adams, J.A. Miller, A coefficient to characterize mixing in solar water storage tanks, Trans. ASME, J. Solar Energy Eng. 116 (1994) 94–99.
[14] M.Y. Haller, C.A. Cruickshank, W. Streicher, S.J. Harrison, E. Andersen, S. Furbo, Methods to determine stratification efficiency of thermal energy storage processes–reviewand theoretical comparison, Sol. Energy 83 (2009) 1847–1860.
[15] E. Andersen, S. Furbo, J. Fan, Multilayer fabric stratification pipes for solar tanks, Sol. Energy 81 (2007) 1219–1226.
[16] A. Campos Celador, M. Odriozola, J.M. Sala, Implications of the modelling of stratified hot water storage tanks in the simulation of CHP plants, Energy Convers. Manag. 52 (8–9) (2011) 3018–3026.
[17] S. Giedré, M. Vytautas, A. Anders N, K. Jonas, Feasibility of CHP-plants with thermal stores in the German spot market, Appl. Energy 86 (11) (2009) 2308–2316.
[18] A. Pablo, M. Marc, G. Antoni, O. Eduard, C. Luisa F, Overview of thermal energy storage (TES) potential energy savings and climate change mitigation in Spain and Europe, Appl. Energy 88 (8) (2011) 2764–2774.
[19] P.C. Eames, B. Norton, The effect of tank geometry on thermally stratified sensible heat storage subject to low Reynolds number flows, Int. J. Heat Mass Tran. 41 (14) (1998) 2131–2142.
[20] I. Simon, L. Wenxian, Numerical simulation of three-dimensional flow dynamics in a hot water storage tank, Appl. Energy 86 (12) (2009) 2604–2614.
[21] M.F. El-Amin, S. Shuyu, S. Amgad, Simulation of buoyancy-induced turbulent flow from a hot horizontal jet, J. Hydrodyn., Ser. B 26 (1) (2014) 104–113.
[22] N. Altuntop, M. Arslan, V. Ozceyhan, M. Kanoglu, Effect of obstacles on thermal stratification in hot water storage tanks, Appl. Therm. Eng. 25 (2005) 2285–2298.
[23] Y. Han, R. Wang, Y. Dai, Thermal stratification within the water tank, Renew. Sustain. Energy Rev. 13 (2009) 1014–1026.
[24] M. Haller, E. Yazdanshenas, E. Andersen, C. Bales, W. Streicher, S. Furbo, A method to determine stratification efficiency of thermal energy storage processes independently from storage heat losses, Sol. Energy 84 (2010) 997–1007.
[25] T. Khurana, B. Prasad, K. Ramamurthi, S. Murthy, Thermal stratification in ribbed liquid hydrogen storage tanks, Int. J. Hydrogen Energy 31 (2006) 2299–2309.
[26] D. Savicki, H. Vielmo, A. Krenzinger, Three-dimensional analysis and investigation of the thermal and hydrodynamic behaviors of cylindrical storage tanks, Renew. Energy 36 (2011) 1364–1373.
[27] A. Zachár, Investigation of a new tube-in-tube helical flow distributor design to improve temperature stratification inside hot water storage tanks operated with coiled-tube heat exchangers, Int. J. Heat Mass Tran. 63 (2013) 150–161.
[28] M. Toyoshima, S. Okawa, An effect of a horizontal buoyant jet on the temperature distribution inside a hot water storage tank, Int. J. Heat Fluid Flow 44 (2013) 403–413.
[29] H. Njoku, V. Ekechukwu, S. Onyegegbu, Analysis of stratified thermal storage systems: an overview, Heat Mass Tran. 50 (2014) 1017–1030.
[30] M. Gasque, P. González-Altozano, D. Maurer, I.J. Moncho-Esteve, R.P. Gutiérrez-Colomer, G. Palau-Salvador, E. García-Marí, Study of the influence of inner lining material on thermal stratification in a hot water storage tank, Appl. Therm. Eng. 75 (2015) 344–356.
[31] P. Geczy-Vig, I. Farkas, Neural network modelling of thermal stratification in a solar DHW storage, Sol. Energy 84 (2010) 801–806.
[32] S.A. Kalogirou, S. Panteliou, Thermosiphon solar domestic water heating systems: long term performance prediction using artificial neural networks, Sol. Energy 69 (2000) 163–174.
[33] Z. Wang, H. Zhang, B. Dou, H. Huang, W. Wu, Z. Wang, Experimental and numerical research of thermal stratification with a novel inlet in a dynamic hot water storage tank, Renew. Energy 111 (2017) 353–371.
[34] J. Dragsted, S. Furbo, M. Dannem, F. Bava, Thermal stratification built up in hot water tank with different inlet stratifiers, Sol. Energy 147 (2017) 414–425.

Study 2

Design the custom built second law model to quantify energy/exergy dispersal of heat pump integrated TES

Paper 3: Second law performance prediction of HP integrated stratified TES system using long short-term neural networks

In this paper a ground source heat pump (GSHP) integrated with thermal energy storage (TES) system available for single family house in the Czech Republic was evaluated for relative exergy balance and second law performance evaluation. For this purpose, second law of thermodynamics was observed in tailoring the entropy and exergy equations. It was made possible to fit these equations to the customized data layer for end to end stratification performance of thermal energy storage (TES), and performance factor (PF) of heat pump (HP) during charge/discharge loop. This means that the second law model equation is derived from the scratch and is used to evaluate end to end energy trial, from grid to tap, from charge to discharge. In addition to novel data layer and derived models and their application to HP integrated TES, detailed application of advanced deep learning algorithms using LSTM neural networks is also demonstrated to model the data thus generated by data layer and to predict the TES layered temperature and efficiency.

Journal of Energy Storage 61 (2023) 106699

Contents lists available at ScienceDirect

Journal of Energy Storage

journal homepage: www.elsevier.com/locate/est

Research papers

Second law performance prediction of heat pump integrated stratified thermal energy storage system using long short-term memory neural networks

Yogender Pal Chandra [a,c,*], Gwang-Jin Kim [b], Tomas Matuska [c]

[a] Department of Environmental Engineering, Faculty of Mechanical Engineering, Czech Technical University in Prague, Technicka 4, 166 07, Prague 6, Czech Republic
[b] University of Freiburg, Freiburg 79104, Germany
[c] University Centre for Energy Efficient Buildings, Czech Technical University in Prague, Czech Republic

ARTICLE INFO

Keywords:
Thermal stratification
Thermal energy storage (TES) and Heat Pumps (HP)
LSTM
ANN

ABSTRACT

Thermal energy storages (TES) are transient state energy devices. These devices are used in renewable energy systems as a buffer for non-coincidence in heat supply and demand. TESs use thermal stratification to ensure high efficiency in heat storage and acquisition. This article is focused on predicting the performance of thermal energy storage (TES) integrated with heat pump using neural networks. In addition, exergy and entropy equations were derived for the calculation and prediction of the stratification efficiency in storage systems and of the performance factor (PF) of renewable energy systems (RES). As for data analytics, real time data-streaming edge devices were customized. The model fitting and prediction were done directly on the edge devices. The key objectives and findings are:

- To demonstrate stream-data processing framework which can graphically represent the stratification decay of an active Thermal Energy Storage (TES) charge/discharge process in real time.
- Derivation of a custom exergy equation for stratification efficiency and streaming it graphically in real time. The optimized key performance index (KPI) at the heat pump end i.e. coefficient of performance (COP) or performance of factor (PF) was 3.3, and at charge and discharge end, in terms of efficiency was 83 % and 84 % respectively.
- A deep neuronal network applying a long short-term memory (LSTM) architecture for predicting stratification deterioration in the charge/discharge cycle with a prediction error below 5 %.

1. Introduction

The key component of renewable energy system is thermal energy storage (TES). Temperature distribution is enforced by buoyancy effect causing discreet layered storage of heat and its delivery. Using this phenomenon, high quality heat is ensured and storage efficiency is increased [1,2]. Water distribution can be present in the stepped or continuous form in the TES. A better assessment of temperature distribution, velocity profiles, in thermal storage tanks at length is given by [3–7]. A study on greater extent solving partial differential questions using neural networs is done by [8]. On contrary, there are some factors which cause the stratification to deteriorate over time, these include primarily mixing at the inlet with cold water, losses to ambient, and internal convection. Stratification indices are mathematical equations quantifying the stratification process. Substantial research is present already discussing these indices. There are stratification measurement indices based on first law of thermodynamics, these include coefficients of stratification, Mix number, Richardson number etc. These indices actually calculate the usable fraction of energy ready to be delivered against stored. Second form of indices are based on second law of thermodynamics ([9]. [3–5]). Second law indices measure total exergy present to the available stored energy during the thermodynamic process of charge or discharge. Logical deduction is that second law indices are equated to stratification efficiency [3–5,9]. This means then an efficient process should always generate lesser entropy comparatively. [10] were the first who researched the second law efficiency. The work of [10] is tightly bounded to the delivery temperature and was applied

* Corresponding author.
E-mail address: yogenderpal.chandra@fs.cvut.cz (Y.P. Chandra).

https://doi.org/10.1016/j.est.2023.106699
Received 16 February 2022; Received in revised form 15 December 2022; Accepted 14 January 2023
Available online 24 January 2023

Nomenclature

ADC	analog to digital convertor
c/C	thermodynamic specific heat capacity (J/kg-K)
DL	deep learning
e	error/loss
E_{com}	compressor electricity consumption
E_p	circulation pump electricity consumption
GSHP	ground source heat pump
HP	heat pump
h	height (m)
H	total height (m)
LSTM	long short-term memory
MLP	multilayer perceptron
NN	neural network
NS	Navier-Stokes
PF	performance factor
PT-100	platinum temperature-100
Q	thermodynamic heat addition (kJ)
Raspi	Raspberry Pi minicomputer
RES	renewable energy source
RNN	recurrent neural network
RSS	residual sum squared
RTD	resistance temperature diode
TES	thermal energy storage
T	temperature (otherwise mentioned in text)
T_{hp}	heat pump outlet temperature
T_0	thermodynamic dead state (ambient)
$T_{hp,out}$	heat pump output temperature
$T_{hp,\ in}$	heat pump input temperature
t	time
V_{cp}	circulation pump flow rate l/h or m^3/s
V_{dis}	discharge rate l/h or m^3/s
W	modified loss coefficient

Greek

ρ	density kg/m^3
λ	penalty term in regularization
Δs	thermodynamic entropy production
η	efficiency
v_{hp}	heat pump flow rate/circulation pump flow rate m^3/s
ξ	exergy (kJ)
η_{st}	stratification efficiency
η_{st} (sh)	stratification eff. during charging

to the discharge process. In this paper, the Rosengarten exergetic equations are rederived for complete charge discharge cycle. The following points are further observed:

- To bring the real time component in the stratification measurement, second law efficiency equations are derived and are fitted to novel stream-data processing edge-device. In this manner, efficiency calculation is improved and is brought to the edge device which helped in envisioning the stratification decay in more dynamic way. The edge devices include two Raspberry Pi [11] minicomputers installed at the experimental test rig. A substantial amount of data engineering was done from ingesting data, data modelling, and finally to visualize data in real time. All the Code and the gif visuals of the physical process is available on the git repository [12]. The visual expression of stratifcation decay will help researchers and academicians for a better understanding of their TES devices and thus will help to improve the industrial testing. A detailed study on visual platforms to study experimentation in the field of efficient storage is done by Guo et al., [3–5].
- The edge computing is further evolved in the area of data engineering by addressing the following:
  - A framework of long short-term memory (LSTM) neural networks was utilized to predict the second law stratification efficiency. The data driven prediction model was correlated and compared with the quantitative formulae driven model.
  - Development of applied deep learning (DL) framework utilizing long short-term memory (LSTM), and multilayer perceptron (MLP) to model the layered temperature and to predict the entropy generation during charging and discharging loop. This will advance knowledge of deep learning frameworks and layered temperature modelling which researchers can use to understand their TES devices when quantitative approach might be restricted. For example, the trained models can be planted on the edge devices itself which can get the real time energy efficiency information without using quantitative calculations at the edge.
  - Hyper-tuning the LSTM neurons so as to improve their capacity to capture more complex local features (information) in the data. For example, discharging is accompanied by complex process of forced convention which has to be captured by model in order to predict the stratification efficiency correctly. Conventional models skip these complex features while only are able to capture more global information from the data. This paper also tried to address this problem as the method improvement.
- Finally, parametric analysis as a correlation matrix will be discussed in relation to performance factor (PF) of heat pump, second law charging efficiency, second law discharging efficiency to reach on a decision about which variables are respecting the energy sustainability.

2. Methods

2.1. Experimental setup

The simple concept of energy in and out is tested. Every irreversible thermodynamic process is accompanied with entropy generation which is the direct measure of the increase in the unavailable energy. The experiments are carried out and this entropy generation was calculated. In this manner de-stratifying entropy was quantitatively measured. The setup is based on a residential ground source heat pump consuming grid power and delivering heat at discrete compressor speeds. The tested TES tank was connected with this heat pump as a buffer heat storage device. Heat pump extracted the heat from the source tank which was constantly heated by thermostatic heater maintained at specific constant temperature. The tested TES was 390 l. Ten PT-100 temperature diodes were attached around the TES longitudinally. This divided the TES into 10 equal temperature layers. TES inlet and outlet temperatures were also tracked. Temperature diodes were calibrated for error of approximately ±0.3 °C. TES was connected with the load tank having a volume of 900 l. There were two water circuits of primary importance – heating circuit with heat pump & TES at its core, and load-TES circuit. Load-TES circuit is attached with a mixing valve to ensure constant discharge temperature. Both circuits had their own flow meter (Seimens) calibrated for error of ±0.5 %. All the data is ingested to the data-stream processing edge device (more on this is in next subsection). Charging was done for a predefined TES temperature with constant flow rate and compressor speed. Discharge loop was actuated for constant tapping temperature once the TES is charged for a predefined value. During the process data was getting ingested already to data streaming device and visuals of stratification indices were created in real time. The heated load tank was cooled down by thermostatic cooler and the experiments were repeated

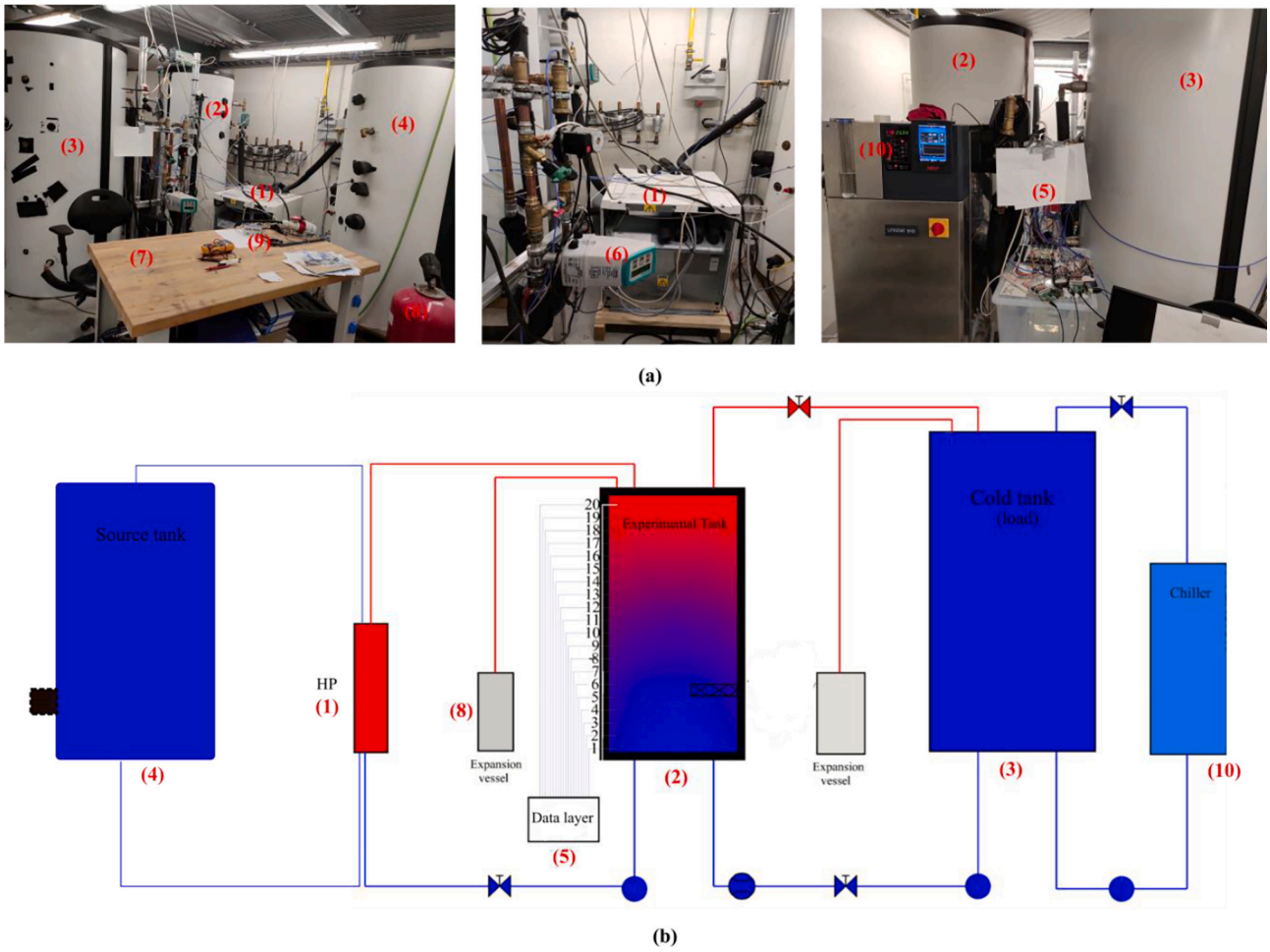

Fig. 1. (a) Experimental rig (see Table 1 for details), and (b) schematic.

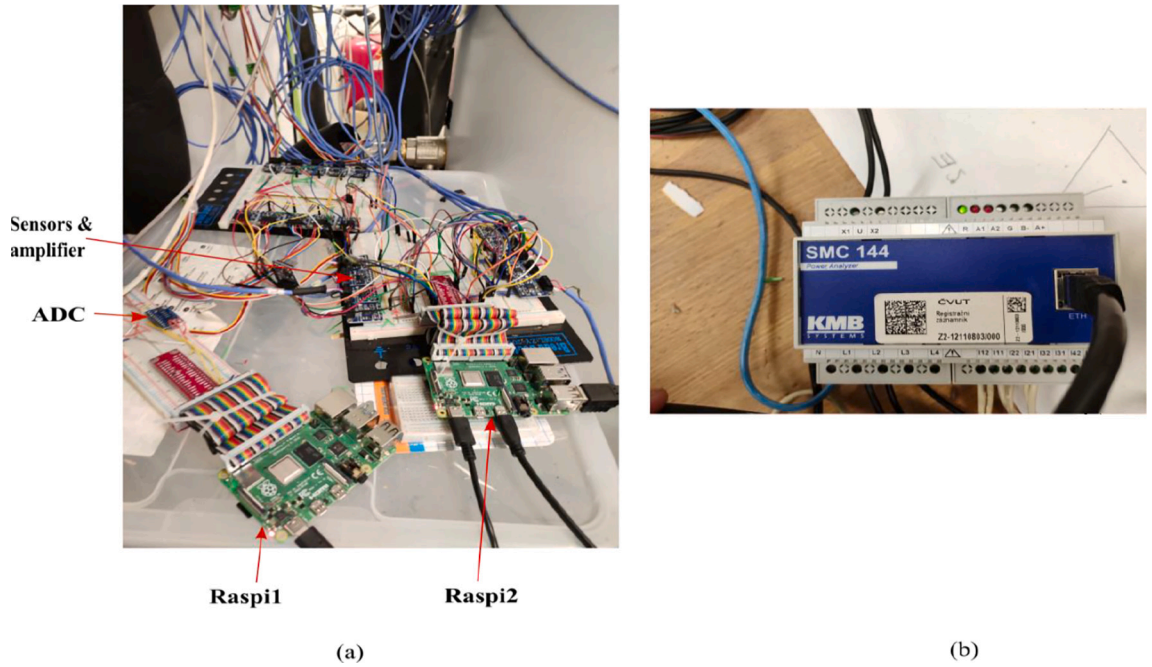

Fig. 2. (a) Raspberry-Pi edge device, and (b) wattmeter.

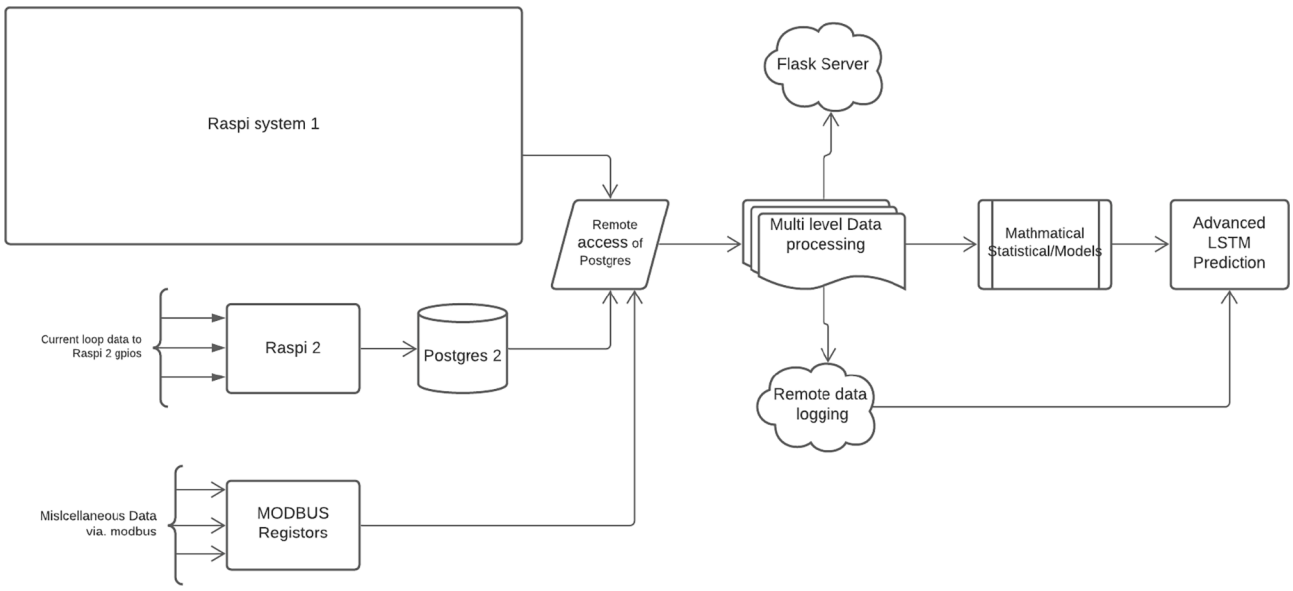

Fig. 3. Edge device workflow.

to enforce reproducibility and accuracy of results. In this way the energy graph was created and analyzed clearly depicting the proportion of grid energy available at tap. This was done by quantitatively calculating the entropy generation, exergy destruction and exergy availability at tap during full process loop. Grid power consumption was assessed using 3-phase wattmeter. A Modbus communication channel was utilized to collect the wattmeter data.

3. Data-streaming edge device

Data-streaming edge device was customized to perform stream processing on the ingested data in near-real time. Exergetic models thus developed were quantitatively fitted with the ingested data. The edge device housed two Raspberry-Pi minicomputers (Ras-Pi1 & Ras-Pi2) powered by Raspbian (Debian Linux distribution), see Fig. 2(a)).

Ras-Pi1 ingested temperature data from the experimental test rig on the other hand Ras-pi2 ingested flow rate information. PT-100 are analog devices, hence an analog to digital converter was used to transform this information before ingesting to the streaming edge device. *MAX31865* [13] was used for this purpose. Time step for data ingestion to the database was 5 s. The code performing this task can be found in the Git Hub repository [14]. Information about grid power consumption was also ingested in the same manner via. Modbus protocol, Fig. 2(b). This information was accessed through proper register address within the Modbus protocol. Error range of each single component is mentioned in Table 2. Ras-Pi1 served as master component performing extremely rudimentary tasks, for example data ingestion, cleaning, transforming. Furthermore, as raspberry-Pi minicomputers are operated headless – no monitoring screen, this makes it extremely essential while operating with higher temperatures, that a secondary web-based data monitoring application be deployed to avert any accident or hazard. In this regard, a Flask framework was also housed in the main server which ingested data into this web application for plots and visuals – thus adding a level of safety against outliers and high temperature accidents. The code for Flask application is freely available in the *GitHub* repository [15]. The workflow over edge device is shown in the Fig. 3.

Extremely important was the data engineering and data science stack used for coding the edge device. These include *Keras, Numpy, Scikit-learn* and *Pandas*. *NumPy* is a fundamental package for scientific computing in Python. It is a Python library that provides a multidimensional array object [16]. *Keras* is a deep learning API written in Python, running on top of the machine learning platform i.e. *TensorFlow* [17], which uses extraordinarily fast computing speed of *NumPy*. *NumPy's* tensors are up to 100 times faster than conventional data structures. Pandas is a fast, powerful, flexible, and easy to use open source data analysis and manipulation tool, built on top of the Python [18]. *Scikit-learn* is an open source machine learning library that supports supervised and unsupervised learning. It also provides various tools for model fitting, data preprocessing, model selection, model evaluation, and many other utilities [19].

Keras actually is built on top of TensorFlow [20]. TensorFlow is an end-to-end machine learning platform - planning and solutions to accelerate machine learning tasks at every stage of machine learning workflow such as preparing data, building ML models etc. *TensorFlow* is finds its application in natural language processing, computer vision, image recognition, high performance scientific commuting (HPC), finding solutions for partial differential equations etc. Keras provides a high-level API to communicate with low level TensorFlow and assists through the model development life cycle – for example, train, test, validation, model creation, hyper parameter tuning etc. It's focus on user experience actually permits easy and frequent prototyping, proof of concept, experimenting, solution design and delivery.

3.1. LSTM architecture

Since the introduction of machine leaning (ML) and deep learning (DL), multi-layer perceptron's (MLPs) have been widely used in engineering problems. MLPs are feed-forward networks, also termed as artificial neural networks (ANNs). In MLP, data flow happens via. The computational matrix $X \rightarrow f(w1,w2...wn) \rightarrow Y$. This lacks of any feedback loop causing vanishing gradient issues in MLPs [21]. That means that the weights start to die out as the information, if forwarded from one layer to another within the network.

Model training and weight adjustment use a technique called stochastic gradient descent. In this technique, the network repeatedly determines the coefficient of the loss function where it has its local minima. Thus, minimizing the loss at each iteration. In simplest form, a network takes X as input variable and predicts Y' as output variable, however the correct output variable is Y i.e. $X \rightarrow f(x) \rightarrow Y$ *Or* Y'. Thus, the loss/cost function as: $error = Y'(predicted) - Y(actual)$. Thus,

$$Cost = \frac{1}{N}\sum (Y' - Y)^2 \tag{1}$$

The aim of the network is minimizing this cost function and thus

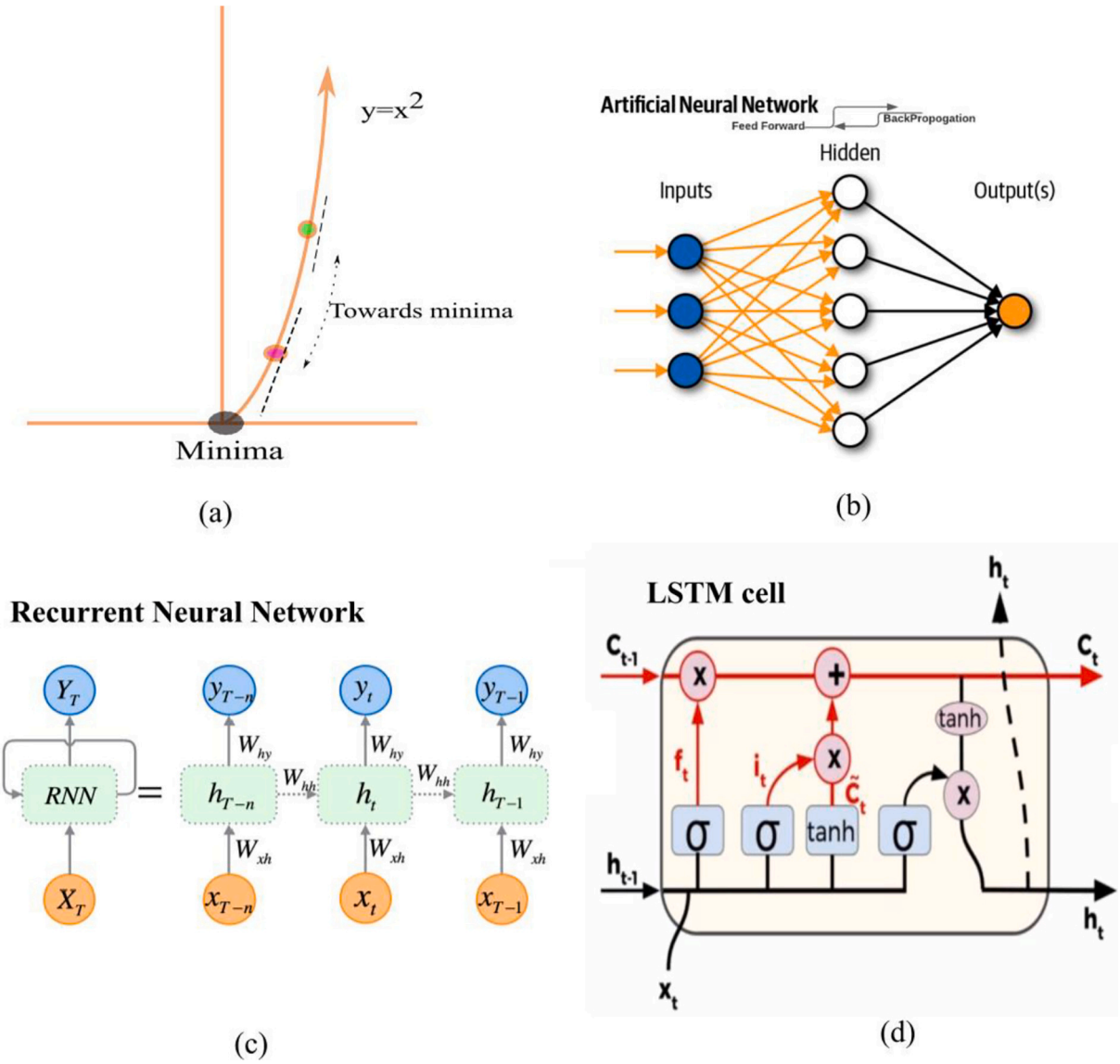

Fig. 4. (a) cost function and minima, (b) MLP architecture (c) RNN structure, and (d) LSTM node. (Fig. 4(c) & (d) modified from: https://bit.ly/LSTMfig 4d; https://bit.ly/LSTMfig 4c).

ensuring the correctness of the predicted output. A parabola $y = x^2$ has its local minima at *(0,0)*, (Fig. 4(a)). Stochastic gradient technique searches slop and intercept of the line pointing towards local minima. Slope of the curve determines the steps towards or away from local minima, see Fig. 4(a). Tangent at green point needs more steps to local minima, comparatively, then the slope at red point, steps are referred as Learning Rate (LR). SGD on this example revels:

$$J_{m,b} = \frac{1}{N}\sum e_i^{\,2} \tag{2}$$

partial derivatives reveal:

$$\frac{\partial J}{\partial m} = 2.e.\frac{\partial}{\partial m}(e) \tag{3}$$

$$\frac{\partial J}{\partial b} = 2.e.\frac{\partial}{\partial b}(e) \tag{4}$$

now,

$$\frac{\partial e}{\partial m} = \frac{\partial}{\partial m}(Y^{'} - Y) \tag{5}$$

and,

$$\frac{\partial e}{\partial b} = \frac{\partial}{\partial b}(Y^{'} - Y) \tag{6}$$

thus,

$$\frac{\partial e}{\partial m} = \frac{\partial}{\partial m}(mX + b - Y) \tag{7}$$

and,

$$\frac{\partial e}{\partial b} = \frac{\partial}{\partial b}(mX + b - Y) \tag{8}$$

this gives:

$$\frac{\partial e}{\partial m} = X \tag{9}$$

and,

$$\frac{\partial e}{\partial b} = 1 \tag{10}$$

plugging Eqs. (9) and (10) in (3) and (4) gives:

$$\frac{\partial J}{\partial m} = 2e.X^{*}LR \, and \, \frac{\partial J}{\partial b} = 2e.LR \tag{11}$$

now since $m^1 = m^0 - \delta m$ & $b^1 = b^0 - \delta b$.

thus,

$$m^1 = m^0 - e.X.LR \tag{12}$$

and,

$$b^1 = b^0 - e.LR \tag{13}$$

LR is the learning rate which is equivalent to steps to be taken towards local minima. In other words, gradients are calculated for each epoch which sustains the information about the minima while LR determines the speed of achieving it. Vanishing gradient occurs with feed forward technique, that means the gradients (Eqs. (2) to (13)) are diminishing in a deep neuronal network. Due to diminishing gradient in MLPs, the gradient reaching the input layer is so little that error function minimizing is compromised. This makes MLPs inefficient to model time series data – the case with TES.

This drawback of MLPs is overcome by recurrent neural network (RNN) with the help of extra feedback or recurrent loop. This recurrent network reduces the vanishing gradient (buy retaining information) to a higher extent thus assisting in capturing local as well as global features from time series data, Fig. 4(b). Fig. 4(c) shows a LSTM cell. LSTM retains the information by receiving preceding cell state, preceding cell output, and existing input vector as input variables. In addition, it passes the information about current state, and output vector to the next cell, Fig. 4(d).

The reduced vanishing gradient with LSTM makes them extremely suitable to model information rich physical processes for example, stratified flows and forced convection – in this case TES. [22] extensively used ANNs and RNNs to predict layered temperature in TES. The input variables were flow rate and preceding temperature values. No load training phase showed promising results, while load phase test results showed a degree of inaccuracy. Authors concluded that the diminishing gradient was the cause of this discrepancy. This paper attempted to address this issue. A better modelling approach was taken, LSTMs were chosen and hyper-tuned. [23] modelled TES with preceding temperature values as input features. Authors also used parameter hyper-tuning to catch local as well as global features from their time series. [24] modelled TES integrated with solar system using neural network. The results were excellent during training while were compromised during testing phase due to vanishing gradient problem. This paper also addressed overfitting problem by taking inputs from three preceding cells. This made more information available for the cells to learn from. A more extensive research on application of machine learning on TES and solar systems is presented by [25], while a review on machine learning application in time series forecasting at length is given by [26]. Thermodynamic application of MLPs is elaborated by [27–30]. Fig. 6 shows the information flow considering LSTM modelling and quantitative equation fitting. As a matter of fact, using LSTM on top of MLPs reduced training and validation losses to an order of magnitude.

3.2. Second law models and performance

To assess the end to end energy performance of TES integrated heat pump system, performance factor of heat pump, and TES's availability, and entropy generation were calculated in real time. The real time availability concept in TES gives an intuitive understanding of stratification destruction during charge discharge loop for varying HP parameters. For this purpose, second law entropy/exergy models are rederived, customized and fitted. In addition, scientific computation with *NumPy* allows temperature dependent thermo-physical properties (such as density) to be easily accommodated into the calculations. The equation was rederived to capture the spontaneity of the physical process [10]. While deriving the following stratification equations, some assumptions are made, firstly, change in entropy is needed to evaluated and is equated to the unavailable energy ($Tds \sim cdT$), this is true for incompressible fluid undertaking reversible process. Secondly, we assume specific heat is constant over all the working temperature range (5–65 °C, as a matter of fact, specific heat changes less than 1 % for aforementioned temperature range). Consider that the system goes from state 1 to 2, then according to the second law of thermodynamics for any incompressible liquid:

$$Tds = cdT \tag{14}$$

where ds is the entropy produced, and c is the specific heat of the incompressible liquid, assuming the process is reversible, this can be affirmed:

$$\int_1^2 ds = \int_1^2 c\frac{dT}{T} \tag{15}$$

this means that the change in specific entropy of tank can be expressed as:

$$\Delta s = s_2 - s_1 = cln\left(\frac{T_2}{Ti}\right) \tag{16}$$

where i is the i^{th} layer. Eq. (15) is valid for thermodynamic reversible process, while Eq. (16) is valid for any process changing its state from 1 to 2. Entropy of whole TES is

$$\Delta s_{total} = c\sum_i^n m_i ln\left(\frac{T_2}{Ti}\right) \tag{17}$$

and the integral form is

$$\Delta s_{total} = \int_0^H \rho(h)\cdot c(h)\cdot(V/10)\cdot ln\left(\frac{T_{hp}}{T_i}\right)dh \tag{18}$$

here density and heat capacity are a function of height. T_{hp} is the heat pump's outlet temperature while T_i is the layered temperature. Exergy can be expressed as

$$\xi_{1-2} = Q_{1-2} - T_0\cdot\Delta s \tag{19}$$

where $\xi_{1\text{-}2}$ is the exergy change (in TES), $Q_{1\text{-}2}$ is the energy change (heat addition by heat pump), and T_0 is the dead state temperature (ambient) below which converting energy to useful work is impossible. Thus,

$$Q_{1-2} = \int_0^t \rho(t)\cdot\dot{v}_{hp}\cdot c(t)\cdot\left[T_{hp,out}(t) - T_{hp,in}(t)\right]dt \tag{20}$$

And exergy is,

$$\xi = \int_0^t \rho(t)\cdot\dot{v}_{hp}\cdot c(t)\cdot\left[T_{hp,out}(t) - T_{hp,in}(t)\right]dt - T_0\int_0^H \rho(h)\cdot(V/10)\cdot C(h)ln\left(\frac{T_{hp}}{T_i(h)}\right)dh \tag{21}$$

and the stratification efficiency η_{st} is,

$$n_{st} = \frac{exergy(\xi)}{energy(Q)} \tag{22}$$

or:

Table 1
Description for Fig. 1 (a), specification of test rig.

Device	Specification	Description	Uncertainty/ Error
(1) Heat Pump	CTC EcoPart 612 M, 5.8 kW Rated Power	Multi-speed	–
(2) TES	390 l, Insulated	Single family house	–
(3) Load tank	900 l, Insulated	Maintained at ambient	–
(4) Source tank	350 l, thermostatically maintained		
(5) Data layer	Raspberry Pi micro computers	2 Raspi communicating with each other	–
(6) Flow meter	Sitrans F M Mag 5000	4–20 mA current loop out	0.4 %
(7) Working table	–	–	–
(8) Expansion valve	–	–	–
(9) Watt meter	3-phase	Communication via. Modbus	–
(10) Thermostatic chiller	Huber Unistat Thermostat	5.3 kW cooling capacity	± 0.5 %

$$n_{st}(ch) = \left[\int_0^t \rho(t)\cdot\dot{v}_{hp}\cdot c(t)\cdot\left[T_{hp,out}(t) - T_{hp,in}(t)\right]dt - T_0\int_0^H \rho(h)\cdot(V/10)\cdot C(h) ln\left(\frac{T_{hp}}{T_i(h)}\right)dh \right] \Big/ \int_0^t \rho(t)\cdot\dot{v}_{hp}\cdot c(t)\cdot\left[T_{hp,out}(t) - T_{hp,in}(t)\right]dt \quad (23)$$

where, v is the heat pump volumetric flow rate. The time derivative of heat addition contributes towards the dynamicity of data analytics hence allowing to scale the process spontaneously. This could allow researchers and engineers to make their TES integrated RE systems better adjusted for real time quantification. In this manner the Rosengarten method was yet employed however completely revamped for a) improved accuracy, and b) for dynamicity addition. Finally, electricity consumption is accessed from Modbus registers of wattmeter, and the HP performance factor (PF) is calculated using the following equation:

$$PF_{hp} = \frac{\sum_{t_i}^{t_n} Q_i}{\sum_{t_i}^{t_n}(E_{comp} + E_p)} \quad (24)$$

E_{com} and E_p are the compressor and circulation pump respectively. The idea is that 1st phase among 3-phases is used by the HP compressor, and the 2nd phase by circulation pump, this data is circulated and stored as 16-digit hexadecimal numbers in different registers each having unique address in hexadecimal digits also. So, there is need to access correct address to get a summed-up and/or unique value of energy consumption per phase and to convert it to human readable float value.

3.3. Hyperparameter tuning

As a general practice, the data is partitioned into train/validation sets. Model performance is determined by accuracy and/or loss. Generally, without any overfit the lower the loss the better the performance. Generalizing the data instead of learning details from it is called overfitting. Overfitting happens when model learns the detailed information along with noise in training data to that extent that it effects the prediction on the test data negatively. The training and validation loss difference is labelled as overfit. Some counter measures against overfit are dropout and regularization [31,32]. Loss is residual sum of square *(RSS)* as expressed by Eq. (25).

$$RSS = \sum_{i=1}^{n}(e)^2 = \sum_{i}^{n}[y_i - (m + bx_i)]^2 \quad (25)$$

As discussed earlier the goal of any machine learning algorithm is to reduce loss. Model hyper-tuning was achieved by number of passes to reduce loss until further improvement appears unlikely. For instance, a simple ANN network resulted in an excessive amount of overfit with a validation loss of 0.025. This overfit was reduced to a greater extent when dropout and regularization techniques were utilized, see Table 1. And so, by using these techniques and simplifying the model we were able to reduce validation loss from 0.024 to 4×10^{-4}. A further discussion on parameter hyper-tuning can be found in the research of [33]. Following are the hyper-tuned NN parameters:

- Addition of Dropout and Regularization layers: Dropout reduces the model output complexity by dropping output from random hidden nodes thus neutralizing their involvement, weights and errors. Either nodes are kept with probability of p or are dropped with probability

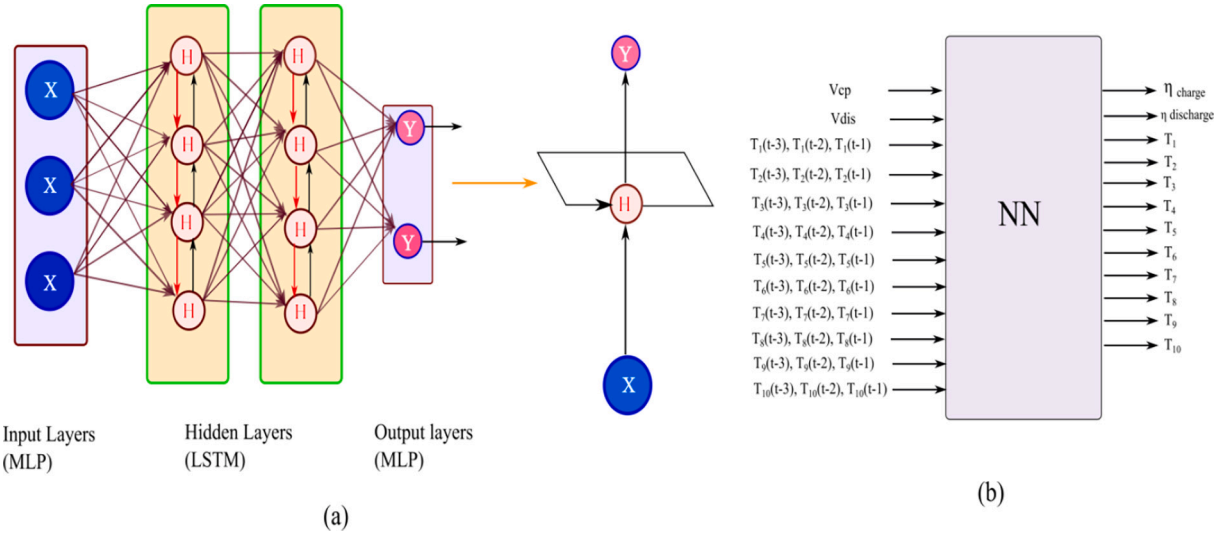

Fig. 5. (a) NN architecture, and (b) Input feature mapping.

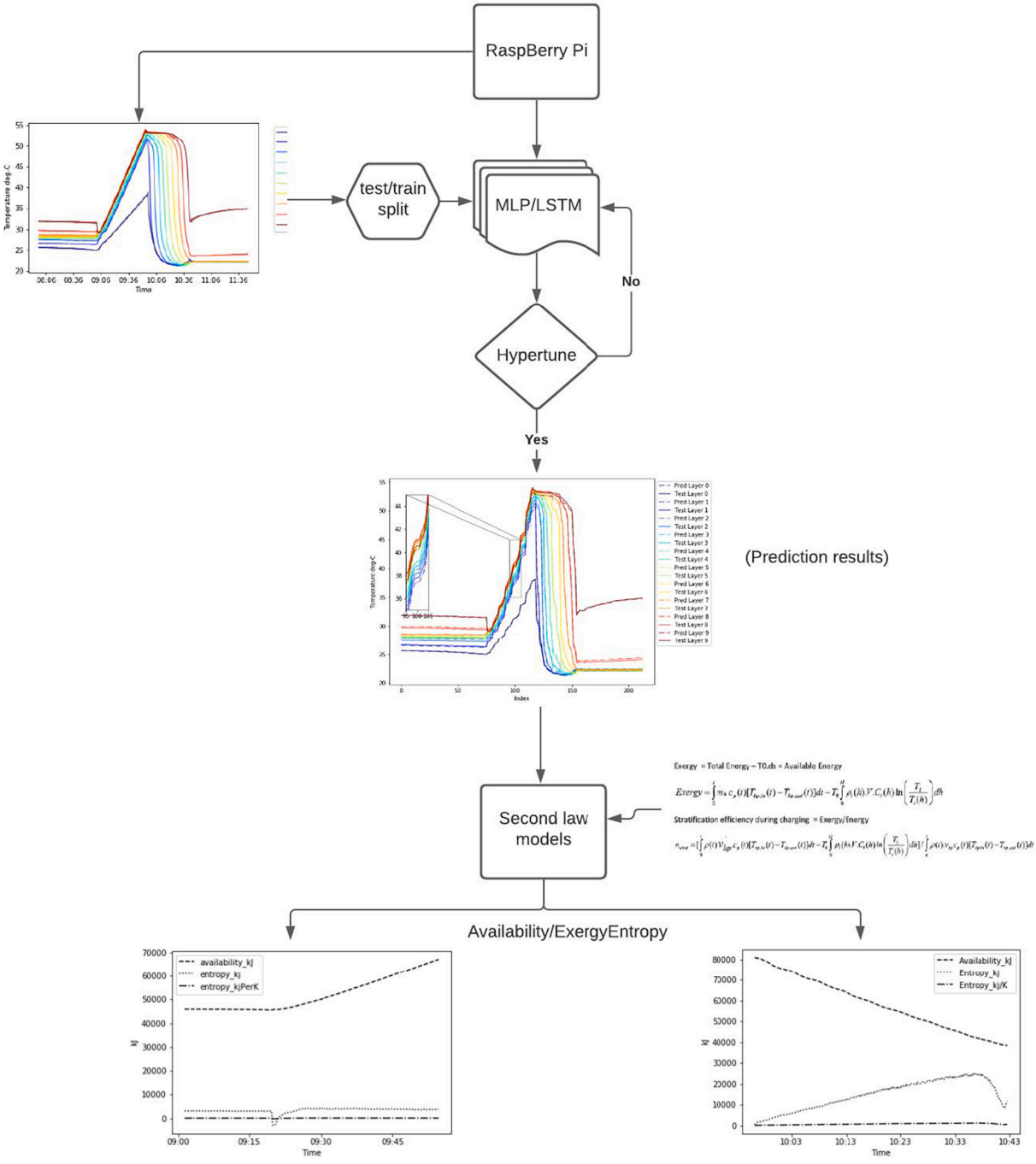

Fig. 6. Workflow over data streaming edge device for prediction task.

of 1-p randomly. This reduces the overfit by breaking the data generalizing pattern among connected nodes. Furthermore, regularization technique works in a way that model is penalized when overfit happens. The fundamental difference between L1 and L2 regularization techniques is about how they modify the loss function by adding a penalty term that is equal to the squared magnitude of the coefficient in L1 and the absolute value of the magnitude of the coefficient L2. The rationale behind these penalties is that by regularizing the loss function (adding coefficient W to RSS) model is enforced to perform lesser than the best (see Eq, (26) and (27)). The overfit for a specific value of W gives the accurate output variable y for input variable x thus minimizing the loss or RSS. This is true with seen data, however with unseen data validation loss increases. This is dealt with by adding penalty term λ to the coefficient W, Eq. (26) & (27). The code for dropout and regularization techniques implemented on the network is available in Git Hub repository [34]. A comprehensive research on these methods in heating systems is done by [35].

$$RSS(L1) = \sum_{i=1}^{n} (e)^2 = \sum_{i}^{n} [y_i - (m + bx_i)]^2 + \lambda \sum_{j}^{m} W_j^2 \tag{26}$$

$$RSS(L2) = \sum_{i=1}^{n} (e)^2 = \sum_{i}^{n} [y_i - (m + bx_i)]^2 + \lambda \sum_{j}^{m} |W_j| \tag{27}$$

- Model simplification itself reduced validation loss by an order of magnitude.

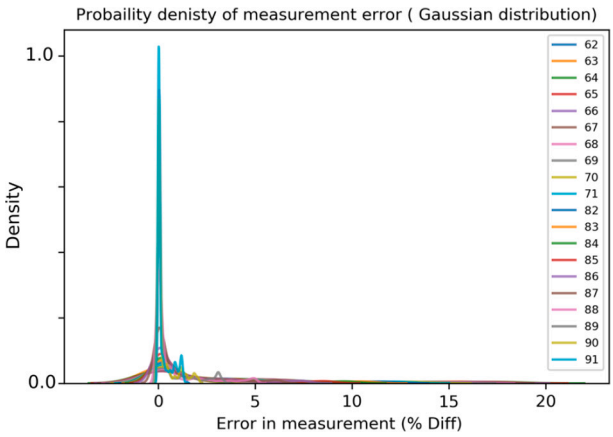

Fig. 7. Probability distribution of error.

- Data normalization was carried within *(0,1)* instead of *(−1,1)*.
- Batch size reduction from 500 to 50.
- 3 Preceding time step temperature values [(t-3), (t-2), (t-1) → *t*] reduced the validation loss further. Fig. 5 (a) and (b) shows the network architecture and feature mapping. Table 3 shows network architecture with training and testing loss.

3.4. Error analysis

This section details the degree of uncertainty in the collected experimental data. Time series data thus collected underwent statistical uncertainty analysis. Probability distribution of error in terms of gauss distribution was analyzed. Multiple tests were conducted on the single variable to guarantee that the results could be reproduced. Error was found on each successive set of data points. This procedure was done until 90 % of the data points were within one or two standard deviations. The probability density of calculated error for a set of data point is detailed in Fig. 7 The measuring sensors were orderly numbered from 62 to 91. Error was roughly normally distributed with 95 % of data points falling under 5 % error. Furthermore, uncertainties in the measuring devices involved is mentioned in Tables 1 and 2.

4. Results and discussions

Jupyter [36] notebook receives a stream of the real-time energy evaluation. The edge devices processed the stream of data they received from the test rig. The data stream was cleaned, stored and processed to fit to the exergy and entropy equations. The source code and gif of real time stream processing and visualization is available on Git Hub [12]. For charging, real time illustration of power consumption, evolution of temperature layers, and exergetic information were considered. For discharging, entropy generation, exergy availability etc. were considered. Modelled data in real time was restored and assembled into still visuals. For parametrization and evaluation. Fig. 8 depicts the entire experimental span put into perspective. Fig. 8(a) shows predicted against measured temperature profile. Hyper-parameter tuning brought down the validation loss to 4×10^{-4}. This is was in contrast to previous passes where validation loss was 0.4. Additionally, overfitting was minimized as was evident by low value of training loss (10^{-3}). Heat pump indices are visualized in Fig. 8(b). These include heat capacity, power consumption, and performance factor. Evidently due to larger temperature lift in the initial stage, power consumption is higher, and thus the performance factor reached to 2.3. In the later stage the temperature lift decreases, this decreases the power consumption as well and consequently performance factor (PF) decreased from 2.3 to 1.8, Fig. 8(b). At the expense of increased power consumption (100 % compressor speed) temperature lift is the highest thus decreasing PF_{hp}.

Fig. 9 shows the availability and entropy during both charging and charging processes. To calculate the availability, thermodynamic energy balance of TES and heat pump was performed using the equations previously developed. Exergetic availability and entropy generation was determined in live mode, gif is available on Git Hub [12]). Once charging stopped discharging was commenced. The energy balance of charging process was again performed by the edge device. Information about availability in terms of exergy and entropy generation was gathered for discharging. Entropy generation during discharge process was measured to be 4000 kJ. Simply stated 4000 kJ of energy was lost during charging. This means that heat pump power consumption was 3.29 kWh for charging the TES to 5.04 kWh. This raised TES's internal energy to 80,000 kJ while the system lost (4000 kJ) as generated entropy – stratification decay. In contrast, discharge generated 20,000 kJ of entropy at 400 l per hour of discharge rate. Fig. 10 highlights the concept of availability for a reversible process undergoing state change. Highest amount of work that can be extracted from system is called availability and it is generally referenced with ambient state. For a reversible process, all energy above ambient is available. Fig. 9 (a) & (b) demonstrates the available energy in charging and discharging of TES under experiment.

Fig. 11 depicts the efficiency predicted against measured. Data-streaming edge device calculated the stratification efficiency using second law equations (Eqs. (21)–(23)) Model development – train, test, validation was done by the data thus gathered separately. To close the feedback loop, prediction was done by the edge device using trained LSTM models previously developed and deployed. One such predicted and calculated data set is depicted in Fig. 11 for charging and discharging. Index is the time representation in the network's terminology. When the compressor was running at 100 % circulation speed, the charge efficiency was found to be around 78.6 %, and discharge efficiency was around 80 %. Fig. 12 (a) shows the 5 % error range and Fig. 12 (b) shows the absolute value of the same during test phase. Loss has been reduced to 10^{-4} (previously it was 10^{-2}) using parameter hyper-tuning. This is shown in Fig. 12 (c) where loss is represented as r^2.

TES and heat pump variables are parameterized. For example, heat pump operating parameters for 50 %, 70 %, and 90 % of the full compressor speed were evaluated for heating side indices. Their effect on entropy generation or TES stratification efficiency was determined during charging. Heating side key performance index was performance factor which was calculated using heat output (heat capacity) and power consumption. Fig. 13 shows these values for 50 %, 70 % and 90 % of heat pump compressor speed. TES temperature evolution is also depicted in the figure. Performance factor was decreasing with the increase in compressor speed. The reason for this was abrupt increase in the temperature lift. Energy threshold for TES was maintained at 80,000 kJ for each experimental case, once reached, heat pump was stopped.

This provided a realistic and fair comparison to evaluate comparative participation of each heat pump's parameter in entropy generation in the TES. 50 % HP parameter showed the highest performance factor, see Fig. 13. In contrast, generated entropy during charging were highest and were resulted by 50 % of compressor speed, making it thermodynamically least efficient, see Fig. 14 (a). Generated entropy during charging is parameterized in Fig. 14 (a) & (b). Fig. 14 confirms that 50 % of compressor speed generates the highest entropy thus maximum destratification during charging. The reason for this is that the low temperature heat addition at a moderately higher flow rate of 700 l per hour causes more mixing. In other words, low compressor speeds are neither efficient from power consumption point of view nor efficient from thermodynamic point of view. Consequently, as apparent in Fig. 14 90 % of compressor speed performed better then preceding cases for the aforementioned reason. Among all, 70 % compressor speed generated the least entropy, see Fig. 14(a). This was due to the fact that that optimal combination of temperature of heat addition and circulation speed was achieved. Thus, it was concluded that 70 % of compressor speed generated the least amount of entropy (3000 kJ), while 70 % and

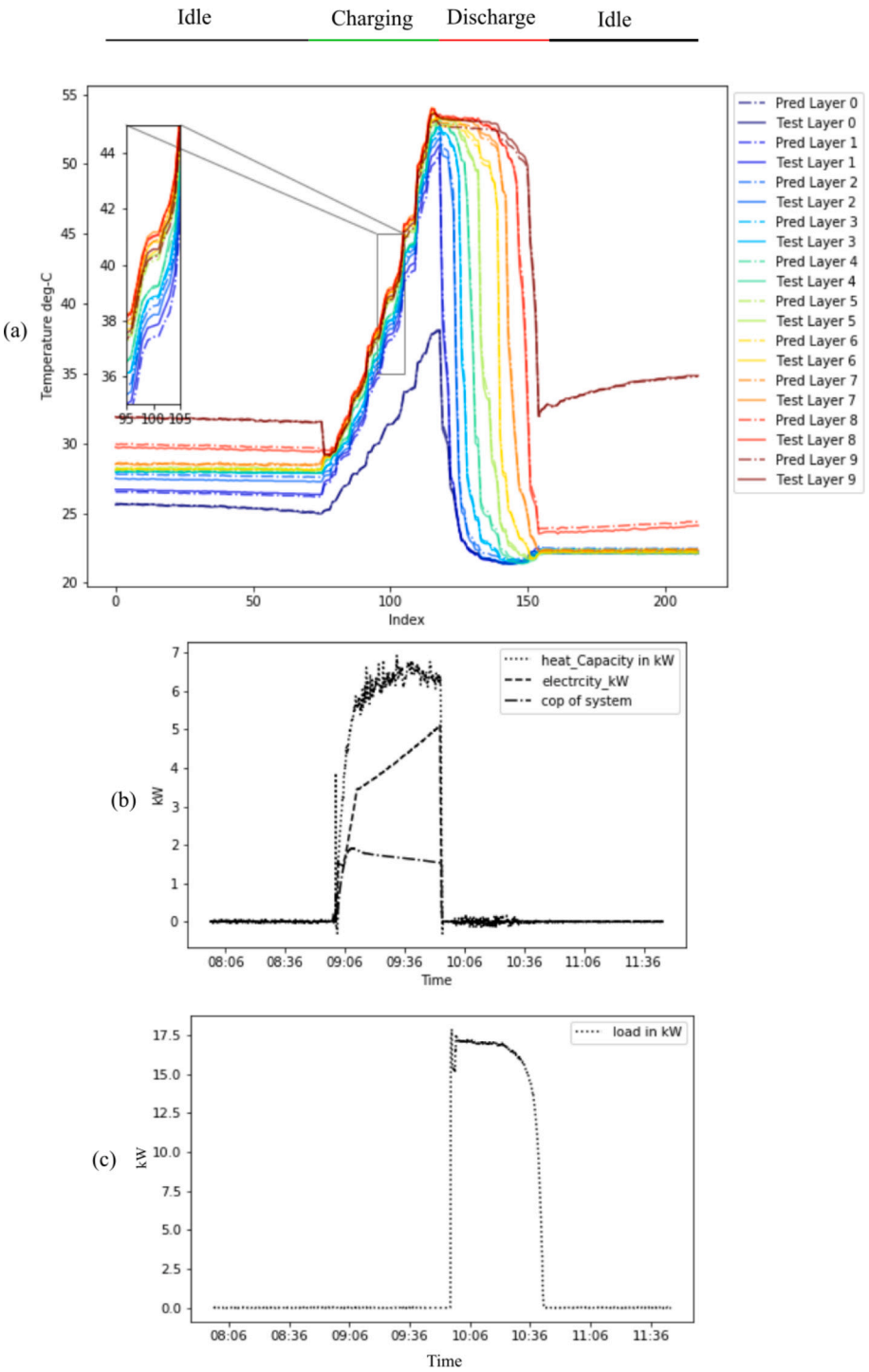

Fig. 8. (a) Temperature profile measured against predicted, (b) Heat capacity, power consumption, Performance Factor, and (c) Load.

90 % of the compressor speeds generated 4700 kJ and 6300 kJ respectively. Fig. 14(b) shows the exergy information for all the cases. Exergy data is in congruence with the entropy data.

Fig. 15 (b) shows the calculated stratification efficiency during charging for all the three cases. The edge device calculated the efficiency using Eq. (23) and streamed it in real time. The stratification efficiency is in congruent with exergy and entropy data.

Fig. 15 (a) shows the predicted efficiency which is congruent with the measured data. For 50 %, 70 %, and 90 % compressor speed, $\eta_{predicted}$ and $\eta_{calculated}$ are approximately 76 % ($\pm$ 1 % $\eta_{predicted}$), 83 % ($\pm$ 2 % $\eta_{predicted}$), and 79 % ($\pm$ 2 % $\eta_{predicted}$) respectively.

Validation loss was brought down to a minimum of 6×10^{-3}. Training loss was ranging between 4×10^{-3} and 6×10^{-3}. The discrepancy between validation and training loss illustrates some overfit. This can further be improved by simplifying the model or feeding the model with better quality and quantity of data.

Exergy and entropy graphs for the discharging process is shown in Fig. 16. Discharging was done at 400 l/h, 600 l/h and 800 l/h. Maximum entropy was generated at 800 l per hour – the highest flow rate. Minimum entropy was generated at lowest flow rate i.e. 400 l per hour. Furthermore, 25,000 kJ of entropy was generated at highest discharge rate while only 6000 kJ at highest charging rate. So, this can be

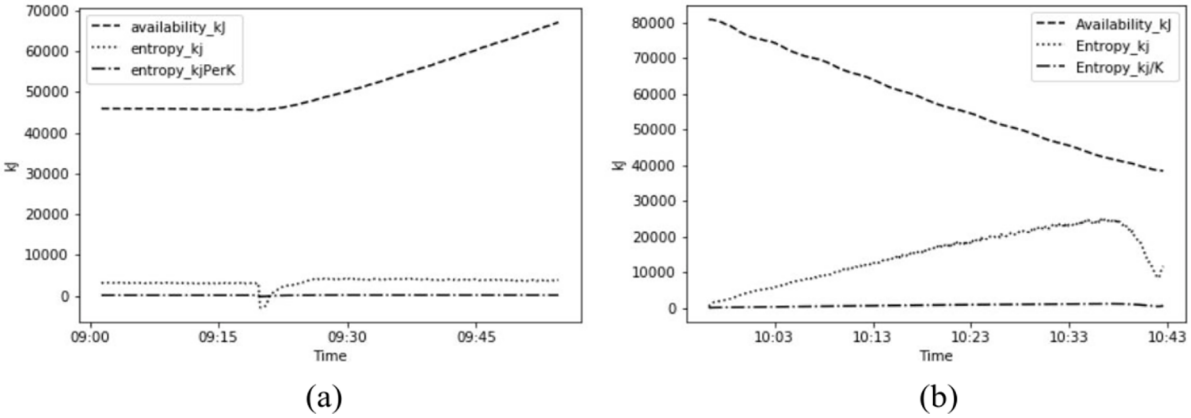

Fig. 9. Availability and entropy at full compressor speed (a) charging, and (b) discharging.

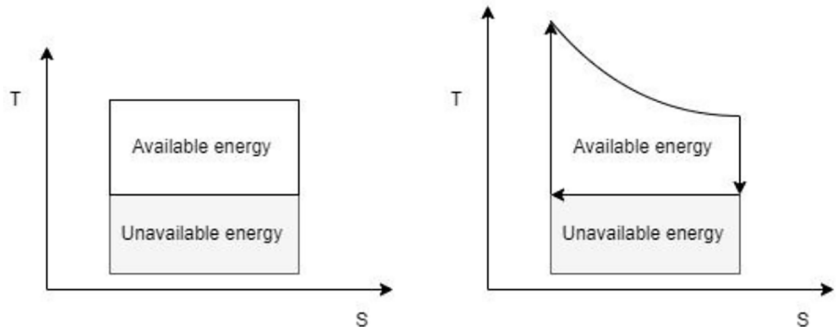

Fig. 10. Concept of thermodynamic availability.

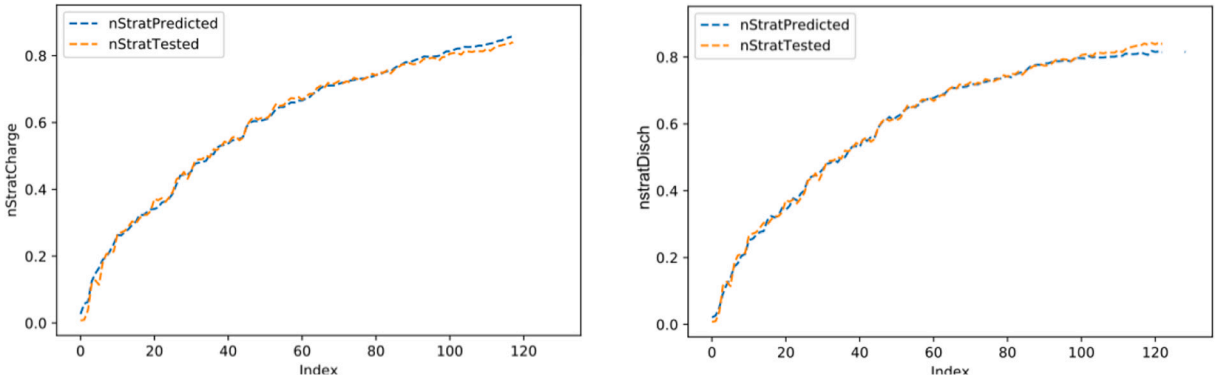

Fig. 11. Stratification efficiency for (a) charging at 100 % compressor speed, and (b) discharging at around 400 l/hour.

concluded that discharging at lowest flow rate while charging at moderately higher flow rates makes the system more efficient thermodynamically.

Fig. 17 (a) shows the discharge phase KPI i.e. stratification efficiency, both predicted as well as calculated. Calculated stratification efficiency has the highest value at 400 l per hour i.e. 84 % (± 0.2 % $\eta_{predicted}$). For 600 l per hour calculated stratification efficiency during discharge was 81 % (± 1 % $\eta_{predicted}$). Finally, for 800 l per hour the calculated stratification efficiency during discharge was around 76 % (± 1 % $\eta_{predicted}$). Fig. 16 (b), (c), and (d) shows the error, represented in terms of r^2 deviation.

As for concluding remarks, the edge device, using the novel exergetic models, calculated the entropy generation during charging. The higher the entropy generation the lower the stratification in the TES. The entropy generation can be minimized by opting optimized charging and discharging indices. Charging indices include correct compressor speed and circulation speed. Discharging indices include discharging flow rate as the most influential parameter. To sum it up, 50 % of compressor speed had the highest performance factor while maximum entropy generation. Thus, thermodynamically, 70 % of compressor speed was more efficient then preceding case because of its equivalent performance factor and lower entropy generation. In addition, it was also determined that stratification decay due to mixing (and resulted entropy generation) is significantly higher during discharge then charging.

5. Conclusion

This paper addressed the stratification measurement of TES in real time mode with custom built data-stream processing edge device and exergetic (quantitative) models. Stratification was also studied using

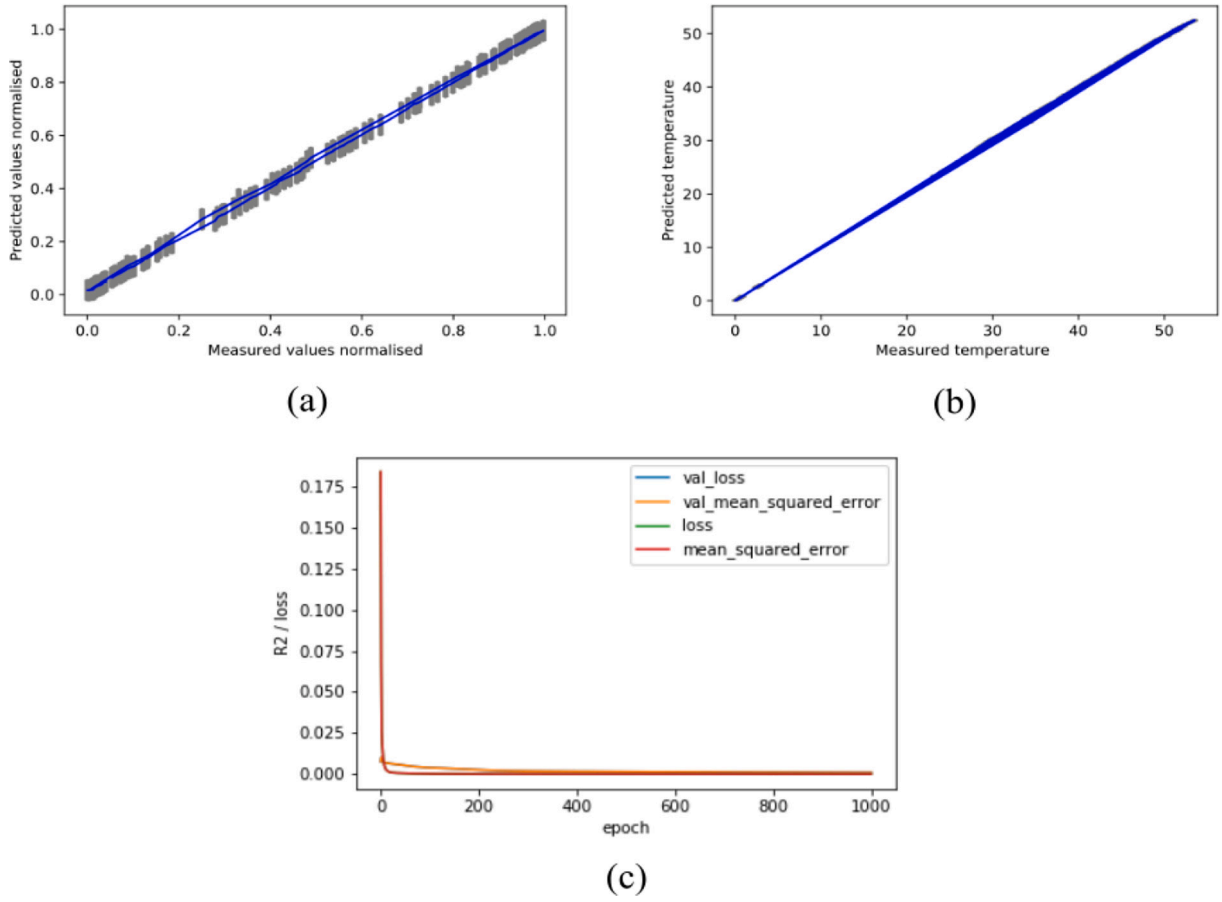

Fig. 12. Predicted against measured temperature (a) Normalized 5 % error range, (b) absolute values, and (c) loss.

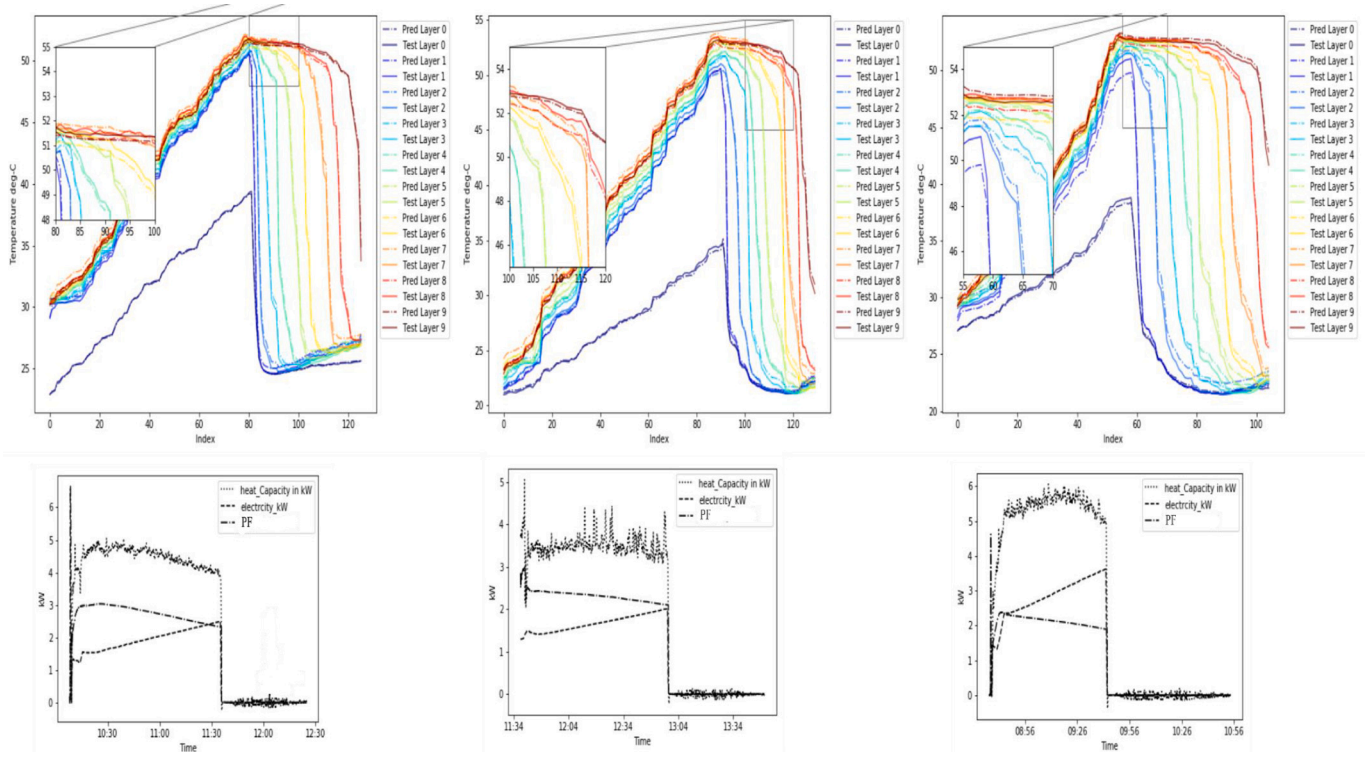

Fig. 13. Predicted against calculated temperature profile along with HP indices – heat capacity, power consumption and PF for (a) 50 % compressor speed (b) 70 % compressor speed, and (c) 90 % compressor speed. Discharge at 400, 600 and 800 l per hour.

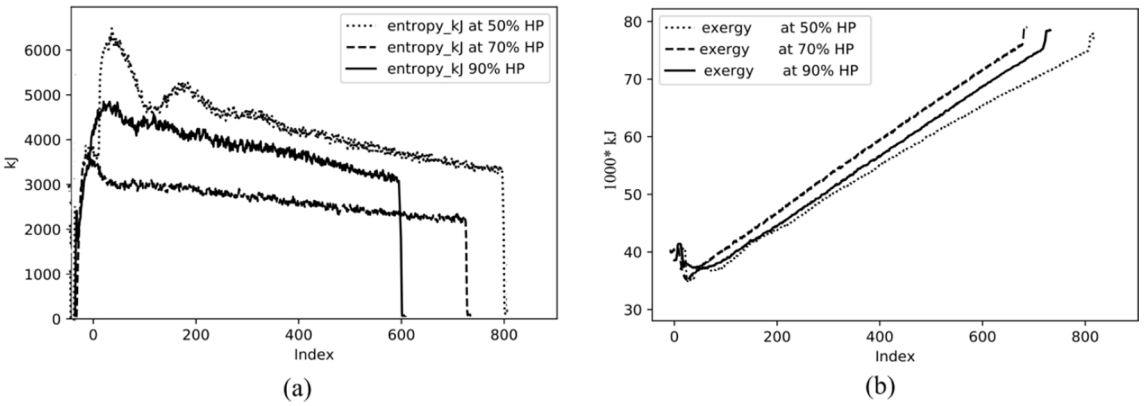

Fig. 14. Comparative (a) entropy generation, and (b) exergy destruction (measured) during charging at 50 %, 70 %, and 90 % of the compressor and circulation speed. Pump circulation rates respectively were – 700, 900 and 1100 l/h.

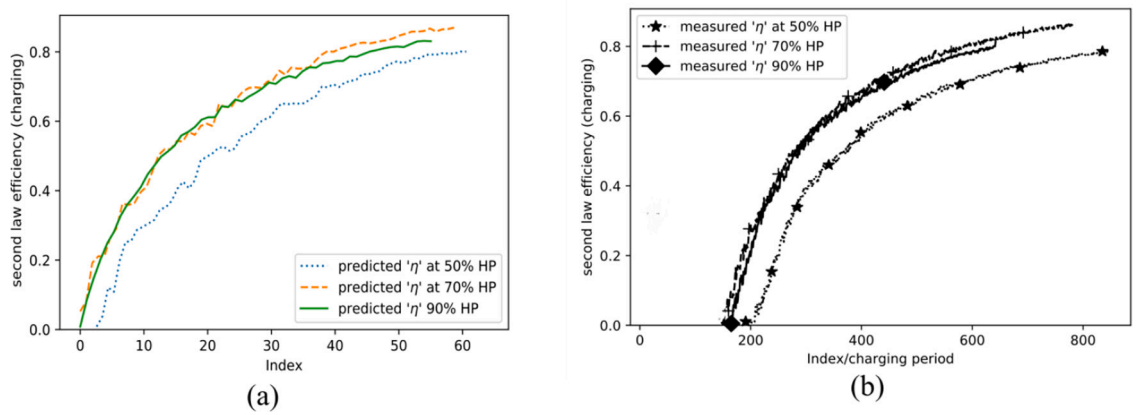

Fig. 15. Stratification efficiency (a) predicted, and (b) calculated at various compressor speed.

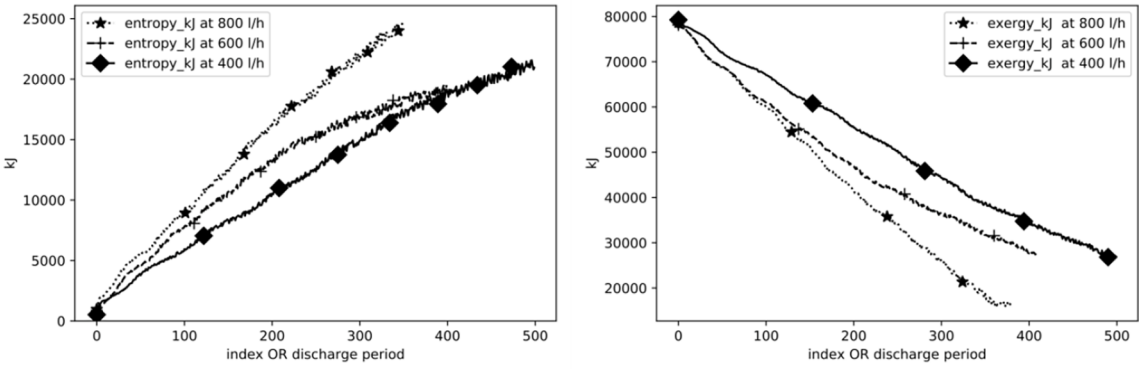

Fig. 16. Measured (a) comparative entropy generation, and (b) exergy delivered during discharge at various flowrates.

data driven neural network approach. In the end, the assumption-based approach (quantitative model) and the assumption-free approach i.e. data driven very nicely confirm and thereby support each other. The following observations are made:

- A TES integrated heat pump used for a single-family house was tested for stratification efficiency and energy balance. And so, end to end energy usage was calculated - from grid to tap.
- Subsequently, custom exergy models were built and were applied to TES using custom data streaming edge device which has the capability to study end to end energy expenses.
- Three distinct compressor speeds and tapping rates were studied using this data-streaming edge device and their exergy disbursement was studied in live mode. It was observed that entropy generation was maximum at highest discharge rate of 800 l per hour i.e. 25,000 kJ (while only 3000 kJ for 900 l/h of charging rate). Furthermore, entropy generation has not only impact on stratification efficiency, however also on performance factor of the heat pump. Making it extremely essential to adjust for inlet flow rate and compressor speed ratio. A PF of 3.2 was obtained at 70 % compressor speed, while maximum discharge efficiency was registered at lowest discharge of around 450 l/h.

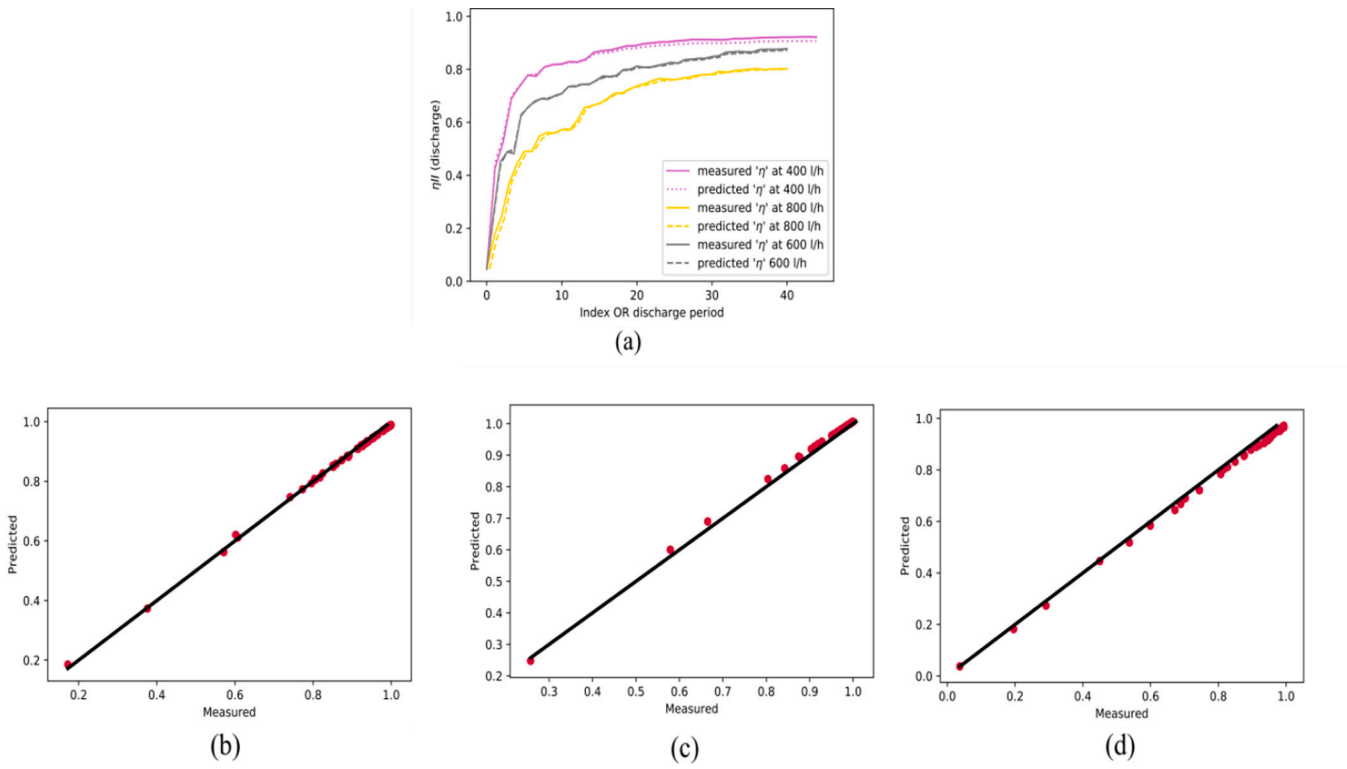

Fig. 17. Stratification efficiency during discharge (a) predicted against measured (b), (c), and (d) R^2 deviation (variance) for 400 l/h, 600 l/h, and 800 l/h discharge.

Table 2
Edge device components with involved uncertainties.

Device	Description	Specification	Uncertainty/ Error/ Accuracy
Raspberry Pi 4	Core component (minicomputer)	8 GB ram	–
Tem. Sensors	Pt100 RTD	4 wire RTD based (ouput: 4–20 mA)	±0.05° C from 80° C to 200 °C
Flow meter	Sitrans F M Mag 5000	Output: 4–20 mA current loop	0.4 %, ±1 mm/ s
Pt100 resistance Amplifier	Adafruit temperature sensor amplifier (MAX 31865)	RTD amplifier and ADC (for Raspi reading)	0.1 % Ω
ADC (ADS1115 I2C module)	Analog to digital converter (for flow meter current loop)	16-bit I2C communication, 4-channel	0.05 V
Watt-meter	3-phase	Communication via. Modbus	–

Table 3
NN architecture.

Layer (type)	Output shape	Training loss	Testing loss
(1) Dense (MLP)	(None, 32)	0.04	0.04
(2) Lstm_1 (LSTM)	(None, 16)	3×10^{-4}	4×10^{-4}
(3) dropout_1 (Dropout)	(None, 16)	–	–
(4) dense_1 (Dense)	(None, 1)	4×10^{-4}	4×10^{-4}

- Data streaming layer along with custom built models give information of TES energy expenses in real time and within 5 % error range. This real time understanding of energy expense can help engineers and researchers to assess their renewable energy devices.
- A neural network model using LSTM was developed and was used to predict the layered TES temperature and efficiency of TES. The error range for temperature and efficiency prediction was observed to be 5 % and 2 % respectively. The LSTM model reproduced the results calculated by exergetic model thus the results calculated by one model or the other was corroborated. The data-driven approach is agnostic and makes no assumptions - but does not give any clue how and which inputs influence the output. The quantitative approach works with assumptions but shows clearly the quantitative relationship between input features and the calculated output, thus helps to deepen the understanding of the processes. Data driven approach in theory is bias-free.

Declaration of competing interest

No conflict of interest exists.

Data availability

The data with the code (deep learning, whole calculation base, flask server and GIF) is available in the GitHub repositories, as referenced in the correct locations within the paper.

Acknowledgment

This work has been supported by the Project TN01000056 - National Centre of Competence CAMEB granted by Technology Agency of Czech Republic.

References

[1] Y.P. Chandra, T. Matuska, Stratification analysis of domestic hot water storage tanks: a comprehensive review, Energy Build. 187 (2019) 110–131.
[2] Y.P. Chandra, T. Matuska, Numerical prediction of the stratification performance in domestic hotwater storage tanks, Renew. Energy 154 (2020) 1165–1179.

[3] J. Guo, Z. Liu, B. Yang, X. Yang, J. Yan, Melting assessment on the angled fin design for a novel latent heat thermal energy storage tube, Renew. Energy 183 (2022) 406–422.
[4] J. Guo, J. Du, G. Liu, X. Yang, M. Li, Compression effect of metal foam on melting phase change in a shell-and-tube unit, Appl. Therm. Eng. 206 (2022), 118124.
[5] J. Guo, X. Wang, B. Yang, X. Yang, M. Li, Thermal assessment on solid-liquid energy storage tube packed with non-uniform angled fins, Sol. Energy Mater. Sol. Cells 236 (2022), 111526.
[6] X. Yang, J. Guo, B. Yang, H. Cheng, P. Wei, Y. He, Design of non-uniformly distributed annular fins for a shell-and-tube thermal energy storage unit, Appl. Energy 279 (2020), 115772.
[7] X. Yang, X. Yang, Z. Liu, X. Luo, J. Yan, Effect of fin number on the melting phase change in a horizontal finned shell-and-tube thermal energy storage unit, Sol. Energy Mater. Sol. Cells 236 (2022), 111527.
[8] L. Lu, X. Meng, Z. Mao, G.E. Karniadakis, DeepXDE: a deep learning library for solving differential equations, SIAM Rev. 63 (1) (2021) 208–228.
[9] M.Y. Haller, E. Yazdanshenas, E. Andersen, C. Bales, A method to determine stratification efficiency of thermal energy, Sol. Energy 84 (2010) 997–1007.
[10] G. Rosengarten, G. Morrison, M. Behnia, A second law approach to characterising thermally stratified hot water storage with application to solar water heaters, J. Sol. Energy Eng. 121 (4) (1999) 194–200.
[11] Raspberry Pi for Industry, n.d.Raspberry Pi for Industry . (n.d.). Retrieved from Raspberry Pi: https://www.raspberrypi.org/for-industry/.
[12] Y.P. Chandra, GitHub [GIF and Code], Retrieved from, 2021, https://github.com/yogenderPalChandra/Raspi1_main_Pt100_FlaskServer.
[13] Adafruit-Industries, n.d.Adafruit-Industries . (n.d.). Adafruit PT100 RTD Temperature Sensor Amplifier - MAX31865. Retrieved from https://www.adafruit.com/product/3328.
[14] Y.P. Chandra, GitHub Code, Retrieved From GitHub, 2021, https://github.com/yogenderPalChandra/Raspi2_second_currentLoop_RemoteMySql/blob/main/FinalScript.ipynb.
[15] Y.P. Chandra, Flask Code, Retrieved from GitHub, 2021, https://github.com/yogenderPalChandra/rpi1_rpi2_FLASK_Heroku.
[16] Numpy-Docs, n.d. Numpy-Docs . (n.d.). Numpy-docs. Retrieved from https://numpy.org/doc/stable/.
[17] Keras-API, n.d.Keras-API . (n.d.). Keras Deep Learning Framework. Retrieved from https://keras.io/api/.
[18] Numpy-Docs, n.d. Pandas-Docs . (n.d.). Pandas API Documentation. Retrieved from https://pandas.pydata.org/docs/reference/index.html.
[19] Scikit-learn-supervised-learning, n.d.Scikit-learn-supervised-learning . (n.d.). Supervised Machine Learning. Retrieved from https://scikit-learn.org/stable/supervised_learning.html#supervised-learning.
[20] TensorFlow, n.d.TensorFlow . (n.d.). Tensorflow Machine Learning Framework. Retrieved from https://www.tensorflow.org/.
[21] I. Goodfellow, Y. Bengio, A. Courville, Deep Learning, first, MIT press, 2016.
[22] P. Géczy-Víg, I. Farkas, Neural network modelling of thermal stratification in a solar DHW storage, Sol. Energy 84 (6) (2010) 801–806.
[23] W. Yaïci, E. Entchev, Performance prediction of a solar thermal energy system using, Appl. Therm. Eng. 73 (2014) 1348–1359.
[24] S.A. Kalogirou, E. Mathioulakis, V. Belessiotis, Artificial neural networks for the performance prediction of large solar systems, Renew. Energy 63 (2014) 90–97.
[25] S.A. Kalogirou, Artificial neural networks in renewable energy systems applications: a review, Renew. Sust. Energ. Rev. 5 (4) (2001) 373–401.
[26] C. Voyant, G. Notton, S. Kalogirou, M.L. Nivet, C. Paoli, F. Motte, A. Fouilloy, Machine learning methods for solar radiation forecasting: a review, Renew. Energy 105 (2017) 569–582.
[27] S.A. Kalogiroua, S. Panteliou, A. Dentsoras, Artificial neural networks used for the performance prediction of a thermosiphon solar water heater, Renew. Energy 18 (1999) 87–99.
[28] A. Mellit, M. Benghanem, S.A. Kalogirou, Modeling and simulation of a stand-alone photovoltaic system using an adaptive artificial neural network: proposition for a new sizing procedure, Renew. Energy 32 (2007) (2007) 285–313.
[29] A. Sencan, K.A. Yakut, S.A. Kalogirou, Thermodynamic analysis of absorption systems using artificial neural network, Renew. Energy 31 (2006) 29–43.
[30] M. Souliotis, S. Kalogirou, Y. Tripanagnostopoulos, Modelling of an ICS solar water heater using artificial neural networks and TRNSYS, Renew,e Energy 34 (2009) 1333–1339.
[31] G.E. Hinton, N. Srivastava, A. Krizhevsky, I. Sutskever, R.R. Salakhutdinov, Improving neural networks by preventing co-adaptation of feature detectors, in: Neural and Evolutionary Computing, Cornell University, 2012. Cite as: arXiv:1207.0580.
[32] N. Srivastava, G. Hinton, A. Krizhevsky, I. Sutskever, R. Salakhutdinov, Dropout: a simple way to prevent neural networks from overfitting, J. Mach. Learn. Res. 15 (56) (2014) 1929–1958.
[33] C. Correa-Jullian, M.J. Cardemil, L.E. Droguett, M. Behzad, Assessment of deep learning techniques for Prognosis of solar thermal systems, Renew. Energy 145 (2020) 2178–2191.
[34] Y.P. Chandra, Github Deep Learning Code, Retrieved from GitHub, 2021, https://github.com/yogenderPalChandra/jospehus_DL.
[35] J.K. Hwang, G.Y. Yun, S. Lee, H. Seo, M. Santamouris, Using deep learning approaches with variable selection process to predict the energy performance of a heating and cooling system, Renew. Energy 149 (2020) 1227–1245.
[36] Jupyter-Lab, n.d.Jupyter-Lab . (n.d.). Jupyter Notebook. Retrieved from https://jupyter.org/.

Study 3

Design intelligent IoT stream processing unit to evaluate energy/exergy and predict the second law stratification efficiency in real time

---

Paper 4: Intelligent data systems for building energy workflow: Data pipelines, LSTM efficiency prediction and more

In this paper, a novel real time stratification performance evaluation and streaming tool (method) for HP integrated TES system was developed. For this purpose, a core computer science application layer was involved – customized data layer using Raspberry Pi single board minicomputers and the other associated data engineering stack. Finally, the custom built second law model developed in study 3 is used to calculate in real time the stratification efficiency during charging. The divergence of this study form study 3 is that this study only talks about the application of real time streaming system in charging mode, in addition to which the second law models are not derived here and are only borrowed and used from study 3.

Paper 5: Energy modeling of thermal energy storage (TES) using intelligent stream processing system

In this paper, the novel data streaming layer is used to evaluate the stratification performance according to indices of stratification which were observed during study 1 and 2. These indices include MIX, Richardson number and temperature profiles for various operational parameters. Even though second law stratification efficiency was not estimated using data streaming layer, neural network architecture is yet used to predict stratification in the form of MIX and temperature profiles as the continuation work from study 2.

Energy & Buildings 267 (2022) 112135

Contents lists available at ScienceDirect

Energy & Buildings

journal homepage: www.elsevier.com/locate/enb

Intelligent data systems for building energy workflow: Data pipelines, LSTM efficiency prediction and more

Yogender Pal Chandra [a,b,*], Tomas Matuska [b]

[a] Czech Technical University in Prague, Faculty of Mechanical Engineering, Department of Environmental Engineering, Technicka 4, 166 07, Prague 6, Czech Republic
[b] Czech Technical University in Prague, University Centre for Energy Efficient Buildings, 27343, Bustehrad, Czech Republic

ARTICLE INFO

Article history:
Received 3 March 2022
Revised 12 April 2022
Accepted 21 April 2022
Available online 27 April 2022

Keywords:
Data acquisition with python and RaspberryPi
Energy storage and smart systems
LSTM
Neural Networks

ABSTRACT

The data collection process for thermal energy storage (TES) system is largely still and restricted to data collection only. This leaves a gap to study the transient state physical process of charge and discharge as it proceeds. In addition, these devices are restricted and cannot perform on spot model fitting, prediction and other data curation techniques. This paper demonstrates the application of intelligent data layer with neural networks for evaluating and predicting end to end performance of heat pump integrated stratified thermal energy storage (TES) system. The data modelling – acquisition, curation, and transformation is done in situ (dynamically). The key objectives are:

- A method to demonstrate the application of data-layer framework to visualize in real-time energy efficiency of TES. To fit the second law of thermodynamics-based exergy model. This will help engineers to intuitively understand the energy efficiency of their devices using novel data pipeline.
- To demonstrate the use-case of hyper-tuned DL framework of LSTM to predict the energy efficiency in the process loop.

Predicted results show tuned correlation with the parametrized experimental data, even during the load phase, where substantial amount of math (convection/mixing) is present for the network to learn (train/test).

1. Introduction

Building sector accounts for an estimated 40% of world's energy consumption and at-least 30% of world's carbon footprints (Serrano et al., (2017)). Thermal Energy Storage (TES) is the major part in building energy consumption and is used for thermal comfort thus it must be evaluated for energy performance. Thermal storage is an essential link in heating systems of buildings due to non-coincidental nature of energy supply & demand [9]. TESs make use of temperature stratification – water is stored and delivered in layers, one after another, due to buoyancy effects of temperature distribution, this improve the performance of storage tanks in the form of enhanced charging and discharging efficiency[8].

Energy efficiency of heating system of building refers to its ability to provide thermal comfort with minimum energy expense. For this purpose, TES systems are generally integrated with Heat Pumps referred as Renewable Energy Systems (RES) due to their lesser carbon footprint then electric heaters or fossil fuel heating systems. A Heat pump transfers heat from cooler environment (typically ground or air) to the TES system using refrigeration cycle, thus consuming grid energy. To reduce this energy consumption and deliver the maximum thermal energy efficiency is very crucial. In the literature, various procedures are devised and studied to assess the TES integrated heat pump system from thermodynamic standpoint[24], Rosengarten et al.,[31,11]. An exergetic study of ground coupled heat pumps is performed by Esen et al., [13], Esen et al.,[18,14–17]. Authors concluded that for the same heat pump operating conditions source temperature can significantly affect exergy availability of the system. In addition to thermodynamic assessment, various researchers used Artificial Neural Network (ANN) approach to predict the performance (Amico & Ciulla, (2022); [12]). Work by [22] is a classic in modelling the temperature stratification in TES. Authors modelled long term measured data using ANNs, taking ambient temperature, mass flow rates and previous time stamp temperature as input. The authors had satisfactory results during the no load periods, however during

* Corresponding author at: Department of Environmental Engineering, Faculty of Mechanical Engineering, Czech Technical University in Prague, Technicka 4, 166 07, Prague 6, Czech Republic.
E-mail addresses: yogenderpal.chandra@fs.cvut.cz (Y.P. Chandra), tomas.matuska@fs.cvut.cz (T. Matuska).

https://doi.org/10.1016/j.enbuild.2022.112135
0378-7788/

Nomenclature

ADC	analog to digital convertor
c/C	thermodynamic specific heat capacity (J/kg-K)
DL	deep learning
E	error/loss
E_{com}	compressor electricity consumption
E_p	circulation pump electricity consumption
GSHP	ground source heat pump
HP	heat pump
H	height (m)
H	total height (m)
LSTM	long short-term memory
MLP	multilayer perceptron
NN	neural network
NS	Navier-Stokes
PF	performance factor
PT100	platinum temperature-100
Q	thermodynamic heat addition (kJ)
Raspi	Raspberry Pi minicomputer
RES	renewable energy source
RNN	recurrent neural network
RSS	residual sum squared
RTD	resistance temperature diode
TES	thermal energy storage
T	temperature (otherwise mentioned in text)
T_{hp}	heat pump outlet temperature
T_0	thermodynamic dead state (ambient)
$T_{hp,out}$	heat pump output temperature
$T_{hp,\ in}$	heat pump input temperature
T	time
V_{cp}	circulation pump flow rate l/h or m_l^3s
V_{dis}	discharge rate l/h or m_l^3s
W	modified loss coefficient
ρ	density kg/m^3
λ	penalty term in regularization
Δs	thermodynamic entropy production
η	efficiency
v_{hp}	heat pump flow rate/circulation pump flow rate m_l^3s
ξ	exergy (kJ)
η_{st}	stratification efficiency
η_{st} (sh)	stratification eff. during charging

the load periods the model showed insufficient accuracy. This however could be the result of diminishing gradient problem of ANNs. This paper as part of method improvement will try to improve the load period DL modelling using LSTM and regularization techniques, since it retains the previous timestamp gradients and hence the vanishing gradient problem is reduced significantly. Dropout and regularization are the cheapest way to reduce overfit [35] & Hinton et al.,[25]. A detailed application of dropout and regularization techniques in deep learning application of heating systems is presented by [26]. Biswas et al., [10] outlined the modelling approach related to the building energy data. Santos et al., [32] studied thermal model and behavior of swimming pools with the help of ANN. Authors used meteorological data as well as geographic location data such as elevation, latitude and longitude as the input to NN models.[18,14–17], applied neural network and compared it with adaptive neuro-fuzzy, and support vector machine approach to study and forecast system performance of ground source heat pump. Yaïci & Entchev,[37], also modelled multilayer TES temperatures using MLPs back-propagation algorithm. Authors concluded that their ANN model was sufficiently tuned to learn from the input data. [28] modelled performance prediction of large solar system using ANNs. Input to the NN was ambient temperature, incident radiation (MJ/m^2) and solar tank water temperature, while the output was the daily average output of the solar system (MJ). In addition, it was apparent from the results few feature selections, caused excellent prediction during training while compromised during validation or testing. This is again either due to vanishing gradient or overfitting problem which is intrinsic in a small dataset (a smaller number of features). This paper will meet this overfitting problem also, by increasing the number of features in the previous time stamps, so the NN has more info to learn from. [18], utilised and found Levenberg–Marguard (LM) algorithm to be most effective over Pola–Ribiere conjugate gradient (CGP) in heat pump systmes performance prediction. A detailed analysis of hyperparameter for temperature sequence prediction in solar thermal systems is done by Correa-Jullian et al., [2]. A more general review of conventional machine learning application in time series forecasting is documented by Voyant et al.,[36] while thermodynamic application of ANN is elaborated by [33], Souliotis et al., [34,30,19,20], Esen et al., [21]. The missing-link in the above approaches is that data collection and prediction are separate tools and need sufficient human intervention and expertise to perform TES performance analysis. In addition, the physical process is transient while the data processing is still. It is necessary to come up with hybrid intelligent method that can automate two approaches and create one expert system which can assess thermodynamic performance of TES system in live mode and predict it using LSTM neural network. Henceforth, below mentioned objectives are observed:

- To accommodate the dynamic (in situ) share in calculation, custom exergy/entropy models are derived using second law of thermodynamics, customized for novel data acquisition layer and fitted as a contribution towards the improved method in terms of correctness and real time animation of the physical process (in detail in section 2). For this task novel data layer was devised and programmed layer using Raspberry Pi-4 (Raspberry Pi for industry, n.d.) systems. Wide range of computing packages was observed which is not limited to PostgreSQL (to store/retrieve dynamic data that is being collected from sensors (RTD, current loop, Modbus)), Pandas/Numpy (to do all the scientific data computing, parsing, transformation, and curation), MatPlot-Lib/Seaborn for an in-situ animated visualization of the stratification decay. The developed code and the gif version of visuals of the process loop is available on the git repository (Chandra, GitHub [GIF and code], 2021). This will considerably improve the intuitive understanding of stratification decay in real time, thus improving the industrial testing of HP integrated TES systems.
- To further enhance the application of full stack data engineering layered around its utility for stratification measurement, this work will try to perform the following:
  - Development of applied deep learning (DL) framework utilizing long short-term memory (LSTM), and multilayer perceptron (MLP) to model the layered temperature and to predict the entropy generation during charging and discharging loop. This will improve the current understanding

of layered temperature modelling using deep learning frameworks at a very fundamental computer science and statistical interface.

- Meanwhile, it is very apparent in the literature that neural networks (NN) are either excessively overfitted and thus are not able to predict during testing phase, or the amount of information to learn during the discharging loop of TES is too large for the NN to handle. While this is true that during load phase due to a complicated natural & forced convection (NS equations) and mixing, the NN is overwhelmed by the information and thus captures only the global superficial features in data, and skips the more important local complex features. There still is possibility to hyper-tune the NN for best prediction. Thus, adding the novelty towards evaluation optimization and demonstration of proposed DL framework, while improving the predicted results during the information intensive load phase of the physical process.

2. Methods

2.1. Experimental testing

Experimental testing is based on simple energy in/energy out approach to quantify energy usage/delivery using exergetic methods described later in this section. Residential ground source heat pump (GSHP) as a RES (renewable energy source) delivers the heat at constant compressor speed and flow rate using grid electricity on one side. On the other side, GSHP is connected with a source tank which is heated by a thermostatic electric heater to constantly supply heat pump (HP) with necessary heat to extract from. The tested tank is 390 L, and its diameter with insulation is nearly 750 mm, top insulation thickness is 120 mm while bottom insulation thickness is 50 mm. To measure the temperature, 10PT-100 temperature sensors are fabricated around the outside of tank wall in an axial direction 40 cm apart, dividing the tank into 10 equal fluid zones. 4PT-100 sensors are also placed each at each inlet and outlet of the tested tank to track any changes in charge/discharge temperature. All the sensors were calibrated for the accuracy around ± 0.3 °C. Tested tank is also connected with a load tank which serves as quasi-infinite load and is approximately 900 L. This makes two circuits of interest – heat pump-testing tank circuit and load-testing tank circuit. Both the circuits are equipped with *Sitrans F M Mag 5000* which is a transmitter-based flow meter by *Siemens* with accuracy of 0.5% to monitor and control flow rates in the circuits. The flow measurements are recorded automatically in the *PostgreSQL* database *via.* integration of 4–20 mA current loop to the designed *Raspberry Pi* based data acquisition system, more on this is in next subsection. Once the testing tank temperature has reached the ambient temperature, charging of the tank is initiated. Once the tank is charged to a predefined temperature, load circuit is switched on carefully for a constant discharge flow rate, thus initiating discharge part of the full cycle. This completes the full charge/discharge cycle and the data just stored has already been analyzed in real time by the novel *Raspberry Pi* based system, thus giving the clear representation and quantification of stratification decay (more on *Raspberry Pi* based system later in this section). The load tank is again cooled by the thermostatic chiller for a constant temperature and the experiment is repeated for the reproducibility and experimental accuracy of the results and for parameter-based analysis to completely understand the energy-cycle of the whole process. The goal of the experiments is simply to model, how much energy is taken from the grid and how much survived during entropy generation of charging/discharging loop. To measure the HP electricity usage, a 3 phase Modbus wattmeter is connected between HP and grid which communicates back again with *Raspberry Pi*. Modbus is a serial communication protocol developed by *Modicon* (now Schneider Electric) in 1979 and in simple terms it is a method to transmit data and information serially between electronics devices. The device requesting the information is called master and the device supplying the information is called slave, in this case Raspberry Pi device is master while wattmeter is slave.

3. Data layer

To stream the real time in-situ energy disbursement from grid to load, we introduced a novel data layer along with custom-made exergetic models. The data layer consists of two Raspberry Pi (Raspi1 & Raspi2) mini computers, both running on *Raspbian* – Debian Linux operating system (Fig. 2(a) Raspberry Pi based system).

Raspi1 stores temperature data from 19PT-100 sensors located at various locations of the test bench, while Raspi2 stores the flow rate data, all in real time. PT-100 are Resistance Temperature Detector (RTD) sensors. When it comes to precision temperature measurement, nothing beats RTDs. RTDs have a resistor most commonly made of platinum, copper, nickel alloys, or various metal oxides that changes its resistance as the temperature is changed. Most commonly, temperature measurement device, or a calibrator is used to convert this resistance back to temperature values according to the conversion table of that RTD type. We used *Adafruit sensor amplifier – MAX31865* for this purpose [1]. We used this type of converter to make sure that all the RTD sensors are calibrated at the same level, thus experimental accuracy and data analysis is not compromised. This conversion is automatically done in *ALMEMO* type of Data systems, however *ALMEMO* devices don't provide the flexibility of real time data evaluation. The flow data reaching Raspi2′s GPIOs (general purpose input output) is in the form of analog current loop (4–20 mA) which is type of output interface of many industrial sensors and since Raspberry Pi's GPIOs are designed to read digital signal, these analog current loop signals are first converted to digital equivalent using an industrial analog to digital (ADC) converter and then connected to Raspi2′s GPIO to read in. Subsequently, this digital value has to be linearly regressed to the actual physical value using intercept equation of line and finally calibrated with what is visible on the flow meter readout. This is done each 5th second the data is logged into each of the Raspi's PostgreSQL-DBs tables through simple one-liner code (Chandra, [GitHub code], 2021). In addition, a short code snippet running in Raspi1 also fetches wattmeter readings *via. Modbus RTU RS-485* serial protocol (Fig. 2(b) wattmeter*). Modbus RTU* is widely used within building management systems (BMS) and industrial automation systems (IAS) due to the simplicity of its architecture of 16-bit hexadecimal 'registers' which can pack and parse floating point, ASCII, tables and other structured data. Modbus registers primarily uses *RS-485* serial interface for master/slave communication which is highly flexible and supported by nearly every commercial data acquisition, monitoring and control programs. Wattmeter stores the 3-phase electricity consumption of HP in kWh in Modbus registers, where it can be accessed using RTU-485 serial interface protocol. Accuracy with specification of the core components is also mentioned in Table 2. Furthermore, since the temperature and flow rate data are stored in different PostgreSQL servers running on different machines, Raspi1 remotely accesses Raspi2′s PostgreSQL tables to fetch its data in a while loop while both are clocked together. This makes sure that all the data (temperature and flow) is stamped with the same time frame. This makes Raspi1 as the main server to perform all the important task including, data transformation, data cleaning, equation fitting etc. Furthermore, to assist the data workflow, intelligence and visualization Raspi1 also exhibits the 'Jupyter-Lab' server [27]. 'Jupyter-

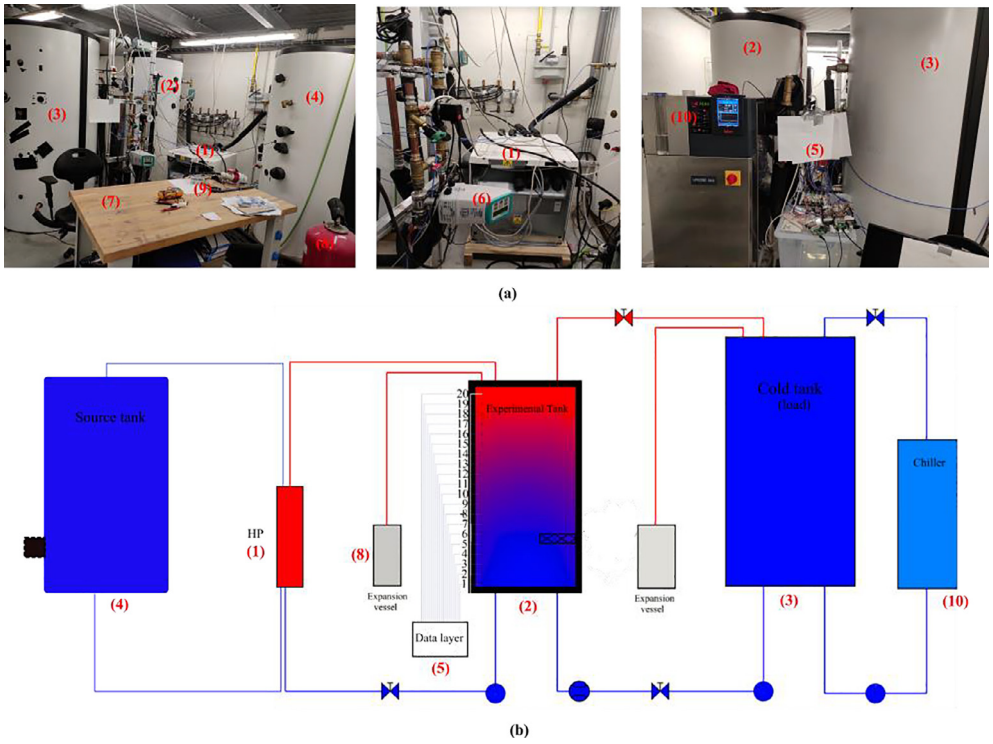

Fig. 1. (a) Experimental setup (Please see Table 1 for details), and (b) schematic.

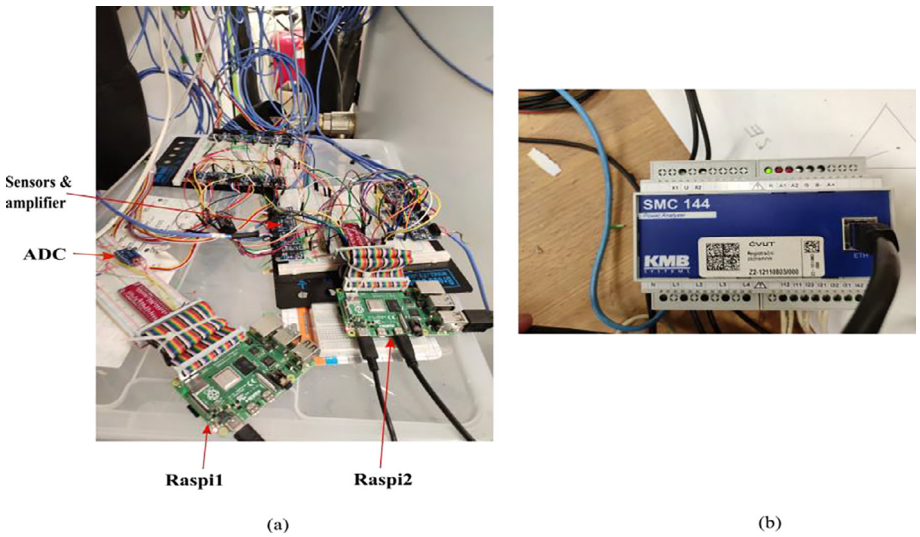

Fig. 2. (a) Raspberry Pi data layer, and (b) Modbus communication wattmeter.

Lab' or 'Jupyter notebook' is web based interactive development and configuration environment to support wide range of data science, scientific computing, machine learning, and deep learning workflows. In addition, attractive feature Jupyter notebook proposes is that it can easily be run in the web browsers – this makes working with Raspberry Pi based data acquisition systems which are characteristically 'headless' (no visual display computer monitors), extremely convenient, and accessible remotely. In addition, since Raspberry Pi's system are headless, the first hand visual of the data is missing in any case of overheating and potential accident. To add second level security and monitoring, Raspi1 also retains 'Flask server' which is constantly logging the data on web-based application server available anywhere outside of local-host for a quick overview of any outliers and potential damage control & remedy since we are dealing with HP with missing visual perspective whatsoever [7]. Flask is a portable micro web framework written in *Python*. The code for Flask application is written in *Python* and is open and freely available to be copied, transferred and used on our *GitHub* repository [3]. The whole workflow is depicted in the Fig. 3.

Equally important, data science stack such as *NumPy, Pandas, scikit-learn* were used along with *Keras (TensorFlow)* as a deep learning framework to build and perform *LSTM* and *MLP* modelling. *NumPy* is a powerful scientific/numerical computing ecosystem which draws the power of *C & Fortran* to *Python. NumPy* indispensably finds its way in the ML & DL applications. Accordingly, *Keras* in

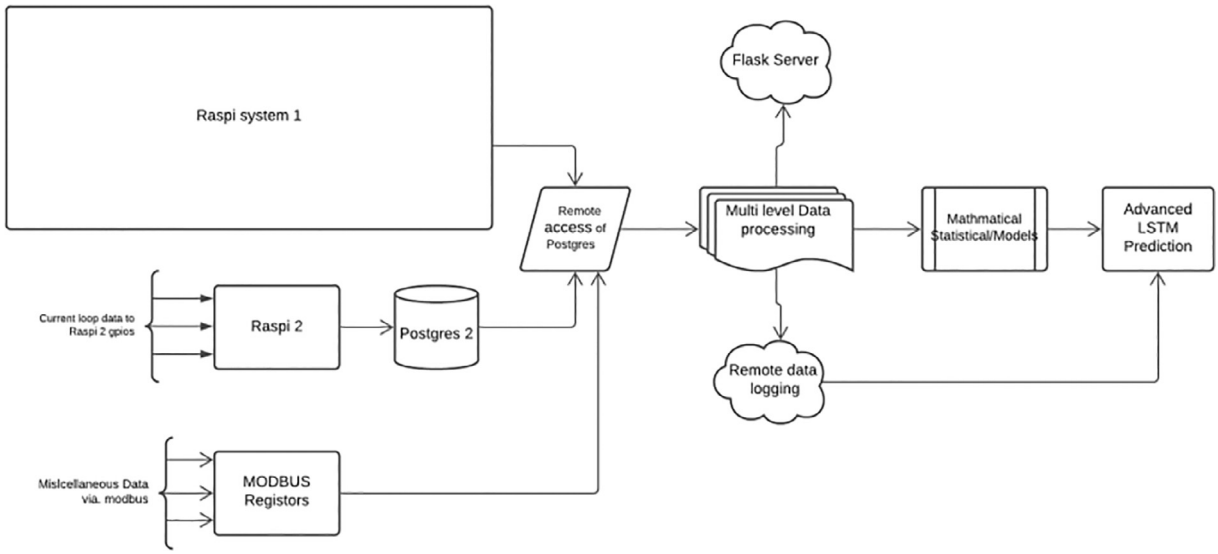

Fig. 3. workflow over data layer.

DL is a computation intensive artificial intelligence (AI) function, which actually demands the unique feature of *NumPy's* numerical packaging in densely packed memory, making *NumPy* 5 to 100 times faster than other data structures, *Python* lists for example, thus making *Keras* work scalable and deployable. Due to this fact, we have used *NumPy* as a data structure to test/train our DL model (more on this later in this section). *Pandas* on the other hand is high level, flexible data wrangling tool built on the top of *Python. Pandas and NumPy* always work hand in hand, data preprocessing/modelling is done using *Pandas* while data-feeding and subsequent NN modelling min *NumPy* tensors. Scikit-learn is a simple machine learning & predictive framework in python. It also provides basic data processing functionality – data normalization, standardization and transformation which comes handy while normalizing the data before feeding the NN, for example.

Finally, NN modelling is done using *TensorFlow* and *Keras. Google's TensorFlow* is an open source DL framework which uses *Python* as an expedient front-end API while still executing high performance *C++* codes in the backend. *TensorFlow* is highly used to train and model NLP (natural language processing), image processing, image classification, and for scientific commuting such as PDEs (partial differential equation) solutions and simulations, to name a few. The workflow of *TensorFlow* is very complex, consisting of series of processing nodes performing mathematical operations on *NumPy* tensors. These mathematical operations are however done in *Python* directed *C++* binaries, thus *TensorFlow* provides high-level abstraction over lower-level nitty-gritty details. *Keras* on the other hand is built on top of *TensorFlow 2.0* ecosystem optimizing and covering every phase of DL workflow *from data* engineering to model training, hyper-tuning and deployment. *Keras* was built for easy and frequent prototyping because of its ease of use and focus on user experience. *Keras's Python* frontend serves as an extreme level of abstraction, although this makes *Keras* comparatively slower, while still *TensorFlow* has adopted it as its core API. To sum up – *"Keras is to Deep Learning what Ubuntu is to Operating Systems"* [29].

3.1. LSTM & MLP principles

MLPs are extensively used in engineering application since the advent of ML & DL. MLP, also called ANN (artificial neural networks) is a class of feed forward neural network and is quintessential structure in DL modelling. MLP is termed as feed forward as the information flows through the $X \rightarrow Y$ *via.* the computational matrix $X \rightarrow f(w1,w2\ldots wn) \rightarrow Y$ thus there is no feedback loop, where the output from NN can be fed back to itself for the adjustment of the weights [23]. This reveals the problem of vanishing gradient of MLPs.

NN are trained using stochastic gradient descent phenomenon (SGD). This means that NN will iteratively find the coefficients of the loss function using calculus at which it has its local minima thus minimizing the loss. For example, consider a DL algorithm which takes X data and predicts *Y'* classifier while actual mapped output is *Y i.e.* $X \rightarrow f(x) \rightarrow Y$ *Or Y'*. This gives an intuitive understanding of the loss/cost function as: *error = Y'(predicted) – Y(actual).* Thus,

$$Cost = \frac{1}{N}\sum (Y' - Y)^2 \tag{1}$$

now the aim of DL algorithm is to minimize this cost function (Eq.1) while finding the parameters (coefficients) at minima, since lower the cost/error between predicted and actual means better the prediction job by NN. For example, parabola, $y = x^2$ as the cost function (Fig. 4(a)), has the minima at this point is *(0, 0)*. SGD will try to find the local minima of this equation along with the values *m (slope) & b (intercept)* in the equation *y = mx + b (equation of line pointing towards the local minima)* using partial derivates. The slope of the curve is determined by drawing tangent to the graph, and by computing this tangent in the direction towards the local minima can be determined – since lesser steepness of slope means towards the local minima and more steepness means away from the local minima, see Fig. 4(a). Tangent at the green point is steeper than the tangent at red point, thus it will take more steps at green then at red to reach local minima, termed as Learning Rate (LR). SGD on this example revels:

$$J_{m,b} = \frac{1}{N}\sum e_i^2 \tag{2}$$

taking partial derivatives (gradient):

$$\frac{\partial J}{\partial m} = 2.e.\frac{\partial}{\partial m}(e) \tag{3}$$

$$\frac{\partial J}{\partial b} = 2.e.\frac{\partial}{\partial b}(e) \tag{4}$$

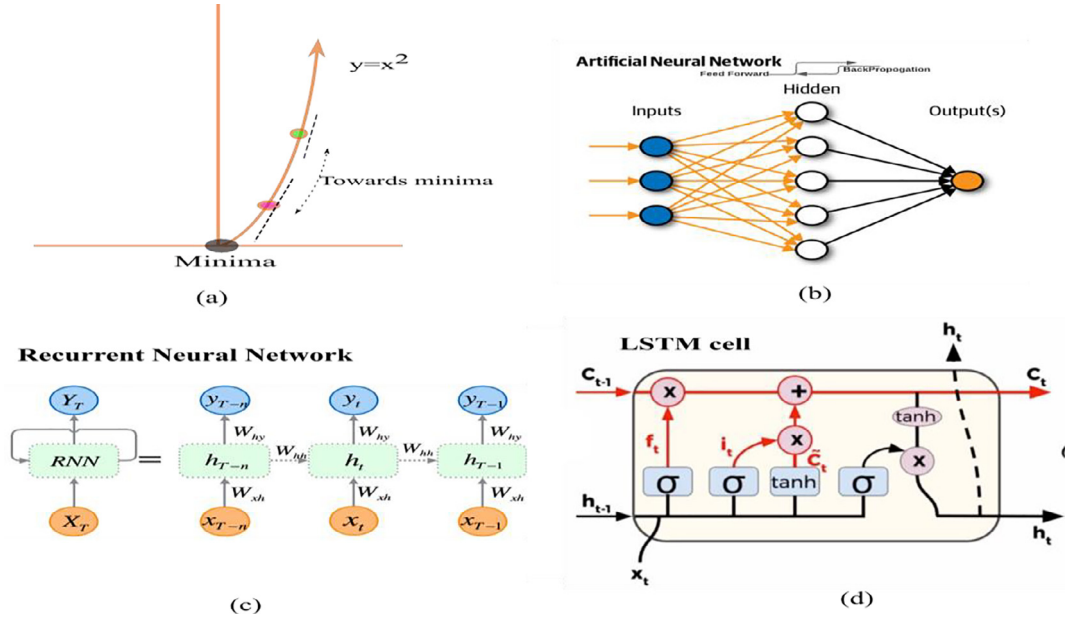

Fig. 4. (a) local minima of a cost function, (b) structure of MLPs, (c) unfolded RNN, and (d) LSTM cell.

now,

$$\frac{\partial e}{\partial m} = \frac{\partial}{\partial m}(Y' - Y) \tag{5}$$

and,

$$\frac{\partial e}{\partial b} = \frac{\partial}{\partial b}(Y' - Y) \tag{6}$$

thus,

$$\frac{\partial e}{\partial m} = \frac{\partial}{\partial m}(mX + b - Y) \tag{7}$$

and,

$$\frac{\partial e}{\partial b} = \frac{\partial}{\partial b}(mX + b - Y) \tag{8}$$

this gives

$$\frac{\partial e}{\partial m} = X \tag{9}$$

And

$$\frac{\partial e}{\partial b} = 1 \tag{10}$$

plugging Eqs. (9) and (10) in (3) and (4) gives:

$$\frac{\partial J}{\partial m} = 2e.X * LR and \frac{\partial J}{\partial b} = 2e.LR \tag{11}$$

now since $m^1 = m^0 - \delta m$ & $b^1 = b^0 - \delta b$.
thus,

$$m^1 = m^0 - e.X.LR \tag{12}$$

and,

$$b^1 = b^0 - e.LR \tag{13}$$

where, LR is the learning rate, which is actually analogous to the size of the steps taken to reach the local minima. Hence to find local minima and coefficients, iterative gradients are calculated for the fed data points using m and b values, each new gradient brings the information about the direction of minima to update the coefficients, and LR determines the how fast is this achieved. One common problem with feed forward, back propagation MLPs is the vanishing gradient, that means the gradients (Eqs. (2) to (13)) are vanishing (diminishing) in a deep NN. The gradients are used to determine the error. However, when there are deep hidden layers in MLPs the gradient reaching the input layer is so small due to 'diminishing gradient' that calculating the errors from it and thus adjusting weights is insignificant. This compromises the search for direction of local minima and thus NNs ability to minimize the cost function. Henceforth, MLPs are unable to capture the sequential features from the input time series data, for example, prediction of layered temperature in TES.

To overcome this limitation recurrent neural network (RNN) architecture is advised. RNN has added the recurrent connection in the hidden state. This looping constraint ensures that sequential features are not skipped due to diminishing gradient (comparatively lower) during the training phase, Fig. 4(b). RNN can extract information more efficiently from time series data, temporal data as well as non-numerical data. Fig. 4(c) depicts LSMT cell (RNN type). The diminishing gradient problem of MLPs and even in RNNs is solved using LSTMs as they retain info. LSTMs are best suited for time series prediction. For intuitive understanding, it receives previous cell state (C_{t-1}) previous cell output (h_{t-1}), and current input vector (X_t) as input variables, and outputs the current state (C_t) and output vector (h_t) to the next cell, Fig. 4(d). As a first layer it has a forget gate which performs linear transformation on current input vector and previous states through sigmoid function (σ) (Fig. 4(d)) and outputs 0 or 1, 1 meaning 'keep the state' and 0 meaning 'forget the state and delete it', Eq. (14). Subsequently works 'current state layer' where yet again one sigmoid function takes previous cell output and current input vector and does some linear transformation on it, Eq. (15). Finally, this layer also has hyperbolic tangent gate which also reads previous cell output and current input vector and outputs candidate value $(\check{C})$ which further is added to the cell state update, Eq. (16).

$$f_t = \sigma(W_f \cdot [h_{t-1}, x_t] + b_f) \tag{14}$$

$$i_t = \sigma(W_i \cdot [h_{t-1}, x_t] + b_i) \tag{15}$$

$$\overset{\vee}{C}_t = \tanh(W_c \cdot [h_{t-1}, x_t] + b_c) \tag{16}$$

The current state is updated using previous cell state current candidate value,

$$C_t = f_t \cdot C_{t-1} + i_t \cdot \overset{\vee}{C} \tag{17}$$

here, the forget gate *f* decides whether to forget what needed to be forgotten and added to the current candidate value multiplied with sigmoidal layer value i_t. And finally, the current output vector h_t is determined by linear transformation through sigmoidal function of previous cell state and current input vector and passes the output through hyperbolic tangent so normalizing the values between (-1, 1), Eq. (18, 19).

$$o_t = \sigma(W_o[h_{t-1}, x_t] + b_0)_t \tag{18}$$

$$h_t = o_t \cdot \tanh(C_t) \tag{19}$$

LSTM can easily model complex physical processes such as natural & forced convection, mixing, and stratified behavior of fluid flow. Fig. 6 elaborates on the workflow of the LSTM predicted TES temperature values and subsequent second law model fitting. LSTMs combined with MLPs are so powerful in learning the local as well as global temporal dependencies from the data that the training/validation losses are actually reduced to the second order of magnitude with minimized.

3.2. Energy performance & second law stratification models

To assess the end to end energy performance of TES integrated HP, HP's PF and TES's availability concept and entropy generation were calculated in real time. For this purpose, second law entropy/exergy models are rederived, customized and fitted. In addition, scientific computation with *NumPy* allows temperature dependent thermo-physical properties (such as density) to be easily accommodated into the calculations. The derivation of the models is out of scope for the intelligent system and its applications to building energy workflow. However, the final version looks like this:

$$n_{st}(ch) = \left[\int_0^t \rho(t) \cdot \dot{v}_{hp} \cdot c(t) \cdot \left[T_{hp,out}(t) - T_{hp,in}(t)\right] dt - T_0 \int_0^H \rho(h) \cdot (V/10) \cdot C(h) \ln\left(\frac{T_{hp}}{T_i(h)}\right) dh\right] / \int_0^t \rho(t) \cdot \dot{v}_{hp} \cdot c(t) \cdot \left[T_{hp,out}(t) - T_{hp,in}(t)\right] dt \tag{20}$$

where, v is the heat pump volumetric flow rate. The time derivative of heat addition contributes towards the dynamicity of data analytics hence allowing to scale the process spontaneously. This could allow researchers and engineers to make their TES integrated RE systems better adjusted for real time quantification. In this manner the exergy models were yet employed however completely revamped for a) improved accuracy, and b) for dynamicity addition. Finally, electricity consumption is accessed from Modbus registers of wattmeter, and the HP performance factor (PF) is calculated using the following equation:

$$PF_{hp} = \frac{\sum_{t_i}^{t_n} Q_i}{\sum_{t_i}^{t_n} (E_{comp} + E_p)} \tag{21}$$

E_{com} and E_p are the compressor and circulation pump respectively. The idea is that 1st phase among 3-phases is used by the HP compressor, and the 2nd phase by circulation pump, this data is circulated and stored as 16-digit hexadecimal numbers in different registers each having unique address in hexadecimal digits also. So, there is need to access correct address to get a summed-up and/or unique value of energy consumption per phase and to convert it to human readable float value.

3.3. Prediction performance accuracy & hyperparameter tuning

Before feeding the NN, data is divided into training and validation sets (sometimes test set too). Performances of the NN is usually expressed either by accuracy or by the loss. Unless there is an overfit, lower loss means better performance. Overfitting is very common problem where model crams the training data instead of learning it. This means NN performs well during training (training loss is marginally low) while validation data is poorly predicted and validation loss differs significantly. This difference in training and validation loss (training loss is significantly lower than validation loss) can be interpreted as an overfit and some measures could be taken to reduce overfitting, for example dropout and regularization are the computationally cheapest methods In regression problems the loss is usually residual sum of square *(RSS)* as expressed in Eq. (22).

$$RSS = \sum_{i=1}^{n} (e)^2 = \sum_{i}^{n} [y_i - (m + bx_i)]^2 \tag{22}$$

The objective of any NN based regression analysis is to lower the RSS. The model is subjected to several *dry-runs* to guess and evaluate the validation loss, and hyper-tuned eliminate overfitting/underfitting problems, in addition to the validation loss reduction. Model hyper-tuning is done in several passes until loss is reduced by several degrees of magnitude until further reduction seem unlikely. For example, simple MLP structure gave a minimum validation loss of 0.024 with excessive overfitting. This was dealt by introduction of LSTMs hidden layers. Overfitting was reduced by introducing regularization and dropout layers, Table 1. In addition, the NN was simplified by removing extra hidden MLP layers this instantly gave a better prediction results by reducing validation loss to around second order of magnitude (0.024 to 4×10^{-4}). Following are the hyper-tuned NN parameters:

- Addition of Dropout and Regularization layers: The function of the dropout is to increase the robustness of the NN by eliminating random nodes output within the layers. Dropout synthetically removes some of the layers output of some of the nodes for a single pass forward, thus neutralizing their weights and their errors. During the training phase (dropout is implemented

Table 1
Description for Fig. 1(a), specification of experimental testing components.

Device	Specification	Description	Uncertainty/ Error
(1) Heat Pump	CTC EcoPart 612 M, 5.8 kW Rated Power	Multi-speed	–
(2) TES	390 L, Insulated	Single family house	–
(3) Load tank	900 L, Insulated	Maintained at ambient	–
(4) Source tank	350 l, thermostatically maintained		
(5) Data layer	Raspberry Pi micro computers	2 Raspi communicating with each other	–
(6) Flow meter	Sitrans F M Mag 5000	4–20 mA current loop out	0.4%
(7) Working table	–	–	–
(8) Expansion valve	–	–	–
(9) Watt meter	3-phase	Communication via. modbus	–
(10) Thermostatic chiller	Huber Unistat Thermostat	5.3 kW cooling capacity	± 0.5%

Table 2
Data layer core components, description, and uncertainties involved.

Device	Description	Specification	Uncertainty/Error/Accuracy
Raspberry Pi 4	Core component (minicomputer)	8 GB ram	–
Tem. Sensors	Pt100 RTD	4 wire RTD based (ouput: 4–20 mA)	±0.05 °C from 80 °C to 200 °C
Flow meter	Sitrans F M Mag 5000	Output: 4–20 mA current loop	0.4%, ±1 mm/s
Pt100 resistance Amplifier	Adafruit temperature sensor amplifier (MAX 31865)	RTD amplifier and ADC (for Raspi reading)	0.1% Ω
ADC (ADS1115 I2C module)	Analog to digital converter (for flow meter current loop)	16-bit I2C communication, 4-channel	0.05 V
Watt-meter	3-phase	Communication via. Modbus	–

only during training phase), individual nodes (neurons) are either dropped out with a probability of 1-p or kept with probability p. This simply shuts down the interconnectedness among the neurons and prevent the network to generalize the data, thus reducing overfit. In addition to dropout, L1 (Lasso) and L2 (Ridge) regularization are also used to prevent overfitting problem. L1 and L2 regularization tend to penalize the NN model by adding complexity term in such a manner that the loss is increased while estimating complex models. The key algorithm behind L1 and L2 is that it modifies the loss function by adding a penalty term equivalent to squared magnitude of coefficient (in L1), and absolute value of magnitude of coefficient (in L2). Regularization treats overfitting as multicollinearity of variables, that means NN is confused by the highly look-alike data points, hence L1 and L2 adds a degree of bias or penalty term to the loss function. The intuition behind adding these penalties, is that L1 and L2 makes sure that the model performs less than perfectly by regularizing the modified loss coefficient value *W (see Eq, (23) and (24))*. The overfitted model means that the *W* value gives the best predicted *y* for input × and the *RSS* is minimized. Certainly, the NN performs best in this case, but only on the seen data, once the NN is tested on the unseen data, the validation loss increases with several degrees of magnitude. So, *L1* and *L2* makes the NN to settle for less-than-perfect model by introducing penalty term λ to the regularized coefficient *W*, Eq. (23) & (24). The code implementing these methods can be reviewed in the GitHub repository (Chandra, Github Deep Learning Code, (2021)).

$$RSS(L1) = \sum_{i=1}^{n} (e)^2 = \sum_{i}^{n} [y_i - (m + bx_i)]^2 + \lambda \sum_{j}^{m} W_j^2 \tag{23}$$

$$RSS(L2) = \sum_{i=1}^{n} (e)^2 = \sum_{i}^{n} [y_i - (m + bx_i)]^2 + \lambda \sum_{j}^{m} |W_j| \tag{24}$$

- Model simplification – hidden neurons reduced from 64 to 32. This alone decreased model complexity and reduced validation loss to an order of magnitude.
- Data normalization is done for a range *(0,1)* instead of *(-1,1)*. This reduced the model confusion in learning local temporal features within the data and predicted results improved.
- Reduced batch size from 500 to 50 (trial and error).
- As an exploratory data analysis EDA initiative, it was determined that previous 3 time stamp layered temperature values [(t-3), (t-2), (t-1) → *t*] reduced the validation loss by further an order of magnitude. This was in contrast to the other fellow researchers where only previous time stamp values were fed to the network. Fig. 5 (a) and (b) respectively shows the NN architecture and input/output mapping, and Table 3 shows layered architecture with number of neurons with training and testing loss of hyper tuned NN. Tables 3a and 3b.

4. Results and discussions

The real time energy assessment is streamed to the *Jupyter* Notebook. The data collected from all the sources of the HP integrated TES system is collected and through a complicated process of data engineering fitted to the equation by data layer. The code and GIF version of this real time presentation is available on the GitHub repository (Chandra, GitHub [GIF and code], 2021) [4, 5]. GIF illustrations demonstrate during charging – layered temperatures values, heat capacity of HP in kW, electricity consumption rate in kW, and second law efficiencies. As animated GIFs could not be put into perspective on hardcopy of this paper, therefore, a restored version of modelled data is collected into still figures for parametrization and assessment. Fig. 6 shows the complete process workflow put into viewpoint from idle charge to discharge and idle again. Fig. 7(a) gives a more still part of the layered temperature data of charge/discharge loop, along with the LSTM predicted values. Validation loss during prediction was reduced down to 4×10^{-4} from 0.4 (the least achievable value) during hyperparameter tuning, while training loss was of the 3rd order of magnitude, showing diminished levels of overfitting. Deep learning code is available on the Git-Hub repository (Chandra, Github Deep Learning Code) [6]. Fig. 7(b) shows the HP parameters during charging of TES – heat capacity and electricity usage in kW, and PF. Electricity usage has steep slope during the initial period due to highest temperature lift, less steep as the temperature lift is reduced and yet absolute value is increasing as the charging process is continued. This decreases the PF_{hp} from 2.3 to 1.8 (Fig. 7(b)), this stems from the fact that current charge loop corresponds to the maximum HP operating parameters *i.e.* 100% compressor and pump speed (∼1100 L per hour) – only two HP parameters made accessible by the HP manufacturer. 100% compressor speed makes sure that the temperature lift is the highest possible at the expense of electricity usage thus contributing to reduced PF_{hp}. After the tank is charged to a sufficient threshold limit (55 °C in this case), discharge process is initiated and the data layer through internal logic operator recognizes the discharge process, and starts to quantify the thermodynamic availability of TES in discharge mode. Exergetic availability and entropy generation is plotted against time, as the intension was to introduce a factor of dynamicity in the second law equation (Eq. (20)). For example, entropy generation and thus stratification destruction at the end of charging was about 4000 kJ. This means 4000 kJ of TES dispensed energy was lost during charging. In another words, HP consumes 3.29 kWh of grid power to charge the TES with 5.04 kWh of heat addition amounting to 1.53 PF_{hp} (nominal PF varies from 3.0 to 1.5) raising its internal energy to 80000 kJ from 45000 kJ, and during the process the system loses 1.12 kWh (4000 kJ) of energy as entropy generation or the stratification decay due to mixing (see Fig. 8(a)). Likewise, the entropy production during load phase reaches as high as 20000 kJ near the end of phase due to cold water injection from the bottom at 400 L/hour (load). The load phases entropy generation decreases the available energy by an amount

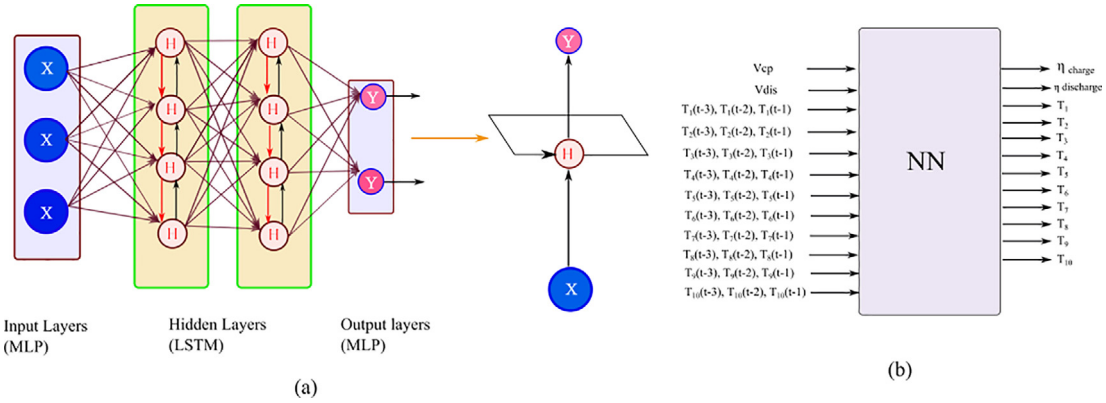

Fig. 5. (a) NN architecture, and (b) Input & output mapping.

Table 3a
NN architecture.

Layer (Type)	Output shape	Training loss	Testing loss
(1) Dense (MLP)	(None, 32)	0.04	0.04
(2) Lstm_1 (LSTM)	(None, 16)	3×10^{-4}	4×10^{-4}
(3) dropout_1 (Dropout)	(None, 16)	–	–
(4) dense_1 (Dense)	(None, 1)	4×10^{-4}	4×10^{-4}

Table 3b
Charging and Discharging efficiencies with PF (∼COP).

Charging at:	50% HP	70% HP	90% HP
PF (∼COP)	3.5	3.2	2.8
Charging Efficiency	76%	83%	79%
Discharge at:	400 l/h	600 l/h	800 l/h
Discharge Efficiency	84%	81%	76%

of 20000 kJ which is in contrast significantly higher by 16000 kJ during charging (see Fig. 8(b)). To clarify the concept of thermodynamic availability (not to be mistaken as absolute heat addition by HP), Fig. 9 shows a reversible process changing its thermodynamic states from state 1 to 2. Availability in this case is the greatest amount of mechanical work that can be obtained from this process. Available energy is referenced to the dead state (ambient in this case) and heat can only be extracted above this state from the system (as parted available and unavailable energy in Fig. 9). Since this is a reversible process, all the energy above the dead state is available for conversion. It equally applies to charge/discharge loop which in addition generates entropy due to the irreversibility in the process thus reshuffling and accumulating for unavailability as demonstrated in Fig. 8(a and b).

Fig. 10 depicts the η of LSTM predicted against measured. Raspberry Pi data layer fits the customized second law efficiencies (Eq. (20)) as the process loop carries on and streams the data on the jupyter Notebook for assessment. Afterwards, the data is retrieved from the local cloud severs for EDA (exploratory data analysis) and preprocessing to feed the LSTM NN prediction. Finally, predicted efficiencies and data layer calculated efficiencies are placed in juxtaposition for experimental and prediction validation as shown by Fig. 10(a) (charge) and Fig. 10(b) (discharge). X-axis represents the index as time representation confuses and reduces the learning rate of the NN. η_{charge} at 100% compressor and circulation speed is around 78.5 %, while $\eta_{discharge}$ around 80%. Fig. 11(a) depicts the 5% error lines plotted for normalized temperature values, while Fig. 11(b) shows the absolute values for hyper-tuned LSTM NN. Fig. 11(c) shows the loss in terms of r^2 error which has been brought down to 4×10^{-4} (from 10^{-2}) during the iterative hyper-tune parameterization of the NN models.

Fig. 12 illustrates parametric viewpoint of the charging and discharging loop at 50%, 70 %, and 90% compressor and circulation speed respectively. The TES layered temperatures along with HP operating parameters – heat capacity in kW, electricity consumption in kW, and performance factor (PF) are studied. The predicted layered temperature is also shown alongside the stratification curves.

Evidently, as the compressor speed is increased, the performance factor (PF) of the system goes down. This is because of higher temperature lift at higher compressor speeds, which eventually consumes more grid power reducing heat pump COP. Consequently, PF of 90% compressor speed is the lowest. By this token, it could be reasonable to assume that 50% compressor speed with PF of 3 should be an optimum choice, however until exergy analysis is performed (Fig. 13b), it wise to say that lower charging rates are prone of diffusive mixing (due to longer charging time and lower ΔT), thus reducing exergy availability in TES. As a result, the temperature profile in case of 70% compressor speed points to a more stratified charging then the rest. This is the reason for smoother transition in the temperature curves and lesser heat capacity in kW (more stratified charging) in case of 70% compressor speed (see Fig. 12b).

Fig. 13(b) illustrates measured second law stratification efficiency as represented by Eq. (20). The data layer calculates the charging efficiency and streams the real time value on 'jupyter notebook', additionally following illustration is the static version of what's represented by Eq. (20). Evidently, the charging efficiency at 50% compressor speed is surprisingly low as compared to rest. This is because the notion of 'the lower the kinetic energy, the lower the stratification decay' is less applicable here due to considerably longer time taken in charging as compared to rest of the compressor speeds. The longer charging time actually takes enough time for diffusion process to act and thus further entropy generation thus decreasing the changing efficiency (see Fig. 13b). Parameter 70% on contrary is a perfect blend of charging flow rate and ΔT so that it out-ways the 90% compressor speed in terms of entropy production.

Fig. 13(a) is the LSTM predicted and in accordance with the calculated efficiency. $\eta_{predicted}$ and $\eta_{calculated}$ (charging) for 50 %, 70%, and 90% HP parameters are approximately 76% (±1% $\eta_{predicted}$), 83% (±2% $\eta_{predicted}$), and 79% (±2% $\eta_{predicted}$).

The validation loss was reduced to a minimum value range between 4×10^{-4} and 6×10^{-4} While, testing loss was between 4×10^{-3} and 6×10^{-3} showing small overfit, however small overfit is always beneficial for further fine tuning. Validation loss and training loss should be low and should be approximately close, representing a good fit. Also, the performance of the NN was tested on the data not seen by the network.

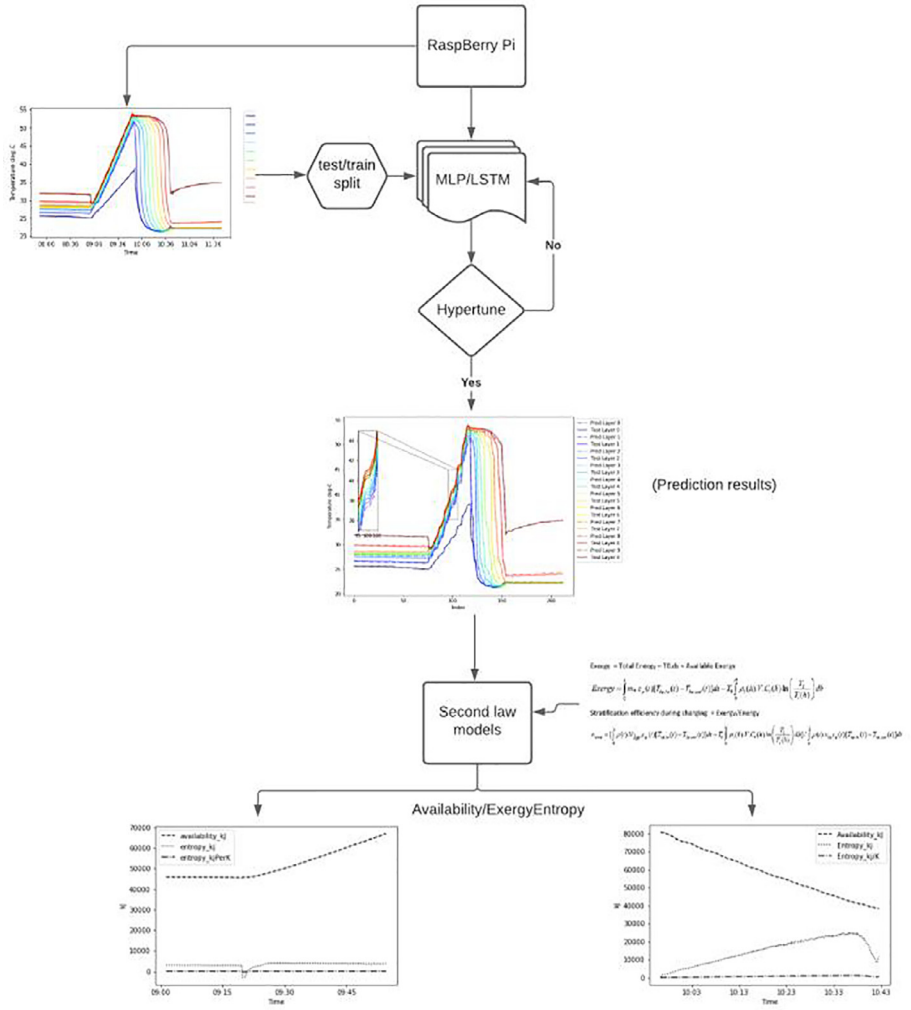

Fig. 6. Workflow for LSTM prediction and subsequent second law model fitting of the predicted data.

Fig. 14(a) demonstrates the LSTM predicted against data layer calculated second law stratification efficiency during discharge. As estimated by entropy and exergy measurements – 400 l/h has the highest $\eta_{calculated}$ approximately 84% (±0.2 % $\eta_{predicted}$), and 800 l/h has the lowest $\eta_{calculated}$ approximately 76% (±1%), while 600 l/h has $\eta_{calculated}$ approximately 81% (±1%). Fig. 14(b–d) are r^2 deviation for each flow rates. To elaborate, the common notion – 'the lower the flow rate, the lower the stratification decay' actually is more applicable here. This is because the higher value of ΔT (and thus the buoyant forces between hot and cold inlet) takes precedence over lower flow rate and the mixing is purely due to hot and cold-water mixing (and lesser due to diffusion). Thus, discharge with 400 l/h has the maximum second law efficiency (84%) then the rest of the flow rates. In Table 3 a comparative map of the results is shown. Comparatively, the charging efficiency is highest at 70% compressor speed with heat pump performance factor of 3.2 and discharge efficiency is highest at lowest flow rate of 400 l/h, due to aforementioned reasons.

In Fig. 15 our exergetic model is compared with Haller et al., [24]. The data form their research was not available as 'csv' file, so other data scrapping and digitizing methods were employed to get the original data points from their paper and are plotted. The data points are normalized for y-axis only, as their charge parameters are rather different, however the simulated tank size in terms of exergy changes is similar to our experimental. The curves show the exergy changes during a full charging period. The authors also performed exergy analysis of standby period along with charging and discharging period with their own exergetic models which are independent of dead state temperature T_0. However, our exergetic models are dependent on dead state as discussed in Fig. 9 and in Eq. (20) and accounts for charging and discharging period only. Likewise, this gave opportunity to compare our models with Haller et al. [24]during charging phase. The comparative study is in accord providing a proof of concept of a part of this study – second law exergetic models. The other part is the method applicability – data layer and its application to the building energy workflow.

For the concluding remarks, the novelty and practical applicability of this work stems from the development of second law exergetic models and 'method application' of custom-built data layer in building energy work-flow and its evaluation. The following points are observed:

- In this paper, a ground source heat pump (GSHP) integrated with TES system available for single family house in the Czech Republic was evaluated for relative exergy balance and second law performance evaluation.
- For this purpose, novel second law models were developed that were fitted in real time with the custom-built data layer thus developed.

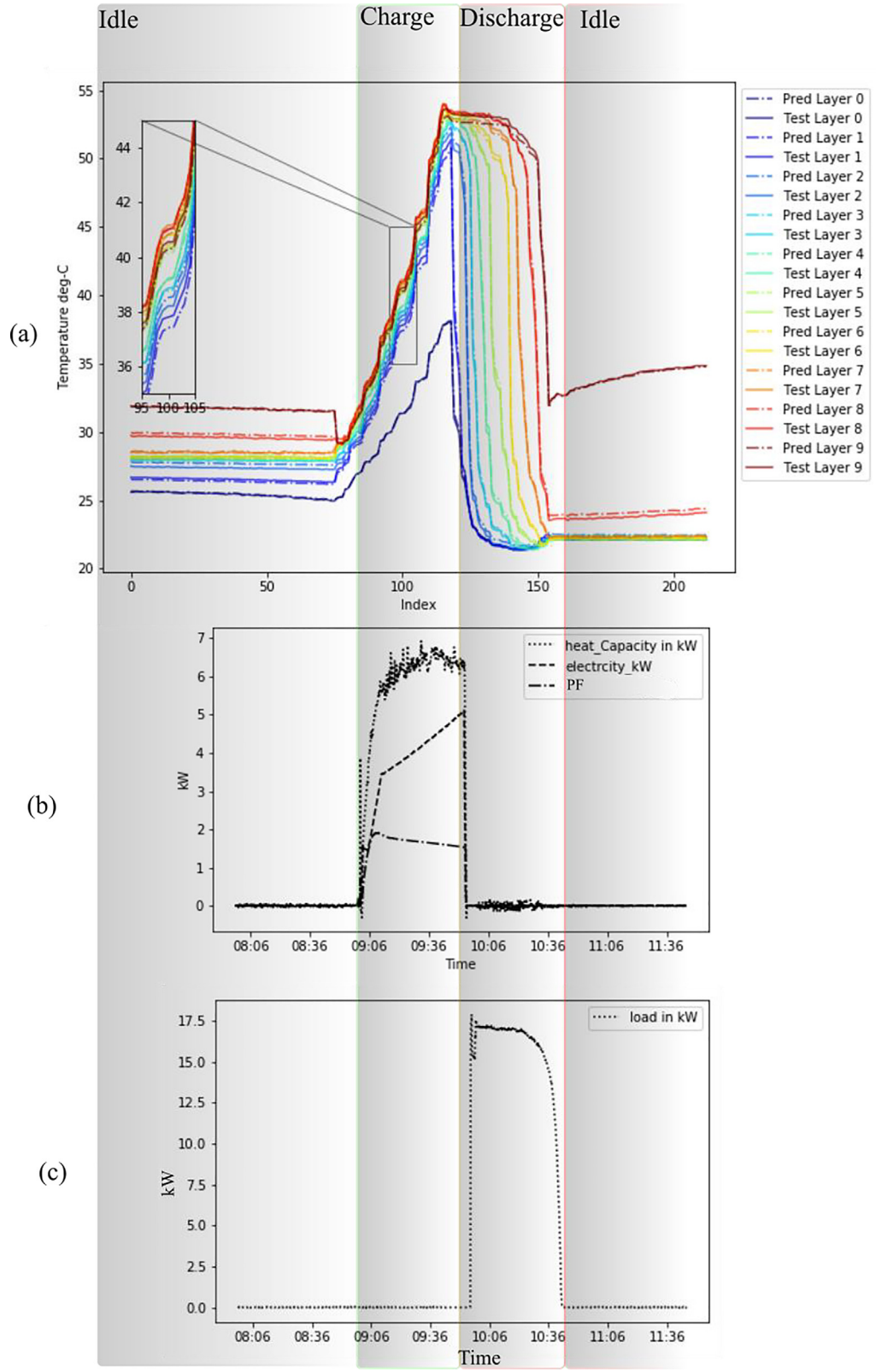

Fig. 7. (a) Layered temperature values LSTM NN predicted vs measured, (b) HP parameters – Heat capacity in kW, Electricity usage in kW, and Performance Factor, and (c) Load in kW.

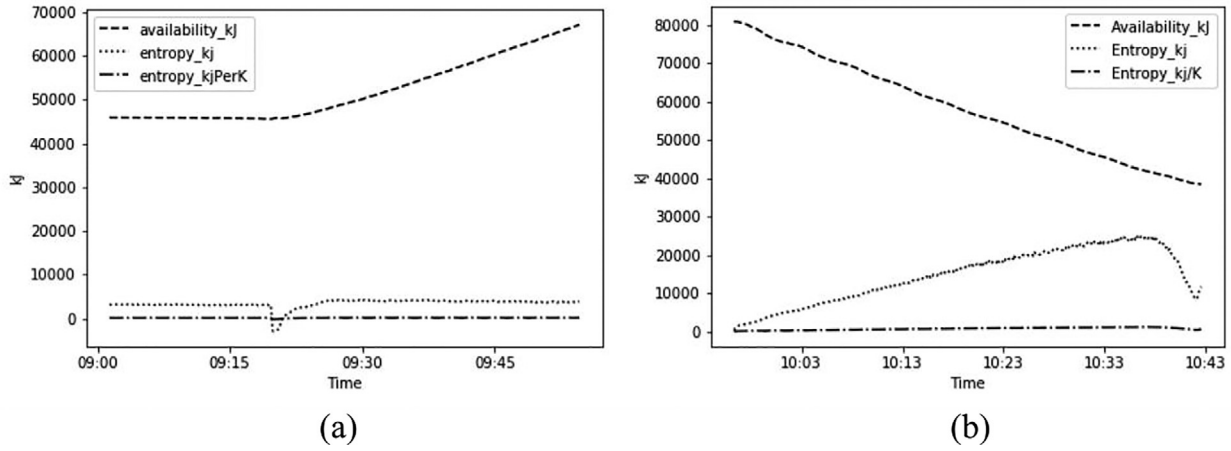

Fig. 8. Availability and entropy of TES at 100% compressor and circulation pump speed for (a) charging, and (b) discharging.

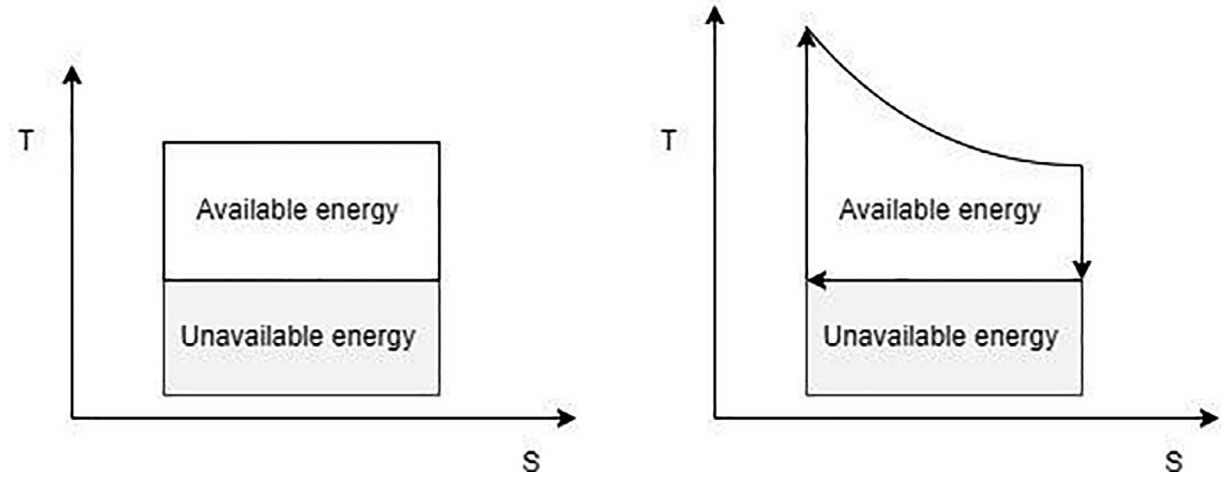

Fig. 9. Availability concept.

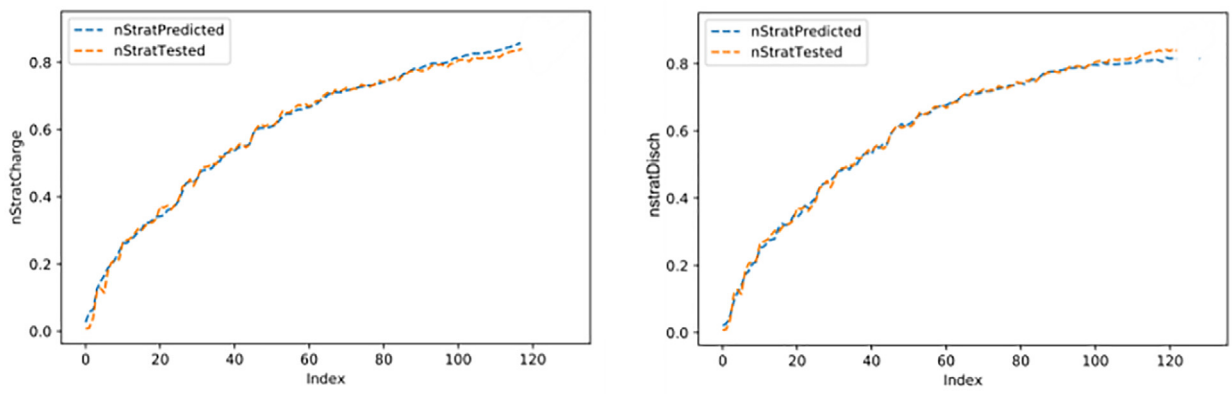

Fig. 10. Second law stratification efficiency for (a) charging at 100% compressor and circulation pump, and (b) discharging at around 400 L/hour.

- Three different typical heat pump charging parameters *i.e.* 50%, 70%, and 90% of the compressor speeds (800 l/h, 1200 l/h and, 1600 l/h of charging flow rates). And, 3 different tapping flow rates *i.e.* 400 l/h, 600 l/h, 800 l/h were experimentally studied and modelled with the data layer and the exergetic models.
- The data layer streams the exergetic information about TES in both charging and discharging mode in real time, thus giving an edge at time scale of seconds in understanding TES systems to energy engineers.

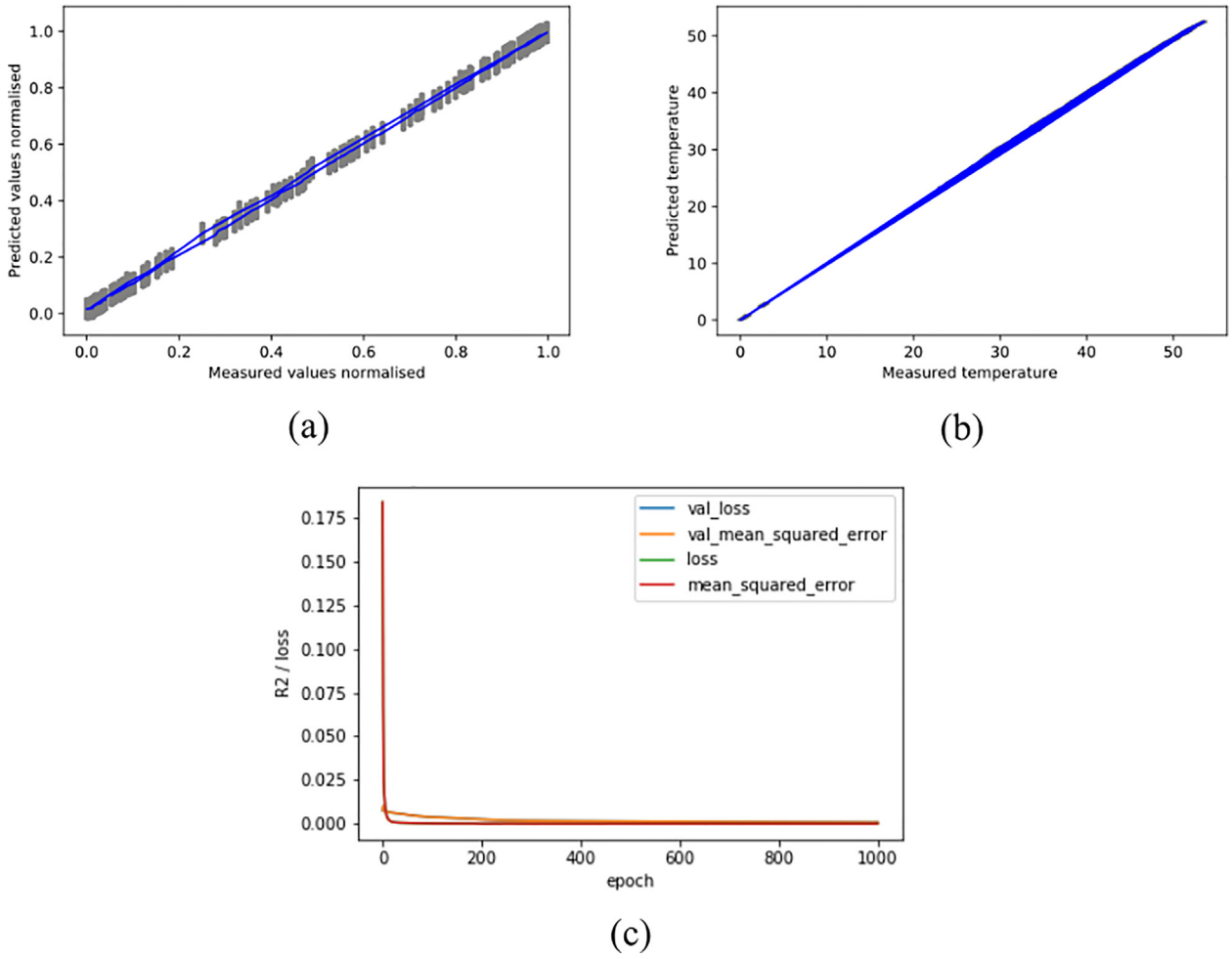

Fig. 11. Predicted against measured layered temperatures (a) Normalized 5% error range, (b) absolute values, and (c) loss, for hyper-tuned LSTM neural network model.

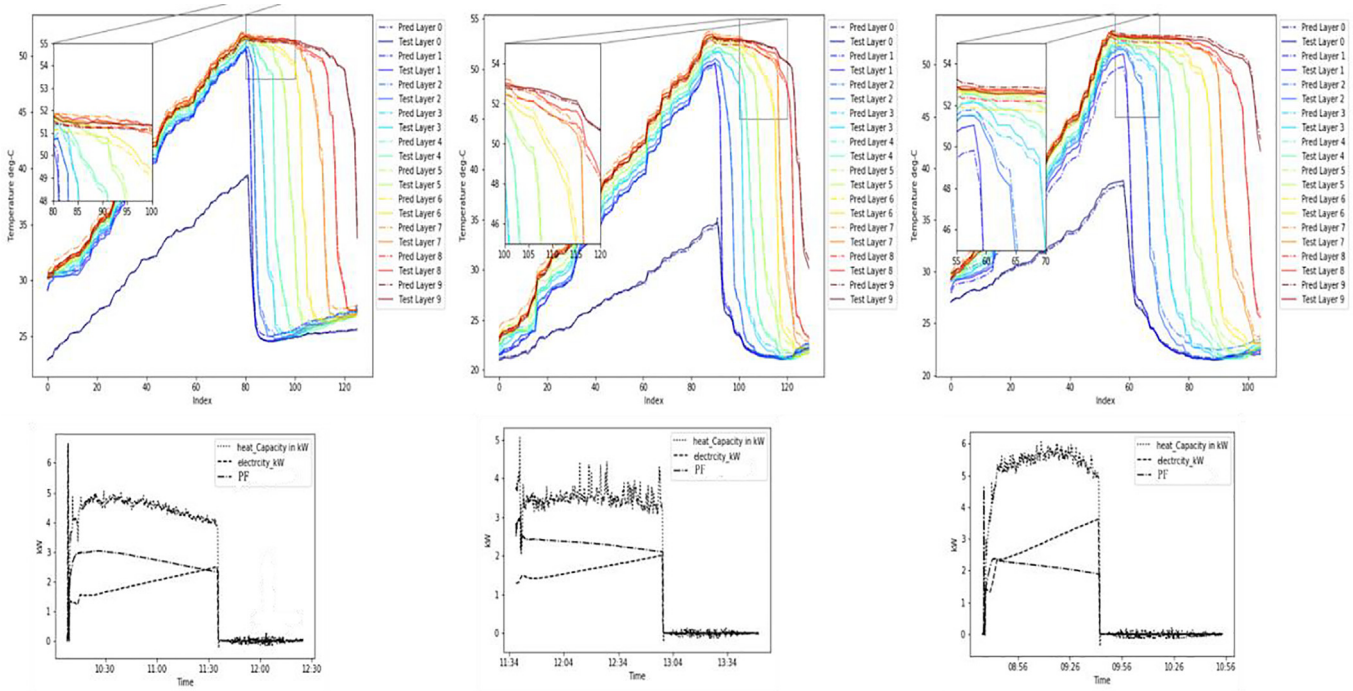

Fig. 12. LSTM predicted against measured layered temperature (charging/discharging) along with HP parameters – heat capacity, electricity and PF for (a) 50% comp. and circulation, (b) 70% comp. and circulation, and (c) 90 % comp. and circulation pump speed. Discharge at 400, 600 and 800 L per hour.

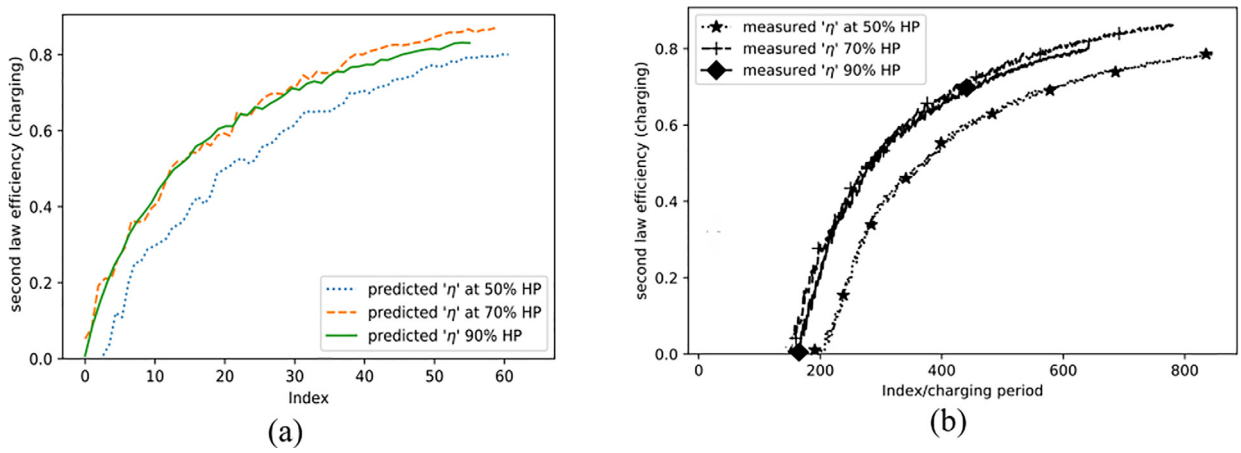

Fig. 13. Second law efficiency (charging) (a) predicted, and (b) measured for 50%, 70% and 90% of compressor and circulation speed.

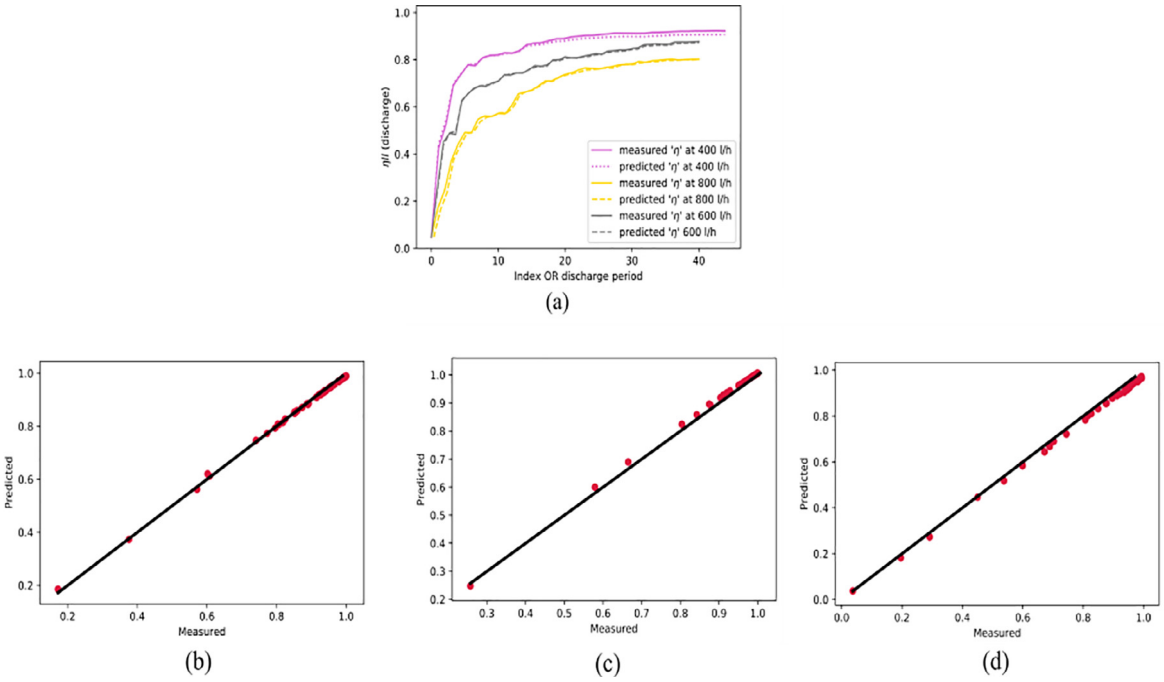

Fig. 14. Second law stratification efficiency (discharge) for (a) predicted against measured at various flowrates, (b), (c), and (d) R^2 deviation (variance) in observed against predicted efficiency for 400 l/h, 600 l/h, and 800 l/h discharge.

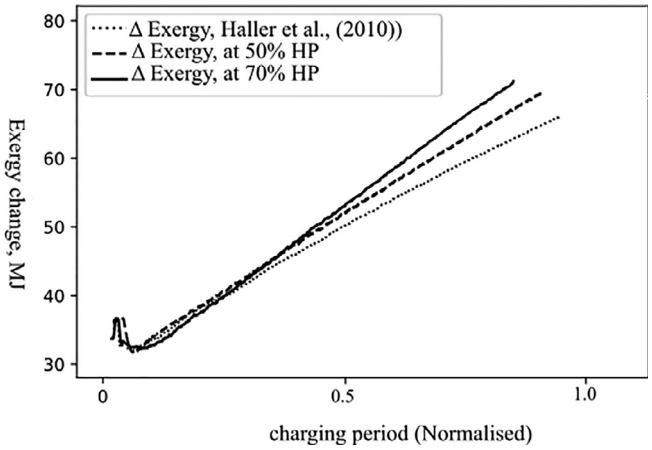

Fig. 15. Second law exergetic model comparison with Haller et al., [24].

- In addition, the data layer streams, end-to-end (from gird to user tapped water) exergy balance of heat pump integrated TES system in live mode. This makes sure that the engineer has clear understanding of the what portion of total energy being taken from grid is getting consumed as entropy during charging/discharging, and what the portion is being consumed by user as the tapped water.
- The application of novel data layer and custom build exergetic model will help engineers to build an energy harmonogram of TES integrated with heat pump system in the Czech Republic and in Europe in general. This can come handy to decide the extant of effectiveness of the current TES system.
- Finally, data layer also performs in-situ performance prediction of the TES system, which can be further extended for long term performance assessment.

- The short-coming of current data layer is that LSTM prediction can be extended for long term prediction. However, for that, experimental data has to be collected for longer periods. In addition, profiles of tapping cycles which are generally used in houses have not been experimentally tested. We believe, this novel data layer along with the custom exergetic model can be systematically applied to tapping cycles to gain meaningful insights regarding gross entropy generation during a week scale of TES system usage in a single-family house for example, and the work in this manner can be further augmented.
- Finally, a comparative study has been performed with previous author to strengthen the arguments made in this work.

5. Conclusion

The motivation for the work was to develop a novel real time stratification performance evaluation and streaming tool (method) for HP integrated TES system. For this purpose, a core computer science application layer was involved – customized data layer using Raspberry Pi single board minicomputers and the other associated data engineering stack. Second law of thermodynamics was observed in tailoring the entropy and exergy equations. It was made possible to fit these equations to the customized data layer in order to stream in real time the end to end stratification performance of TES, and PF of HP during charge/discharge loop. This real time evaluation gives a better perspective about the energy efficiency of RES system and thus could help engineers and researchers. Accordingly, complete charge and discharge tests were performed on the test bench. In addition, detailed application of advanced deep learning algorithms using LSTM neural networks is also demonstrated to model the data thus generated by data layer and to predict the TES layered temperature and efficiency. The experimental curves correspond well with LSTM predicted curves, with layered temperature having error within ± 5% and efficiency error within ± 2%. The accuracy to NN is determined by the minimized loss and the loss was reduced down to 6×10^{-4} by parameters hyper-tune methods. The experimental data was used for training and validation of the NN. Vanishing gradient problem was reduced to a much greater extent (which is a major problem with standard MLPs) with the use of advanced memory retaining LSTM nodes.

As of the experimental side, it is concluded that entropy generation in TES effects the PF (∼COP) of HP during charging. Thus, it is necessary to optimize correct conditions of circulation flow rate and compressor speed. Charging efficiency was highest at 70% compressor speed with performance factor (PF – COP) of 3.2, while discharging efficiency was highest at lowest flow rate of 400 l/h. The exergy balance presented in this paper from stratified charging to delivery measures the effective utility of heat pump integrated with TES system.

Declaration of Competing Interest

The authors declare that they have no known competing financial interests or personal relationships that could have appeared to influence the work reported in this paper.

Acknowledgments

This work has been supported by the Project TN01000056 - National Centre of Competence CAMEB granted by Technology Agency of Czech Republic.

References

[1] Adafruit-Industries. (n.d.). *Adafruit PT100 RTD Temperature Sensor Amplifier – MAX31865*. Retrieved from https://www.adafruit.com/product/3328.
[2] C. Correa-Jullian, M.J. Cardemil, L. Droguett, E., Behzad, M., Assessment of Deep Learning techniques for Prognosis of solar thermal systems, Renewable Energy 145 (2020) 2178–2191.
[3] Chandra, Y. P. (2021, 06 12). *[Flask Code]*. Retrieved from GitHub: https://github.com/yogenderPalChandra/rpi1_rpi2_FLASK_Heroku.
[4] Chandra, Y. P. (2021, July 10). *[GitHub code]*. Retrieved from GitHub: https://github.com/yogenderPalChandra/Raspi2_second_currentLoop_RemoteMySql/blob/main/FinalScript.ipynb.
[5] Chandra, Y. P. (2021, July 24). *GitHub [GIF and code]*. Retrieved from GitHub: https://github.com/yogenderPalChandra/Raspi1_main_Pt100_FlaskServer.
[6] Chandra, Y. P. (2021, 06 12). *Github Deep Learning Code*. Retrieved from GitHub: https://github.com/yogenderPalChandra/jospehus_DL.
[7] Chandra, Y. P. (n.d.). *Sensor Data*. Retrieved from https://raspi-flask.herokuapp.com/.
[8] Y.P. Chandra, T. Matuska, Stratification analysis of domestic hot water storage tanks: A comprehensive review, Energy & Buildings 187 (2019) 110–131.
[9] Y.P. Chandra, T. Matuska, Numerical prediction of the stratification performance in domestic hotwater storage tanks, Renewable Energy 154 (2020) 1165–1179.
[10] M.A.R. Biswas, M.D. Robinson, N. Fumo, Prediction of residential building energy consumption: A neural network approach, Energy 117 (2016) 84–92.
[11] A.A. Dehghan, A. Barzegar, Thermal performance behavior of a domestic hot water solar storage tank during consumption operation, Energy Conversion and Management 52 (1) (2011) 468–476.
[12] B. Bektas Ekici, U.T. Aksoy, Prediction of building energy needs in early stage of design by using ANFIS, Expert Systems with Applications 38 (5) (2011) 5352–5358.
[13] H. Esen, M. Inalli, M. Esen, K. Pihtili, Energy and exergy analysis of a ground-coupled heat pump system with two horizontal ground heat exchangers, Building and Environment 42 (10) (2007) 3606–3615.
[14] H. Esen, M. Inalli, A. Sengur, M. Esen, Modelling a ground-coupled heat pump system using adaptive neuro-fuzzy inference systems, Int. J. of Refrigeration 31 (1) (2008) 65–74.
[15] H. Esen, M. Inalli, A. Sengur, M. Esen, Artificial neural networks and adaptive neuro-fuzzy assessments for ground-coupled heat pump system, Energy and Buildings 40 (6) (2008) 1074–1083.
[16] H. Esen, M. Inalli, A. Sengur, M. Esen, Forecasting of a ground-coupled heat pump performance using neural networks with statistical data weighting pre-processing Int, J. of Thermal Sciences 47 (4) (2008) 431–441.
[17] H. Esen, M. Inalli, A. Sengur, M. Esen, Modelling a ground-coupled heat pump system by a support vector machine, Renewable Energy 33 (8) (2008) 1814–1823.
[18] H. Esen, M. Inalli, A. Sengur, M. Esen, Performance prediction of a ground-coupled heat pump system using artificial neural networks, Expert Systems with Applications 35 (4) (2008) 1940–1948.
[19] H. Esen, F. Ozgen, M. Esen, A. Sengur, Modelling of a new solar air heater through least-squares support vector machines, Expert Systems with Applications 36 (7) (2009) 10673–10682.
[20] H. Esen, F. Ozgen, M. Esen, A. Sengur, Artificial neural network and wavelet neural network approaches for modelling of a solar air heater, Expert Systems with Applications 36 (8) (2009) 11240–11248.
[21] H. Esen, M. Esen, O. Ozsolak, Modelling and experimental performance analysis of solar-assisted ground source heat pump system, Journal of Experimental and Theoretical Artificial Intelligence 29 (1) (2017) 1–17.
[22] P. Géczy-Víg, I. Farkas, Neural network modelling of thermal stratification in a solar DHW storage, Solar Energy 84 (6) (2010) 801–806.
[23] I. Goodfellow, Y. Bengio, A. Courville, Deep Learning, MIT press, 2016.
[24] M.Y. Haller, E. Yazdanshenas, E. Andersen, C. Bales, A method to determine stratification efficiency of thermal energy, Solar Energy 84 (2010) 997–1007.
[25] Hinton, G. E., Srivastava, N., Krizhevsky, A., Sutskever, I., & Salakhutdinov, R. R. (2012). Improving neural networks by preventing co-adaptation of feature detectors. *Neural and Evolutionary Computing, Cornell University*, Cite as: arXiv:1207.0580.
[26] J.K. Hwang, G.Y. Yun, S. Lee, H. Seo, M. Santamouris, Using deep learning approaches with variable selection process to predict the energy performance of a heating and cooling system, Renewable Energy 149 (2020) 1227–1245.
[27] Jupyter-Lab. (n.d.). *Jupyter Notebook*. Retrieved from https://jupyter.org/.
[28] S.A. Kalogirou, S. Karellas, V. Badescu, B. Braimakis, Exergy analysis on solar thermal systems: A better understanding of their sustainability, Renewable Energy 85 (2016) 1328–1333.
[29] Keras-API. (n.d.). *Keras deep learning framework*. Retrieved from https://keras.io/api/.
[30] A. Mellit, M. Benghanem, S.A. Kalogirou, Modeling and simulation of a stand-alone photovoltaic system using an adaptive artificial neural network: Proposition for a new sizing procedure, Renewable Energy 32 (2007) (2007) 285–313.
[31] G. Rosengarten, G. Morrison, M. Behnia, A second law approach to characterising thermally stratified hot water storage with application to solar water heaters, J. Sol. Energy Eng 121 (4) (1999) 194–200.

[32] E.T. Santos, L.E. Zárate, E.M.D. Pereira, Hybrid thermal model for swimming pools based on artificial neural networks for southeast region of Brazil, Expert Systems with Applications 40 (8) (2013) 3106–3120.
[33] A. Sencan, K. Yakut, A, Kalogirou, S. A., Thermodynamic analysis of absorption systems using artificial neural network, Renewable Energy 31 (2006) 29–43.
[34] M. Souliotis, S. Kalogirou, Y. Tripanagnostopoulos, Modelling of an ICS solar water heater using artificial neural networks and TRNSYS, Renewable Energy 34 (5) (2009) 1333–1339.
[35] N. Srivastava, G. Hinton, A. Krizhevsky, I. Sutskever, R. Salakhutdinov, Dropout: A Simple Way to Prevent Neural Networks from Overfitting, Journal of Machine Learning Research 15 (56) (2014) 1929–1958.
[36] C. Voyant, G. Notton, S. Kalogirou, M.L. Nivet, C. Paoli, F. Motte, A. Fouilloy, Machine learning methods for solar radiation forecasting: A review, Renewable Energy 105 (2017) 569–582.
[37] W. Yaïci, E. Entchev, Performance prediction of a solar thermal energy system using, Applied Thermal Engineering 73 (2014) 1348–1359.

Available online at www.sciencedirect.com
ScienceDirect
Energy Reports 8 (2022) 1321–1335
www.elsevier.com/locate/egyr

TMREES22-Fr, EURACA, 09 to 11 May 2022, Metz-Grand Est, France

Energy modeling of thermal energy storage (TES) using intelligent stream processing system

Yogender Pal Chandra[a,b,*], Tomas Matuska[b]

[a] *Czech Technical University in Prague, Faculty of Mechanical Engineering, Department of Environmental Engineering, Technicka 4, 166 07, Prague 6, Czech Republic*

[b] *Czech Technical University in Prague, University Center for Energy Efficient Building, 273 43, Buštěhrad, Czech Republic*

Received 2 August 2022; accepted 3 August 2022
Available online xxxx

Abstract

Thermal energy storage (TES) is the core element of renewable energy system (RES) and can considerably affect its overall efficiency. An effective thermal energy storage (TES) should enhance the stratification by restricting inlet mixing. In this paper, an experimental study is presented to evaluate the performance of thermal energy storage (TES). Discharging of the tank was conducted with different inlet flow rates to assess the effect of inlet mixing on thermal stratification. Results are quantified in terms of temperature distribution, MIX, and Richardson number and were visualized to predict the behavior of TES. In addition, the data parsing is done in live mode with ad-hoc built stream-processing data layer. Finally a methodology for time series prediction in the context of TES using high end LSTM network is framed. It was concluded that discharging rate of 800 l/h has the maximum mixing and thus the worst stratification, while prediction efficiency fell well within 5.2% of the error range.

Peer-review under responsibility of the scientific committee of the TMREES22-Fr, EURACA, 2022.

Keywords: Thermal energy storage (TES); Data streaming with RaspberryPi and Python; Renewable Energy

1. Introduction

The best defense against demand-side and supply-side non-coincidences, particularly with solar thermal systems, is the application of thermal energy storage (TES). This makes TES a crucial component of renewable energy systems (RES). Enhancing the functionality of this critical part can greatly reduce the amount of supplement grid energy needed for TES and eventually for entire building [1]. Thermal stratification is frequently observed and promoted property of TES which greatly influences its thermal efficiency [2]. Likewise, a functional TES system must meet certain technological requirements, as also detailed in Fig. 1. These include maintaining hot and cold-water layers in a stratified fashion, minimized mixing and dead water weight, to name a few.

* Corresponding author at: Czech Technical University in Prague, Faculty of Mechanical Engineering, Department of Environmental Engineering, Technicka 4, 166 07, Prague 6, Czech Republic.
E-mail address: yogenderpal.chandra@fs.cvut.cz (Y.P. Chandra).

https://doi.org/10.1016/j.egyr.2022.08.012

Peer-review under responsibility of the scientific committee of the TMREES22-Fr, EURACA, 2022.

Nomenclature

ADC	Analog to digital converter
ANN	Artificial neural network
β	Thermal expansion coefficient (1/K)
DL	Deep learning
e	Error/loss
E_j	Energy content of jth fluid element
GSHP	Ground source heat pump
GR	Grashofs number
g	Gravitational constant (m/s^2)
J	Mean squared error
LR	Learning rate
LSTM	Long short-term memory
M	Moment of energy (J m)
M_{str}	Moment of energy of perfectly stratified TES (J m)
$M_{full-mix}$	Moment of energy of fully mixed TES (J m)
M_{exp}	Moment of energy of experimental TES (J m)
MIX	Dimensionless MIX number
ρ	Density of water (kg/m^3)
RTD	Resistance temperature diode
RNN	Recurrent neural network
Re	Reynolds number
SGD	Stochastic gradient descent phenomenon
ΔT	Temperature diff. (^oC/K)
v	Characteristic velocity
W	Potential energy (J)
y	Height
z	Distance in y direction

Due to the low density of hot water, stratification is therefore encouraged by having hot water enter at the top of the tank [3,4]. However, allowing the hot and cold water to mix will lower the available temperature and, as a result, the quality of the energy delivered at load (Fig. 2).

Numerous researchers employed the Neural Network (NN) technique to the thermal performance forecasting and prediction [5,6]. Work by Géczy-Vg, P., and Farkas, I. (2010) [7] is a standard in the field of thermal stratification modeling in TES. A typical procedure to model the NN is to feed the network with previous time point values These data points can be temperature profiles, flow rates or any other feature which is known to govern the thermal performance of TES system. Careful feature engineering is needed to select such features. The authors' findings were satisfactory when there was no load, but the model's accuracy deteriorated during the load phase. Nevertheless, the declining gradient issue with NN could be the cause of it. In our study, this shortcoming will be addressed. We will use especial cell called LSTM (long short-term memory) which stores previous weights and gradients in its memory. This significantly dampens vanishing gradient issue which is prevailing in common ANN cell. In addition, we will demonstrate two approaches to curb overfit — regularization and layer dropout (Srivastava et al. 2014 [8] & Hinton et al. 2012 [9]). A through application procedure of this is also detailed by Hwang et al. (2020) [9] in their study of application of machine learning in building heating system. Yaci & Entchev (2014) [10] demonstrated an interesting back-propagation technique to model multilayer TES temperatures. The researchers asserted that the used network was sufficiently optimized to retain the learned features from input data during training. A condensed research on application of ANN in thermal systems is provided by Sencan et al. (2016) [11], Souliotis et al. (2009) [12], and Melit et al. (2007) [13]. Voyant et al. (2017) [14] offered a thorough study of classical

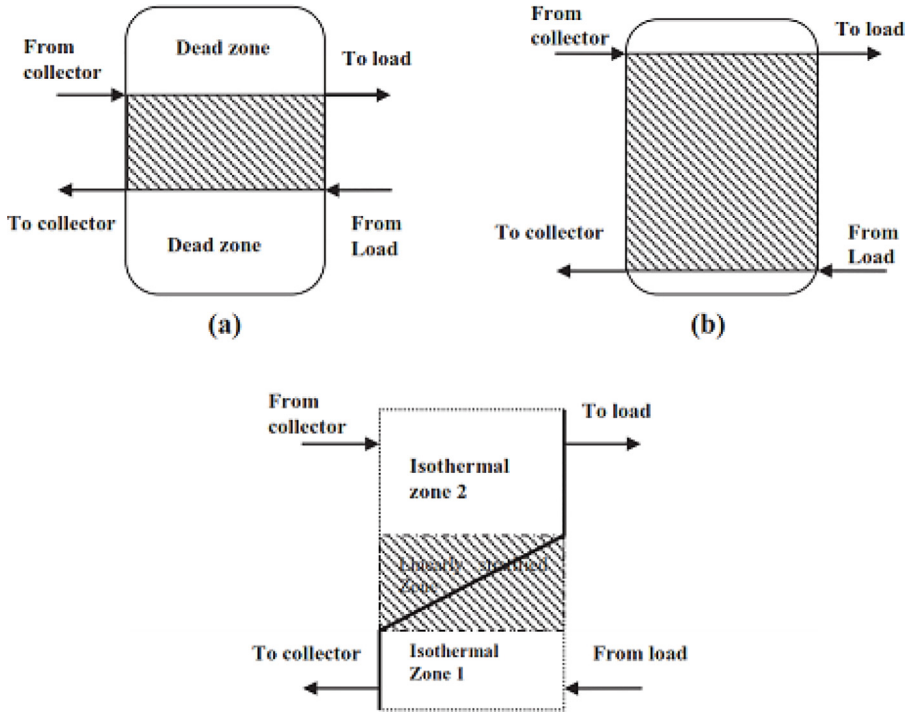

Fig. 1. (a) and (b) Position of inlet and outlet for efficient and economic concerns in SDHW, and (c) thermal stratification in the same [2].

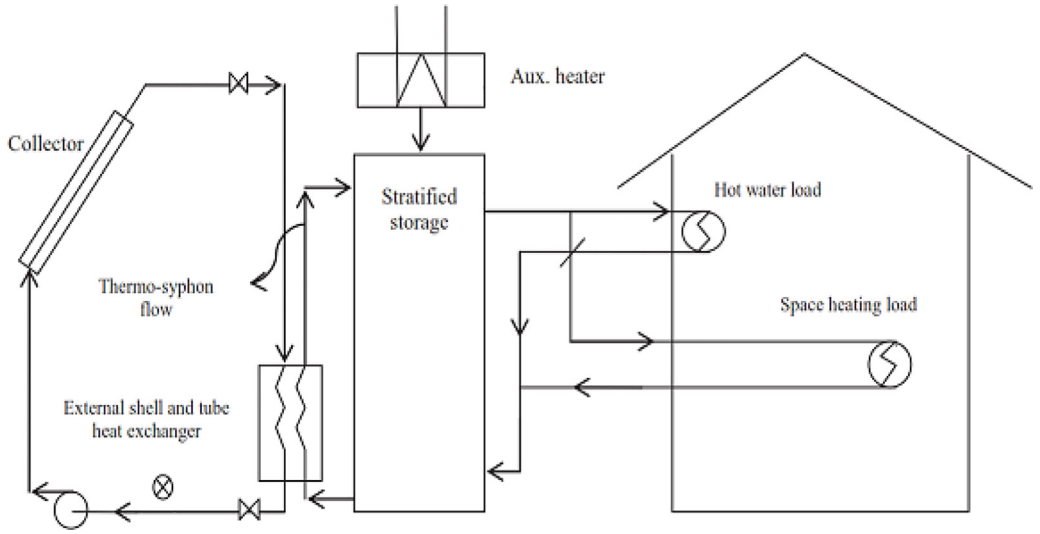

Fig. 2. Stratification in solar domestic hot water (SDHW) combi-system [2].

regression and deep learning application in forecasting time series data. The drawback with these techniques is that data curation and prediction are separate tools against TES analysis and require proper human experience in both directions. Therefore, it is recommended to conduct both operations at the end devices itself — stream-processing layer, thus closing the loop. Moreover, the discharge process is dynamic, while the data collection is still, adding another degree of restriction.

Henceforth, to combine and automate both above operations — data stream-processing and TES analysis along with prediction, a smart system has to be fabricated. The following key objectives are observed:

- A technique for demonstrating the use of the data-streaming-layer structure to view the energy efficiency of TES in real-time. To fit the thermal indices by utilizing unique data stream in real time. This will assist engineers to optimize TES systems for thermal efficiency.
- To provide methodology for time series prediction in the context of TES using high end LSTM network.

Even in the load phase, which involves a significant amount of mathematical representation of convection/mixing for the network to learn (train/test), the predicted results demonstrate excellent correlation with the parametrized experimental data

2. Experimental setup and procedure

A 397l TES measuring 500 mm in diameter and 1905 mm in height makes up the test rig as depicted in Fig. 3. TES has 200 mm thick insulation. 20 PT-100 RTD temperature diodes equally spaced are built around the TES to monitor temperature distribution, dividing TES into 20 equal nodes. Inlet and outlet temperatures were also measured likewise. The TES has an expansion unit attached to compensate any volumetric changes during cooling and heating cycle. TES is charged *via.* external thermostatic electric heater up to a single digit degree of precision in temperature. Thermostatic heater can be set to discreet temperature values 60 degrees for example. As indicated

(a)

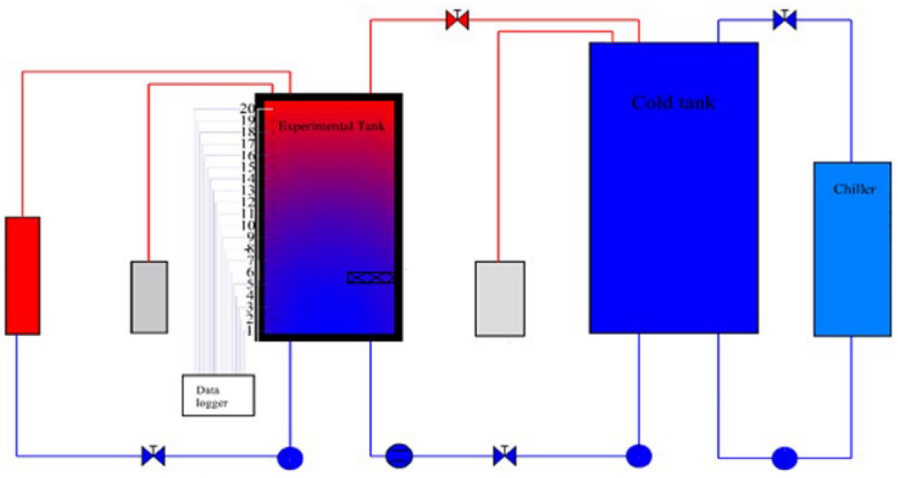

(b)

Fig. 3. (a) Experimental facility to test the commercial TES, (b) Schematic view of the same.

in Fig. 3(a), the discharge procedure is controlled by adjusting several one-way valves. Two loops come into picture-discharge loop and charge loop. Discharge loop forms between TES and cold-water tank, while charge loop forms between TES and chiller. Discharge entails closing down chiller loop while carefully controlling and monitoring the flow rates of 200, 400, 600, and 800 liters per hour. After full discharge of TES, discharge loop is closed, while the charge loop with thermostatic cooler is switched on, thus completing one charge and discharge cycle. In addition, the data has already been collected and has undergone real-time analysis using ad-hoc built novel stream-processing data layer. This quantifies the destratification process in real time. The reproducibility of tests was observed.

3. Data stream-processing layer ('data in motion')

We propose an innovative data stream-processing method to stream the energy disposal of TES in real time. Two Raspberry Pi (Raspi1 & Raspi2) computers booted with Raspbian operating system make up the layer, see Fig. 4(a). Raspi1 and Raspi2 both collect data in real time. Primary master Pi collects volumetric flow rate in contrast to secondary slave Pi which collects the temperature values from the 20 RTD sensors positioned across the experimental rig. A PT-100 sensor is a type of Resistance Temperature Detector (RTD), which changes its current value with the change in temperature. Sensor data is logged into *PostgreSQL* (database) server running on Pi. This is performed every fifth second (Chandra, [GitHub code], 2021) [15]. Additionally, Raspi1 server retrieves grid energy consumption values using Modbus RTU RS-485 protocol, see Fig. 4(b). Table 1 mentions the precision of the stream-processing layer's components. The primary master server is the Raspi1 which carries out all significant data engineering operations, such as data curation, parsing, transformation and energy model regression. In Fig. 5 the work flow representation of the stream-processing layer. Raspi1 as the master server makes all necessary API calls, executes data churn processes, and accesses the Raspi2's *PostgresSQL* table values remotely.

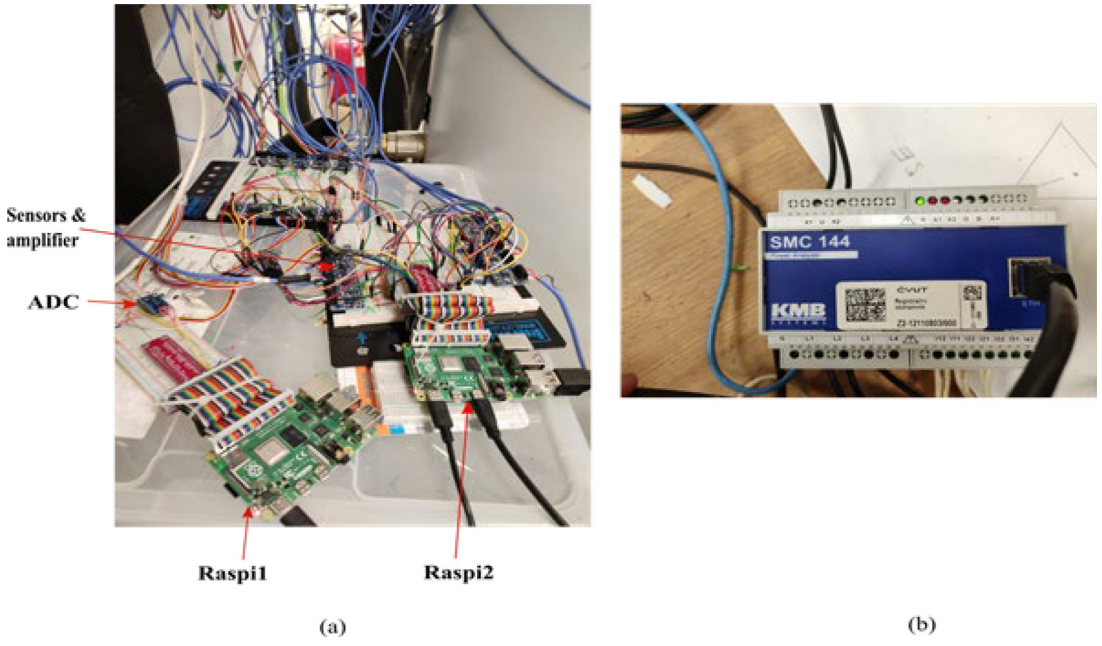

Fig. 4. (a) Raspberry Pi data streaming layer, and (b) Modbus communication wattmeter.

Worth to mention is machine learning framework used in time series prediction i.e. *Keras*, data engineering stacks *i.e*. *NumPy*, *Pandas,* and *Scikit-learn*. The super-fast computing capacity of *'C'* is borrowed to *Python* by the robust numerical computing framework known as *NumPy*. *NumPy* is a necessary component of machine learning or deep learning applications. NumPy array manipulation is 5 to 100 times faster than other data structures like Python lists, for instance, thus finding its application in the deep learning. *Keras* uses *NumPy* array in test/train process because of its super-fast speed. This also makes *Keras* scalable. The high-level data parsing tool such as *Pandas* comes handy for data transformation before converting it to *NumPy* arrays and eventually feeding to the network. NumPy

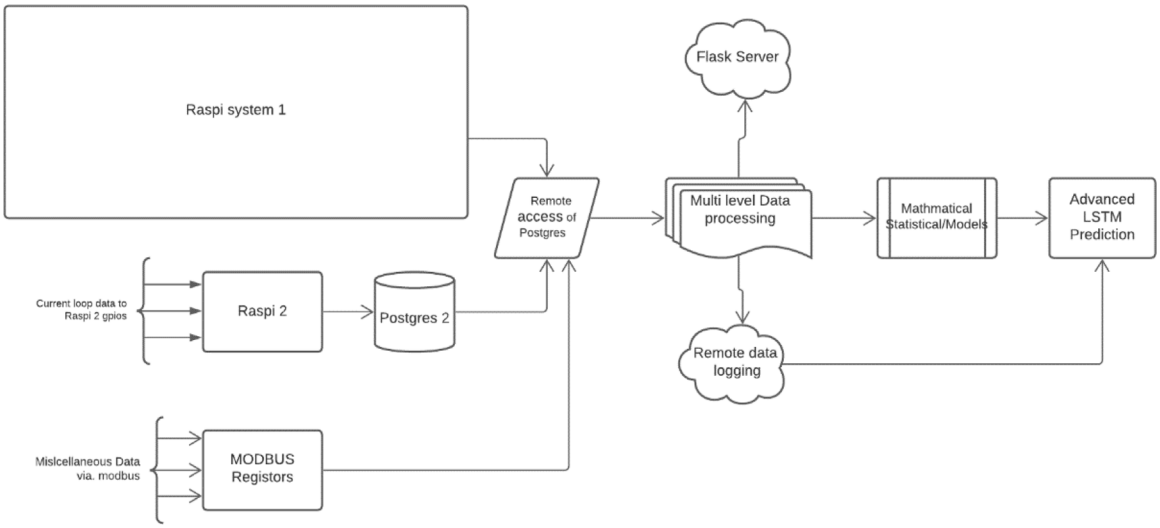

Fig. 5. Workflow over data streaming layer.

Table 1. Data layer core components, description, and uncertainties involved.

Device	Description	Specification	Uncertainty/error/accuracy
Raspberry Pi	Core component (minicomputer)	8 GB ram	–
RTD sensors	Pt100 RTD	4 wire RTD based (ouput: 4–20 mA)	±0.05 °C from 80 °C to 200 °C
Flow meter	Siemens F M Mag 5000	Output: 4–20 mA current loop	0.4%, ±1 mm/s
Pt100 resistance Amplifier	Adafruit temperature sensor amplifier (MAX 31 865)	RTD amplifier and ADC (for Raspi reading)	0.1% Ω
ADC (ADS1115 I2C module)	Analog to digital converter (for flow meter current loop)	16-bit I2C communication, 4-channel	0.05 V
Watt-meter	3-phase	Communication via. Modbus	–

and Pandas are inseparable; Pandas is used for data preparation and modeling, while *NumPy* tensors/arrays feed the network. Scikit-learn is a machine learning package bundle wide range of functionality. It offers fundamental data processing capabilities, such as normalization, standardization, and transformation, which comes handy during data preparation.

Finally, *TensorFlow* and *Keras* are used for time series prediction and predictive modeling. *TensorFlow* is a deep learning framework that runs on top of high-performance C++ in the backend, while using Python as a quick front-end API. Natural language processing (NLP), image classification, scientific computing, solutions for partial differential equations are common use cases for TensorFlow. TensorFlow's workflow is extremely complicated and maintains a set of distributed nodes that perform computational math on *NumPy* tensors. The computation is carried out in Python wrapped C++ binaries. *TensorFlow* in this manner offers high-level abstraction. Likewise, *Keras* is wrapper on the *TensorFlow 2.0* ecosystem facilitating and abstracting away every step of the deep learning workflow including data engineering and training/testing. Because of its simplicity and emphasis on the user experience, *Keras* was designed for quick proof of concept and prototyping. Python API for *Keras* provides high degree of abstraction due to which *TensorFlow* has accepted it as its fundamental API.

4. Energy methodology

4.1. MIX number

The energy distribution is assessed based on temperature contours and the bulk energy held within the TES [16,17]. Moment of energy calculation at each TES segment facilitates the mixing process quantification at layer level [2]. By adding the sensible energy content up to the jth vertical storage segment and weighting it

according to its height, as specified by Eq. (1), the moment of energy of a thermal storage tank is computed thus taking energy as well as temperature profiles into consideration, see Eq. (2).

$$M_E = \sum_{j=1}^{j} y_j . E_j \tag{1}$$

$$MIX = \frac{M_{str} - M_{\exp}}{M_{str} - M_{full-mix}} \tag{2}$$

The MIX is a dimensionless number and falls within 0 and 1. It is a measure used to assess the TES's performance. Full stratification of TES is represented by value 0; fully mixed TES is represented by value 1, provided both TESs stores the same energy content.

4.2. Richardson number

Authors [2] frequently evaluated stratification using the Richardson number. The ratio between the potential energy needed for mixing and the turbulent kinetic energy available for it is represented by this dimensionless number. Mixed storage is denoted by a lower Ri value, while stratified storage is denoted by a higher Ri value. Eqs. (3) and (4) explain this (4)

$$Ri = \frac{W}{K.E.} = \frac{\frac{g}{\rho} . \frac{d\rho}{dz}}{\left(\frac{\delta \upsilon}{\delta z}\right)^2} \tag{3}$$

$$Ri = \frac{g\beta \Delta T L}{\upsilon^2} \tag{4}$$

5. LSTM & ANN fundamentals

The stochastic gradient descent phenomenon is used to train NN (SGD). In order to minimize the loss, NN will iteratively determine the coefficients of the loss function at which it has its local minimum (Calculus). Consider a DL algorithm taking X and predicting Y′, while the actual output is Y, i.e. X→ f(x) →Y Or Y′. Error = Y′(predicted) - Y(actual) provides an intuitive comprehension of the loss/cost function.

The stochastic gradient descent phenomenon is used to train NN (SGD). In order to minimize the loss, NN will iteratively determine the coefficients of the loss function at which it has its local minimum (Calculus). Consider a DL algorithm taking X and predicting Y′, while the actual output is Y, i.e. X→ f(x) → Y Or Y′. Error = Y′(predicted) - Y(actual) provides an intuitive comprehension of the loss/cost function.

$$\frac{\partial e}{\partial m} = \frac{\partial}{\partial m}(Y' - Y) \tag{5}$$

The goal of the DL algorithm is now to minimize this cost function (Eq. (1)) while locating the parameters (coefficients) at minima, as a lower cost/error between the predicted and actual values indicates a better prediction performance by NN. For instance, the minima of the cost function $y = x^2$ (Fig. 4(a)) is at (0, 0). SGD will use partial derivates to try and identify the local minima of this equation as well as the values for the slope and intercept in the equation $y = mx + b$ (line pointing towards the local minima). The slope of the curve can be found by drawing a tangent to the graph in the direction of the local minima. Slope's steepness indicates either in the direction or away from local minima (see Fig. 4). (a). Tangent at the green point is steeper than the tangent at the red point, it will require more steps at green than at red to reach the local minima, which is known as the learning rate (LR). SGD therefore indicates:

$$J_{m,b} = \frac{1}{N} \sum {e_i}^2 \tag{6}$$

taking partial derivatives (gradient):

$$\frac{\partial J}{\partial m} = 2.e.\frac{\partial}{\partial m}(e) \tag{7}$$

$$\frac{\partial J}{\partial b} = 2.e.\frac{\partial}{\partial b}(e) \tag{8}$$

$$\text{now, } \frac{\partial e}{\partial m} = \frac{\partial}{\partial m}(Y' - Y) \tag{9}$$

$$\text{and, } \frac{\partial e}{\partial m} = \frac{\partial}{\partial m}(Y' - Y) \tag{10}$$

$$\text{thus, } \frac{\partial e}{\partial m} = \frac{\partial}{\partial m}(mX + b - Y) \tag{11}$$

$$\text{and, } \frac{\partial e}{\partial b} = \frac{\partial}{\partial b}(mX + b - Y) \tag{12}$$

$$\text{this gives: } \frac{\partial e}{\partial m} = X \tag{13}$$

$$\text{and, } \frac{\partial e}{\partial b} = 1 \tag{14}$$

plugging Eqs. (13) and (14) in (7) and (8) gives:

$$\frac{\partial J}{\partial m} = 2e.X * LR \text{ and } \frac{\partial J}{\partial m} = 2e.X * LR \tag{15}$$

now since $m^1 = m^0 - \delta m \& b^1 = b^0 - \delta b$,

$$\text{thus, } m^1 = m^0 - e.X.LR \tag{16}$$

$$\text{and, } b^1 = b^0 - e.LR \tag{17}$$

where, the magnitude of the steps needed to get at the local minima is essentially equivalent to the learning rate, or LR. Therefore, iterative gradients are calculated for the input data points using m and b values in order to locate local minima and associated coefficients. Each new gradient offers information about the direction of minima to update the coefficients, while LR controls how quickly this is accomplished. The vanishing gradient, or more specifically, the fact that the gradients (Eqs. (5) to (17)) are disappearing (diminishing) in a deep NN, is a typical issue with feed forward, back propagation MLPs. The error is usually calculated using gradients, however, diminishing gradient phenomenon in case of deep MLPs causes minimal gradient to reach the input layer. Thus, compromising the quest of local minima and its direction and hence minimization of cost function. As a result, MLPs are left with very limited proficiency to extract the sequential features from the input time series data, such as the prediction of layered temperature in TES.

Recurrent neural network (RNN) architecture is suggested as a way to get around this restriction. RNN has an advantage of hidden feedback loop. This feedback loop preserves the information and the problem of diminishing gradient is reduced significantly. This helps in retaining the sequential features during training phase, Fig. 6(b). RNN can extract information from time series data, temporal data, and non-numeric data more effectively. The LSMT cell, a type of RNN is shown in Fig. 6(c). LSTMs are used to alleviate the diminishing gradient problem in MLPs and even RNNs as they store information in short term memory. Time series prediction is where LSTMs shine. The LSTM network architecture and input/output mapping are depicted in Fig. 7(a) and (b), respectively. Table 2 displays the architecture clearly depicting hidden layers and losses. The volumetric discharge rate and the last three timestamps of temperature values are the network's inputs, and its output is the current MIX and layered temperature values.

Table 2. NN architecture.

Layer (Type)	Output shape	Training loss	Testing loss
(1) Dense (MLP)	(None, 32)	0.04	0.04
(2) Lstm_1 (LSTM)	(None, 16)	3 x 10^{-4}	4 x 10^{-4}
(3) dropout_1 (Dropout)	(None, 16)	–	–
(4) dense_1 (Dense)	(None, 1)	4 x 10^{-4}	4 x 10^{-4}

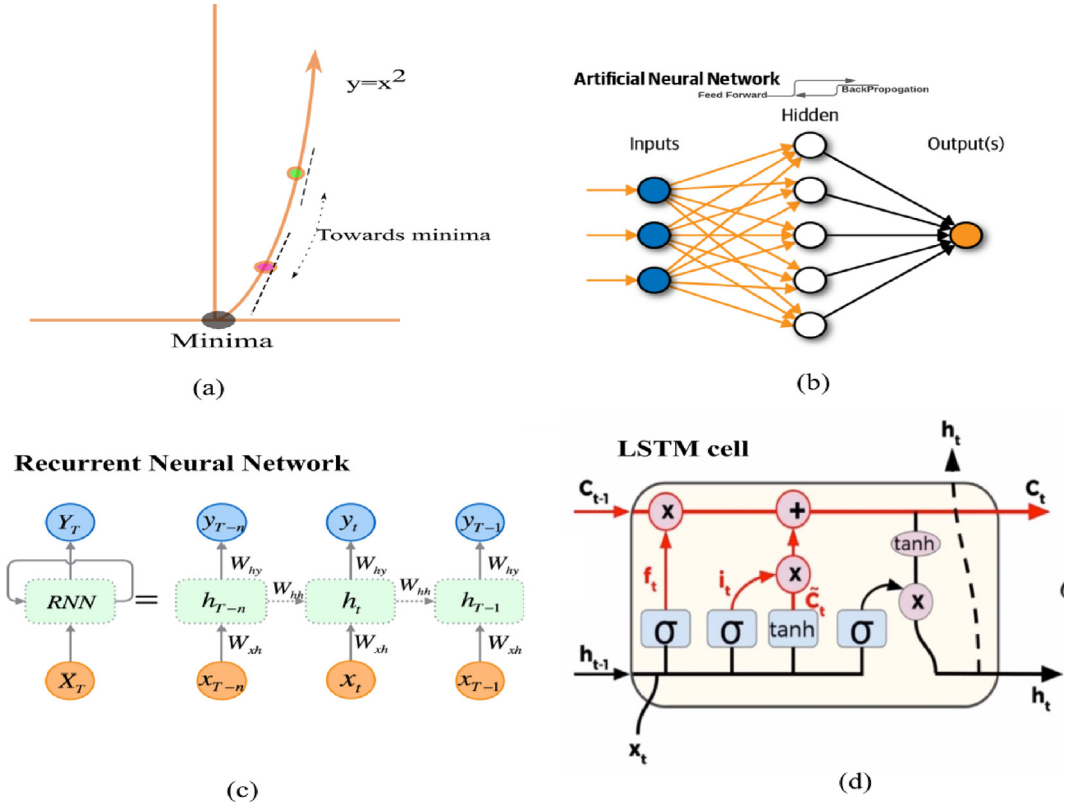

Fig. 6. (a) local minima of a cost function, (b) structure of MLPs, (c) unfolded RNN, and (d) LSTM cell (Fig. 6(c) & (d) modified from: https://bit.ly/LSTMfig4d; https://bit.ly/LSTMfig4c).

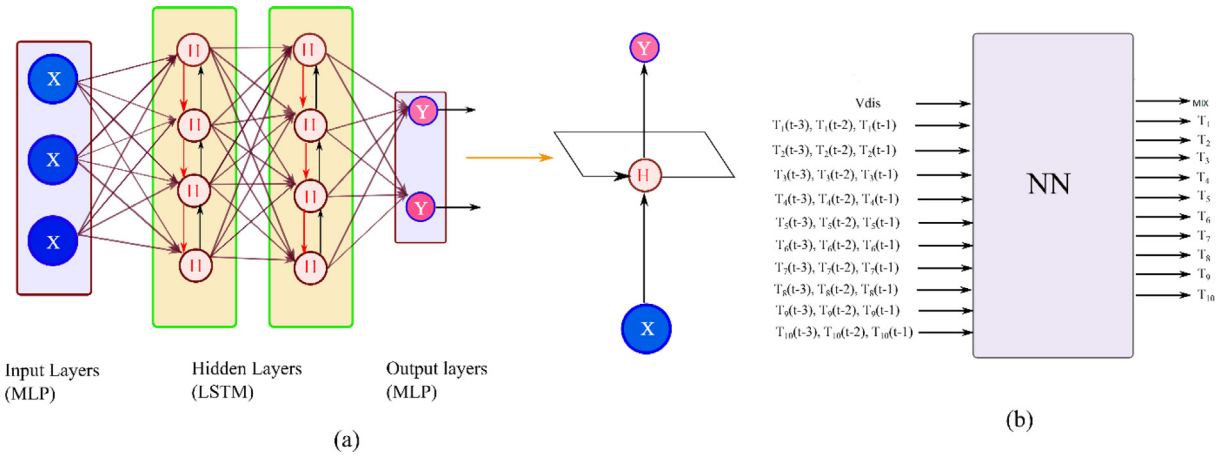

Fig. 7. (a) NN architecture, and (b) Input & output to network.

6. Results and discussions

6.1. Temperature distribution

The Jupyter Notebook receives a stream of the real-time energy evaluation. Data from experimental facility is collected and underwent through a series of data engineering process before fitting to the energy models by data

layer. The code and GIF presentation are both accessible on the GitHub repository [15]. A restored version of the modeled data is collected into still figures for parametrization and evaluation because animated GIFs could not adequately convey perspective in the hardcopy of this work.

The tank was maintained at 60 °C before discharging for each Inlet flow rate. This was important to compare various inlet flow rates with base tank temperature. During discharge, the inlet water temperature was held constant at 20 0.2 °C. Each intake had a discharging test at four different flow rates: 200 l/h, 400 l/h, 600 l/h, and 800 l/h. The amount of time it took for the inlet water to completely replace the water in the tank is known as the replacement time. To examine the impact of flow rates on the temperature distribution during discharging, the temperature distribution and outflow water temperature throughout one replacement time were recorded. Unit replacement time is different for each flow rate and hence to evaluate and analyze the discharging performance at various flow rates, the dimension-less discharging time was developed. Three distinct flow rates were used, and each experiment lasted one unit of replacement time. The findings of the experiment were examined in one-unit replacement time at various flow rates. The accompanying Fig. 8 displays the development of both the discharging procedure and the temperature profile at various nodal locations (20 nodes). Unit replacement time for 200 l/h is 1.985 h. It is clear that compared to other flow rates, 200 l/h demonstrates superior stratification. For larger flow rates, the top layers' temperature is

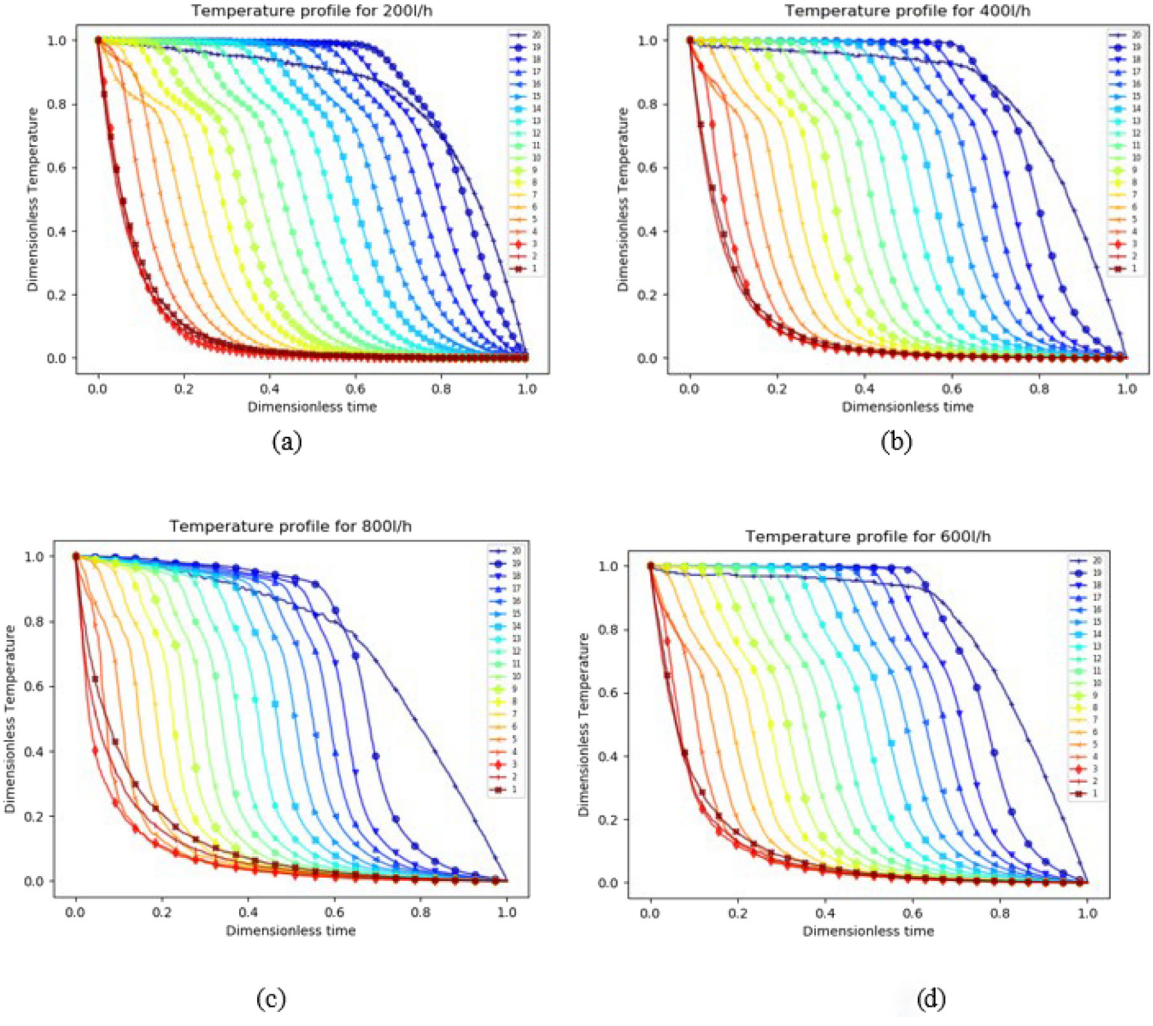

Fig. 8. Temperature profile at (a) 200 l/h, (b) 400 l/h, (c) 600 l/h, (d) 800 of discharging rate (Fig. 6(c) & (d) modified from: https://bit.ly/LSTMfig4d; https://bit.ly/LSTMfig4c).

higher and more stable than its counterpart. The strongest mixing occurs at the inlet and even at higher level for 800 l/h.

20th layer actually does not participate in the plug flow, due to its geometrical position above the tank outlet. For 400, 600, and 800 l/h the unit replacement time is 0.99, 0.66, and 0.499 h, respectively. The temperature of the 18th layer, the topmost layer involved in the plug flow, was at its lowest (52 °C) for 800 liters per hour while at 59.2 °C for 200 l/h during 60% of discharge.

6.2. MIX number

The MIX number analyzes the tank based on both the vertical temperature profile and the total energy stored in the tank, as opposed to temperature gradients which eventually uses temperature profiles. In other words, the MIX number postulates the mixing process in the tank by evaluating the momentum of energy ME as indicated by Eq. (1), which is based on both the energy and temperature distribution.

Fig. 9 displays the computed MIX number for the 60 – 20 °C discharge at flow rates of 200, 400, 600, and 800 l/h. Eq. (2) indicates that the MIX number varies between 0 and 1, but the important question is how slowly. The MIX number's ascent is lowest at 200 l/h, followed by 400 l/h, then 600 l/h, and greatest at 800 l/h. The figure clearly shows that at t* = 0.4, MIX is around 0.4 for 200 l/h and 0.6 for 800 l/h.

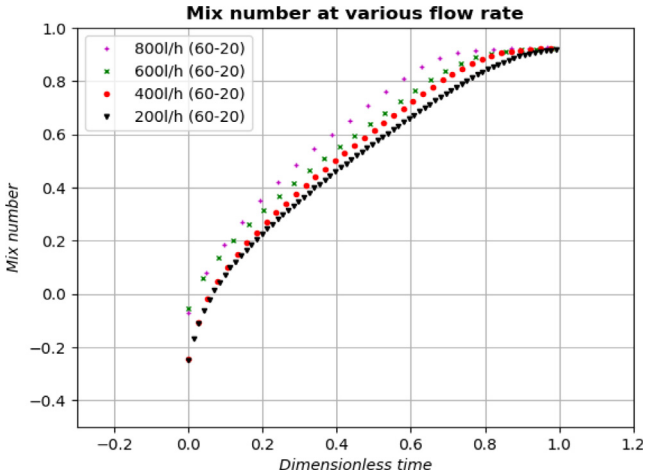

Fig. 9. MIX number analysis at different flow rates.

6.3. Richardson number

The buoyancy, which is influenced by both the gravity and the impact of the temperature on the density of the heat transfer medium, helps to define the thermal stratification inside the storage tank. In reality, the Richardson number ($Ri = Gr/Re^2$) is always considered a major factor in the stratification progress. Fig. 10 denotes the evolution of the

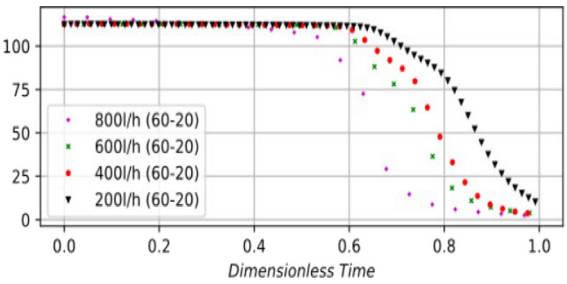

Fig. 10. Richardson number at different flow rates.

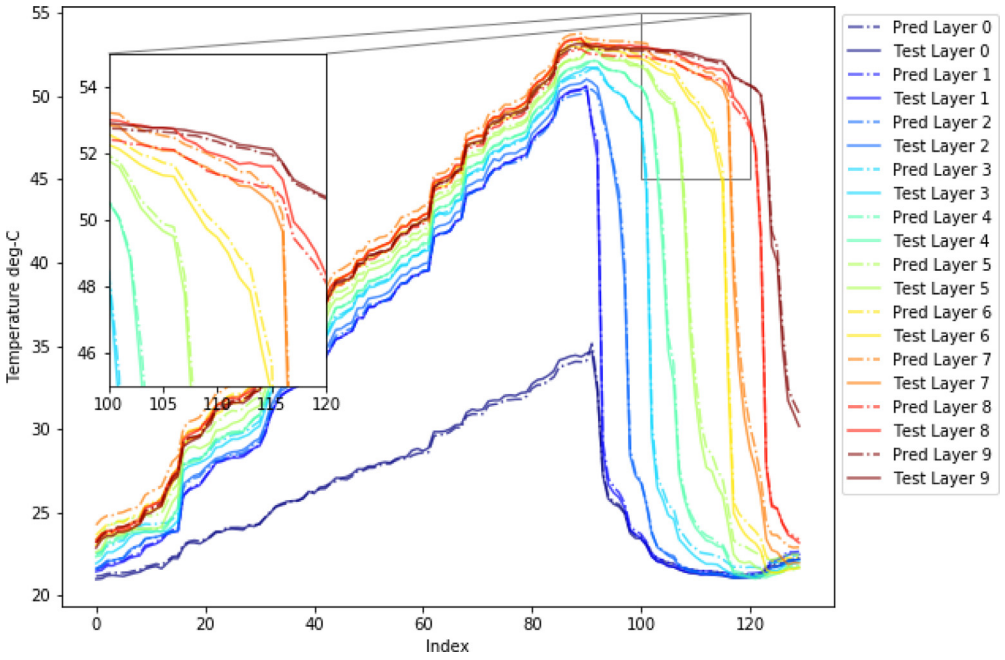

Fig. 11. Predicted against measured layered temperature for 1200 l/h discharge rate.

Richardson number as a function of the dimensionless time for different discharging processes. As per definition, tank sustains better stratification at lower flow rates. In other words, *Ri* is increased as flow rate is decreased from 800 to 200 l/h. For example, *Ri* at $t^* = 0.6$ for 800 l/h is nearly 75, while for 200 L/h it is approximately 120. $t^* = 0.6$ being the dimensionless time at which 60% tank is already discharged.

6.4. LSTM network prediction

The comparison of measured and predicted temperature distribution is plotted in Fig. 11. Given the mixing induced by high inlet flow rate, stratification destruction is apparent. Likewise, the MIX number predicted versus experimentally calculated is shown in Fig. 12(a). As the process is carried forward, the data layer assesses energy models and broadcasts the results to the "Jupyter Notebook" for further analysis. The information is then retrieved from the cloud servers for exploratory data analysis (EDA) and for prediction tasks using neural network. As time representation confounds and slows the learning algorithm of the network, the X data points have carefully been chosen as indexes. Fig. 12(a) demonstrates the extent of mixing at such a high flow rate. MIX at 1200 l/h is almost peaking 1. In contrast, Fig. 9 shows lesser levels of exergy destruction due to lesser intensity of flow, with MIX staying around 0.90. The normalized temperature distribution are displayed in Fig. 12(b) against observed values with an acceptable tolerance of 4%. The r-squared loss is reduced from 10^{-2} to 4×10^{-4} in model tuning process, refer Fig. 12(c).

Validation loss falls within 4×10^{-4} and 6×10^{-4}. Slight overfit is evident despite lowest reported testing loss. As a matter of fact, slight overfit is desirable for additional tuning of network. Validation and training loss need to be minimal and reasonably similar to each other, signifying the best possible good fit. The effectiveness of network was evaluated with the unseen data during testing phase.

In the final remarks, it should be noted that the main goal of this work is to demonstrate the 'data in motion' algorithm to assess the TES performance in near real-time. Stream-processing pipeline calculates the thermal indices, such as MIX and Richardson number and subsequently the degree of stratification destruction in TES. This cutting-edge stream-processing pipeline, presumably would assist engineers and researchers to intuitively understand the energy performance of their TES. The noteworthy observations are:

- This study assessed the destratification process and thermal efficiency of TES for single family house frequently available in the Czech market

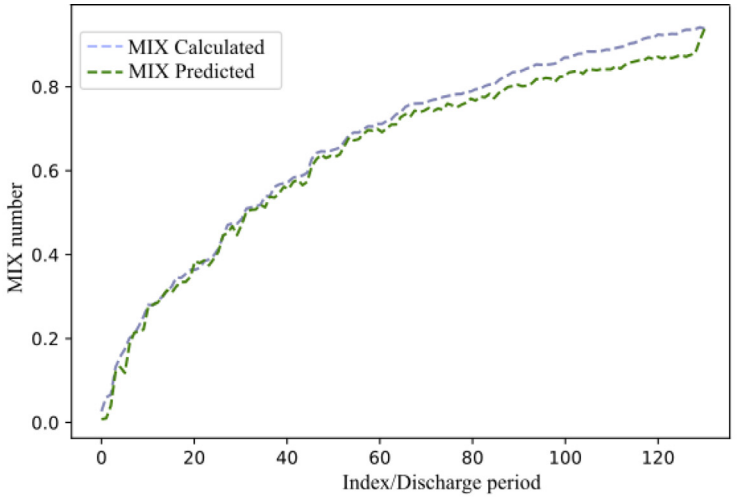

(a)

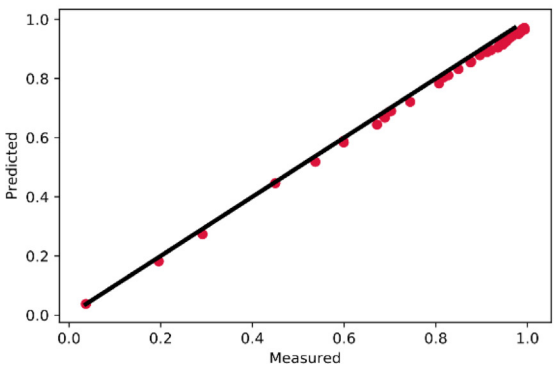

(b)

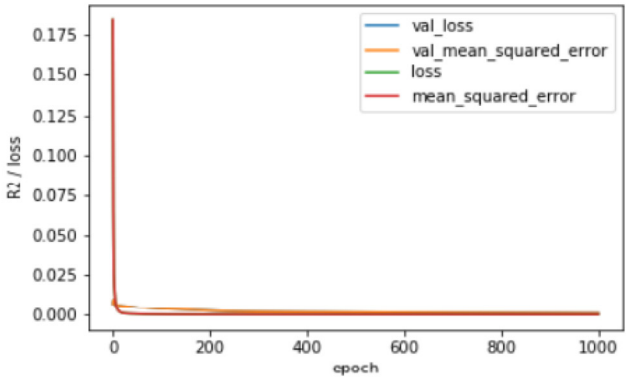

(c)

Fig. 12. Predicted against measured (a) MIX number, (b) error range ∼5%, and (c) mean square error.

- For the stated purpose, initially, TES temperature dispersion is measured using resistance temperature diodes' (RTDs). Next, thermal indices like MIX &Richardson numbers are reviewed to confirm the findings. Assessment is made using stream processing layer dedicated for real time evaluation.
- Distinct flow rates of 200 l/h, 400 l/h, 600 l/h, and 800 l/h were studied in this work.
- Stream-processing layer gives a competitive edge to the energy researchers by logging the thermal performance in real time. Researchers will be fully cognizant about the percentage of the total energy which is thermodynamically inaccessible due to stratification destruction.
- The future work with current stream-processing layer can thoughtfully be the long-time evaluation of TES. For long time energy forecasting, extended duration of data collection is required with proper domestic tapping profiles. It is advisable to methodically use this unique stream-processing layer and the energetic models along with domestic tapping cycles to obtain insightful knowledge about thermodynamic losses, within a month's span of TES operation.

- The novelty of the work lies within the application of the stream-processing layer which essentially assists to create energy dispersion 'harmonogram' of TES. This is useful particularly in determining thermal performance of TES available in market of the Czech Republic.

7. Conclusion

Destratification seriously limits the effectiveness of TES. Full stratification in TES facilitates higher energy delivery with lower grid energy consumption. The decomposition of temperature at every layer was found to be increased with the rise in inlet flow rate thus polluting the energy content in the TES.

The creation of an innovative real-time stream-processing tool, which can evaluate the stratification performance of TES system with minimum human intervention served as the driving force behind this study. Stream processing layer is fabricated using a broad range of tech stack - Raspberry Pi single board mini-computers and wide spectrum data science and data engineering stack, for instance. This ad-hoc designed stream-processing layer was used to perform regression on energetic indices. Additionally, a thorough implementation of cutting-edge Machine Learning algorithm is illustrated for the time-series prediction workflow. The data thus collected by stream-processing layer is used to perform prediction workflow - temperature distribution and TES efficacy.

According to test results, extreme destratification due to intense mixing occurs at discharge of 800 l/h. The prediction and testing data correspond well within 5% error range. This is true for both temperature as well as efficiency data points. Training loss was brought to its lowest value of 6×10^{-4} using hyper-tune techniques, determines the precision of network.

Declaration of competing interest

The authors declare that they have no known competing financial interests or personal relationships that could have appeared to influence the work reported in this paper.

Data availability

The authors do not have permission to share data.

Acknowledgments

This work has been supported by Project TN01000056 - National Centre of Competence CAMEB granted by Technology Agency of Czech Republic.

References

[1] Cruickshank CA, Harrison SJ. Heat loss characteristics for a typical solar domestic hot water storage. Energy Build. 2010;42(10):1703–10.
[2] Chandra YP, Matuska T. Stratification analysis of domestic hot water storage tanks: A comprehensive review. Energy Build. 2019;187:110–31.
[3] Jaluria Y, Gupta SK. Decay of thermal stratification in water body for solar energy storage. Sol Energy 1982;28:137–43.
[4] Dehghan AA, Barzegar A. Thermal performance behaviour of a domestic hot water solar storage tank during consumption operation. Energy Convers Manage 2011;52:468–76.
[5] D'Amico A, Ciulla G. An intelligent way to predict the building thermal needs: ANNs and optimization. Exp Syst Appl 2022;191:116293.
[6] Ekici BB, Aksoy UT. Prediction of building energy needs in early stage of design by using ANFIS. Expert Syst. Appl. 2011;38:5352–8.
[7] Géczy-Víg P, Farkas I. Neural network modelling of thermal stratification in a solar DHW storage. Sol. Energy 2010;84(6):801–6.
[8] Srivastava N, Hinton G, Krizhevsky A, Sutskever I, Salakhutdinov R. Dropout: A simple way to prevent neural networks from overfitting. J. Mach. Learn. Res. 2014;15(56):1929–58.
[9] Hinton GE, Srivastava A, Krizhevsky I, Sutskever R, Salakhutdinov N. Improving neural networks by preventing co-adaptation of feature detectors. In: Neural and evolutionary computing. Cornell University; 2012, Cite as arXiv:1207.0580.
[10] Yaïci W, Entchev E. Performance prediction of a solar thermal energy system using. Appl. Therm. Eng. 2014;73:1348–59.
[11] Sencan A, Yakut K, Kalogirou SA. Thermodynamic analysis of absorption systems using artificial neural network. Renew. Energy 2006;31:29–43.
[12] Souliotis M, Kalogirou S, Tripanagnostopoulos Y. Modelling of an ICS solar water heater using artificial neural networks and TRNSYS. Renew. Energy 2009;34:1333–9.

[13] Mellit A, Benghanem M, Kalogirou SA. Modeling and simulation of a stand-alone photovoltaic system using an adaptive artificial neural network: Proposition for a new sizing procedure. Renew. Energy 2007;32:285–313.
[14] Voyant C, Notton S, Kalogirou ML, Nivet C, Paoli F, Motte G, Fouilloy A. Machine learning methods for solar radiation forecasting: A review. Renew. Energy 2017;105:569–82.
[15] Chandra YP. GitHub [GIF and code]. 2021, Retrieved from GitHub: https://github.com/yogenderPalChandra/Raspi1_main_Pt100_FlaskServer.
[16] Davidson JH, Adams DA, Miller JA. A coefficient to characterize mixing in solar water storage tanks. Trans ASME J Sol Energy Eng 1994;116:94–9.
[17] Haller MY, Cruickshank CA, Streicher W, Harrison SJ, Andersen E, Furbo S. Methods to determine stratification efficiency of thermal energy storage processes–reviewand theoretical comparison. Sol Energy 2009;83:1847–186.

References

1. Haller et. al, A method to determine stratification efficiency of thermal energy storage processes independently from storage heat losses, Solar Energy, 84 (2010) 997–1007
2. Rosengarten et. al, A second law approach to characterising thermally stratified hot water storage with application to solar water heaters. Journal of Solar Energy Engineering, 1999, 121(4): 194 – 200
3. Haller et. al, Methods to determine stratification efficiency of thermal energy storage processes – Review and theoretical comparison, Solar Energy, 83 (2009) 1847–1860
4. A. Campos Celador, M. Odriozola, J.M. Sala, Implications of the modelling of stratified hot water storage tanks in the simulation of CHP plants, Energy Conversion and Management 52 (2011) 3018-3026
5. S. Giedre, M. Vytautas, A. Anders N, K. Jonas, Feasibility of CHP-plants with thermal stores in the German spot market, Applied Energy 86 (11) (2009) 2308-2316
6. A. Pablo, M. Marc, G. Antoni, O. Eduard, C. Luisa F, Overview of thermal energy storage (TES) potential energy savings and climate change mitigation in Spain and Europe, Appl. Energy 88 (8) (2011) 2764-2774.
7. W. Yaici, M. Ghorab., E. Entchev, S. Hayden, Three-dimensional unsteady CFD simulations of a thermal storage tank performance for optimum design, Applied Thermal Engineering, 60 (2013) 152-163
8. Data Science, What is Neural Network, 2022, Retrieved from: https://www.sevenmentor.com/what-is-neural-network
9. Shujaat Hasan, Recurrent Neural Network and it's variants…, Analytics Vidhya, 2020, Retrieved from: https://medium.com/analytics-vidhya/recurrent-neural-network-and-its-variants-de75f9ee063